Electrical-Impedance Biofeedback Instrument for Swallowing Rehabilitation

---

A thesis submitted in partial fulfilment of the requirements for the Degree of Masters of Engineering in Electronic and Electrical Engineering

by

Christopher J. Chester

University of Canterbury

March 2014

Abstract

Biofeedback is an important tool in the rehabilitation of several dysphagic conditions. This thesis presents an investigation into using bio-impedance as a technique for providing biofeedback of the swallowing sequence, specifically sequencing in the pharynx. The motivation behind this project was to find an alternative rehabilitation tool for detecting pharyngeal sequencing, as the current tool of pharyngeal manometry is invasive and non-portable. This investigation included the design and creation of a bio-impedance measuring device named the Guided Utility for Latency in Pharyngeal Sequencing (GULPS). This system was continued from a previous unpublished investigation at the University of Canterbury, where an initial prototype was designed and created. It was found that this pre-existing system had numerous faults in both its hardware and software, limiting the use of the device.

Electrical impedance across the throat can be determined by applying a known constant amplitude current signal across the throat and recording the corresponding voltage. This impedance has been shown to change during a swallowing sequence due to a change in the structure of the throat. The principle used in this project was to investigate if two positions of impedance measurement could be used to determine the sequencing of the pharynx during a swallow. The design of the GULPS device was influenced by the pre-existing system and several prototypes were built to obtain a system capable of providing two channels of impedance measurement. Software was adapted from the pre-existing system to interface with this hardware to provide a system that could be attached to an external computer.

Various electrode positions for the final device were trialled aimed at measuring two similar, but temporally separated, impedance waveforms. It was found that positioning the electrodes close to the approximate position of the pharynx with a 40 mm gap between channels allowed for two temporally separated channels to be produced with three distinct features: two peaks and one trough in each of the GULPS waveforms. The GULPS device with these electrode positions was trialled on three 'healthy' subjects and one dysphagic subject. The three features could be identified in both impedance waveforms in all four subjects.

To determine if the identified features related to the sequencing of the pharynx, the GULPS device was trialled alongside the current conventional method for detecting pharyngeal sequencing, pharyngeal manometry. The results from these trials revealed a potential relationship between the temporal separation of the second peaks found in the GULPS waveforms and the temporal separation of the pressure peaks from pharyngeal manometry. The GULPS device was trialled alongside pharyngeal manometry on one 'healthy' and one dysphagic subject. A linear regression between peak-to-peak latencies between the two methods had an R^2 value of 0.347 for the 'healthy' subject and 0.241 for the dysphagic subject. However, these peaks were often difficult to detect, and could only be detected in 64% of swallows in the 'healthy' subjects using the GULPS device in a standalone fashion and in 23% of swallows when used concurrently with manometry.

As the current GULPS device is unable to produce the desired results in a consistent manner, no definitive conclusions can be drawn on the ability of using bio-impedance to measure the pharyngeal sequence. Notwithstanding, substantial progress has been made towards a device for reliable measurement of pharyngeal sequencing and, together with the clinical benefits to be gained, more than justify further research and development into GULPS for dysphagia rehabilitation.

Acknowledgements

I would like to thank my supervisors, Dr Paul Gaynor, Dr Richard Jones, and Dr Maggie-Lee Huckabee for their continued help and support throughout this project. Their input throughout the entire project was extremely helpful and I really appreciate the time and effort they put into reviewing and correcting this thesis. I would like to thank the electrical technicians who helped fabricate and design the prototype circuit boards, notably Mike Cusdin. Thanks also to all the subjects who agreed to be part of the device trials.

A special thanks to my family and Hannah - for their continued support and belief over these past two years. Their encouragement and support has always allowed me to strive to succeed.

Contents

CHAPTER 1

Introduction

Geddes & Baker, authors of the series *Principles of Applied Biomedical Instrumentation* [1], state that in the biomedical sciences the use of biomedical instrumentation is a valuable tool for transforming a biological event into an electrical signal. With an event available in an electrical format, it is much easier to obtain the advantages of modern computing and to display the desired information. The use of biomedical instrumentation offers a different approach for solving problems in the field of medical research and treatment. For example, the ability to record the data for future examination at different display speeds, either faster or slower, allows for retrieval of information missed at the time of measurement. Geddes & Baker stated that, in biomedical sciences, instrumentation for the purpose of quantification in measurement has not been explored in all available areas, and a major task yet to be accomplished is to develop the tools and technology for solving the problems of detection and quantitative measurement of living processes.

This thesis covers the use of engineering techniques and approaches in the medical application of biological feedback to a specific application. Biological feedback (biofeedback) is an invaluable tool in many medical fields for rehabilitating conditions through the use of instrumentation. Biofeedback is a process through which information regarding physiological reactions and parameters is conveyed through electrical signals, often audible or visual. Information such as blood pressure and skin temperature, which are not consciously controllable by an individual, are often relayed through the use of

biofeedback [2]. Fields which incorporate biofeedback are numerous and exist over a wide range of applications including the treatment of functional constipation, bronchial asthma, and balance disorders [3].

Biofeedback is often provided with some form of applied biomedical instrumentation. These instruments can provide visual or audio signals as feedback for rehabilitation. An example of instrumentation is the use of surface electromyography to provide feedback of a patient's pelvic floor muscle activity as a rehabilitation tool for functional constipation [4, 5]. In this treatment the patients use a visual representation of the data from their pelvic floor muscles as feedback to regain the correct functional use of these muscles to avoid constipation. Similarly, biofeedback in the treatment of bronchial asthma provides a method of rehabilitation. A technique discussed by Anokhin *et al.* [6] visualizes a patient's external respiration rhythm through the use of a custom respiration corrector. The patient then attempts to synchronize this visible rhythm with a desired reference rhythm. Even the condition of vertigo, a balance disorder, can be addressed with the use of biofeedback [7]. This is again achieved through the use of visual biofeedback, where vertigo is induced and a visual representation of the efforts applied in order to counteract the symptoms is provided as feedback. These efforts include head rotations and eye movements, and allow for patients to isolate techniques which provide the best results in avoiding vertigo.

Treatment for swallowing disorders (dysphagia) is a field in which behavioural rehabilitation techniques are emerging [8]. The exact prevalence of dysphagia is unknown. Epidemiologic studies, however, indicate that the prevalence may be as high as 22% in those over 50 years of age [9]. It has been documented that approximately 10 million Americans are evaluated each year with swallowing difficulties, both over and under 50 years of age [10]. The field of dysphagia treatment often incorporates the use of biofeedback, where it has been found that providing patients with biofeedback allows for several debilitating swallowing conditions to be treated effectively [11]. The New Zealand Brain Research Institute is one facility that uses biofeedback as a technique for dysphagia rehabilitation [12].

Initial investigation work was performed in 2011 by the University of Canterbury in association with the New Zealand Brain Research Institute to develop a device to provide swallowing biofeedback. This device aimed to investigate the use of electrical-impedance measurement data as a form of biofeedback for the dysphagic feature of pharyngeal mis-sequencing. Pharyngeal mis-sequencing occurs when several swallowing muscles

contract at the same time, rather than in a sequential order; this is covered in more detail in Chapter 2. This device was not completed but provided a conceptual basis to build on for a follow-up device.

This thesis presents the continuation of development of a dysphagia rehabilitation biofeedback device, for research purposes and potential clinical use. The work completed in this study included development of a working device known as the Guided Utility for Latency in Pharyngeal Sequencing (GULPS). This procedure included redesigning most of the hardware from the previous work and building all new prototypes in order to obtain a consistent and reliable two channel bio-impedance measuring device. In addition, the software used in the previous solution needed to be heavily adapted for use with the GULPS hardware.

The contents of this thesis include nine chapters outlining the creation and testing of the current GULPS device, where the initial focus is on previous research and development. Chapter 2 provides a background on swallowing disorders and current rehabilitation methods, including bio-impedance. This chapter covers normal swallowing movements, potential dysphagic features (including pharyngeal mis-sequencing), and the current, as well as potential future, methods of rehabilitation. Following this chapter, an outline of the previous work completed in developing a bio-impedance device is covered in Chapter 3. This chapter details the design of the previous device and how it was examined and tested to outline its problems and shortcomings.

Chapter 4 through to Chapter 6 include the work performed in developing the GULPS device. Adaptations and improvements to the previous design are outlined in Chapter 4. This chapter provides an explanation of the steps taken, as well as the reasoning, in developing the current GULPS device. A large part of obtaining a consistent device was reliant on the electrodes; the electrode choices and placements are therefore outlined in Chapter 5. Chapter 6 then covers the improvements and bug fixes performed on the previous software design in order for it to be compatible with the new hardware.

Chapter 7 covers the various testing and trials of the GULPS device on test rigs and subjects. This chapter includes protocols used, approvals gained, as well as the actual results of the device. Chapter 8 details the analysis of the results gained, including explanations of performance characteristics. The final chapter, Chapter 9, includes conclusions and potential advice and guidance for any future development of the device.

CHAPTER 2

Background

This chapter outlines the background principles and theories used in this thesis. The topics covered in this chapter include an overview of the basics of swallowing and issues that can occur while swallowing. This leads onto the specific issue of pharyngeal mis-sequencing, and the associated current rehabilitation techniques. Finally, a brief outline of alternative methods used for dysphagia rehabilitation and their suitability for rehabilitating pharyngeal mis-sequencing is presented, with an overview of bio-impedance and its applications.

2.1 Swallowing Biomechanics

Swallowing is normally conceptualized as happening in several distinct phases, namely, the oral phase, the pharyngeal phase, and the oesophageal phase. Ekberg [8] states that the swallowing sequence consists of these three anatomically and functionally separated, but integrated, areas which act as a hydrodynamic pump. Each of these compartments operate independently but, for a successful swallowing process, finely tuned coordination between the compartments is required. In addition to these three phases, a fourth stage can be included in the discussion of normal and abnormal swallowing. This phase occurs prior to the oral phase and is known as the pre-oral phase [13]. In this section each of the four stages of swallowing will be highlighted and given a brief description.

2.1.1 Pre-oral Phase

The pre-oral phase is summarized by Daniels and Huckabee [13] to be a valuable tool in conceptualizing the swallowing sequence. A model containing the pre-oral phase considers a strong interaction between the pre-swallowing and swallowing behaviours. The pre-oral phase encompasses the pre-oral motor, cognitive, and psychosocial elements involved during ingestion, such as attention, eating behaviour and feeding method, all of which could impact swallowing efficiency and safety [14]. The pre-oral phase is of particular importance for patients with head-injuries, where cognitive deficits are recognized as a substantial factor influencing feeding and swallowing [15]. The pre-oral phase is therefore important for rehabilitation purposes and allows for the utilization of sensory modulation of taste and smell for rehabilitation of patients with dysphagia [16].

2.1.2 Oral Phase

The oral phase of swallowing is described by Jones [17] as an almost entirely voluntary stage of swallowing that involves ingestion and mechanical formation of the bolus; a bolus is the collection of food or drink in the mouth that has been chewed and is ready to be swallowed. This stage requires use of many of the facial muscles, muscles for mastication, and tongue muscles as well as the supporting bones and cartilage. The positions of various anatomical features used in the oral phase can be seen in Figure 2.1. The oral phase uses the structures between the lips and the pharyngeal inlet, where the tongue is a major part of the oral centre. The tongue is responsible for creating a bolus which is then propelled quickly from the front to the back of the oral cavity, allowing the bolus to be passed to the pharynx.

2.1.3 Pharyngeal Phase

Jones [17] describes the pharynx as being a group of more than 24 muscles with intricate anatomical relationships. In the pharyngeal phase these muscles must function together to transport a bolus from the oral cavity to the oesophagus. The position of the pharynx can be seen in Figure 2.1, where it is connected to both the oesophagus and the larynx. Events that occur in the pharyngeal stage occur in a precise sequence and can be explained as occurring early or late in the swallowing sequence. The early stage of the swallowing sequence includes sealing of the nasopharynx, propulsion of the bolus into the pharynx with elevated hyoid bone and larynx, and sealing of the pharyngeal inlet [17]. The late stage is comprised of the restoration of the hyoid bone and larynx to the original position and clearance of the bolus into the oesophagus.

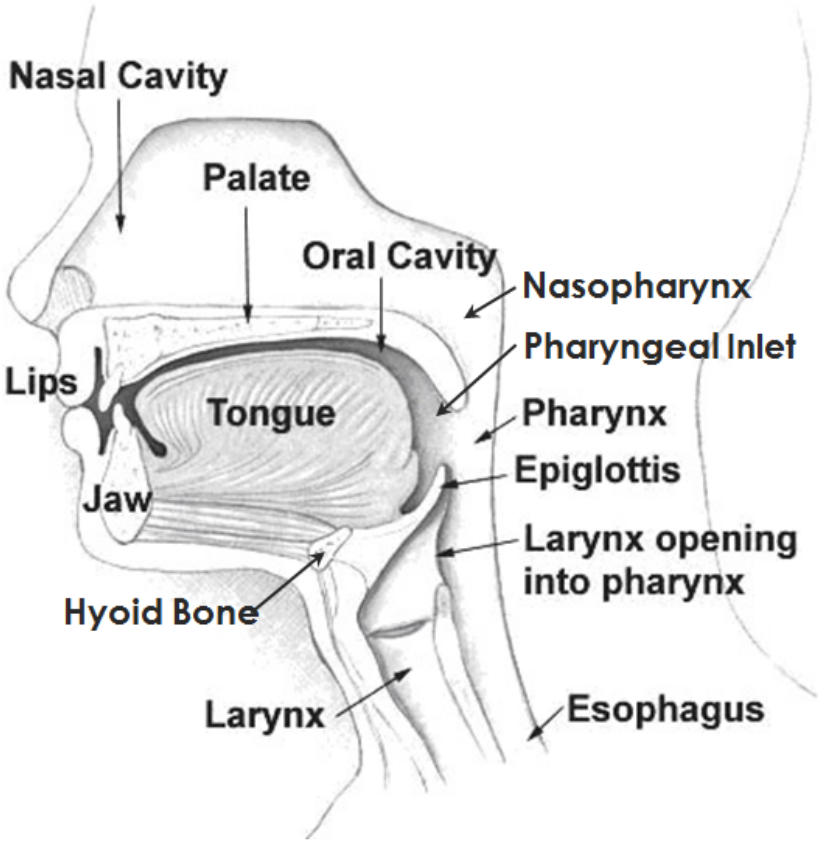

Figure 2.1: *Diagram of the primary anatomical structures involved in swallowing. The oral cavity, pharynx, and oesophagus are the three major areas of interest [18].*

Each of these stages is an important part of the swallowing sequence to ensure success and safety of swallowing. Sealing the nasopharynx (nasal end of the pharynx) stops the bolus from entering the nasal passage. In combination with this, the raising of the hyoid bone and larynx prevents the bolus entering the airway. The final means of preventing escape of bolus material is the closing of the pharyngeal inlet which prevents regurgitation of the bolus into the oral cavity. The late stage of the swallowing sequence consists of using the muscles of the pharynx in sequence to clear the bolus and reset the positions of the hyoid bone and larynx. The muscle movements in these stages can be seen in Figure 2.2.

Daniels & Huckabee [19] stated that the action of propelling a bolus through the pharynx is accomplished by the combination of several muscles. Following the anterior hyoid movement a sequencing of these muscles creates pressure to propel the bolus through the pharynx. The muscles primarily used in the sequencing of pressure in the pharynx are the superior, middle, and inferior constrictor muscles. These muscles can be seen in

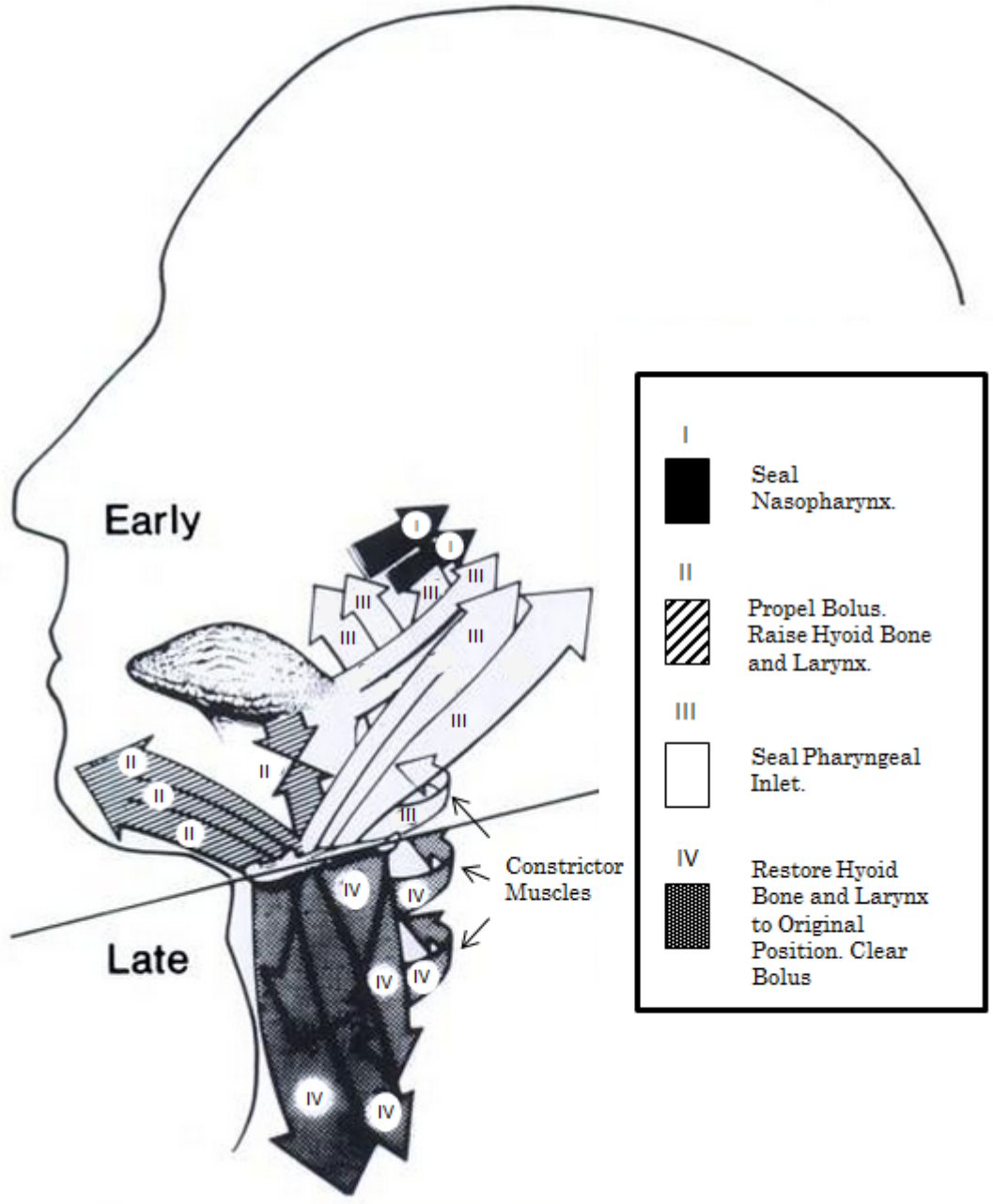

Figure 2.2: *The muscles and sequences responsible for early and late activity during the pharyngeal stage, as shown by Jones [17].*

Figure 2.3, where the order of muscle activity is from top to bottom (superior to inferior). In regards to the early or late swallowing movements, the superior constrictor muscle is first used after the base of the tongue has been raised in the early stages. The superior constrictor muscle is used to pull base of the tongue to the pharynx's posterior wall to seal the pharyngeal inlet. This movement applies pressure on the bolus, forcing it downwards. This same muscle, along with others, is then used to shorten the pharynx. While these

steps occur, the other two sequencing muscles of the pharynx are used to clear the tail of the bolus. This pressure sequencing moves the bolus into the oesophagus, where the inferior constructor muscle brings the upper oesophageal sphincter (UES) up to meet this oncoming bolus through its movement of the laryngeal structures.

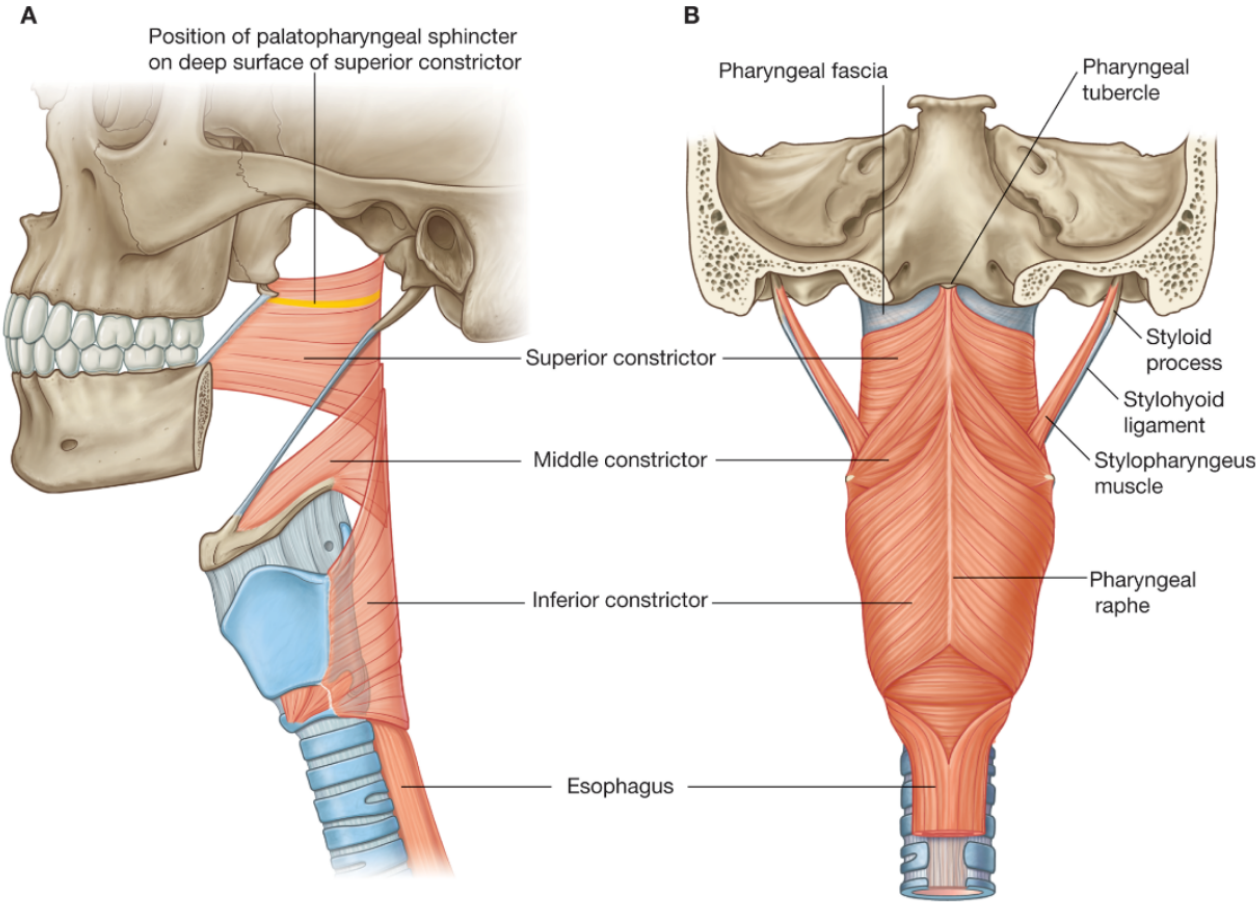

Figure 2.3: *The constrictor muscles used to clear the bolus in the pharyngeal phase [20]. (A) Lateral view. (B) Posterior view.*

2.1.4 Oesophageal Phase

The oesophageal phase of the swallowing sequence is the simplest phase. The oesophagus consists of sphincters which act alongside a contraction wave of muscles during this phase to pass the bolus to the stomach [21]. These sphincters include the upper oesophageal sphincter (UES) and the lower oesophageal sphincter (LES). The UES opens when the bolus enters the oesophagus from the pharynx. This bolus is then pushed through to the LES by sequential muscle contraction in the oesophagus. This muscle contraction is

called peristalsis and occurs in two separate waves to clear the bolus. Once the bolus has reached the bottom of the oesophagus the LES opens and releases the bolus into the stomach.

The overall swallowing sequence can be seen in Figure 2.4, where images taken from a video x-ray of the oral and pharyngeal phases are visible, and the oesophageal stage is about to occur. The operation and integration of all of these phases is very complex, this complexity means that any disruption to the swallowing sequence can be potentially hazardous.

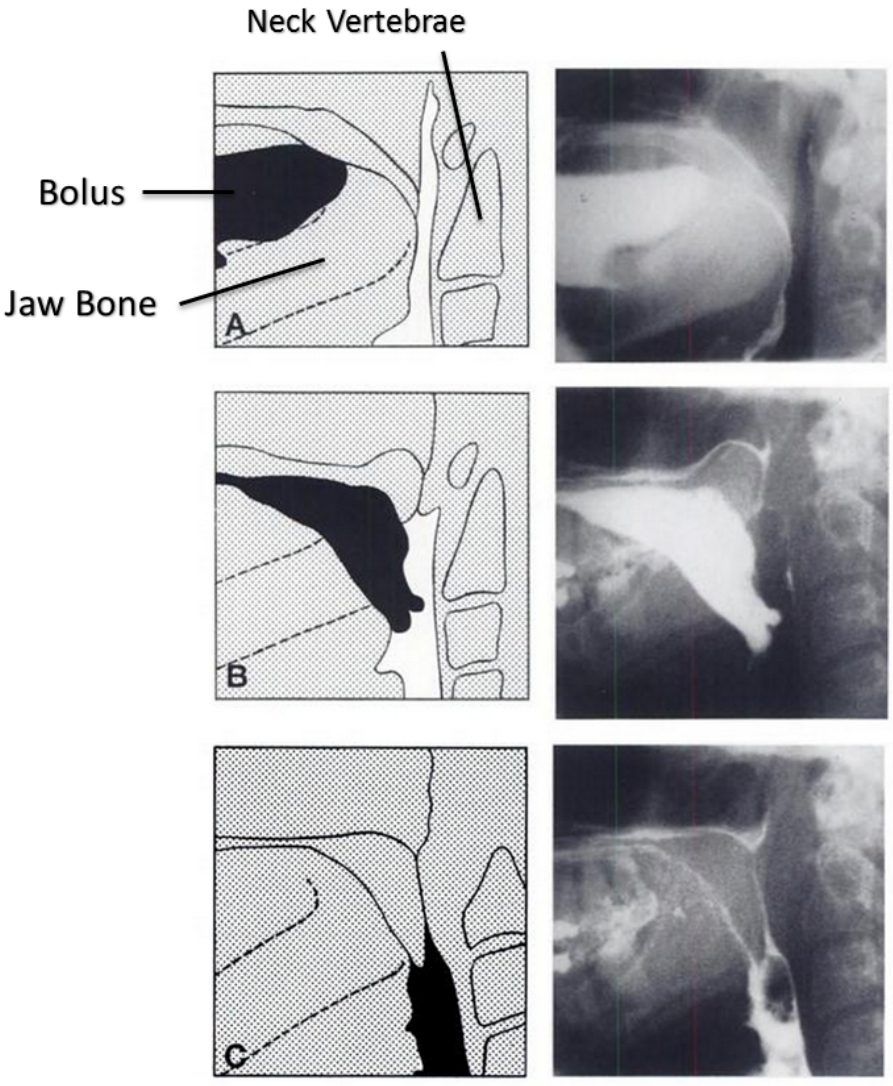

Figure 2.4: *Three x-ray frames from a swallowing sequence from 'Normal and Abnormal Swallowing' [17]. (A) Shows the bolus in the oral stage. (B) The bolas passing to the pharynx. (C) Bolus being passed to the oesophagus from the pharynx.*

2.2 Swallowing Disorders (Dysphagia)

The disorder of *dysphagia* is defined by Leopold & Kagel [22] as a disturbance of the intake or transport of food from the mouth to the stomach. Furthermore, it includes behavioural, sensory, and motor disorders in preparation for swallowing. This covers the four phases of swallowing, where dysphagia is a disruption in any of these phases. Dysphagia can be caused by one of two types of problems: something obstructing the pharynx or oesophagus, or impairment of the use of muscles and nerves controlling swallowing. The former can be caused by inflammation or growths in the pharynx or oesophagus. This form of dysphagia is an impairment of the biological structure and any treatment is focussed upon repairing the structure of the pharynx. Muscle and nerve malfunction can be caused by stroke, traumatic brain injury, neurodegenerative disorders, and immune system problems. These disorders may require treatment of the underlying neurological disorder and swallowing therapy. These treatments can often be in addition to any procedures performed for the original injury, such as surgery undertaken for head trauma. Both types of dysphagia can potentially result in a feeding tube placed directly into the stomach if oral feeding is unsafe or inadequate [23].

2.2.1 Forms of Dysphagia

As normal swallowing is a very complex physiologic function, dysphagia can present as a wide variety of pathophysiologic impairments in any of the swallowing phases. Problems in the oral phase can exist from deficits in muscle tone and function controlling the the lips, jaw, and tongue. Logemann [24] stated that potential issues with the lips can include a neurological or a structural problem which prevents the lips from fully closing, allowing food to fall from the mouth. Alternatively, a pocket between the facial muscles and the skeleton can be formed due to a lack of muscle tone in the mouth. This pocket can collect a great deal of residue during a swallowing event. These issues are problematic, but in the oral phase a problem with the tongue can be the most debilitating. The tongue is a very important feature of the oral cavity stage of swallowing as it is responsible for not only emptying the oral cavity of food but also forming a bolus. If the tongue is impaired in either the vertical or lateral directions swallowing becomes far more difficult.

In addition to dysphagia caused by issues with the oral phase, there are several other dysphagic conditions due to the impaired function of the pharynx. One of the main issues is an absent or delayed pharyngeal swallow, resulting in food or water entering the lungs (aspiration) before the pharyngeal swallow [24]. In addition, weakness or lack of coordination of the pharyngeal swallow can cause post-swallow pharyngeal residual,

nasal redirection, and aspiration of food or fluid into the airway [19]. A failure of the UES to relax can result in difficulty transferring the bolus into the oesophagus. Parkinson's disease and stroke are common causes for dysphagia of both the oral and pharyngeal type. Due to the complexity of pharyngeal swallowing, specific pathophysiologic conditions are often difficult to isolate or even detect [25]. One of these conditions is pharyngeal mis-sequencing.

2.2.2 Pharyngeal Mis-sequencing

Recent research has identified a specific pathophysiologic feature of dysphagia characterized by pharyngeal mis-sequencing. Pharyngeal mis-sequencing is a condition where the patient has lost temporal separation and sequencing of pharyngeal pressure and occurs most often in patients with brainstem injuries. This condition causes contraction of pharyngeal muscles simultaneously rather than in sequence, causing major difficulties when eating and drinking. Pharyngeal mis-sequencing seriously impairs a person's ability to swallow and increases the likelihood of aspiration [26].

Little information is available on pharyngeal mis-sequencing and its cause is still unknown. Pharyngeal mis-sequencing has not been explicitly reported in literature, hindered by the reliance of videofluoroscopic swallowing studies for swallowing diagnosis and infrequent use of pharyngeal manometry. The New Zealand Brain Research Institute (NZBRI) has only recently started diagnosing patients with pharyngeal mis-sequencing issues, based on manometric evidence. This diagnosis has led to a manuscript documenting the condition by Huckabee *et al.* [27]. This manuscript outlines the characteristics of the condition as well as its previously undocumented nature.

2.3 Current Biofeedback Methods for Rehabilitation of Pharyngeal Mis-sequencing

Typically biofeedback modalities using in dysphagia treatments try to capture three different types of signals: swallowing images, pharyngeal sound, and surface electromyography (sEMG). Swallowing images are captured using the techniques of ultrasound [28], videoendoscopy [29], and videofluoroscopy [30]. Swallowing rehabilitation using these techniques have traditionally been focused on increasing the strength of swallowing to increase bolus flow and reduce pharyngeal residual [31]. Since pharyngeal mis-sequencing is a deficit of temporal separation, rather than strength of swallowing, a different biofeedback technique for rehabilitation is needed.

The University of Canterbury Swallowing Rehabilitation Research Laboratory based at the New Zealand Brain Research Institute (NZBRI) has been working with a cohort of patients who suffer from pharyngeal mis-sequencing from both New Zealand and abroad in order to rehabilitate their swallowing. It has been found that providing a subject with biofeedback of pressure patterns in the pharynx can help a patient learn how to retrain pharyngeal sequencing to obtain a more normal pattern. This biofeedback is provided through the use of pharyngeal manometry which provides ongoing, temporally sensitive information regarding the generation of swallowing pressure and position to a patient. This biofeedback can be used to relay information on pharyngeal dynamics to the patient, allowing them to adapt their swallowing technique. This is done until a more conventional sequencing of the swallow appears in the feedback.

2.3.1 Pharyngeal Manometry

The current method used in this laboratory for providing this pharyngeal biofeedback is that of pharyngeal manometry. The manometer is a device that measures pressures at multiple sensor locations. The sensors are very sensitive, accurate, and have an excellent frequency response. Standard, discrete sensor manometry, often also used in conjunction with fluoroscopy, measures pressures at various points in the pharynx. The device currently used at the NZBRI measures upper-pharyngeal, mid-pharyngeal, and upper-oesophageal sphincter (UES) pressures. The timing and magnitudes of these pressures when used in conjunction with fluoroscopy provide the clinician with important diagnostic information. Most importantly, it provides quantitative data to supplement the qualitative fluoroscopic assessment of pharyngeal/UES events before, during, and after swallowing [32]. Example waveforms from pharyngeal manometry are shown in Figure 2.5.

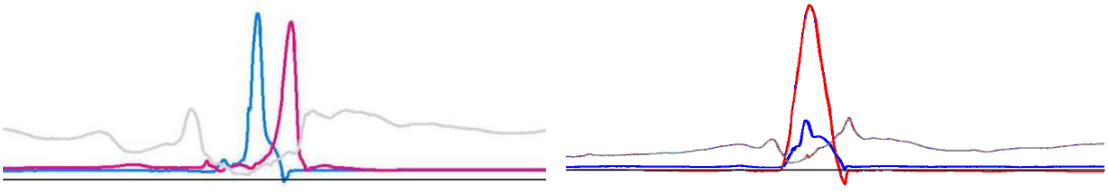

(a) *Normal swallow.* ***(b)*** *Mis-sequenced swallow.*

Figure 2.5: *Example waveforms from pharyngeal manometry, the blue waveform in each figure relates to the top sensor in the pharynx and the red relates to the bottom sensor. The grey waveforms are for the sensor located in the UES.*

The pharyngeal manometer, by its nature, is intrusive, and potentially uncomfortable and upsetting for the patient. An example of a transnasal catheter can be seen in Figure 2.6, where an inserted transnasal catheter is also shown in Figure 2.7. This manometer is used in a stand-alone set-up with patients, where a patient views a live display of the pressures on a monitor screen. This current solution has been found to allow some patients to regain substantial swallowing capability. Therefore, providing a patient with biofeedback of their swallowing pattern gives the opportunity for patients to increase the quality of their swallows.

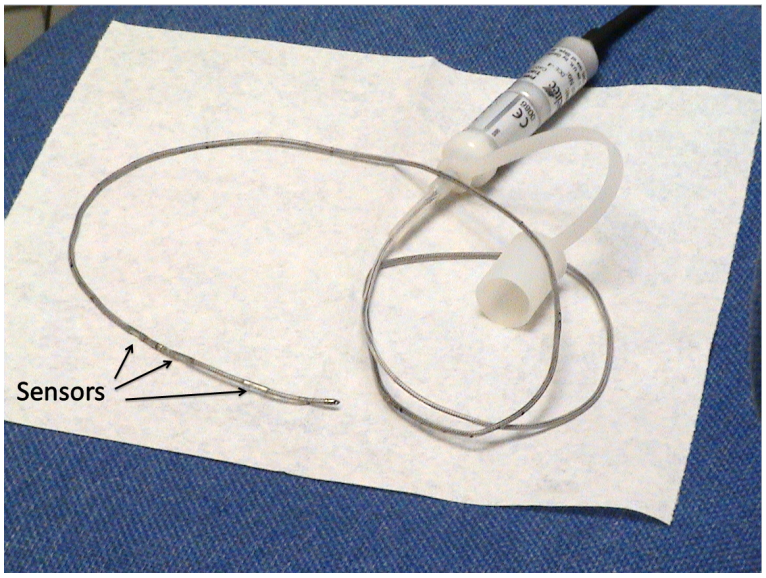

Figure 2.6: *The transnasal catheter (manometer) used in the treatment of pharyngeal mis-sequencing.*

2.3.1.1 Drawbacks of pharyngeal manometry

Though pharyngeal manometry is a useful tool in the rehabilitation of pharyngeal mis-sequencing it does have several drawbacks. The drawbacks of the current method are:

1. A physically invasive nature.
2. A lack of portability.
3. Reliance on expensive equipment.
4. The need for placement of the manometer and supervision of the biofeedback session by a trained swallowing specialist.

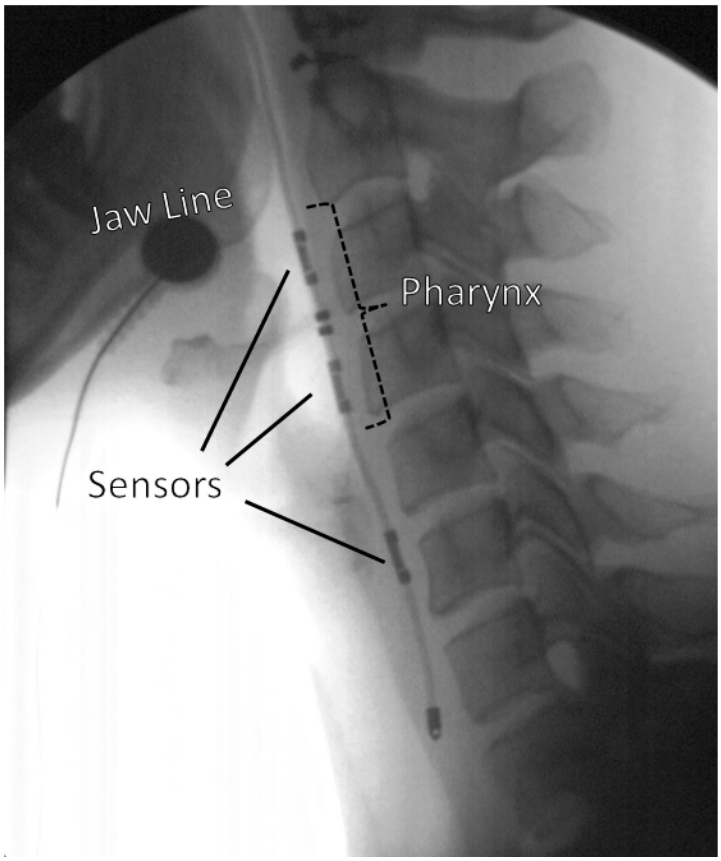

Figure 2.7: *Image of an inserted manometer, image taken using videofluoroscopy. This image shows the placement of two pressure sensors in the pharynx, as well as an additional sensor in the upper oesophageal sphincter (UES).*

One of the key features of the current manometry treatment provided by the NZBRI is the ongoing nature of the rehabilitation. Normally, two sessions are performed daily over an intensive one-week period to enable patients to gain a normal swallowing movement. Ongoing treatment is then attempted, in which patients attend weekly sessions to continue their rehabilitation. It has been found that patients who are unable to continue the treatment after the initial week are more likely to revert to pharyngeal mis-sequencing behaviour after a period of time. Continuous, or at least longer-term, treatment is therefore required to give patients the best possible chances of recovery.

A new device is therefore desired that provides the advantages of pharyngeal manometry, without its drawbacks. The features required from a new device include:

1. Temporally sensitive to change
2. The ability to detect sequenced pattern of pharyngeal constriction
3. Less invasive than pharyngeal manometry

4. Portable to allow for continued treatment

With these criteria in mind, a new solution was investigated.

2.4 Alternative Approaches for Rehabilitation of Pharyngeal Mis-sequencing

Several potential approaches for providing a subject with biofeedback information to assist with the rehabilitation of pharyngeal mis-sequencing were considered. These methods range from existing techniques for measuring other dysphagic conditions to the use of not yet applied methods such as muscle mapping as a form of feedback [30,33]. In addition, other techniques used to provide biofeedback in other fields were analysed to determine their suitability. Each of these solutions were evaluated against the features required from a new device.

2.4.1 Non-Invasive Techniques

2.4.1.1 Muscle Mapping

Muscle mapping is a technique involving the recording of surface electromyography (sEMG) signals and representing each of these signals as a separate muscle action [34]. The technique of sEMG involves testing the electrical activity of muscle fibres individually and collectively. This electrical activity can be recorded via surface electrodes, during periods of rest (spontaneous activity), and during periods of voluntary muscle contraction [35]. These electrical pulses can then be mapped to a two- or three-dimensional model to allow for biofeedback of the muscle movements.

Muscle mapping has presented itself as a useful tool in providing biofeedback in other clinical areas. Milosevic *et al.* [33] have gathered data on using muscle mapping in trunk muscle synergies. This technique used self-organizing maps to encode the EMG responses into a 2-D projection for visualization. Clinical devices have been developed for trunk muscle mapping purposes. A muscle pattern recognition device for biofeedback on the trunk and neck muscle activity has been developed by Edgerton *et al.* [36].

The technique of muscle mapping is a useful tool in areas of the body that have specific muscles that are easy to isolate with sEMG devices, but will likely have limited application in pharyngeal swallowing. The pharynx is too complex to isolate specific muscles using sEMG alone [37]. As mentioned in Section 2.1, there are a high number of muscles

responsible for the pharyngeal phase of the swallowing sequence (Figure 2.2). Needle electrodes could be used to isolate the required muscles for sequencing, however this would result in the device becoming more invasive than the current manometry solution. Due to these limitations, a muscle mapping device would likely not be able to deliver on the requirement of needing an ability to detect the sequenced pattern of pharyngeal constriction.

2.4.1.2 Bio-impedance

Bio-impedance is a biofeedback technique based upon measuring the electrical impedance of biological tissue, rather than the electrical signals produced by the body (as done with sEMG). The premise behind bio-impedance is that a change in the composition of the body local to the area being investigated will result in a changing impedance of that area [38]. Bio-impedance can be used to determine various aspects about the human body such as the fluid content of a specific area, or defects in the tissue [39, 40]. This technique provides a non-invasive method of determining and evaluating a change in composition of the body at many positions simultaneously.

Previous research has been conducted into the use of bio-impedance as a method for evaluating the swallowing process. Kusuhara *et al.* [41] designed and built an impedance pharyngography device to assess swallowing functions based on changes in electrical impedance of the neck during a swallow. This study used a four-electrode bio-impedance measuring device in order to determine the changing impedance of the neck. It was validated against a swallowing sound measurement system in order to determine the characteristics of the bio-impedance signal. Kusuhara *et al.* concluded that the waveform reflected changes in impedance caused by laryngeal movement. The work done by Kusuhara *et al.* [41] provided evidence that an impedance-based device could be used to identify specific positions in the swallowing sequence. These positions can be seen in Figure 2.8, where the central stage (II) is the pharyngeal stage.

Kusuhara *et al.* [41] also highlighted alternative techniques used in dysphagia diagnosis which are not suitable for evaluation of the pharynx. The complex structure of the pharynx is difficult to delineate by ultrasonography; it is impossible to swallow during a videoendoscopy.

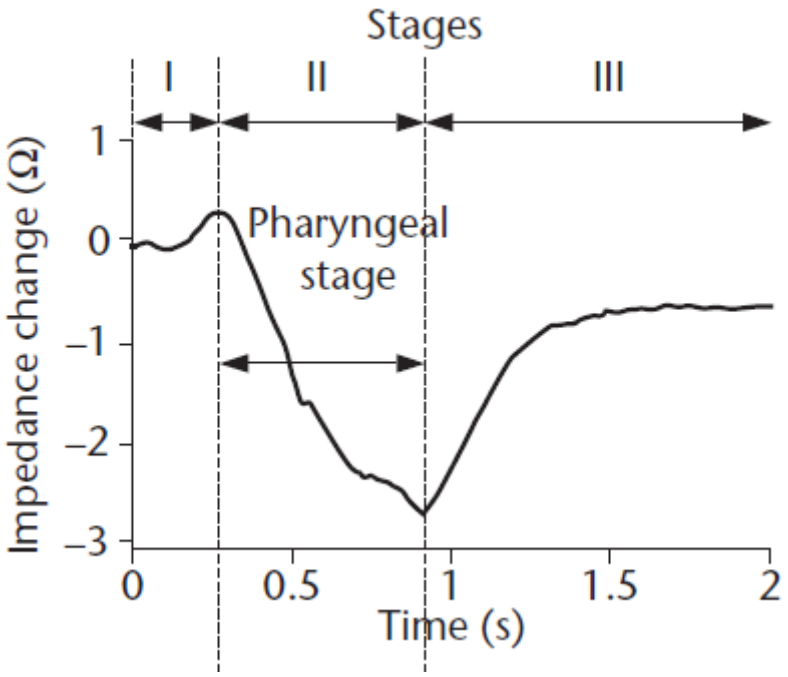

Figure 2.8: *Impedance measurements during a swallow, from Kusuhara et al. [41].*

2.4.2 Invasive Techniques

There are several invasive techniques for providing biofeedback on swallowing other than pharyngeal manometry. These techniques include the use of videofluoroscopy, axial pressure measurement, and fibre-optic endoscopic evaluation, all of which provide useful biofeedback information for other dysphagia conditions [11, 42, 43].

2.4.2.1 Videofluoroscopy

Videofluoroscopy is commonly used as a diagnostic technique with patients who suffer from dysphagia as it allows for a visual representation of the throat. Videofluoroscopy is effectively a video x-ray of the throat which provides an internal view of the swallowing sequence [30]; a still image of a videofluoroscopy session can be seen in Figure 2.7. This technique is particularly useful when trying to diagnose a condition but, due to exposure to radiation and demands of the set-up, videofluoroscopy is not used for rehabilitation. This invasive exposure to radiation means that videofluoroscopy is not an option for rehabilitation.

Another critical issue currently limiting videofluoroscopy in the treatment of pharyngeal mis-sequencing is that pharyngeal sequencing cannot be adequately detected. The issues of not having a high enough time-resolution to be able to detect the pharyngeal sequencing and lack of observability are severely limiting factors of videofluoroscopy [43]. These limitations, along with the fact that videofluoroscopy cannot be used for rehabilitation purposes due to radiation exposure, categorically rule out videofluoroscopy as potential rehabilitation solution.

2.4.2.2 Axial Force Measurement

Axial force measurement has been developed with oesophageal dysphagia and was considered as a potential biofeedback modality for pharyngeal mis-sequencing. Axial force measurement has been found by Gravesen *et al.* [42] to obtain a more complete picture of oesophagus movement when paired with manometry. The most recent design of the force measurement uses impedance to measure the force provided by the oesophagus. This works by having two electrodes, one attached to each side of a gel filled bag. When a force is applied to the bag the electrodes separate, increasing the impedance between the two electrodes. An image of this device can be seen in Figure 2.9, in which two electrodes are suspended in a gel bag. When an axial force is applied to the gel bag, the electrodes separate as the gel bag is moved away from the relatively stationary section of the device.

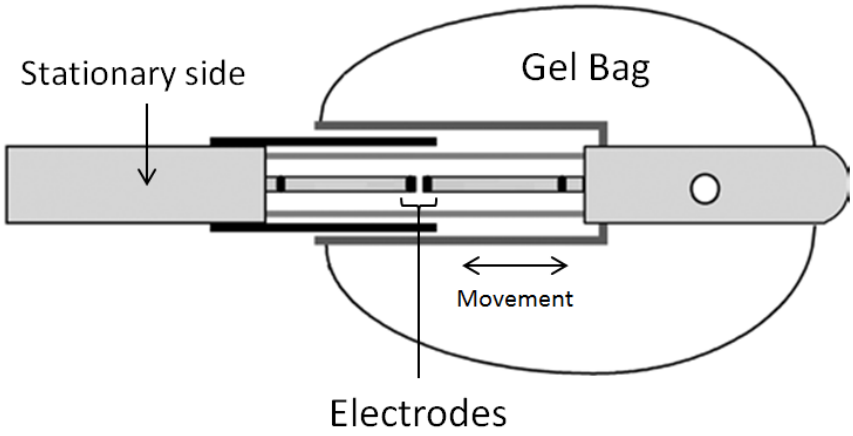

Figure 2.9: *Axial force measurement device designed by Gavesen et al. [42]. This device separates the electrodes suspended in the gel bag when an axial force is applied. The thick black and dark grey lines represent rigid plastic cylinders that ensure that the construction will not bend. The gel bag moves away from the stationary section when an axial force is applied.*

The main difference between this technique and manometry is that the device measures an axial (lengthways) force of the oesophagus, whereas manometry measures radial force. This form of measurement is invasive like manometry and is not well documented, with less than ten instances before the research completed by Gravesen *et al.* [42], where Gravesen has published four instances [42, 44–46]. On top of the difference of measurement technique, manometry and this axial force measurement differ in the type of instrumentation device used. The gel filled bag used with this technique may be appropriate for use in the oesophagus but filling the pharynx with a gel filled bag would be hazardous for a patient. The pharynx is part of the airway as well as the anatomy responsible for swallowing, where blockage of the airway would lead to suffocation. Axial pressure measurement is therefore not an appropriate rehabilitation technique.

2.4.2.3 Fibre-optic Endoscopic Evaluation of Swallowing

The main disadvantage of videofluoroscopy is its inability to act as a rehabilitation tool for dysphagic conditions due to extended exposure to radiation. Fibre-optic endoscopic evaluation of swallowing (FEES) is a potential alternative to this. FEES allows for a visual biofeedback technique of displaying a live video feed from inside the patient's throat by using fibre-optic video. Traditionally FEES has been used as a diagnosis tool, rather than a tool for rehabilitation [47].

FEES has the ability to be used as a standalone biofeedback treatment or in conjunction with another treatment method. FEES is a newer, reliable, and valuable technique that can be used to assess pharyngeal dysphagia, determine aspiration risk, and guide the management of dysphagia [48]. Sun *et al* [49] reported promising findings when using FEES in combination with neuromuscular electrical stimulation as a form of dysphagia rehabilitation. In addition, studies reviewed by Langmore [11] stated that FEES has been shown to help in the rehabilitation of dysphagic patients suffering from neck cancer. These findings show FEES's potential to be used as a rehabilitation technique, rather than just a diagnostic tool.

The main issue with FEES is that it offers similar problems to the current pharyngeal manometry solution, where no easily determinable advantages are available. The criteria imposed for a desired rehabilitation device are not fulfilled by FFES, where FEES is an invasive rehabilitation solution and if often non-portable [50]. The lack of fulfilment of these criteria, and lack of improvement on the pharyngeal manometry technique led to this technique not being used as the alternative solution.

2.4.3 Choice of Technique

Bio-impedance was chosen as the biofeedback technique to be investigated over the other possible approaches due to its non-invasive nature and related research that had promising results [41]. The invasive methods of biofeedback provided in the previous section offer similar problems to the currently used manometry technique. In addition, the high number of muscles responsible for swallowing, as seen in Figure 2.2, makes muscle mapping unusable when trying to isolate the specific muscles used for the sequencing of pressure [37]. Further analysis was able to be conducted into bio-impedance in order to outline its basic theory as well as its potential application to detection of pharyngeal sequencing.

2.5 Bio-Impedance Feedback

2.5.1 Bio-Impedance Overview

As mentioned in Section 2.4.1.2, bio-impedance measures the electrical impedance of a biological event in order to determine various characteristics of that event. Biological cells may be modelled as a group of three electronic components, namely extracellular space, intracellular space, and the cell membrane [1]. The extracellular space is represented as a resistor in parallel with the intracellular space and the cell membrane; the intracellular space is modelled as a resistor and the cell membrane is modelled as a capacitor as seen in Figure 2.10. A brief introduction provided by Holder [38] stated that both the extracellular space and intracellular space are highly conductive, due to their high concentration of salt ions. Measuring the impedance characteristics of both the intracellular and extracellular space allow for certain characteristics of the cell to be determined.

When measuring the impedance characteristics of biological element the frequency of operation is highly correlated to the impedance experienced [1]. At lower frequencies (generally less than 100 Hz), almost all the current flows through the extracellular space, so the total impedance is largely resistive and is equivalent to that of the extracellular space. This is due to the lipid membrane of the cells being an insulator, preventing low frequency current from passing through the cells. An example of low frequency current paths is shown in Figure 2.11, where the current is forced to pass around the cells. Holder [38] stated that this extracellular space is only about 20% or less of the total tissue, resulting in relatively high impedance. At higher frequencies (generally higher

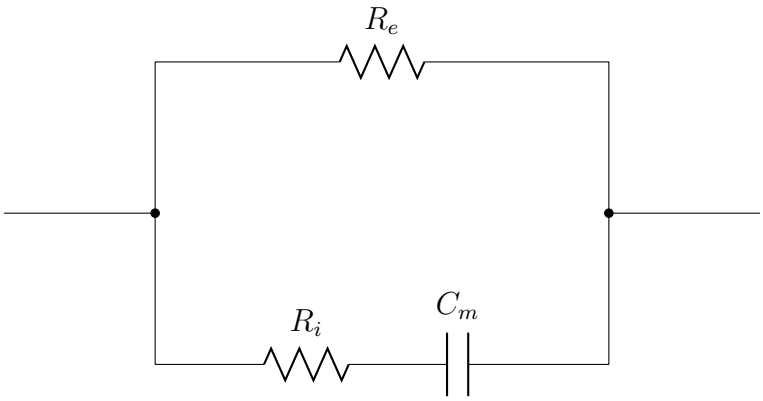

Figure 2.10: *Biological cell modelled by a basic circuit. R_i and R_e are the resistances of the intracellular-space and extracellular-space resistances respectively, where C_m is the membrane capacitance.*

than 100 Hz), the current can cross the capacitance of the cell membrane and so enter the intracellular space as well. It then has access to the conductive ions in both the cellular spaces, so the overall impedance is lower. Frequency of operation is therefore an important aspect of any bio-impedance measuring device.

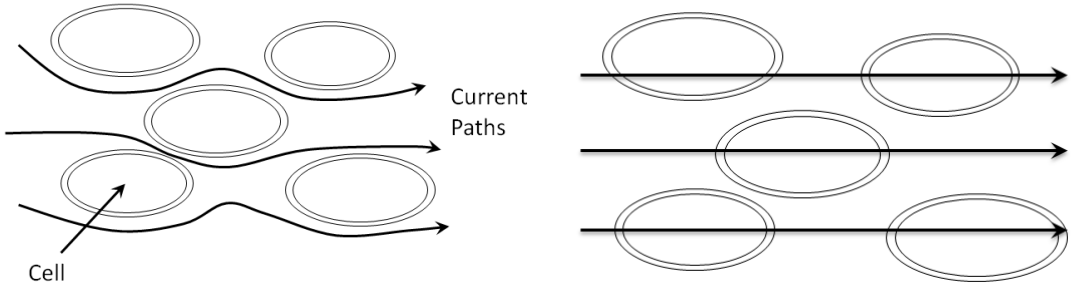

(a) *Low frequencies* ***(b)*** *High frequencies*

Figure 2.11: *Path of current through cells at both low and high frequencies.*

2.5.2 Bio-Impedance Applications

Bio-Impedance has been used in several medical fields prior to this study, including analysis of breast tissue, the respiratory system, body water, and even determining a patient's identity. These investigations include finding the impedance across various sections of the body, sometimes at various frequencies, in order to identify certain properties of the tissue.

2.5.2.1 Breast Tissue Analysis

The electrical conductivity of many tumours, in particular the malignant tumours of the breast, may significantly differ from the conductivity of surrounding normal tissue [40]. Several papers have looked into the use of impedance as a method of early detection and preliminary diagnosis of breast tumours [51, 52]. Cherepenin *et al.* [51] provided initial research into imaging the distribution of conductivity regions below the skin surface in 3D. The system was able to visualize various states of the breast, suggesting the possibility of application to breast cancer detection. In addition, Jossinet [52] provided research into the variability of impedance in normal and pathological breast tissue. This study provided evidence on the difference in the impedance of pathological and normal tissue. This information was collected across various frequencies from the voltage and phase differences in the received signals.

2.5.2.2 Respiratory Applications

Electrical impedance techniques in the respiratory area are used primarily in apnoea detection in newborns and for tracking changes in chest fluid accumulation [39, 53, 54]. Baker [53] has however carried out research into the use of bio-impedance to indirectly measure the respired volume in surgical patients. This technique, although not as accurate as some of the alternative techniques, provided a non-invasive method of measuring the volume of air respired.

2.5.2.3 Electrical Impedance Tomography

In addition to using the electrical impedance techniques for measuring characteristic properties of the human-body, electrical impedance can be used to create a more complete image of the tissue measured [55]. The technique of electrical impedance tomography (EIT) has had several proposed applications, including lung function [55], detection of breast cancer [56], imaging of brain function [57], and imaging of the thorax [58]. EIT measures several electrical impedances through an area of interest (such as the lungs) through the use of multiplexing and then constructs an image of the tissue of the area of interest. These images are reconstructed through the use of complex algorithms that relate the measured potentials with the impedance at the various points measured [59]. These impedance values are then related to the properties of the targeted tissue, where a relatively high impedance would relate to a property such as an air gap. Using these relationships an image of the estimated tissue pattern is formed.

Lionheart [59] stated that the problem of recovering an unknown conductivity from the boundary data is severely ill-posed. This is due to the impedance measurements being "non-local", which means that the impedance being measured is not only representative of a straight line between the measuring electrodes. The impedance measurement includes all surrounding tissue to the path being measured, where any parallel current paths are included in the measurement [60]. This non-local property of EIT is one of the principal reasons that EIT is difficult. It means that to find the conductivity image one must solve a system of simultaneous equations relating every voxel to every measurement.

2.5.2.4 Additional Applications

Surgical patients are ideal subjects for bio-impedance measurements due to their prone position and lack of movement, which can affect bio-impedance readings. This has led to several bio-impedance applications targeting surgical patients [61, 62]. Hannan *et al.* [61] describes a bio-impedance system for assessing a patient's extracellular and total body water. It is stated that using a two frequency approach of bio-impedance measurement a patient's water content can be measured.

A further novel idea for the use of bio-impedance has been put forward by Cornelius *et al.* [62], where bio-impedance can be used as a way of identifying a person. The idea behind this project was that each individual's tissue would respond in a unique way to alternating current of different frequencies. This is due to each person having a unique reactive and resistive component to their tissue at a specific point in their body (such as their wrist). With this in mind, an individual's measured bio-impedance at various frequencies could be recorded and used as a unique identifier.

All of the mentioned applications of bio-impedance highlight the versatility of bio-impedance in medical applications for providing biofeedback. The investigation of bio-impedance as a potential technique for the rehabilitation of pharyngeal mis-sequencing was therefore determined to be viable line of research. The expected impedance response to a swallowing event was able to be estimated using the same principles used in the bio-impedance applications mentioned above, where an impedance change due to a change in biological geometry can be detected.

2.5.3 Swallowing Bio-Impedance

The underlying theory of operation for swallowing bio-impedance is that a change in impedance in the throat corresponds to a swallowing event. As a swallowing event occurs, the pharynx experiences a change in geometry due to pressure from the pharyngeal muscles. This change in geometry causes an air-filled cavity to be closed off, resulting in a decrease in the impedance between the electrodes. A visual representation of the changing geometry of the pharynx can be seen in Figure 2.12, where the air gap can be seen to decrease during a swallowing sequence. Results from a study performed by Hughes *et al.* [63] suggest that the exclusion of air from the larynx and pharynx is the major factor influencing the change in conductivity when a solution of low conductivity material is swallowed. The impedance change due to the geometry change in the pharynx was outlined as the most likely feature of bio-impedance to correspond to sequencing of the pharynx.

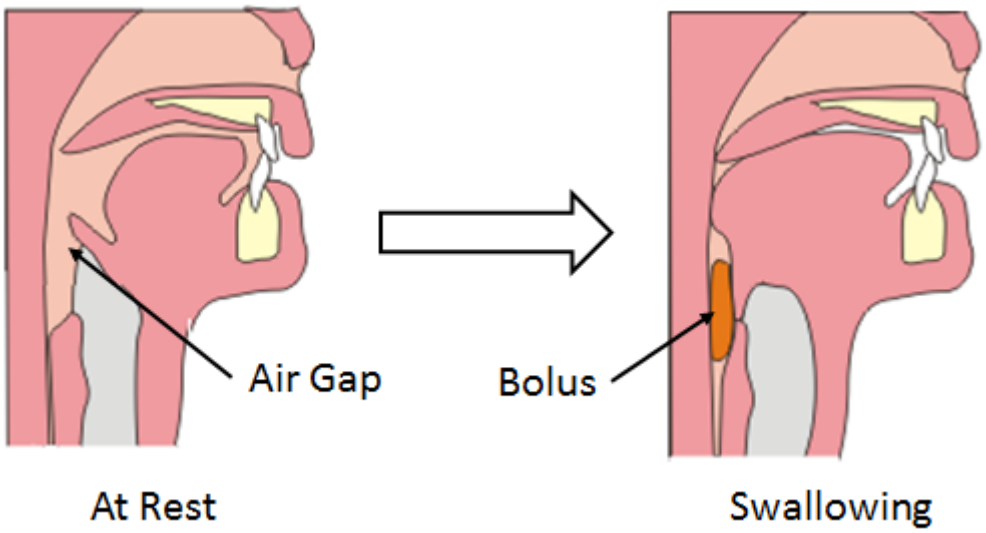

Figure 2.12: *Visual representation of two instances in the swallowing sequence, where the air gap across the pharynx closes during a swallowing event [64].*

Due to human tissue's ability to be modelled by a set of parallel resistances and capacitances a constant amplitude current waveform can be used to determine the impedance of the tissue [1]. The resultant voltage drop across a throat with a current with a known frequency and a constant amplitude can be used to determine the impedance of a circuit. A model of this expected circuit to be measured in the throat can be seen in Figure 2.13, where a variation in the rms output voltage is expected to relate to a swallowing event. A reduction in the voltage amplitude as the current amplitude remains constant corresponds to a decrease in throat impedance.

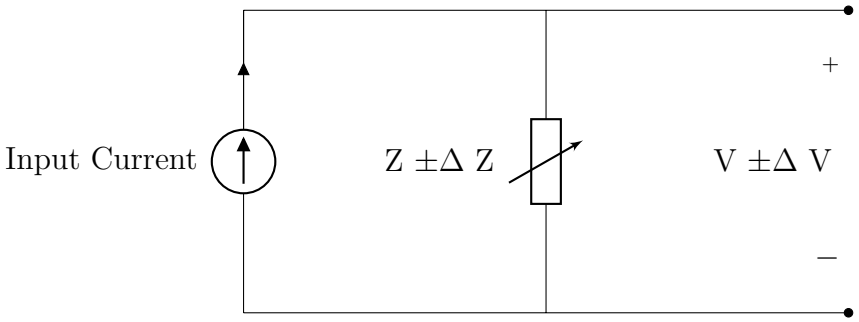

Figure 2.13: *Basic principle of throat impedance sensing circuit.*

A decrease in the voltage across the throat is expected to correspond to the pharyngeal constriction at the position of impedance measurement. This idea is partially supported in concept by work performed by Kusuhara *et al.* [41] as mentioned in Section 2.4.1.2. Kusuhara *et al.* found that single-channel impedance meter was able to monitor swallowing functions of subjects. This information was not relayed back to the patient however, and was used as a proof of concept rather than a biofeedback tool. This technique was stated to be able to determine the occurrence of the different phases of swallowing during a swallowing event. However, as mentioned in Section 2.4, a device that could determine the sequencing of the pharynx was desired. Since the device by Kusuhara *et al.* could only determine when the pharyngeal phase was occurring, rather than the actual sequencing of the pharynx, a device which could provide more detail was needed. This idea therefore needed to be extended to include at least two points of reference in the pharynx for bio-impedance measurement in an attempt to determine the pharyngeal sequencing.

2.6 Summary

The swallowing sequence is a complicated process, where the pharyngeal stage alone requires synchronization between multiple muscle groups. Physical and neurological disorders can cause complications in the swallowing sequence and lead to dysphagia. One pathophysiological feature of dysphagia targeted for treatment is that of pharyngeal mis-sequencing. This form of dysphagia is currently treated by providing visual biofeedback of the swallowing sequence to a patient. This feedback is currently produced using a technique called pharyngeal manometry, which is an invasive and non-portable system. Several alternate techniques to pharyngeal manometry were outlined as potential methods of providing biofeedback, including both invasive and non-invasive techniques. The method chosen to be further investigated was that of bio-impedance, where bio-

impedance is used in several other medical fields to provide biofeedback. Swallowing bio-impedance consists of measuring the impedance across a patient's neck at various positions and using this as a proxy for manometric biofeedback. It is expected that changes in impedance will correspond to the swallowing event.

CHAPTER 3

GULPS Prior Development Overview

The following chapter provides details of the research and development of the bio-impedance device prior to the current project, and study. These details include a history of development, from the inspiration to the completion of the initial prototype. Following this, a section on the initial system is presented, in which the system is described and the functional modules outlined. Finally, a section on the evaluation of this prototype is provided, including required improvements and additions to the device.

3.1 History

The development of the Guided Utility for Latency in Pharyngeal Sequencing (GULPS) initially started in 2011 as a joint project between the Department of Electrical and Computer Engineering at the University of Canterbury and the New Zealand Brain Research Institute (NZBRI). This project was part of an ongoing study into alternative methods for dysphagia rehabilitation. The initial prototype of the bio-impedance measuring device was completed by Andrew Nicholas as part of a final year engineering project and summer research project at the University of Canterbury at the beginning of 2012. This device provided an important conceptual basis to work from, but only provided one working channel, which was itself faulty.

The initial prototype was constructed to interface with a Python-based software tool called *Biofeedback in Swallowing Skill Training* (BiSSkiT), also created at the University of Canterbury as part of a final year engineering project by Ben Han. BiSSkiT was a tool developed to interface with a separate, commercially available, surface electromyography

(sEMG) measuring device called *MyoPace*. The BiSSkiT software provided a one-channel display of the output of the *MyoPace* device. Integration of the initial GULPS hardware with the BiSSkiT software was attempted but was never completed due to limitations in the operating speed of the system.

3.2 System Description

This section describes the state of operation of the GULPS device prior to this thesis. Included in this section is an overview of the system design including the components used, a description of the data protocol used, and the positioning of the electrodes found to be most effective. Most the information in Section 3.2 is summarized from reports (unpublished) by Nicholas.

3.2.1 System Overview

The description of the initial device can be simplified to essentially a 2-channel impedance measuring system. Two channels of impedance measuring hardware exist, each to measure at a different position on the neck. The purpose of these channels is to measure spatiotemporal differences in the swallowing sequence. Each channel can be divided into the four following sections, where each section can then be broken into several modules:

1. Electrodes to transmit and measure the signals in the throat.
2. Current generating circuitry to produce the constant amplitude current signal across the throat.
3. Voltage measuring circuitry to measure the voltage change, and hence the impedance change, across the throat.
4. Microcontroller to sample the signals and communicate with a PC.

A block diagram of this system can be seen in Figure 3.1. In this figure the top row of modules for each channel is the current generating section and the bottom row is the voltage sensing section.

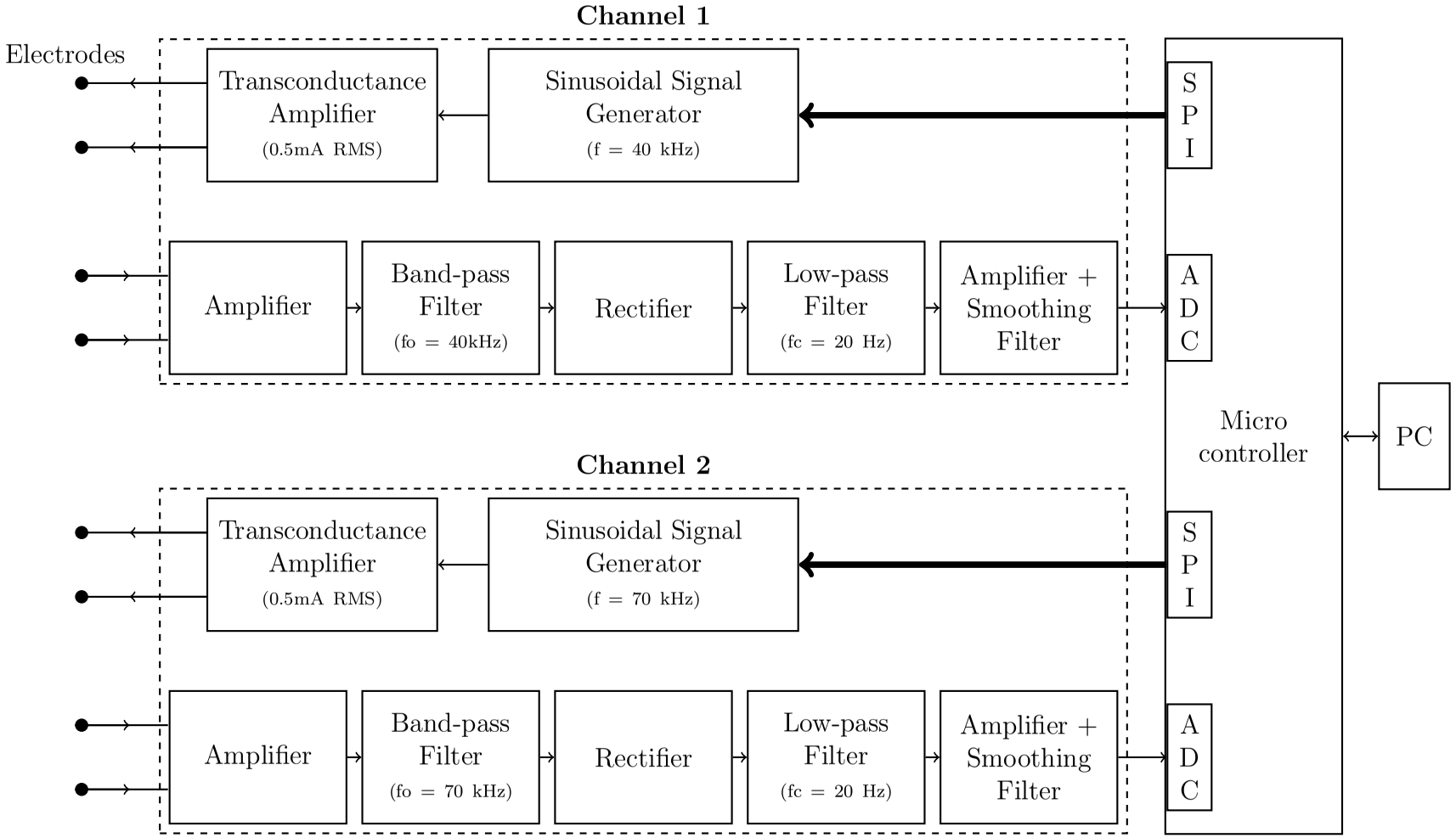

Figure 3.1: *Block diagram of the initial prototype, in which two channels and eight electrodes were used to measure the impedance change at two different locations. Each channel can be broken into two sections, where the top row of modules is a current generating section and the bottom row is a voltage measuring section.*

3.2.1.1 Electrodes

Electrodes were chosen to be used as the method of applying and measuring the electrical signals across a throat. A set of four electrodes per channel were used to detect the change in impedance. This is known as a tetrapolar circuit [53]. After experimentation, a tetrapolar circuit was found to be more effective than a two electrode approach. A tetrapolar configuration of the electrodes minimizes the effect of a changing electrode/skin interface impedance and surface impedance value of the neck. Schwan and Ferris [65] stated that boundary tissue can be polarized by the introduction of an electric current, causing the resulting boundary to change with ac current, but not necessarily in phase with the ac current. The tetrapolar circuit prevents the changing impedance of the surface tissue from impacting the impedance measurement. Tetrapolar circuits measure the impedance at a separate location to where the electric current is being applied, therefore avoiding the changing electrode/skin interface impedance [65].

The electrodes of choice were chosen to be Ambu Blue Sensor BRS electrodes [66]. Several other electrodes from various manufacturers were tested, where the pros and cons of each were evaluated. The Ambu Blue electrodes were chosen due to their small size, comfort, and ability to produce the smoothest waveforms.

3.2.1.2 Current Generation

The function of the current generating circuitry was that of creating a constant amplitude, and constant frequency, current waveform to be applied across the throat. This was achieved by using two separate modules: a sinusoidal signal generator and a voltage to current converter. The voltage to current converter was in the form of a transconductance amplifier which would provide a constant amplitude current signal. The measured voltage drop due to this constant current would allow for the change in impedance across the throat to be measured.

To be able to measure the impedance across a patient's throat, impedance variation was used to modulate the applied current waveforms by the equation $\Delta V = I \times \Delta Z$. The changing impedance (ΔZ) would modulate the applied constant amplitude current (I) to the frequency band of the changing impedance, where the result is the voltage (V) measured across the throat; modulation allowed for multiple channels to be used. An example of this modulation can be seen in Figure 3.2, where amplitude modulation is used to obtain the output voltage at the combined frequencies of the current and change of impedance signals. This output signal contains the modulated signal from the measured channel, as well as an attenuated signal from the other channel (at a different centre frequency).

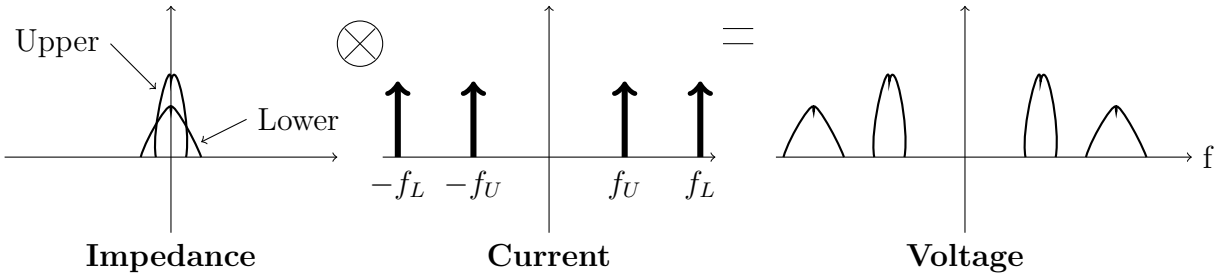

Figure 3.2: *Frequency domain example of how the modulation of the current occurs, where amplitude modulation of both the lower and upper channel's current waveforms occurs ('lower' and 'upper' identifying relative position on the throat). This example shows the measurement of the upper channel, where the resulting voltage waveform is comprised of the modulated current waveform from the upper channel, as well as the modulated current waveform from the lower channel (modulated with a different impedance signal).*

Sinusoidal signal generation: The sinusoidal signal generator creates a constant frequency sinusoidal wave to be applied across the throat. The frequencies chosen were 40 kHz and 70 kHz respectively for each channel. These frequencies were chosen specifically not to be integer multiples of each other to minimize harmonic interference between channels. The frequency band was chosen to be similar to that used by Kusuhara *et al.* [41] in their investigation into bio-impedance characteristics of the throat.

A direct digital synthesis (DDS) programmable waveform generator was used to create a constant frequency sinusoidal waveform. The integrated chip (IC) used was the AD9833 by Analog Devices [67]. The AD9833 was a digitally programmable sinusoidal signal generator which required a connection to the microcontroller's serial peripheral interface (SPI) ports to program the operating frequency of the IC. In addition to this, an external clock module was required to set the output waveform. The clock generation IC used was the LTC6900 resistor set oscillator by Linear Technology [68], this was set to a clock frequency of 2 MHz. A block diagram for the set-up of this module can be seen in Figure 3.3.

Transconductance amplifier: To be able to create a voltage across the throat which would reflect the change in impedance of that throat, and to ensure a safe current was used at all times, a transconductance amplifier was used. The current applied was limited to 0.5 mA rms for each channel as the recommended maximum rms current for an electrical signal across a human was 1 mA [41], where this was halved because two channels were being used.

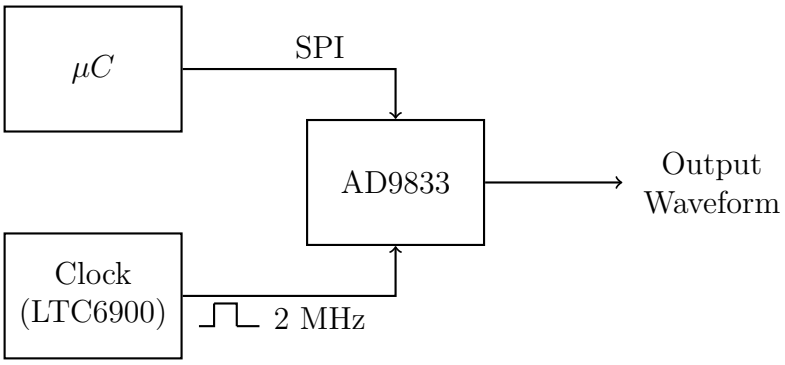

Figure 3.3: *Block diagram of the sinusoidal signal generation module of the initial device. The AD9833 programmable waveform generator is programmed with an external serial peripheral interface (SPI) connection to the microcontroller (μC). An external connection to the LTC6900 clock module was also required to set the output sinusoidal signal.*

The transconductance amplifier used to create the constant amplitude current signal was the LM13700N by Texas Instruments [69]. This transconductance amplifier was set-up in a single-ended configuration (as seen in Figure 3.4), where an attenuated version of the sinusoidal signal (with the use of a voltage divider formed by R_{div1} and R_{div2}) with its dc component removed (via a high-pass filter formed by C_{hp} and R_{hp}) was used as the input. This attenuation of the input signal was to avoid saturation of the amplifier as well as to limit the size of the output current. The high-pass filter had a cut-off frequency of f_c =4.8 kHz. The transconductance of this circuit was set through the i_{set} pin in the amplifier, where the current into this pin was set to attenuate the output current signal to below the maximum 0.5 mA rms level.

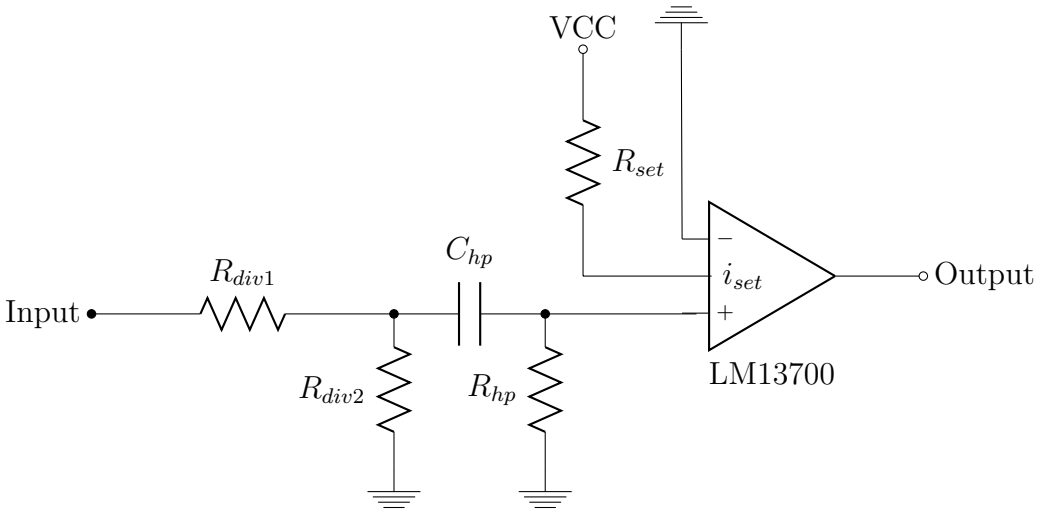

Figure 3.4: *Set-up of the LM13700 transconductance amplifier circuit module in the initial prototype. This shows a voltage divider followed by a high-pass filter, and finally the transconductance amplifier.*

3.2.1.3 Voltage Measurement

In order to retrieve the desired signal, the measured signal had to be continually processed through several voltage detection circuit modules as shown in Figure 3.1. These modules included an amplifier, a band-pass filter, a rectifier, a low-pass filter, and finally an ac smoothing filter. Each of these modules provided a different function in measuring the changing impedance of each channel.

Amplifier: The amplifier was directly connected to the voltage-sensing electrodes to amplify the received signal to a level where the ADC could effectively read the signal. An instrumentation amplifier was used due to its high common mode rejection ratio and high input impedance. This amplifier was used in a differential mode, with one electrode is on each side of the throat. The amplifier chosen was the AD620 by Analog Devices [70]. This instrumentation amplifier's gain was controlled by an external resistor connection, where a variable resistor was used to control the gain. Each input to the instrumentation amplifier was ac coupled, where high-pass filters were used with a cut-off frequencies of $f_c = 16$ Hz. This circuit can be seen in Figure 3.5.

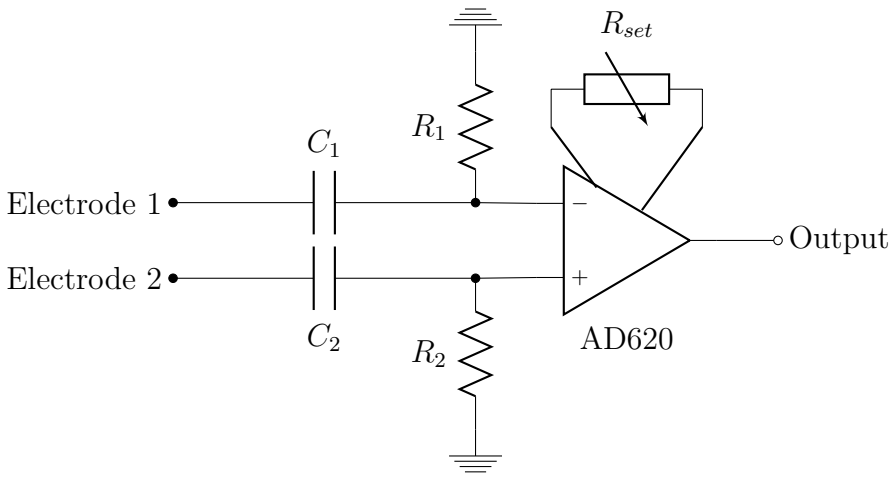

Figure 3.5: *Set-up of the AN620 instrumentation amplifier circuit module in the initial prototype.*

Band-pass Filters: High Q factor band-pass filters were used to isolate the desired channel's signal and remove inter-channel interference as well as other noise, most notably 50 Hz mains noise. Each filter was set-up with its respective centre frequency of 40 kHz and 70 kHz, with a pass-band bandwidth of 10 kHz and a stop-band attenuation of 100 dB for both channels. The ICs used for this section of the circuit were the LTC1562-2 active RC filters by Linear Technology [71]. Two of these filters were cascaded together for each channel to create a 16^{th} order band-pass filter.

Rectifier: In order to identify the change in impedance during a swallowing sequence the received signal must be demodulated, where the signal experiences amplitude modulation as a result of the change in impedance. The method used to do this was that of envelope detection. This was broken up into two steps: rectification and smoothing.

The signals were able to be half-wave rectified rather than full-wave rectified due to the modulation frequencies being substantially larger than the highest frequency in a swallowing sequence, which is approximately 20 Hz for measured pressure waveforms. This frequency was found by analysing the frequency responses of several swallowing measurements with pharyngeal manometry, where the resulting frequency responses can be seen in Figure 3.6. The half-wave rectification was accomplished using a Schottky diode. To complete the envelope detection the rectified signal was passed through a low-pass filter in the next module.

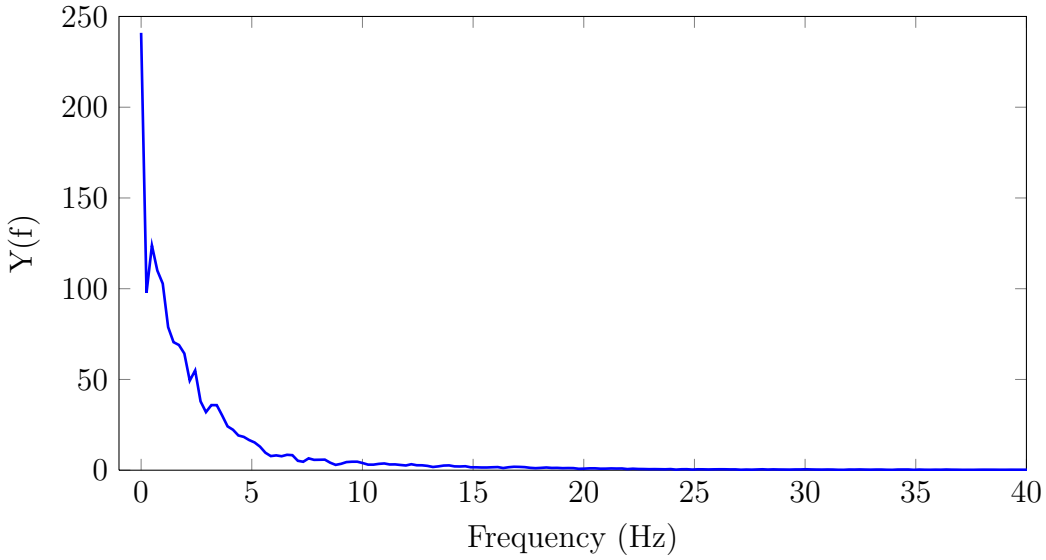

Figure 3.6: *Combined frequency responses from a set of 16 manometry signals.*

Low-pass Filter: A low-pass filter was used for two purposes: smoothing of the rectified signal and as an anti-aliasing filter for the ADC. Smoothing the rectified signal completed envelope detection and demodulation of the signal. To do this the LTC1068 clock-tunable, quad second-order IC by Linear Technology [72] was used to set-up an 8^{th} order low-pass filter. The filter had a pass-band cut-off frequency of 20 Hz, where 100 dB of attenuation was designed to occur by 40 Hz; the cut-off frequency was chosen to be (i) below 50 Hz to attenuate any mains noise still remaining and (ii) high enough to include the spectral content of the swallowing impedance signals.

Final Amplifier/Filter: The final module of each channel was used to modify the waveform to look like the waveforms gained using pharyngeal manometry. A manometry pressure waveform increases in value as the throat closes and has almost no dc component. Five features therefore needed to be added in this step in order to complete the processing of the signal, these features were:

1. Remove the dc component.
2. Amplify the signal.
3. Invert the signal to make it resemble a manometry reading.
4. Offset the signal to fall within the ADC's range (0 - 5V).
5. Filter the signal with a third order low-pass filter to smooth the signal and act as an anti-aliasing filter.

This module was completed by designing the five features around a pair of central operational amplifiers: the AD8622 dual op-amp IC from Analog Devices [73]. The design for this module can be seen in Figure 3.7. In order to remove the dc component of the signal, a high-pass filter with a very low cut-off frequency of 0.08 Hz was used. This cut-off frequency had to be very low as the circuit needs to capture very low frequencies. The high-pass filter is a passive filter using the combination of a large capacitor (C_{hpf}) and the resistor (R_{gain1}) to create a single-pole high-pass filter before the amplifier.

The remaining processing stages of the signal, consisting of inverting, amplifying, offsetting, and filtering the signal were designed to use the two op-amps in the AD8622 IC. The amplification and inversion of the signal was done through an inverting amplifier set-up, where the gain of -150 V/V was used. This inverting amplifier is shown in Figure 3.7, where the R_{gain1} and R_{gain2} resistors set the gain of the amplifier. A dc offset of 1.67 V was also added through this amplifier, which is one third of the available 0 V to 5 V range. This off-set allowed for a larger positive voltage swing than negative voltage swing in the signal without the risk of saturation of the amplifier. As this is an inverting circuit this corresponds to a larger negative impedance swing, which is characteristic of a swallow; swallows were found to have a large impedance drop, with a smaller impedance increase. Finally, the signal was passed through a third-order low-pass filter to smooth the signal and act as an anti-aliasing filter. This filter consisted of a passive low-pass filter cascaded with a second-order Sallen-Key filter. This filter was designed to have a cut-off frequency of 8 Hz, where it was found that using a cut-off frequency of 8 Hz, rather than the initial frequency of 20 Hz, still allowed for all relevant information to be retrieved.

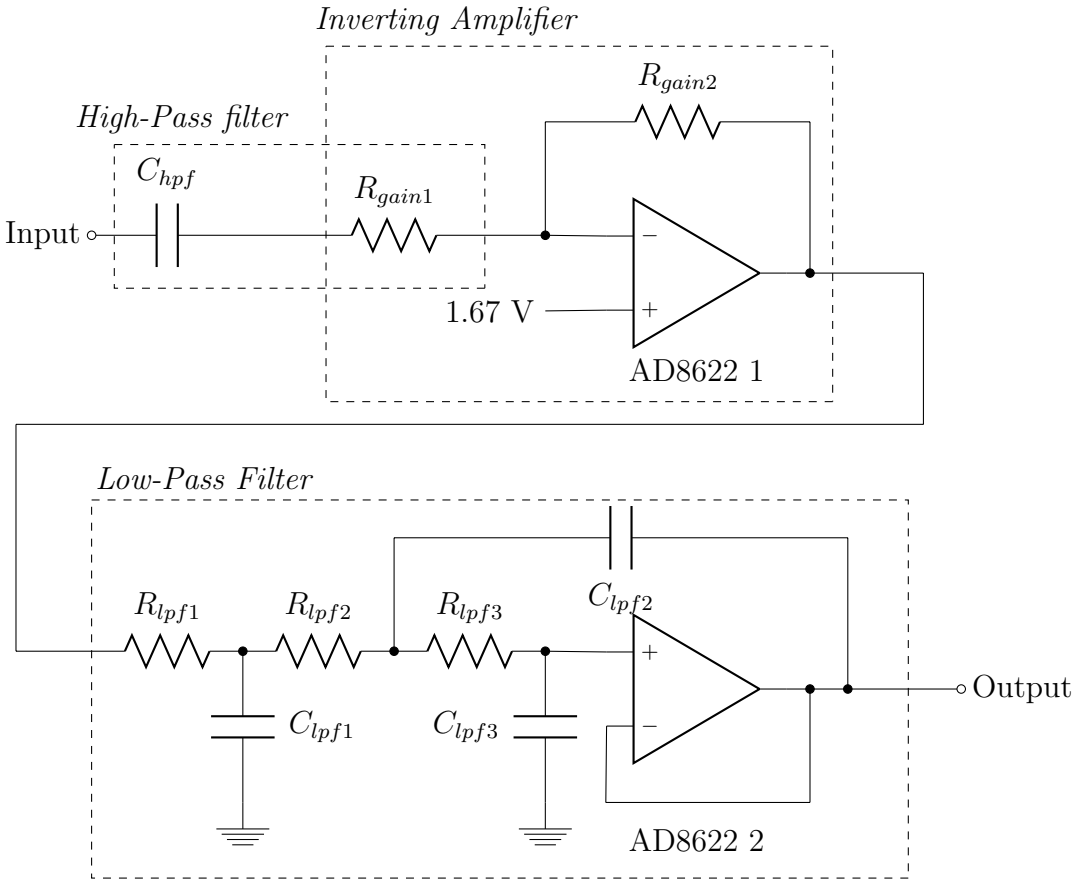

Figure 3.7: *Set-up of dual AD8622 operational amplifiers for the ac amplifier circuit module in the initial prototype. Three blocks of circuitry consisting of a high-pass filter, inverting amplifier, and the low-pass filter were used to process the signal in this stage.*

3.2.1.4 Microcontroller

The microcontroller in this prototype had two purposes, to convert the analogue signal to a digital signal in order to interface with a PC, and to configure the signal generators. The method used to communicate with the computer was through an universal asynchronous receiver/transmitter (UART) protocol. To configure the signal generators, the serial peripheral interface (SPI) ports of the microcontroller were used. The microcontroller used was the dsPIC30F3013 microcontroller from Microchip Technology [74].

3.2.1.5 Computer

A Windows-based PC is used to display and store the data generated by the initial device. The UART interface connects to one of the computer's COM ports and communicates with the altered BiSSkiT software through this. The software was written in Python [75] and requires several additional Python modules to be installed.

3.2.2 Software Integration

Software for both the microcontroller and the desktop computer was developed or modified to allow signals from the GULPS device to be viewed in a computer monitor. The firmware for the microcontroller had to be written to set-up a device that could measure and transmit signals. To view this transmitted signal the BiSSkiT software needed to be adapted. This adaptation included a serial data protocol to be developed in order to encode the signals for transmission using the UART ports of both the computer and microcontroller.

3.2.2.1 Firmware

In order to operate the microcontroller firmware was written in the C programming language to sample and transmit the signals from the impedance measuring channels. The microcontroller had three main functions in the previously developed project, namely: sampling the signals using the on-board ADCs, setting-up the waveform generators using the SPI ports, and communicating with a computer via the UART port. The modules used to complete these processes can be seen in Figure 3.8, where the adc12, uart, and spi modules are provided by Microchip Technology [74] for programming.

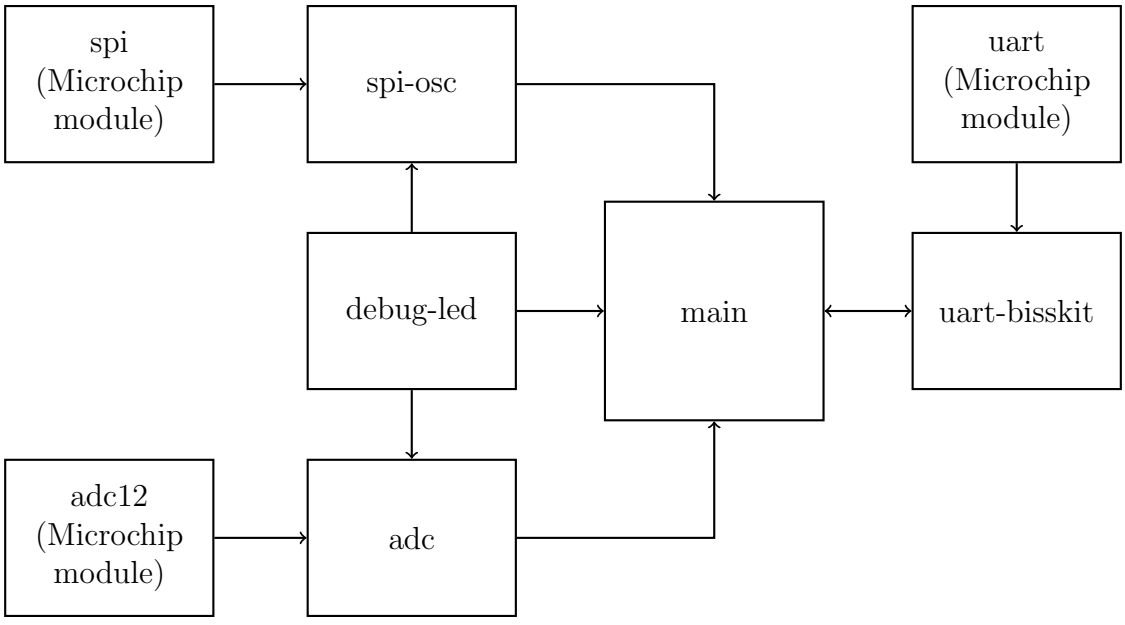

Figure 3.8: *Modular design of the firmware used for the pre-existing prototype.*

The microcontroller's firmware was designed to complete several initial functions followed by a main-loop for continual data processing. A flow diagram of the structure of the software can be seen in Figure 3.9. This structure shows that the SPI ports were initially set-up to program the waveform generators before any data processing occurred. After the

SPI ports are set-up the ADC and UART modules are initialized and then continuously operated through the use of a main-loop. This loop periodically samples the ADC values and the resultant information is transferred over the UART connection. This main-loop was set-up to transmit data at a rate of 10.2 Hz to the connected computer.

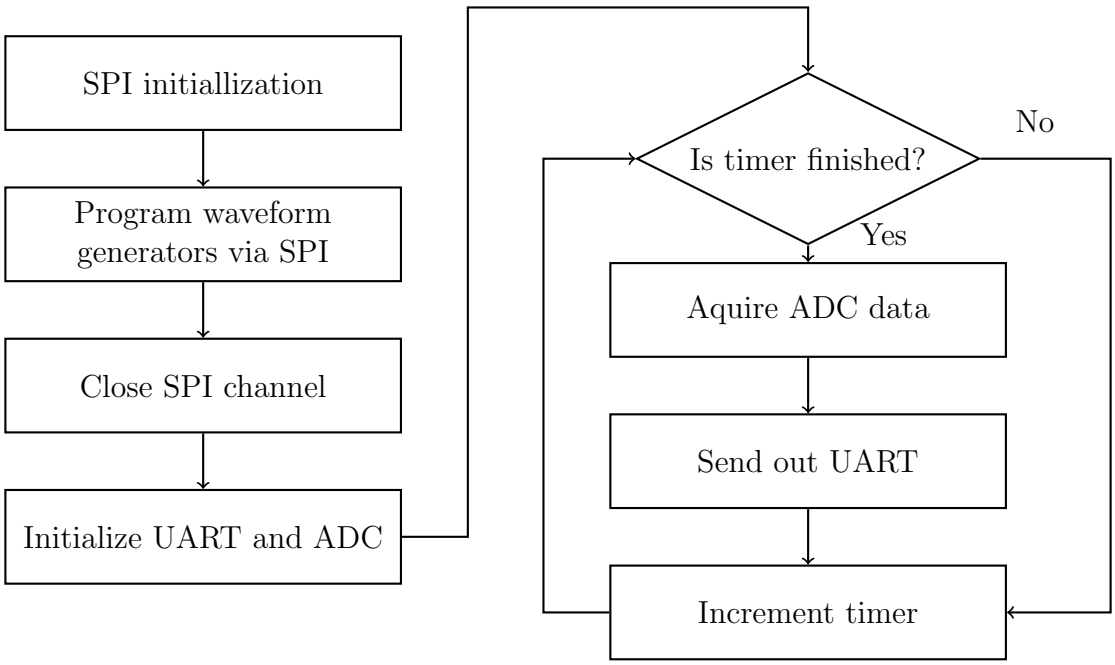

Figure 3.9: *Structure of the software for the microcontroller used in the pre-existing prototype.*

3.2.2.2 BiSSkiT Software Adaptation

In order to display the desired waveform from the initial GULPS device the pre-existing BiSSkiT software was adapted to display the impedance measurement waveforms. The software was adapted to display one channel of impedance measurement data, where the displayed channel was chosen in the firmware. In order to do this the serial interface module of the BiSSkiT software was adapted to interpret data with the GULPS device's data protocol.

3.2.2.3 Serial Data Protocol

A custom protocol was designed for interaction between the GULPS device and the adapted BiSSkiT software in order to transmit the impedance data. The UART connection of the microcontroller connects to a computer via an RS232 protocol serial-to-USB connection cable and is set up to transmit at a baud rate of 115200 bits/s. A virtual COM port is set-up on the PC which communicates to the device using the BiSSkiT software. The ADC on the microcontroller was a 12-bit converter which required the information

to be split into two bytes. The lower eight bits are sent in the first byte, followed by the higher four bits that are padded to eight bits and sent in the second byte. A third byte was also sent as a synchronizing byte that allows BiSSkiT to be able to determine the start of each 12-bit data block sent; this byte was sent preceding the ADC data. A box diagram of this protocol can be seen in Figure 3.10.

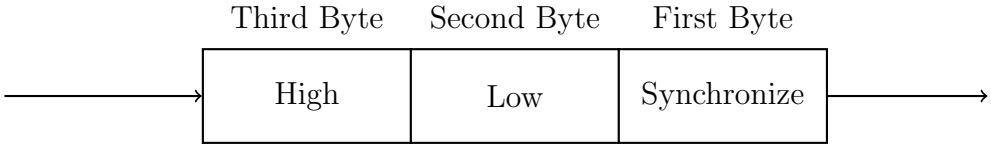

Figure 3.10: *Data packet format sent through the UART connection.*

3.2.3 Electrode Positioning

It was reported that in order to obtain a distinguishable temporal separation of the swallowing features between the waveforms in the two channels, the electrodes needed to be placed on well specified areas on the neck. Initially, the temporal separation between the peaks of the two inverted impedance waveforms was used to determine the sequencing of the pharynx, in which the hope was that the temporal separation between the peaks would correlate to the pressure peak temporal separation seen in manometry. The peak in the inverted impedance waveform was initially used to determine when the pharynx was completely closed and exhibiting the peak pressure at the position of the electrodes. The positions of the electrode placements used can be seen in Figure 3.11.

3.3 Evaluating the Initial Solution

The first prototype of the bio-impedance measuring device provided some promising initial results into developing a pharyngeal sequencing detection device, but was very erratic, difficult to set-up, and had lost functionality in one of the channels. In addition to the hardware performance, the software response was extremely slow and could only provide one channel at a time. This delay in the response made the software unusable. The results gained from the initial prototype were obtained through an oscilloscope. An example of an output when both channels were operating can be seen in Figure 3.12.

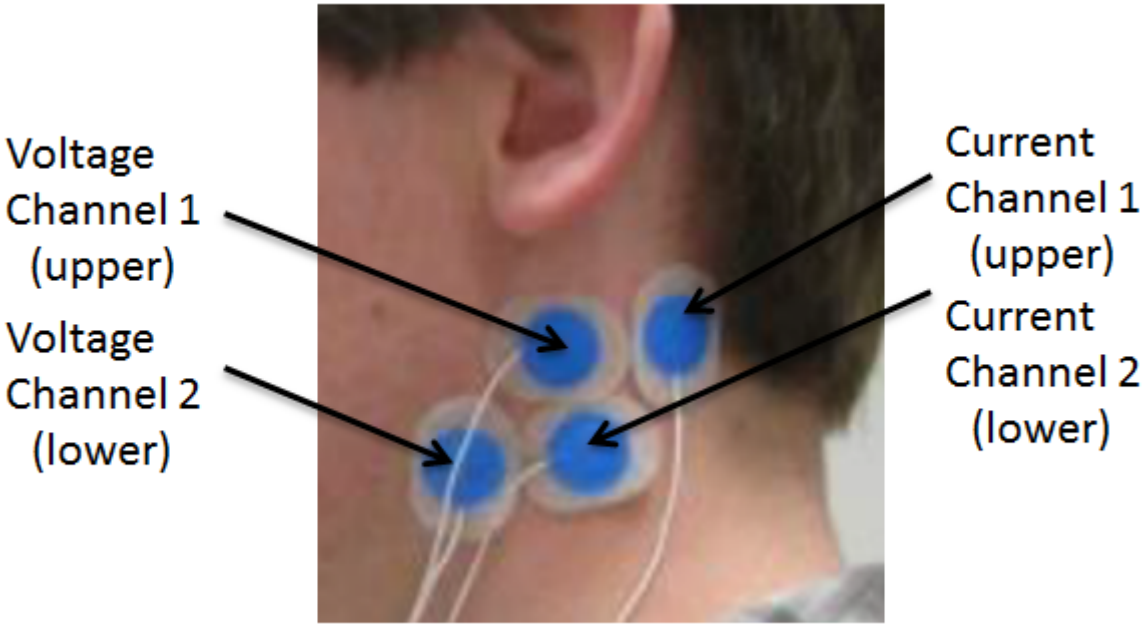

Figure 3.11: *The positioning of the electrodes reported to be most effective in the initial prototype (each electrode shown is paired with a matching electrode on the opposite side of the neck). The current injection electrodes for each channel were located at the back of the neck, and the voltage measurement at the front.*

3.3.1 Tests of Initial Prototype

At the beginning of the current project, thorough testing and investigation was performed on the initial prototype to try and identify the problems which caused the prototype not to work as expected. These tests included checking each module of the board for functionality, where the various modules of the board can be seen in Figure 3.1. The only modules found to be working correctly were the modules on the 40 kHz channel's voltage sensing line, and the microcontroller. This was in contrast to the report associated with the previous prototype, where the entire circuit was reported to operate but not to perform the desired functions consistently. Both current injection sections were not working as expected as well as the second channel's voltage sensing modules, which had several integrated chips missing from the prototype. It was found that the power supply was also not working correctly.

The tests performed in order to analyse the modules consisted of using waveform generators, dc power supplies, and oscilloscopes to try and isolate each module. To test the current generation modules, the board was connected to a $\pm$ 5 V bench-top power-supply. These current sources were designed to work with only a single dc supply and a connection to a microcontroller to program the signal generating chips. The voltage sensing

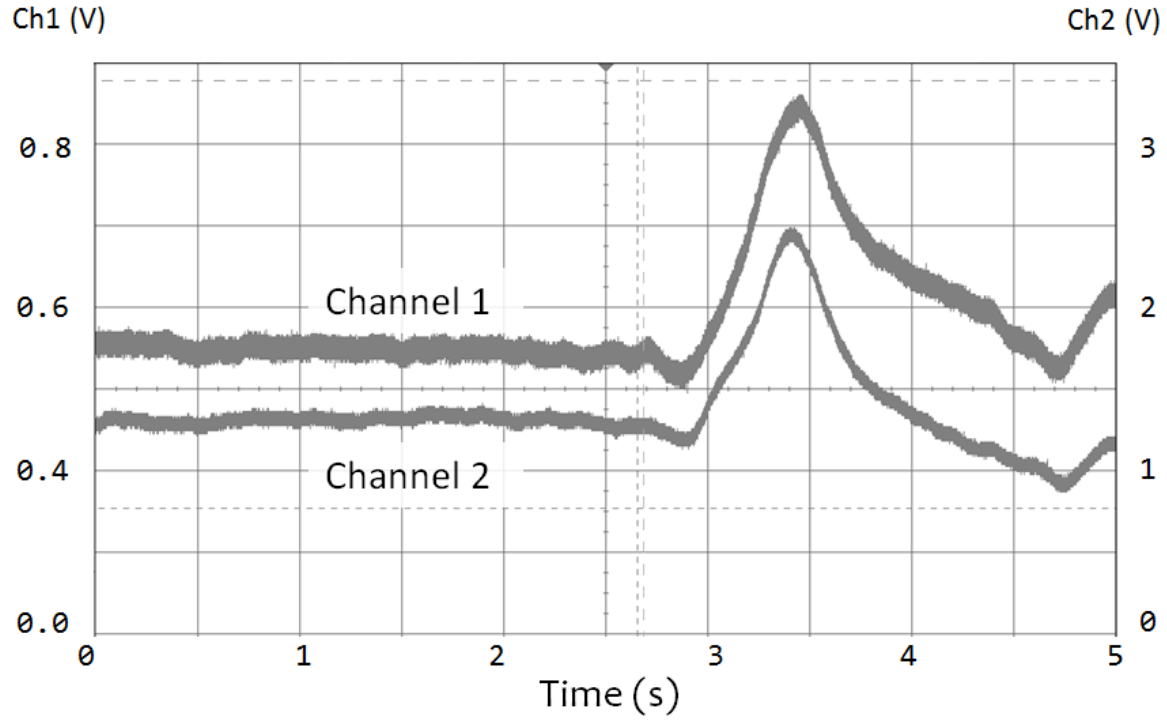

Figure 3.12: *Two channel output from the initial prototype, where the Channel 1 (top) waveform represents the top set of electrodes, and the Channel 2 waveform represents the bottom set of electrodes. The two outputs have different scales, where the scale of Channel 1 is on the left hand side, and Channel 2 on the right.*

circuitry was tested by connecting stable waveform generators to the inputs of the amplifier to determine the response to the tuned frequency as well as the channel's ability to reject noise. The other frequencies used to simulate noise included the other channel's tuned frequency and a 50 Hz signal representing mains noise.

3.4 Objectives

The previous work carried out was useful for showing the potential of using impedance to measure pharyngeal sequencing, but the actual prototype was essentially non-functional. The previous research and development was therefore useful but no device was available with which to compare performance from the current project. The primary objectives of the current project were:

1. Develop a modular prototype of the original circuits to allow for investigation and testing of the initial model to be easily performed.

2. Perform testing on the modular prototype to discover any issues and features that could be improved.

3. Design and build an advanced prototype that would produce clearer, more consistent results.

4. Develop the BiSSkiT software to allow for the new prototype to produce meaningful, easily viewed results on multiple channels.

5. Perform extensive testing of the device on healthy subjects to ensure proper function, as well as identifying features, such as proper electrode placement.

6. Perform a comparison of the results gained from the use of bio-impedance measurements, and the results gained from alternate methods, such as pharyngeal manometry and videofluoroscopy.

7. Preliminary evaluation of the instrument as a rehabilitation device on dysphagic subjects with pharyngeal mis-sequencing.

3.5 Summary

Previous work was done in developing a bio-impedance measuring device for dysphagia rehabilitation research by the University of Canterbury. This device used two channels with current generation and voltage measurement sections. This device provided some promising initial results but its operation was erratic and unreliable. In a review of the original hardware for this device it was found that very few of the modules were working at the beginning of this project. In addition to the hardware, the interfacing software was not working as desired, where the speed performance was so slow the software was unusable. The required improvements to the device were outlined as several hardware and software improvements to obtain a working prototype. This project's objectives were then detailed, in which creating working hardware and software were the first objectives, followed by evaluation of the device on both healthy and dysphagic patients.

CHAPTER 4

Hardware Design

Reliability is a key feature of medical instrumentation, where concerns about reliability involve the consistency and/or repeatability of measurements made with the instrument [76]. For this project, reliability corresponded to obtaining consistently achievable impedance readings from two impedance measuring channels. At the start of this project, the pre-existing bio-impedance device was reported to only be able to achieve single channel performance, as the second channel of hardware was implemented, but was not working. Testing proved that even the reported working channel was, in fact, faulty (as stated in Chapter 3).

This chapter covers the procedure undertaken to identify problems in the previous design and the steps taken to achieve a working version of the hardware. Firstly, the development of an easily adjustable modular prototype was explored to isolate any faults and easily identifiable improvements on the previous design. Continuation of the design process is then described, in which a second prototype was built. The second prototype refined and condensed the modular prototype into a single board. Evaluation of this second prototype is then presented, with outlines of the sections of the prototype still needing improvement. Finally, a description of the final GULPS hardware prototype is provided. The aspects described include: improvements to the second prototype, overall performance of the system, and components used.

4.1 First Prototype: Modular Prototype

The first prototype to be designed and built was a modular prototype consisting of several circuit boards which were able to be connected and interchanged. A block diagram of the modules used can be seen in Figure 4.1, where each channel can be broken into three major blocks. Each block identifies a specific module. The three major blocks for each channel are the current generation module, instrumentation amplifier module, and the filtering module. In addition, two universal modules are implemented in the circuit, in the forms of the power supply and microcontroller (μC).

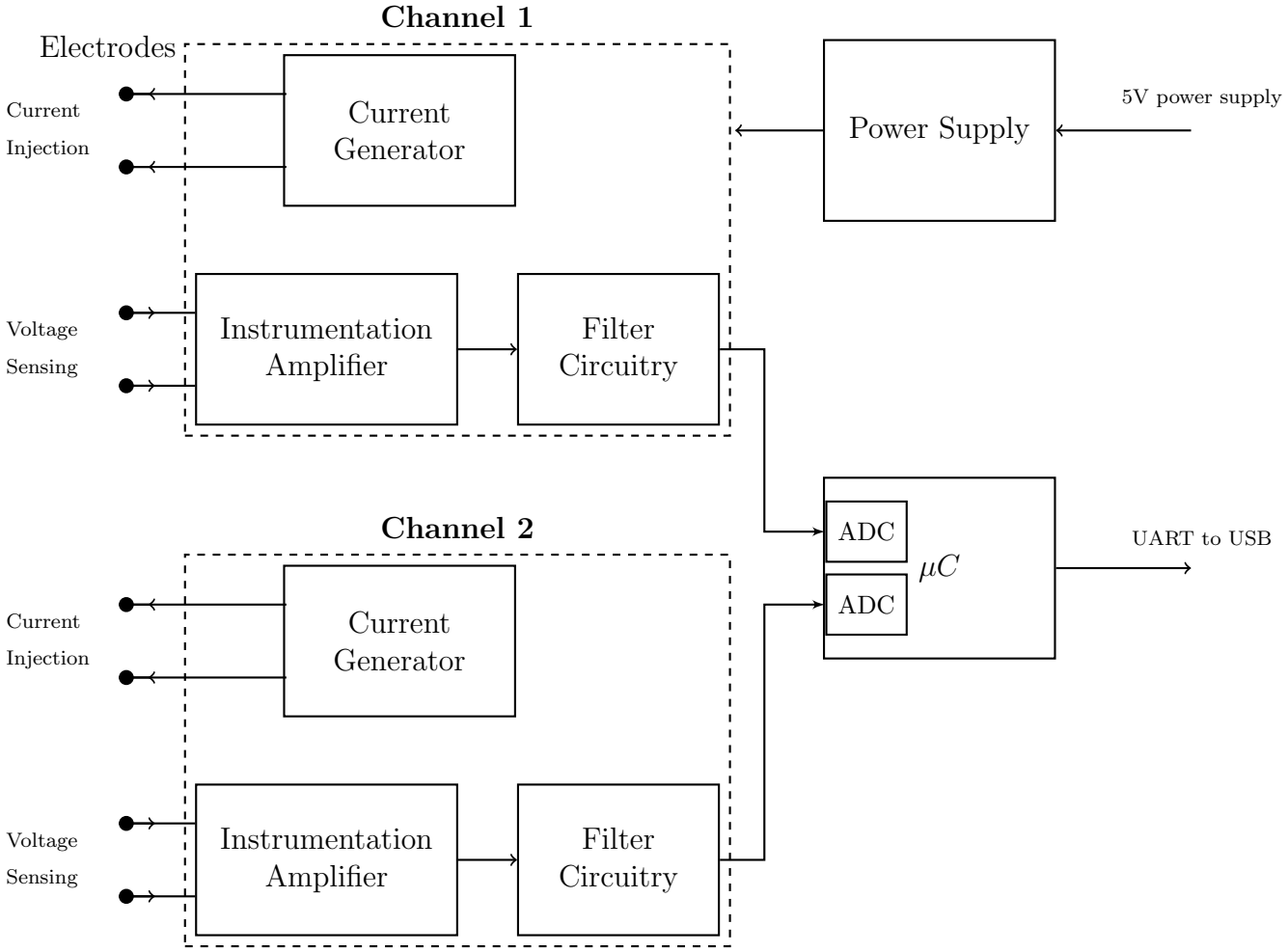

Figure 4.1: *Block Diagram of the first modular prototype of the GULPS hardware developed in this project.*

With the first goal of the prototype development identified as producing one working impedance measuring channel, the first task undertaken was to try and adapt the previously developed device in order to get one of its channels working. Due to the 40 kHz channel of the previously developed device needing the fewest corrections, namely a new current generation module and power supply, it was decided that this channel would be investigated first. The current generation and power supply modules were therefore the first modules investigated.

4.1.1 Current Generation

The previous solution for current generation was to use a precision digital sine-wave generator in combination with a transconductance amplifier IC. Both of these chips had been reported to cause several problems in the set-up of a constant current generation circuit. The precision waveform generator had encountered several issues due to its need for constant interaction with the microcontroller, as-well as needing an external clock connection. These drawbacks limited the usefulness of the digital generator and it was therefore ruled out as an option for the first prototype. The transconductance amplifier also was not operating as desired in the original prototype, and was a contributing factor in the malfunction of the current generation circuit. Due to this problem, and the availability of several alternative solutions, the previous transconductance amplifier design also was not used in this prototype.

Waveform generator: The aim of the waveform generator module was to create a suitably sinusoidal waveform with an easily adjustable frequency. Several options were investigated for the waveform generator, with voltage-controlled oscillators (VCOs) and clock generators being the primary focus. These types of integrated circuits were stand-alone modules which would not have to rely on other sections of the circuit, unlike the precision digital sine-wave generator. A VCO was the chosen component for the signal generation module for the first prototype design. A VCO allowed for the waveform frequency to be easily altered by changing a reference voltage, where this voltage was controlled by a voltage divider ratio through the use of a variable resistor.

A square-wave generating IC was used to create the oscillatory waveform in this circuit due to the lack of appropriate sinusoidal waveform generators. Analogue sinusoidal waveform generator ICs capable of producing frequencies between 1 and 100 kHz were sparse, as the circuitry used for producing waveforms for these types of applications tended towards digital waveform synthesizers [77]. The electronics retailer Element14 [78] had no currently produced components that matched this criteria, resulting in square-wave oscillators being the remaining choice for IC based stand-alone oscillators. Other

methods of generating sinusoidal waveforms were investigated, such as biasing op-amps in order to obtain an oscillating signal [79, 80]. The techniques reviewed include the Wien-bridge, phase-shift, bubba, and quadrature oscillators. These techniques required several more discrete components in order to set the operating frequency than the square-wave generating ICs. This would become an issue if the centre frequency had to be changed, either to match the band-pass filter's centre frequency or for investigation of another frequency. A square-wave generating IC was therefore chosen as the frequency generating technique to achieve an easily changeable operating frequency, where a relatively sinusoidal waveform could be achieved by low-pass filtering the square-wave.

The 74HC4046ad phase-locked loop (PLL) with an on-board VCO by Philips Semiconductors [81] was chosen as the waveform generator. This IC allowed for the VCO to act as a stand-alone waveform generator, where a variable resistor in combination with a capacitor could be used to change the frequency. A passive band-pass filter network was set-up following the VCO in order to obtain the fundamental frequency, as well as removing the dc component to centre the wave about 0 V. The values for these passive filters were chosen to allow the fundamental frequency through but to mostly block the harmonics of that frequency; square waves consist of a fundamental frequency and then higher odd harmonics of that frequency, as well as a dc component [82].

The design of this band-pass filter created a low-pass cut-off at 72 kHz and a high-pass cut-off at 10 kHz and can be seen in Figure 4.2; the oscillator's fundamental frequency was 40 kHz. The low-pass cut-off frequency was chosen to be high enough to allow for the fundamental frequency of square-wave through without attenuation, while being low enough the filter out remaining harmonics of the signal. The lowest harmonic frequency to be filtered was 120 kHz (3rd harmonic), which had an expected amplitude of three times less than the fundamental frequency [82]. In order to create the frequency cut-off value of 72 kHz the resistor and capacitor values of the low-pass filter stage of the band-pass filter had to be calculated. Using the equation $f_c = 1/2\pi RC$ for a passive low-pass filter a 1 nF film capacitor and a 2.7 kΩ resistor were used in order to gain the desired frequency [83].

In the high-pass filter section of the band-pass filter the cut-off frequency was chosen to be 10 kHz in order to remove the dc component of the signal. This frequency was chosen to be less than the fundamental frequency of 40 kHz, while still significantly higher than the dc component of the signal to ensure high attenuation. The cut-off frequency for this filter was again determined by the equation $f_c = 1/2\pi RC$, where the frequency cut-off

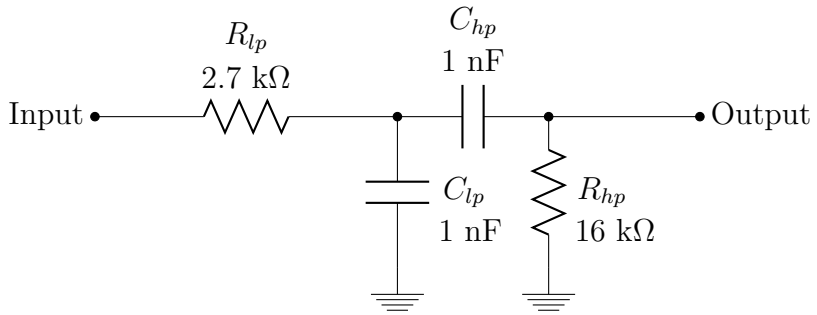

Figure 4.2: *Circuit diagram of the band-pass filter used to convert the square-wave input from the waveform generator to a predominately sinusoidal wave with no dc component for the transconductance amplifier output.*

was now a high-pass frequency cut-off [83]. Again a 1 nF capacitor was used, where a 16 kΩ resistor was used to obtain the cut-off frequency of 10 kHz. With the sinusoidal waveform generator set-up, a transconductance amplifier was then needed to complete the current generation module.

Transconductance amplifier: Due to reported difficulties in using the transconductance amplifier IC in the previous project, a simple, easily testable, transconductance circuit was designed. An op-amp voltage-to-current conversion circuit was chosen to be the method of creating a constant amplitude current. This circuit can be seen in Figure 4.3, where a voltage divider is feeding into the voltage-to-current converter. This voltage divider provided attenuation to the signal to avoid saturation of the input of the amplifier, as well as limiting the output current. The principle of this circuit is that the op-amp will hold the inverting input terminal voltage at the same level as the non-inverting input terminal. This voltage is then applied across the resistor R_{trans} and the resulting current (I_{out}) is applied across the throat. This current is directly proportional to the input voltage. The equation relating the input voltage to the output current (I_{out}) is $I_{out} = V_{div}/R_{trans}$, where the V_{div} value is the voltage-divided input voltage. These equations were used to set the values of R_{trans} and the voltage dividing resistors to limit the output current to below the previously determined maximum allowable rms current of 0.5 mA [41].

The component values used for the transconductance amplifier were chosen to obtain a constant output current of 0.5 mA, with an attenuated input voltage into the amplifier. The input voltage into the voltage divider was a predominantly sinusoidal waveform with an amplitude of 2.5 V and an rms voltage of 1.77 V from the waveform generating circuitry. A voltage divider was used to attenuate this voltage by a factor of 15.7 by using the resistor values of 100 kΩ and 6.8 kΩ as shown in Figure 4.3. R_{trans} was then chosen through the equation $I_{out} = V_{div}/R_{trans}$, where these were all rms

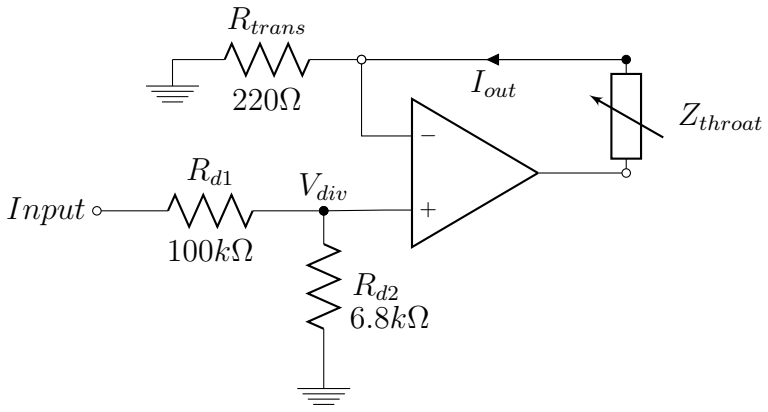

Figure 4.3: *Circuit diagram of the op-amp transconductance amplifier used in the first modular prototype in this project.*

values. The desired rms current value of 0.5 mA and the voltage divided rms value of 1.77 V × 1/15.7 = 0.11 V could then be placed into this equation. The equation then became R_{trans} = 0.11 V/ 0.5 mA = 220 Ω. This was conveniently an available e12 resistor value.

The input impedance of this module was limited by the voltage divider feeding into the voltage-to-current converter. This effectively gave the module an input impedance of these resistors in series (107 kΩ), as the input impedance of the voltage to current converter is the input impedance of an op-amp which has a very high value [84]. This input impedance causes the high-pass filter from the waveform generation module's cut-off frequency to shift to 11 kHz as it now sees its 16 kΩ resistor in parallel with the 106 kΩ input impedance. There is also an additional attenuation to the signal due to the voltage divider set-up by the output impedance of the waveform generation module and the input impedance to the transconductance module. This attenuation was calculated to be about a 30%, where the measured voltage at the input to the op-amp was 78 mV rms rather than 113 mV. This resulted in an expected rms output current of 0.35 mA using the equation $I_{out} = V_{div}/R_{trans}$, where V_{div} = 78 mV. It was decided that these discrepancies would not significantly affect the circuit operation and this design could be used. The cut-off frequency was essentially the same with the calculated input impedance. The additional attenuation of the signal would affect the constant current waveform produced, but only by decreasing its amplitude. A lower rms constant current values is acceptable as it allows for a greater margin between the current used and the safety limit of 0.5 mA. The output current was not required to be a specific value as long as it was close to, but less than, the 0.5 mA limit.

4.1.2 Power Supply

One of the contributing factors to the pre-existing device not working correctly was the issue of the the power supply not delivering a reliable -5 V voltage rail. This negative voltage was required to produce a constant amplitude current signal symmetrical about zero amps, as well as being needed for the signal measurement circuitry. A new power supply was therefore needed in order to deliver a stable -5 V voltage rail.

A dedicated bench-top power supply was used at this stage of the circuit design to provide constant positive and negative voltage rails of $\pm$ 5 V. The use of a consistent power supply at this early stage was chosen as it allowed for the other modules to be examined without the potential of an unstable power supply module corrupting the signals. The power supply had to be addressed at a later stage in the design, as a bench-top power supply does not provide a portable option for powering the device.

4.1.3 Evaluation of Channel One

With the remaining functioning modules from the 40 kHz channel(Ch1) substituted into the initial prototype, Ch1 could then be tested. Initially, the channel was tested by using a network of fixed and variable resistors to mimic a human throat's resistive elements. Holder [38] stated that most human tissue can be treated as a combination of resistive and capacitive elements. At this stage, it was assumed that most of the impedance across the throat at the frequencies chosen was resistive. Saulnier [77] stated that the load impedance range of biological tissue typically range from 100 Ω to 10 kΩ, which is a function of electrode size, excitation frequency and the tissue type. A dummy impedance circuit with a base resistance of 1 kΩ was used, with a 50 Ω variable resistor in series to imitate a swallowing sequence (Figure 4.4). The value of 50 Ω was chosen as the available impedance change as it allowed for a wider, yet reasonably similar, change of impedance as that found by Kusuhara *et al.* [41] to occur during a swallow; Kusuhara *et al.* stated that the change in impedance during a swallowing event was around 5 Ω.

The results from the testing can be seen in Figure 4.5, where a sharp change in the measured voltage corresponds to the variable resistor being altered. The ranges of resistances viewed by each of the channels was between 1 kΩ and 1.05 kΩ. This changing output was viewed through the system software which had been debugged to allow for real time display of the data (Chapter 6). The y-axis scale corresponds to the signal values measured at the ADCs' inputs, rather than the actual impedance values. In addition, the x-axis scale does not correspond to usable information, were an arbitrary

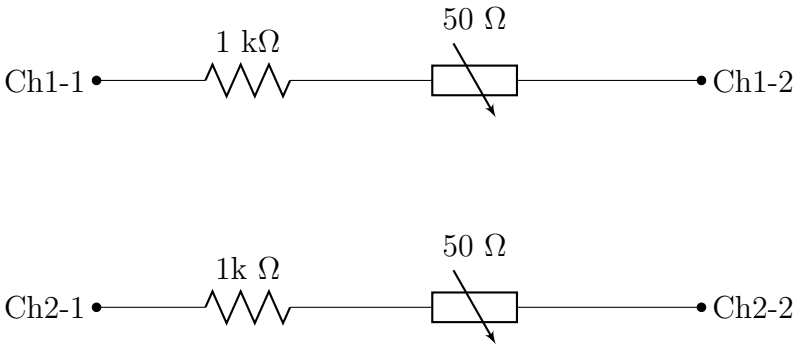

Figure 4.4: *Circuit diagram of the original two channel dummy load circuit.*

step value present in the pre-existing software was used as the time base (not time in seconds). This step value was not constant and is explained further in Chapter 6. This time base was later improved upon to allow for accurate time values to be obtained.

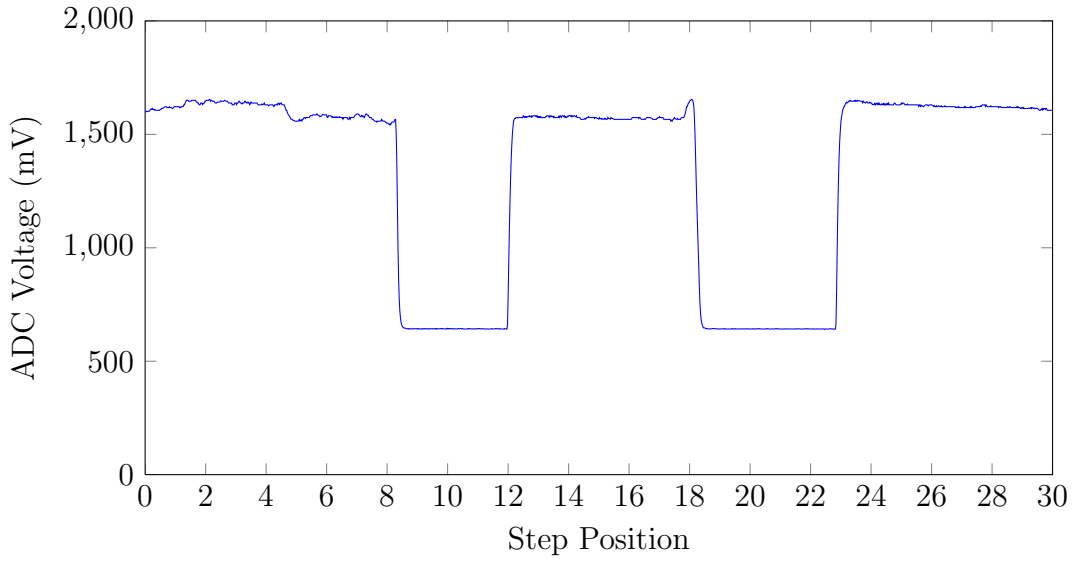

Figure 4.5: *Output waveform of one channel of impedance measurement using the remaining functioning modules from the initial prototype. The impedance change being measured was that of a resistor network designed to imitate a throat's impedance.*

The trials on this dummy circuit indicated that the circuit was working as desired, with the changing output signal reflecting the changing variable resistor's value. The second channel of the modular prototype could then be developed in order to measure two impedance changes simultaneously.

4.1.4 Two Channel Modular Prototype

With the first channel working as expected, the second channel was then able to be designed. The second channel was essentially the same as the first channel, except centred around a frequency of 70 kHz instead of 40 kHz. As the 70 kHz channel(Ch2) was reported to be the channel that caused the most issues in the pre-existing device, it was decided that the circuit would be redesigned in order to be confident about its operation. This meant recalculating the biasing component values for both the band-pass and low-pass filters in the system. In addition, the schematic was changed in order to mimic the implemented prototype, rather than the recorded schematic of the pre-existing device; the recorded circuit and the implemented circuit of the pre-existing device differed in the design for the final amplifier. A simple block diagram of the two channel modular prototype can be seen in Figure 4.6, where new current generating and signal conditioning circuitry (instrumentation amplifier and filtering module) were needed for the 70 kHz channel.

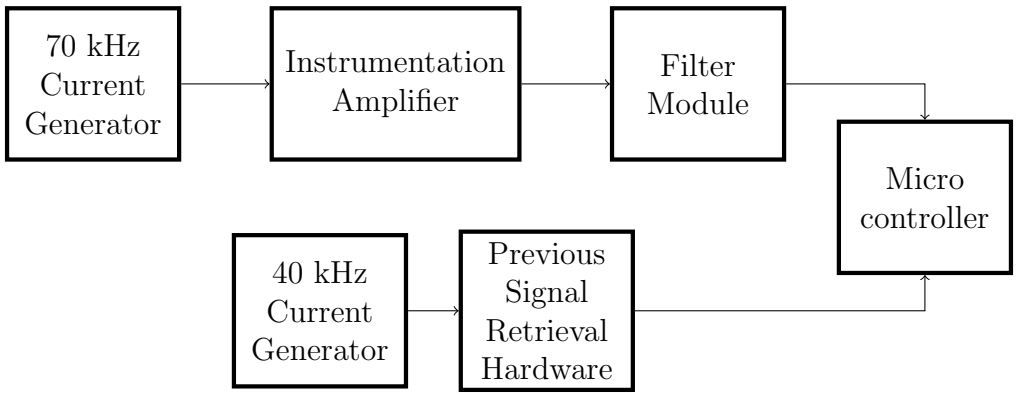

Figure 4.6: *Simple block diagram of the circuit boards used in the two channel modular prototype.*

4.1.4.1 Current Generation

In the creation of the current generation circuitry for the second channel, the same modules as used in the first channel were implemented, namely, a waveform generator followed by a transconductance amplifier. The waveform generator was essentially the same as the first channel due to the frequency being set by a variable resistor. However, to provide the desired output waveform, the centre values of the passive band-pass filters need to be changed to accommodate a centre frequency of 70 kHz, rather than 40 kHz. In order to do this, R_{lp} (Figure 4.2) was changed to 1.5 kΩ to give a low-pass cut-off of 106 kHz; the same high-pass filter values were used to keep cut-off frequency of 10 kHz. The transconductance amplifier following this module was identical to that used in the first channel (Figure 4.3).

4.1.4.2 Instrumentation Amplifier

The instrumentation amplifier was chosen to be an identical design to the amplifier used in the 40 kHz channel, as testing and investigation into the design had confirmed that the amplifier was performing correctly. A variable resistor was attached to the amplifier circuitry in order to be able to adjust the amplification, this was the same set-up as the initial prototype shown in Chapter 3.

4.1.4.3 Filter Module

The filter module was the module that required the most alterations from the pre-existing 70 kHz channel design outlined in Chapter 3. A block diagram of the necessary changes in design of the filter module is shown in Figure 4.7. As shown in this figure, each section in this module needed to be edited, from changing resistor values in filters, to adding a completely new amplifier to the circuit.

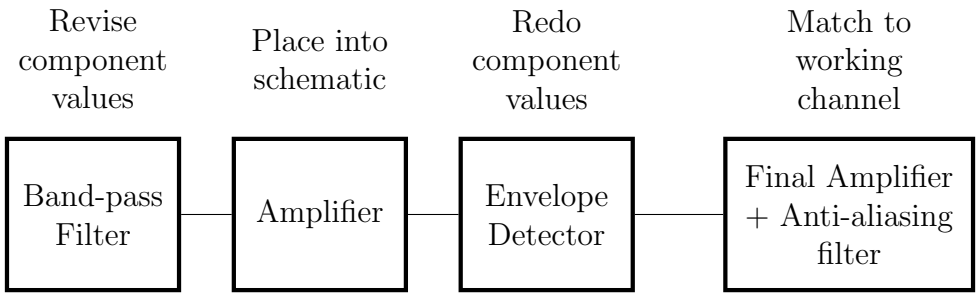

Figure 4.7: *Block diagram of the filter module used in the two channel modular prototype.*

Band-pass filter: The design of the band-pass filter incorporated the same LTC1562-2 active RC quad universal filter chip by Linear Technology [71] as used in the pre-existing prototype, where different biasing component values were used. This chip uses three external resistors per filter to set the centre frequency, gain, and Q factor values. The circuit was designed to have a centre frequency of 68.4 kHz, a Q value of 6.45, and a unity gain, using equations from the chip's data sheet [85]. The Q value of 6.45 was chosen to give a cut-off frequency of around 5 kHz either side of the centre frequency. This resulted in lower and upper cut-off values calculated to be 63 kHz and 73.7 kHz. The circuit and expected frequency response of this circuit were created using the FilterCAD software tool by Linear Technology [86]; the response of the filter and can be seen in Figure 4.8. The filter has a centre frequency close to 70 kHz and there is substantial attenuation at the other frequencies of interest (40 kHz and 50 Hz).

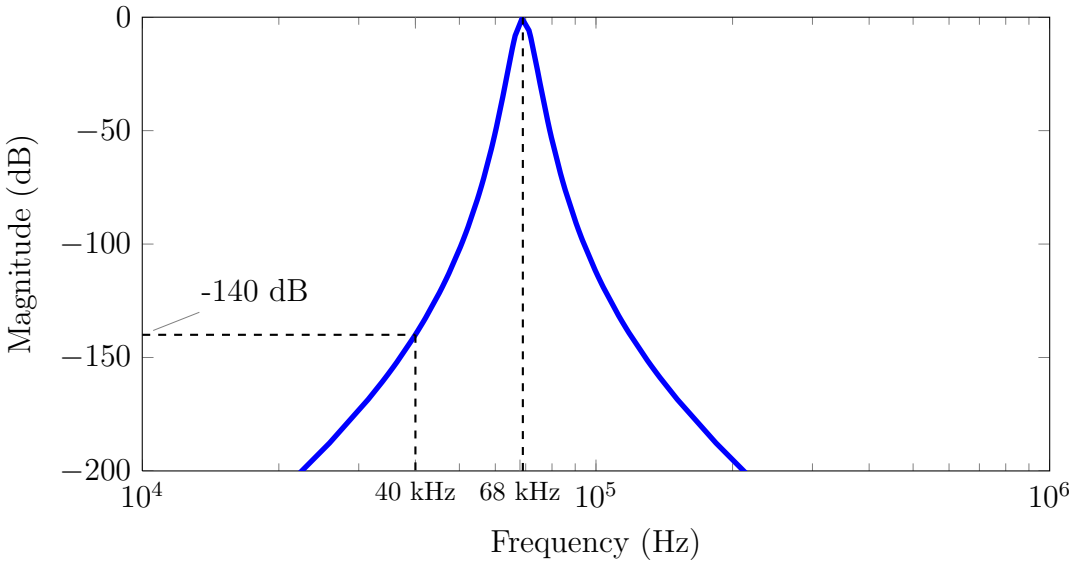

Figure 4.8: *Frequency response of the 70 kHz band-pass filter in the modular prototype.*

Amplifier: One of the problems encountered while using the LTC1562-2 active filtering chips was that the actual gain was less that the expected gain. This gain could not be easily increased by altering the band-pass filter circuit without distorting the output waveform. A separate amplifier module was therefore implemented. This amplifier stage was implemented in the previous design, but had not been documented. This module uses a non-inverting amplifier configuration with a gain of 3 V/V in order to compensate for the attenuation from the band-pass filter module, and can be seen in Figure 4.9. The resistors used to attain this gain were 5 kΩ for R_{gain1} and 10 kΩ for R_{gain2}. This gave a gain of 3 V/V through the equation $A_V = (1 + R_{gain2}/R_{gain1})$ [84], where A_V is the voltage gain provided by the amplifier. The amplifier also provided a buffering stage between the band-pass filter and the envelope detector, where the non-inverting amplifier provided a high input impedance and a low output impedance [84].

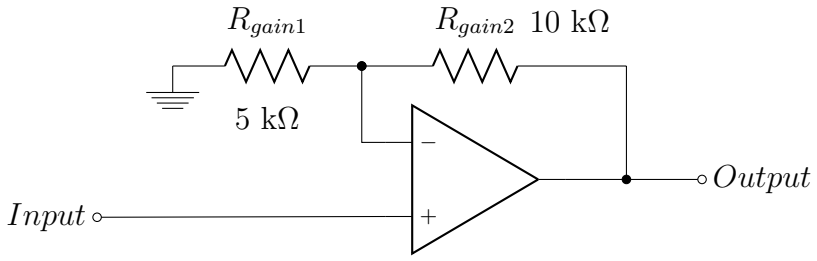

Figure 4.9: *Circuit diagram of the non-inverting op-amp gain stage between the band-pass filter and the low-pass filters*

Envelope detector: As with the pre-existing prototype, an envelope detector followed the band-pass filter's compensating amplifier. The envelope detector consisted of a half-wave rectifier (a diode), and a low-pass filter. The low-pass filter design was kept very similar to the design used in the pre-existing prototype, where the previous solution used the LTC1068 active low-pass filter IC by Linear Technology [72]. Since the low-pass filter's primary task is to demodulate the received signal to baseband, the filters could be the same for both channels, as the baseband frequency was very similar between channels. When constructed, however, this module did not work as expected and high frequency oscillations occurred on two of the op-amp stages. After investigation no clear explanation could be found for these oscillations, where the circuit was identical to the working module in the pre-existing device. It was concluded that the oscillations were due to malfunctioning stages in the IC itself, where an oscillation frequency much higher than the pass-band is most likely caused by the dynamics of the op amp [87]. These stages could be bypassed due to the order of the low-pass filter being substantially higher than needed. The frequency of the signal needing to be filtered (70 kHz) was several decades higher than the cut-off frequency of 20 Hz. This meant that the original eighth-order filter was able to be reduced to a fourth-order filter through the use of the bypasses without any significant change to the resulting signal from the filter. Further reductions in filter order were able to be completed later in development.

Final Amplifier + Anti-aliasing filter: The final amplifier and anti-aliasing section was the last module of the filter circuit to be implemented. Again, this module was identical to the module in Ch1 due to the signals at this stage of the circuit being very similar. The main issue with the implementation of this module was the differences between the schematic diagram for the pre-existing device and its actual implemented construction. Due to the first channel having working hardware, it was decided that the design present in the hardware would be used in preference to the design in the schematic. This meant implementing a three-pole passive RC-filter as the anti-aliasing filter, rather than an active filter as specified in the schematic. This effectively divided the module into the two sections as shown in Figure 4.10. The initial section of this module is a high-pass filter feeding into an inverting amplifier with 150 V/V gain and the second section is an anti-aliasing filter for the microcontroller's analogue to digital converter. The amplifier used gain resistors of $R_1 = 1$ kΩ and $R_1 = 150$ kΩ, where the gain of the inverting amplifier is governed by the equation $A_V = -R_2/R_1$ [84]. A capacitor of 1 mF was combined with the R_1 resistor to create a high-pass filter to remove the dc component of the signal.

It was decided at the outset of this project that the dc component of the impedance signal would be removed from the measurement (as with the previous project) in an attempt to maximize the dynamic range of the changing impedance signals received. The impedance characteristics relating to the movement of the pharynx during a swallowing sequence were relatively unknown at the outset of this project. Therefore to minimize the risk of not having a great-enough dynamic resolution to detect all of the waveform's features a high-pass filter was implemented, where it was the changing impedance that was identified as the main feature of interest, not the static impedance. The high-pass filter preceding the final amplifier was implemented to remove this static component of the signal, where a filter with a cut-off frequency of 0.16 Hz was initially used. The manometry waveforms analysed in Chapter 3 all occurred in a time frame of less than 2 s, therefore 0.5 Hz was identified as the lowest frequency for the sequencing of a swallow.

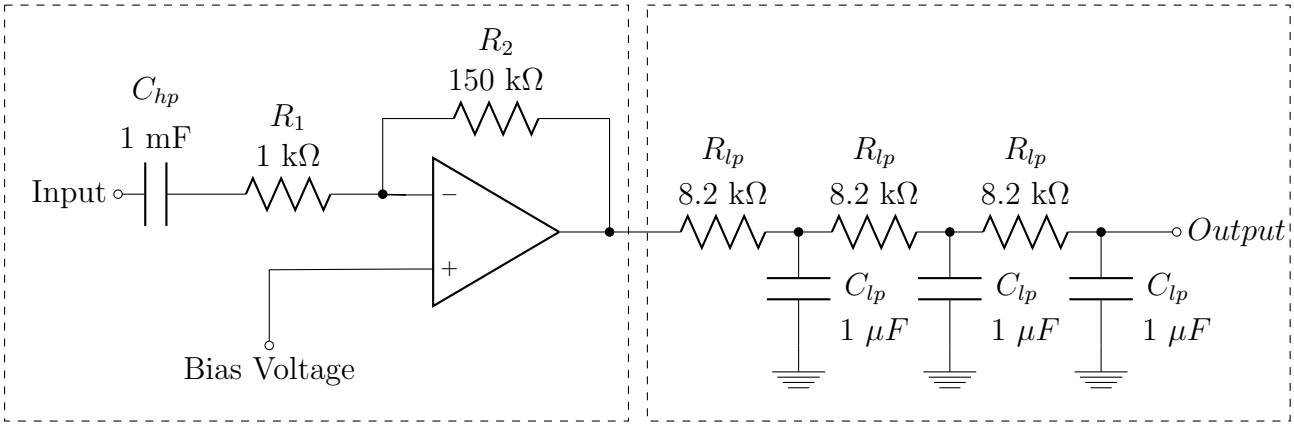

Figure 4.10: *Circuit diagram of the final amplifier and anti-aliasing filter set-up used in the modular prototype. The box on the left-hand side is the inverting amplifier, and on the right is the passive low-pass filter.*

One feature of this module that had to be investigated was the low input impedance due to an inverting amplifier being used. In order to reduce unwanted attenuation between modules, the input impedances had to be very high compared to the output impedance of the previous module. The value of the input impedance of an inverting amplifier is governed by R_1 and C_{hp} [84], where the lowest value would occur at high frequencies and is governed by R_1. This relatively low input impedance did not pose a problem, however, due to the output impedance of the envelope detection module being so low. The LTC1068 IC included an inverting amplifier as the last stage of the low-pass filter module. This inverting amplifier gave the module a very low output impedance [84]. This allowed for an inverting amplifier to be used in the final module without the concern of the input impedance being too low.

For the second part of this module, a three-pole passive RC filter was implemented as an anti-aliasing filter. The anti-aliasing filter was originally designed to have a cut-off frequency of 20 Hz, the same as the envelope detector's low-pass filter. This was accomplished by using a signal-pole RC filter and the equation $f_c = 1/2\pi R_{lp}C_{lp}$ to gain a cut-off frequency (f_c) of 20 Hz [83]. Values of $C_{lp} = 1$ μF and $R_{lp} = 8.2$ kΩ were chosen to gain this frequency. However, this filter was expanded to a three-pole passive filter (the same order used in the pre-existing prototype) by cascading three of these low-pass filters together to increase the stop-band attenuation. The primary reason for this was to ensure any 50 Hz noise present at the final module was significantly attenuated. This increased filter order caused the 3 dB cut-off frequency to decrease to 9.9 Hz. This was calculated using the transfer function of the filter (shown in Equation 4.1), where the cut-off frequency was able to be found by using the values of $C_{lp} = 1$ μF and $R_{lp} = 8.2$ kΩ. Though lower than the desired 20 Hz, this cut-off frequency was still large enough to allow for the majority of the information present in a swallowing signal to not be attenuated. Of the data located below 20 Hz in the manometry waveforms collected only 6% was located between 10 and 20 Hz, where the remaining 94% was less than 10 Hz.

$$-3dB = (\frac{1}{R_{lp}C_{lp}j\omega_c + 1})^3 \tag{4.1}$$

This passive low-pass filter output does however cause the output impedance of the ac amplifier section of the circuit to be relatively high. This is not a serious problem as the module feeds into an ADC, which has a high input impedance. Passive anti-aliasing filters have a higher output impedance and a longer settling time than an active filters. However, a filter with a large capacitor value will work to charge the ADC's capacitor quickly and negate this problem [88]. Due to the final C_{lp} value of 1 μF being so much larger than the ADC's sampling capacitor value of 18 pF [74] the use of a passive anti-aliasing filter was found to be appropriate.

4.1.4.4 Evaluation of the Two Channel Modular Prototype

With all of the modules created for the two-channel modular prototype, the next step was to test the system. In order to test the system, all of the modules had to be combined to create the full system. This full system was initially tested on a combination of fixed and variable resistors, as initially done with Ch1. This resistor network was required to be extended to two channels in order to simulate using two channels on the neck. These two channels were interlinked in order to determine the effect of inter-channel interference, as well as to more effectively mimic the expected impedance of a throat. The effect of a tetrapolar circuit was however ignored at this stage of the design, where the current injection and sensing points for each channel were the same. The resistor network can

be seen in Figure 4.11, where the resistance for each channel was chosen to be similar to that used in the one-channel prototype of 1 kΩ ± 50 Ω. The inter-channel resistance was chosen to be 220 Ω as it was expected the tissue impedance separating the channels would be less than the skin impedance but more than the change in impedance during a swallow. The results from the tests on this prototype can be seen in Figure 4.12.

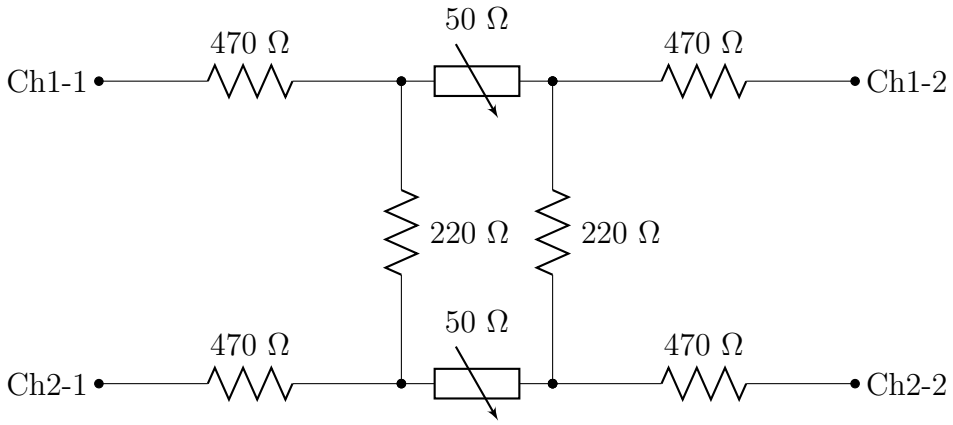

Figure 4.11: *Circuit diagram of the two channel test circuit used to mimic the expected throat impedance used for the first prototype.*

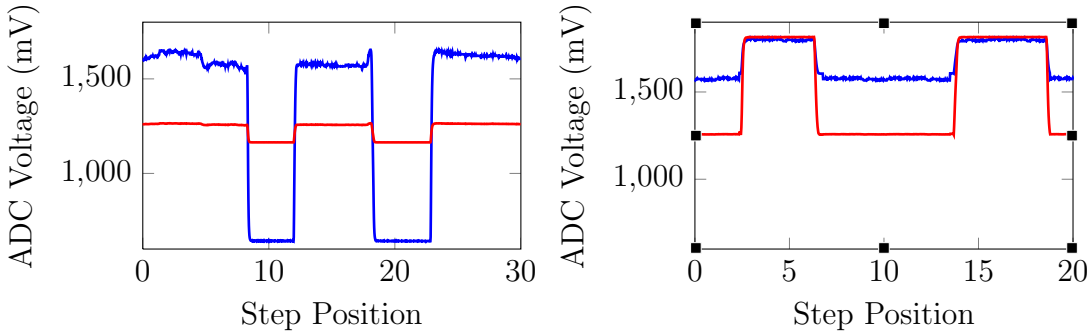

(a) *40 kHz channel impedance change* ***(b)*** *70 kHz channel impedance change*

Figure 4.12: *Waveforms produced when the variable resistors were changed in each channel of the test circuit in Figure 4.11, where the 40 kHz channel is the blue line and the 70 kHz channel is the red line. (a) The response when the variable resistor on the 40 kHz channel is changed. (b) The response when the variable resistor on the 70 kHz channel is changed.*

The tests performed on the passive resistor network allowed for the basic function of the circuit to be investigated with what was expected to be a similar load to that provided by a human neck. The results shown in Figure 4.12 indicated that both of the channels were able to detect a small change in impedance in the resistive network. The change in impedance of one channel resulted in a change in both channel's waveforms. This was expected, as Figure 4.11 shows there is a parallel impedance path for each channel

through the two 220 Ω resistors and the other channel's variable resistor. However, undesired features were the differing levels of the signal in each channel and the noise level on the 40 kHz channel. The differing levels of the waveforms needed to be adjusted to gain a similar settled dc value for each channel, as well as a similar change in voltage.

The inter-channel interference was difficult to determine from the output of the two channels due to both the medium, and the other channel's voltage signal, changing at the same time. The inter-channel interference was therefore investigated by monitoring the band-pass filter output of the 70 kHz channel; the 40 kHz channel from the previous prototype had a very compact circuit layout around the band-pass filter and was difficult to test. The waveform following the band-pass filter in the 70 kHz channel can be seen in Figure 4.13, where only the frequency from the 70 kHz channel is visible. This was as desired and meant that the band-pass filter was filtering the other channel's signal to an insignificant level. In addition to this test, the presence of any radiated noise between channels was investigated by using two separate, unconnected, impedance channels. This was done by using the same test circuit (Figure 4.11) without the inter-channel 220 Ω resistors. It was hoped that each channel's output waveform would be immune to any changing signals in the other channel. The resulting waveforms can be seen in Figure 4.14, where no detectable change in the 70 kHz channel could be seen when the 40 kHz channel's impedance was changed.

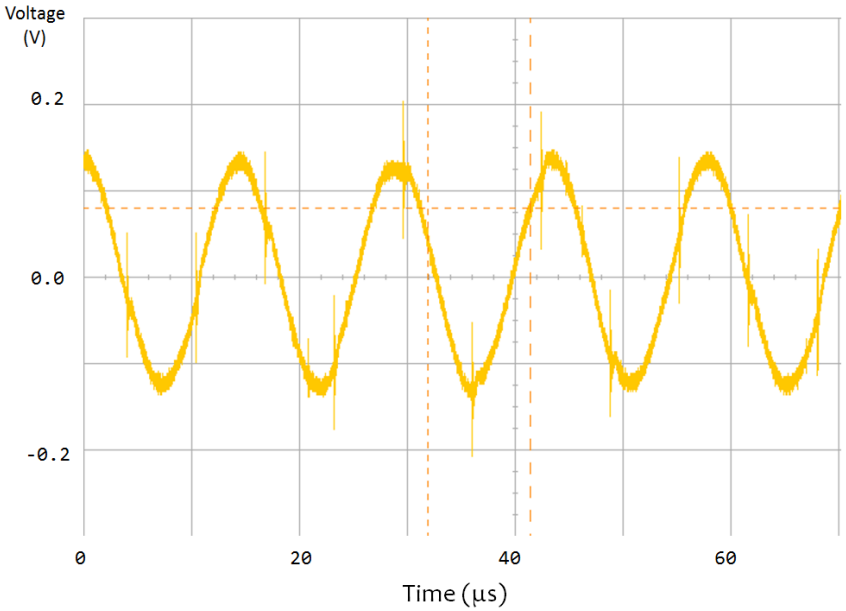

Figure 4.13: *Output of the band-pass filter in the 70 kHz channel of the modular prototype. The load used for this circuit is the resistor based dummy impedance circuit.*

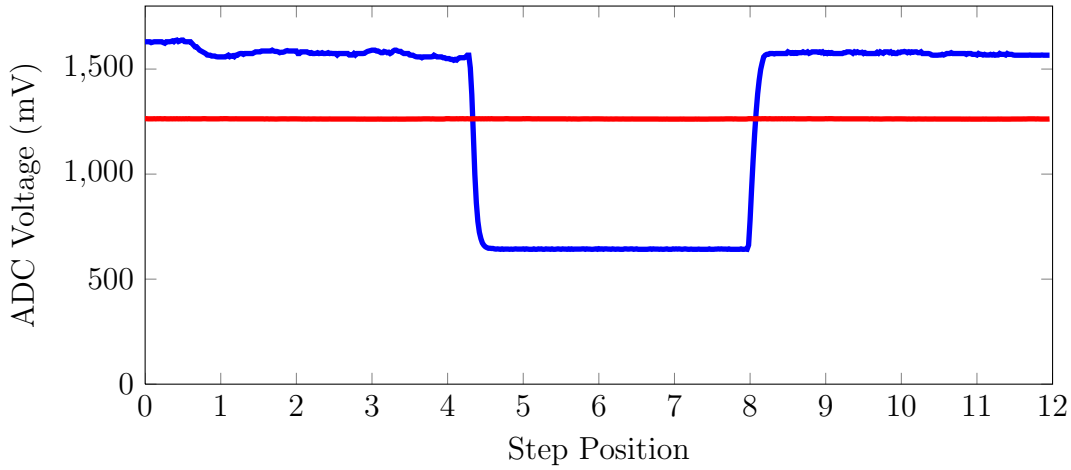

Figure 4.14: *Output waveforms of the first modular prototype, where the device measured was two independent test channels. The blue waveform corresponds to the 40 kHz channel, and red waveform is the 70 kHz channel.*

With the testing on the dummy impedance circuit completed, the system was trialled with electrodes and a human neck. Representative resulting waveforms are shown in Figure 4.15, where it can be seen that two different signals were able to be obtained. However, as with the dummy load, the signals had different gains and dc offset values. The results gained from this prototype provided a proof of concept of the project, where changing impedance measurements were able to be viewed at two different locations on the neck at the same time. The results from this prototype were only useful for examining the hardware functionality, as the results gained were unusable for swallowing analysis. As with the initial Ch1 results (Figure 4.5), the horizontal x-axis did not correspond to seconds and the y-axis was the voltage measured at the ADC. Even though the device could not determine the impedance value of the throat, at this stage the gains of the circuit had to be significantly decreased from those used with the dummy load in order to be able to determine a changing impedance. This meant that the overall impedance of the throat was significantly lower than estimated for the dummy load, meaning the dummy load would need to be adjusted to gain a similar behaviour to that of the throat.

The investigation of the two channel modular prototype allowed for two channels of impedance across the neck to be measured but several issues with the prototype remained. The measured waveforms were not as similar as desired, even when using the purely resistive load. This was due to the circuitry of each of the channels still being significantly

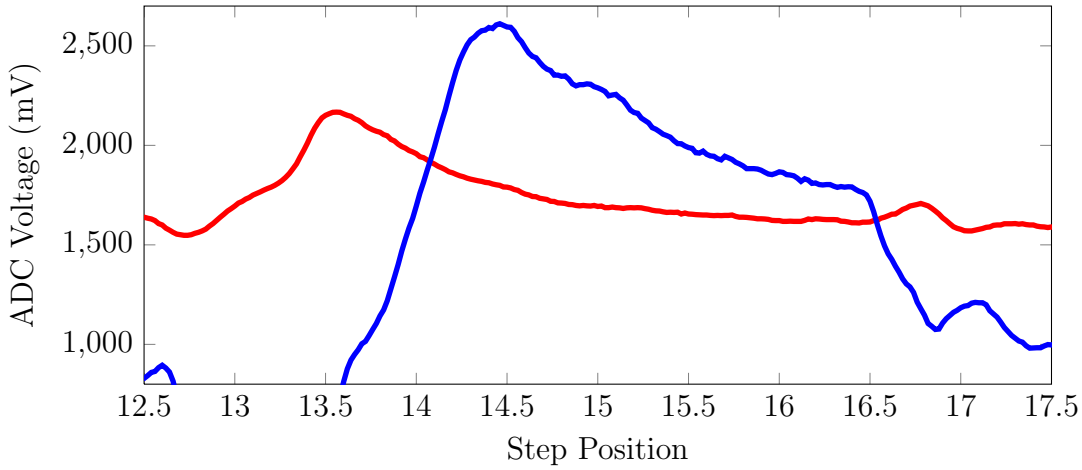

Figure 4.15: *Output waveforms of the first modular prototype, where the device measured the impedance across a human throat. The blue waveform corresponds to the lower positioned 40 kHz channel, and red waveform is the higher positioned 70 kHz channel.*

different, where the voltage gains and dc offsets existing in both channels were not closely matched. These issues, combined with the problem of the device not being portable due to its dependence on the bench-top power supply, resulted in a new prototype design being implemented.

4.2 Second Prototype: Single Board Design

The aim of the second prototype board was to create two complete functioning impedance measuring channels based on the first modular prototype, and condense the result into one portable board. The channels had to operate identically, except for being at different frequencies. The design process for this second prototype was to combine the correctly operating module designs for the first modular prototype with redesigned modules from the pre-existing prototype. This meant that the same design used in Figure 4.6 was implemented, except the previous signal retrieval hardware block was to be redesigned. To do this, the 40 kHz signal retrieval modules from the pre-existing prototype were redesigned to replicate those designed for the 70 kHz channel in the first modular prototype. These modules included the instrumentation amplifier module and the filtering modules, where a similar process was used to that described in Section 4.1. A new power supply also needed to be designed to enable a portable solution.

A new design was not needed for all of the 40 kHz signal retrieval hardware. Only the band-pass filter module needed to be redesigned. This was due to the 40 kHz channel being very similar to the 70 kHz channel past the point of the band-pass filter module, where the instrumentation amplifier designs were also identical. The modules therefore requiring a new design were the band-pass filter and the power supply.

4.2.1 Band-pass Filter

The LTC1562-2 active filter chip by Linear Technology [71] was again used to create a band-pass filter, with the centre frequency at 40 kHz. The design produced a theoretical unity gain, Q factor of 2.87, and a centre frequency of 38 kHz. A Q factor of 2.87 produced a low frequency cut-off of 31.5 kHz and high frequency cut-off of 44.8 kHz. This Q factor was chosen to be lower than the value used in the 70 kHz channel to allow for the filter to have the same 10 kHz bandwidth. The expected frequency response of this filter, produced by the FilterCAD program by Linear Technology [86], can be seen in Figure 4.16. Again, an additional stage of amplification was required after the filter to compensate for the band-pass filter's actual less than unity gain.

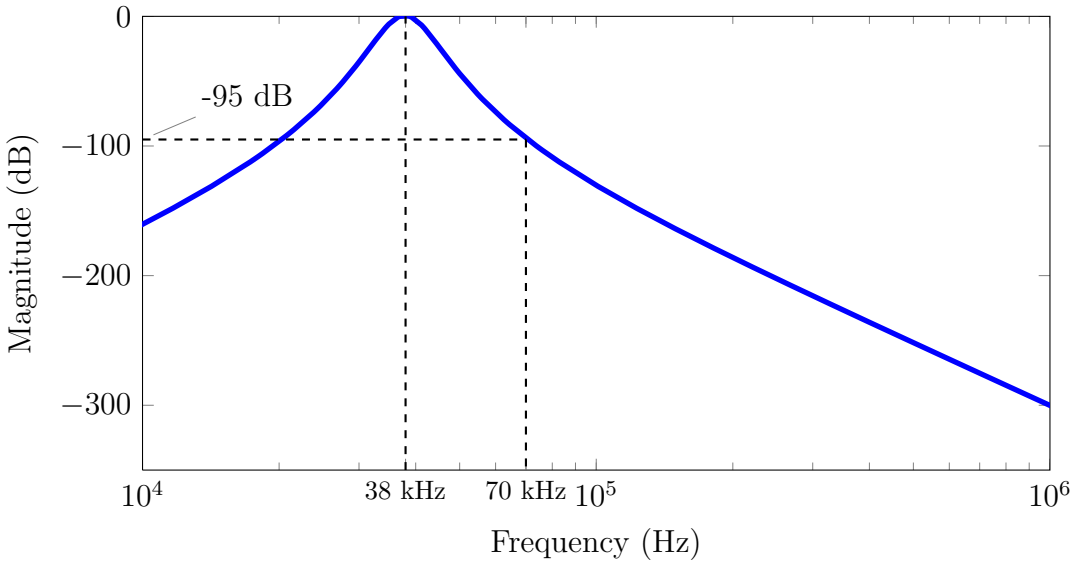

Figure 4.16: *Frequency response of the 40 kHz band-pass filter in the single board prototype (that is, the second prototype).*

4.2.2 Power Supply

In order to create a portable prototype, the power supply for the board needed to be become portable as well. Several alternatives to the power supply chip used in the pre-existing prototype were trialled in order to fix the problem of excessive noise on the negative power rail. The negative rail voltage from the power supply designed for the pre-existing prototype can be seen in Figure 4.17, where the maximum peak-to-peak noise was 544 mV. Several alternative power inverting chips were trialled with little improvement between chips. It was therefore decided that using voltage regulators to set the voltage would be the most practical solution for providing a stable power supply voltage. Positive and negative adjustable voltage regulators were used to maintain a steady voltage under load. In order to do this, a 6 V voltage source and the previously used TPS6755 voltage inverter by Texas Instruments [89] were used.

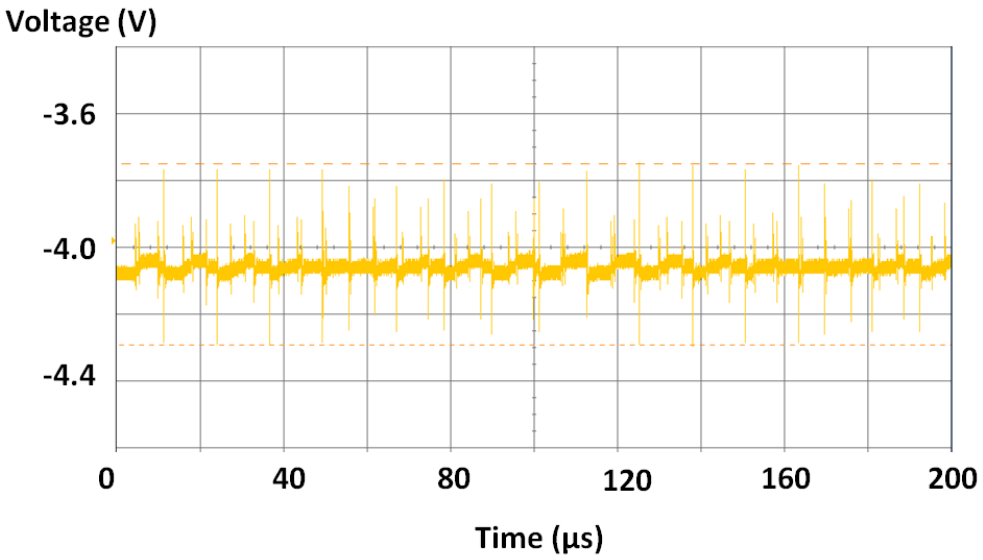

Figure 4.17: *Negative supply rail voltage from the power supply circuit designed for the initial prototype.*

The voltage source was the RBE850 adjustable ac-to-dc transformer-isolated external adaptor by Avico [90]. A transformer-isolated supply was used in preference to a switch-mode supply, where it was found that external plug-in switch-mode power supplies trialled were not actually fully isolated. An unacceptable leakage current for a medical device (over 100 μA [91]) was measured when using a switch-mode power supply. The transformer-isolated supply fell below this leakage current limit. Using the voltage source, a negative voltage rail was achieved by implementing the voltage inverter. The output voltage of the voltage inverter is determined by reference and feedback resistors, which were biased to give an output voltage of -6 V. The circuit

diagrams for these regulators and the voltage inverter can be seen in Appendix A.3 in Figure A.16. The components for the voltage inverting circuit were chosen from the TPS6755's datasheet [89], where the equation $R_{fb} = |V_o|R_{ref}/(1.22)$ relates the output voltage to the R_{fb} and R_{ref} resistors. The resistor value of $R_{ref} = 10$ kΩ was suggested by the datasheet. Therefore to obtain an output voltage of -6 V a R_{fb} of 49 kΩ was used.

The output voltages for each rail were designed to be regulated to 4.4 V and -4.4 V respectively. This was done with the use of the LM317 and LM337 regulators by Texas Instruments [92, 93]. These regulators allowed for exact voltages to be achieved and maintained, with the additional advantage of adding circuit protection against power surges and incorrect input voltages. To obtain these voltages two regulating resistors were set to $R_{reg1} = 2.7$ kΩ and $R_{reg2} = 6.8$ kΩ, where the equation governing the output voltage for both of the regulators was $V_{out} = 1.25 \times R_{reg2}/R_{reg1}$ [92, 93]. The voltages were chosen to be below 5 V to allow for the regulators to have a voltage drop of more than 1.25 V between the input and output. Having a voltage drop of greater than 1.25 V allows for the regulators to provide effective stabilization [93]. Ideally the output voltages would have been left at ±5 V which could have been achieved by raising the input voltages. This was not available however, as the TPS6755 required the input and output voltages to have a voltage difference of no greater than 12 V [89], so the chip was already operating at its limit. The resultant waveforms for these rails can be seen in Figure 4.18.

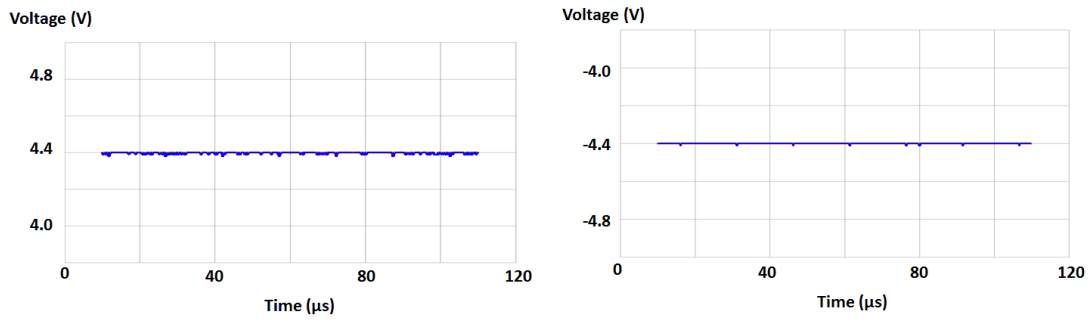

(a) *Positive Rail.* ***(b)*** *Negative Rail.*

Figure 4.18: *Power supply rails for the regulated portable power supply.*

A lower power supply voltage would not affect most of the modules due to their need for a stable rail voltage rather than a precise voltage, but there are however two sections of the circuit that relied on a precise rail voltage. These sections were the waveform generation module and the final amplifier module. The waveform generation module created a rail-to-rail square-wave, where the rails were the positive rail and the earth reference. This meant that instead of a 5 V square-wave a waveform with a amplitude

of 4.4 V was produced. This voltage was 12% less than the value used to calculate the output current and meant that the constant current waveform would have a rms value of 0.31 mA rather than the previously calculated 0.35 mA. It was decided that no compensation for this attenuation was needed at this stage due to the current still being relatively close to the outlined 0.5 mA limit, however any further attenuation to this value would need to be addressed. In regards to the final amplifier module, the dc offset for the ADC was dependent on the positive voltage rail directly. This voltage would be decreased from 1.5 V to 1.32 V with the change in the rail voltage. Since 1.5 V was chosen as an arbitrary value for the offset originally, the change to 1.32 V was acceptable as the change in impedance due to a swallow was expected to increase the output voltage of the inverting amplifier as stated in Chapter 3.

With the power supply and band-pass filter designed, the full prototype was able to be built and tested. The developed circuit for the prototype can be seen in Appendix B in Figure B.1. This prototype was developed on two boards, one for the power supply and one for the rest of the circuit. This was done due to the original prototype power supply being without the voltage regulators and therefore having a noisy supply voltage. As with the modular prototype, there were difficulties constructing the band-pass and envelope detection modules. These issues were due to the ICs not behaving as expected. Both the band-pass filter ICs and the ICs responsible for creating a low-pass filter in the envelope detector had stages of the filters malfunctioning. The band-pass filter in the 70 kHz channel and the low-pass filter in the 40 kHz channel each had one stage that had to be bypassed. Due to these filters being such high-orders originally(16^{th} and 8^{th} order respectively), the device was still able to function with this decreased filter order, but this was still undesirable as it lowered the attenuation applied to unwanted signals.

4.2.3 Evaluation

With the second prototype developed, the solution then needed to be evaluated to ensure that the circuit design was appropriate to be used in the final prototype. The evaluation was conducted by examining the outputs of each module of the circuit for both a dummy load (as outlined in Section 4.1.4.4) and a real throat impedance. These tests were hoped to outline which modules were working as desired, as well as determining the final values of components to be used; several easily adaptable variable resistors were used in this prototype which were to be replaced by fixed value components in the final prototype.

The criteria used to choose component values consisted of aiming to make the signal sampled by the microcontroller as large as possible, while avoiding the risk of saturation and voltage clipping. To achieve these goals, the gain of the amplifiers throughout the circuit were required to be tuned to sufficiently amplify the desired signal, while avoiding saturation. In order to limit the amplification of noise the signal was amplified as early as possible in the voltage sensing line. This was due to operational amplifiers and other noise sources existing throughout the circuit, where amplification earlier in the signal processing hardware allowed for noise amplification to be minimized [94].

In order to optimize the gain of each amplifier, the amplifier circuits were designed to operate at half their voltage range for a standard swallow. To achieve this, the voltage change was measured at each amplification stage during a swallowing event. The amplifier's gain was then set to ensure the signal produced could double in amplitude before reaching the amplifier's voltage limits. This margin in the circuitry allowed for patients who have a higher impedance across their throats to use the device; a higher impedance could be caused by different electrodes or a larger neck. The two amplifiers that needed to be adjusted were the initial instrumentation amplifiers and the final amplifiers. The band-pass filters' compensating amplifiers did not need to be changed as they were aiming for an overall unity gain when combined with the band-pass filters. The values of the variable resistors governing the gain of the instrumentation amplifiers were adjusted to achieve an overall gain of 42.1 V/V. The final amplification stage of the circuit produced a gain of 22 V/V.

With the amplification values set, the output waveforms during a swallowing event could be analysed. Again, these values were used to determine if the channels were working as desired, where optimal positioning of the electrodes had not been found. The resulting waveforms can be seen in Figure 4.19, where the waveforms were recorded using an updated version of the interfacing software (outlined in Chapter 6). As the recorded waveforms show, the channels were operating similarly. Further investigation into each module confirmed this, where signals similar to those desired were present at each stage.

Another task that could then be completed was to set the dummy load impedance to match the actual impedance measured from a throat. The original dummy load impedance was found to be significantly higher than the actual throat impedance in the previous prototype, and needed to be changed to allow for the device to operate with the newly set gains. This was achieved by measuring the output of the instrumentation amplifier module of one channel during a swallow and then changing the resistance of the dummy load until it matched this waveform. Both the peak voltage and the peak

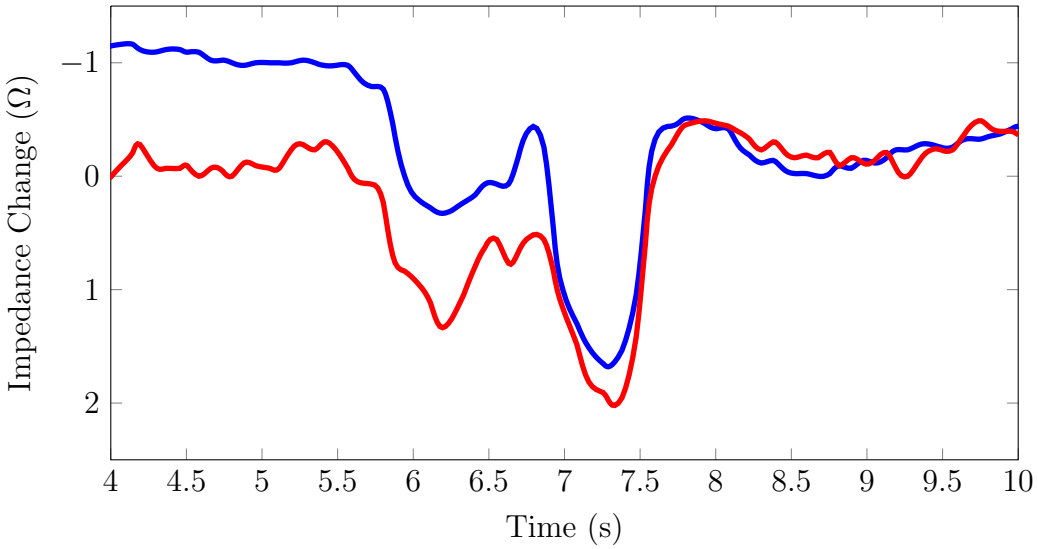

Figure 4.19: *Output waveforms of the second prototype, where the device was measuring the impedance across a human throat. The blue waveform corresponds to the top channel (40 kHz), and red the bottom (70 kHz).*

voltage change during a swallow were investigated in order to try and obtain a useful dummy circuit. It was found that using a base resistance of approximately 60 Ω with a changing impedance of 3 Ω would produce similar waveforms to a swallowing event in the throat. A changing impedance of around 10 Ω was chosen to be used in the dummy load to allow for greater range to be examined. This changing impedance was achieved by using a 50 Ω variable resistor in parallel with a 12 Ω resistor(a 10 Ω variable resistor was not readily available at the time of construction). The new circuit diagram for the dummy load can be seen in Figure 4.20. The inter-channel resistance was removed at this stage in order to clearly examine each channel without a change in the other channel's impedance affecting it. An example of the impedance measurement made with the dummy circuit can be seen in Figure 4.21. This shows how each channel was able to operate independently with a similar response. Different changes in the impedance were measured for each channel, where the changes in impedance were abrupt and over the full 10 Ω range.

Even though this prototype provided a working two channel impedance measurement of a throat, there were several drawbacks of this circuit. These drawbacks included: modules that did not perform consistently, and the need to calibrate the variable resistor values governing the operating frequencies and gains of each channel. The filter modules were

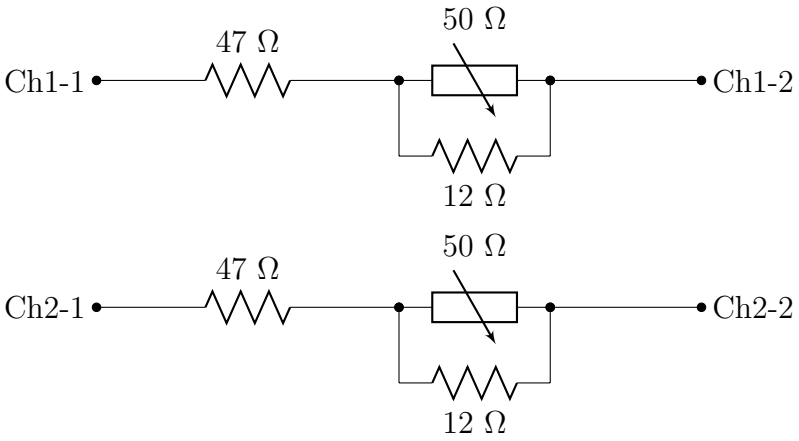

Figure 4.20: *Circuit diagram of the redesigned two channel dummy load circuit.*

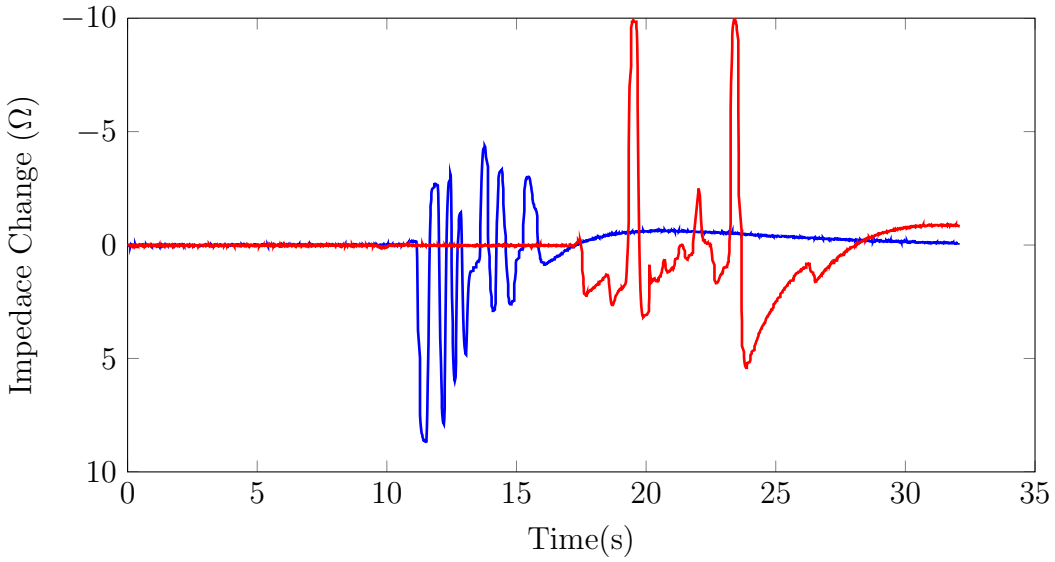

Figure 4.21: *Output waveforms of the second prototype, where the device was measuring the impedance across the dummy impedance circuit. The blue waveform is from the 40 kHz channel and the red dashed waveform is from the 70 kHz channel.*

difficult to use as several of the chips used had one or more sections which would not work as expected. This occurred in both the band-pass and low-pass filter modules, where the faulty sections of the chips needed to be bypassed. These drawbacks led to the design and construction of a third and final prototype.

4.3 Third Prototype: Final GULPS Hardware Design

With a two-channel working prototype achieved, a final prototype could be constructed. This final prototype was designed to have isolated circuitry with set component values to achieve a device with very little set-up required for use. This section provides the details for the final prototype design, including components used and alterations made to the previous two channel prototype (that is, the second prototype).

The final circuit design has a similar module pattern to the previous prototypes, where the major changes to the final circuit occurred in the voltage detection and filtering modules. These changes included the addition of dedicated high-pass filter modules to remove the dc component of the signal, as well as the addition of amplifiers for an auxiliary analogue output. These changes can be seen in the block diagram of the final prototype in Figure 4.22. Additionally, the post band-pass filter amplification modules, shown in Figure 4.7, were removed. These modules were removed as they were effectively part of the previous band-pass filter modules and were compensating for the unexpected behaviour of the band-pass filter ICs. The final modules used in the design are as following:

- Current Generation
    1. Sinusoidal Wave Generator
    2. Voltage to Current Converter
- Voltage Detection
    1. Instrumentation Amplifier
    2. Band-pass Filter
    3. Envelope Detector
    4. High-pass Filter
    5. Amplifier
        - Digital Output + (anti-aliasing filter)
        - Analogue Output
- Output
    - Digital

1. Microcontroller
2. UART to USB converter

– Analogue
    1. Co-axial output

Each module is outlined in the following sections, where each module is covered once as they are essentially identical for each channel. Justifications of each module design, as well as an example of the output of each module are included in each of these sections. The examples of the operation are shown for the 70 kHz channel, where the only differences between channels is the operating frequency. Any differences in the module design between channels is due to different component values, rather than a different design circuit topology or design technique. These differing values, as well as the complete circuit diagrams used, can be seen in Appendix A.

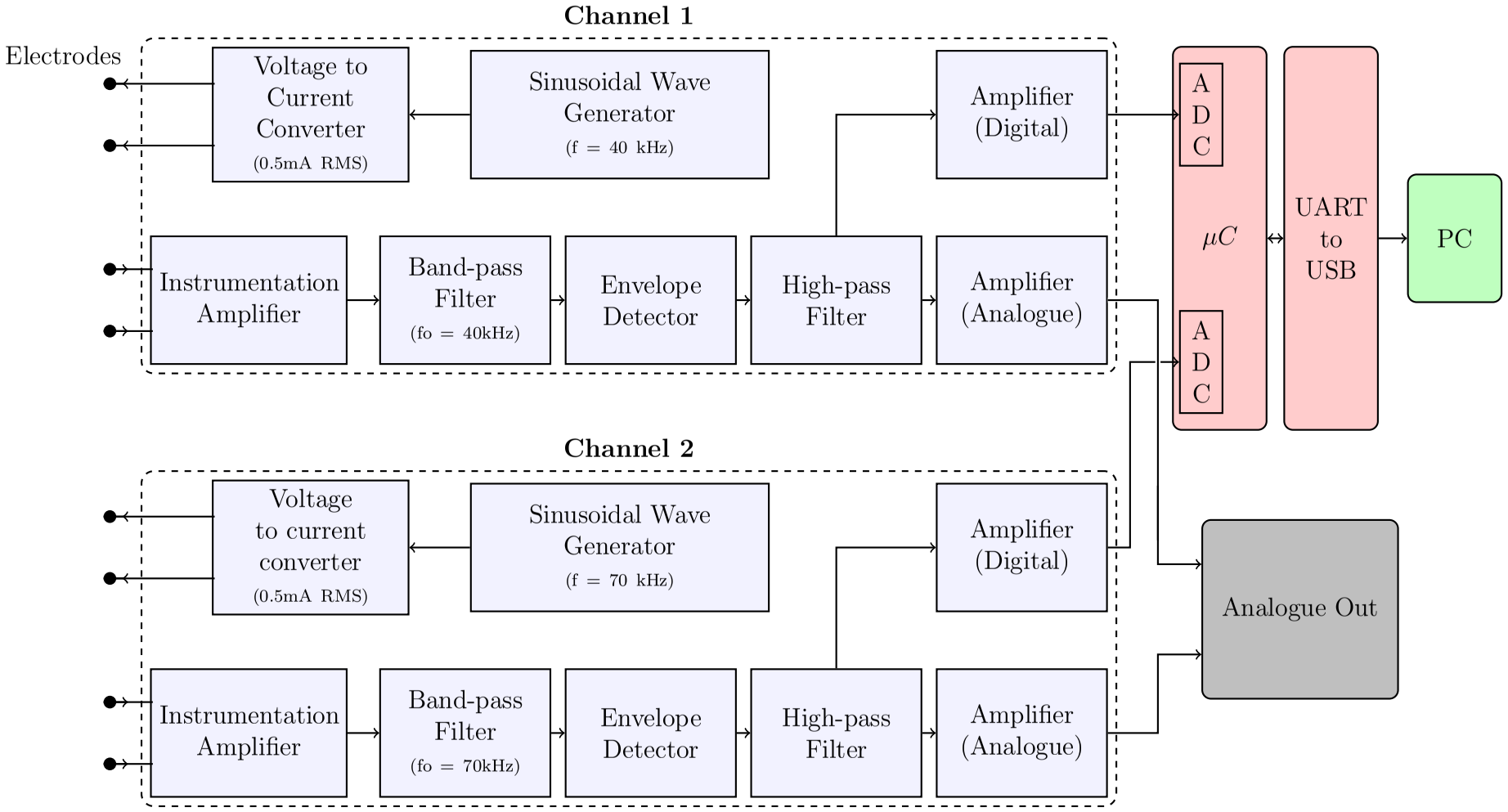

Figure 4.22: *Block diagram of the modules used in the final prototype.*

4.3.1 Current Generation

The current generation design used in the final prototype aimed to use a similar design to that used in the previous prototype, where the major difference was the use of a fixed frequency waveform generator in place of the adjustable VCO used previously. The channel frequencies were decided to be kept at 40 kHz and 70 kHz for the remainder of this project due to the promising results obtained using these frequencies in previous prototypes. These results included being able to measure a changing impedance during a swallow, as well as the lack of inter-channel interference experienced.

4.3.1.1 Sinusoidal Wave Generator

The sinusoidal waveform generating circuitry was altered from the previous prototype to incorporate a constant frequency generating module for each channel. In order to do this, the previous VCO used was replaced by a resistor-set oscillator. The IC chosen was the LTC6900C by Linear Technology [68] which is a low-power resistor-set oscillator which produces a square-wave output, similar to the previous VCO option. This oscillator was chosen in preference to the previously used VCO due to a lower component count, but, most notably, because the frequency could be more accurately set for each channel. This was due to the LTC6900 using just resistors to set the frequency values, where the VCO used a combination of capacitors and resistors. It is difficult to attain exact capacitor values, where capacitor values can change significantly over time [95], and relatively accurate, constant frequency values for each channels were desired.

The oscillator chips in each channel were biased based on the equation from the oscillator's datasheet [68] in order to achieve frequencies of 40 kHz and 70 kHz. The equation governing the frequency of operation was $f_{osc} = 10M \times 20k/(100 \times R_{set}))$. R_{set} values of 50.3 kΩ and 28.5 kΩ were used to create frequencies of 39.8 kHz and 70.2 kHz. These square waves were then passed through passive filters (Figure 4.2), as done in the previous prototypes, to create a predominantly sinusoidal waveform symmetrical about 0 V. The only difference in these passive filters was the use of a 1.8 kΩ resistor in place of the 1.5 kΩ resistor in the 70 kHz channel's low-pass filter section. This change was made in order to decrease the cut-off frequency of the filter from 106 kHz to 88 kHz, as the operating frequency was now set to 70 kHz. Previously the cut-off was set higher to allow for the operating frequency to be increased. An example of the waveform produced by this module of the prototype can be seen in Figure 4.23, where the result is an approximately sinusoidal waveform at 70 kHz. Though this waveform is not an ideal sinusoid it was decided that due to the relatively large frequency separation between channels and the frequencies being non-integer multiples of each other this waveform would be acceptable

to use. The load for this waveform was the dummy load shown in Figure 4.20. The circuit diagrams for the signal generation modules of the final prototype can be seen in Appendix A.1 in Figure A.1 for the 40 kHz circuit and in Figure A.8 in Appendix A.2 for the 70 kHz signal.

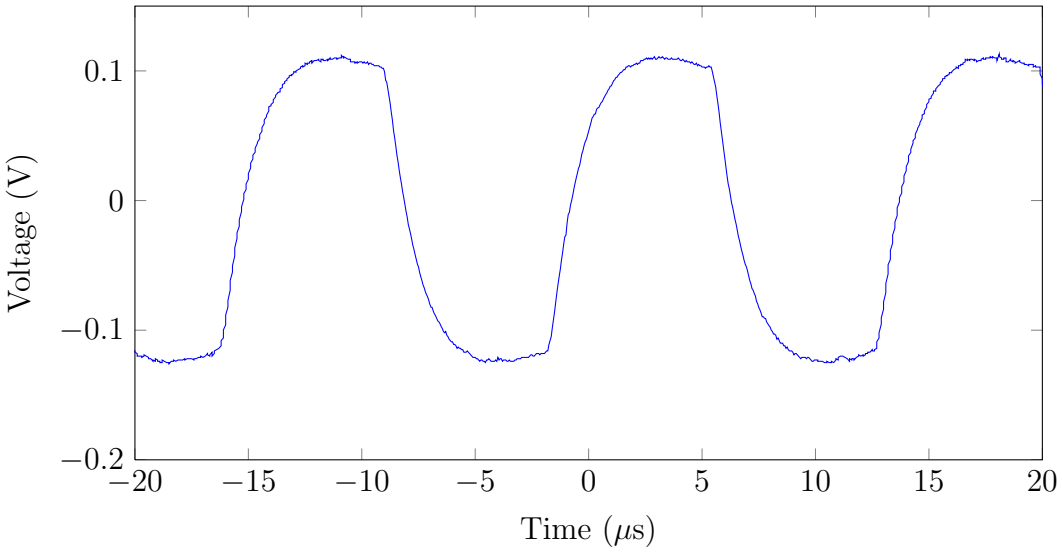

Figure 4.23: *The signal measured at the output of the signal generating module in the 70 kHz channel. The dummy impedance was the load for this measurement.*

4.3.1.2 Voltage-to-Current Converter

The voltage-to-current converter was kept the same as in the previous prototype due to this module working as expected as well as having fixed component values. The basic set-up of this circuit can be seen in Figure 4.3. The op-amp used in this circuit was the MCP6H01 rail-to-rail operational amplifier by Microchip Technology [96]. This amplifier was chosen to take advantage of the rail-to-rail operation and the ability to use dual supply voltages up to ±8 V. The circuits for the voltage to current converters can be seen in Figure A.2 (Appendix A.1) for the 40 kHz module and Figure A.9 (Appendix A.2) for the 70 kHz module.

4.3.2 Voltage Detection

The design of the voltage detection section of the final prototype was significantly different to the previous prototypes, due to the use of different filtering chips. The only modules that remained similar to those used in previous prototypes were the modules of the instrumentation amplifier and the final amplifiers. The band-pass and envelope detection modules used different filtering chips for this design, and the high-pass filter was split into its own module.

4.3.2.1 Instrumentation Amplifier

The only change to the design of the instrumentation amplifier for this final prototype was to incorporate a fixed value resistor for setting the gain in preference to a variable resistor. The instrumentation amplifier used for this module was the AD620AN by Analog Devices [70], this was the same amplifier used in the previous prototypes. This amplifier performed as expected and is described by its manufacturer as a low cost, high accuracy instrumentation amplifier that requires only one external resistor to set a gain between 1 to 1000 V/V [70]. The low noise, low input bias current, and low power of the AD620 make it well suited for medical applications. A gain setting resistor of 1.2 kΩ was used to give the differential amplifier a constant gain of 42.1 V/V through the equation $A_V = 49.4k\Omega/R_g + 1$. This gain was set to allow for the received signals to be amplified as much as possible to avoid the need for amplification later in the circuit, while limiting the voltages to below the saturation points of the amplifier (roughly ±4 V). Examples of the type of signals measured at the output of the instrumentation amplifier module can be seen in Figure 4.24. The waveform in Figure 4.24a was measured using the dummy impedance load, where the signal measured is only from the 70 kHz channel. In Figure 4.24b however, the signal across a neck is presented and is comprised of both 70 kHz and 40 kHz signals, as well as other electrical signals present in the human body. Both channels were attached to the neck for this measurement. The unwanted electrical signals, including the signal from the other channel, are filtered out by the band-pass filter.

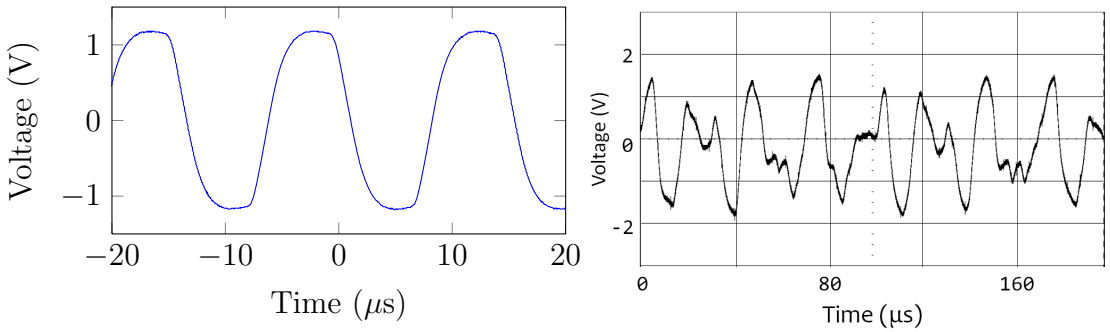

(a) *Dummy load.* ***(b)*** *Neck load.*

Figure 4.24: *The signals measured at the output of the instrumentation amplifier module of the 70 kHz channel in the final prototype.*

The circuit diagram used for the instrumentation amplifier module can be seen in Figure A.3 (Appendix A.1) and Figure A.10 (Appendix A.2). The two channels used the same circuit for this module. These circuits were very similar to the circuit used in the pre-existing prototype described in Chapter 3. This was due to the module operating as desired, therefore not needing a redesign. The module however could be improved

by removing the high-pass filter at the input to each the instrumentation amplifiers. Saulnier [77] stated that instrumentation amplifiers used in bio-impedance measuring circuits could be connected directly to the electrodes. These high-pass filters limit the input impedance of the instrumentation amplifier, where the input impedance will be essentially 100 kΩ (that is, the input resistors connected to ground). This impedance is much greater than the measured impedance of the throat at the frequencies used in this device (around 60 Ω) so should not affect performance.

4.3.2.2 Band-pass Filter

The band-pass filter module was redesigned for both channels to use a different active filter IC to isolate each channel's signal. The UAF42AU filter IC by Texas Instruments [97] was used in preference to the previously used LTC1562-2 ICs by Linear Technology [71], as the UAF42AU was found to provide a more reliable solution to filtering the signal, with the added advantage of being a cheaper, readily available alternative. The solution was considered to be more reliable due to all of the modules on the chip working as expected, where the previously used used LTC1562-2 chips were found to often have faults. In addition, the waveform after the filter appears to better resemble a sinusoidal waveform (Figure 4.25a) than the previous filter (Figure 4.13). Two ICs were again cascaded for each channel to create the band-pass filter. The values of the external resistors used to set the filter specifications were chosen by using the equations provided in the datasheet [97]. The resulting filter characteristics are shown in Table 4.1. Again, the Q factors were designed to give each filter a similar bandwidth. The only issue with these filtering modules is that the voltage at which they started distorting the waveform was found to be reasonably low (1.5 V peak). The gain value was therefore set at 0.5 × to allow for the band-pass filters to operate without distortion during a high change in impedance. This attenuation had to be compensated for later in the circuit.

Channel	**Gain**	**Center frequency** f_0	**Q factor**	**Low cut-off frequency** f_1	**High cut-off frequency** f_2
1	0.5	39.8 kHz	2.83	33.4 kHz	47.4 kHz
2	0.5	70.2 kHz	5.94	64.5 kHz	76.4 kHz

Table 4.1: *Final design band-pass filter characteristics.*

The output waveform of the band-pass filter is a modulated version of the impedance waveform, where the waveform will be centred at the channel's frequency with the information about the impedance contained in the signal. An example of the output waveform can be seen in Figure 4.25, where both the centre frequency and the impedance information can be seen in the two waveforms.

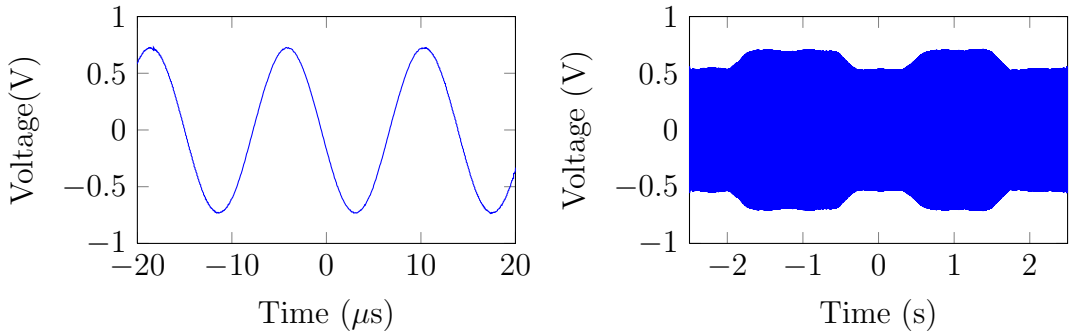

(a) *Short time-frame* ***(b)*** *Long time-frame*

Figure 4.25: *The signal measured at the output of the 70 kHz band-pass filter module of the final prototype. This signal is shown with short and long time-frames, where the signal now only contains information located around the band-pass filter's centre frequency. The impedance change information can be seen in the envelope of the signal in the long time-frame. The load for this example was the dummy impedance load.*

The circuit diagrams for the band-pass filter modules are shown in Figure A.4 (Appendix A.1) for the 40 kHz band-pass filter, and Figure A.11 (Appendix A.2) for the 70 kHz filter. These circuits took advantage of the filtering IC's low output impedance and high input impedance to minimize unwanted attenuation [97].

After the circuit was constructed, it was found that each of the UAF42AU filtering chips provided only a second-order band-pass filter, in contrast to the eighth-order filters provided by the previously used LTC1562-2 chips. This oversight meant that each channel only had a fourth-order band-pass filter instead of the desired 16^{th}-order filter, again cascading two filter chips. This meant that the attenuation of any inter-channel interference would not be as great, potentially corrupting the signal. It was found that by substituting in the values from Table 4.1 into Equation 4.1 the frequency response of the fourth-order band-pass filters could be found [97], where A_{gain} is the gain of the filter, ω_n is the center frequency of the filter in rads/s, and Q is the quality factor of the filter. The attenuation experienced by a 70 kHz signal in the 40 kHz channel was calculated to be be 27.7 dB and the calculated attenuation experienced by the 40 kHz signal in the 70 kHz channel was 40 dB. These lower-than-desired attenuations, most notably the

27.7 dB attenuation, could potentially allow for the desired signal to be corrupted by the other channel's signal. This module's order should therefore be increased in any following prototypes. This could be done by either cascading more UAF42AU chips or choosing a new filtering technique to produce higher-order filters.

$$\frac{V_{out}}{V_{in}} = \frac{A_{gain}\omega_n^2/Q^2 s^2}{(s^2 + \omega_n/Qs + \omega_n)^2} \tag{4.1}$$

4.3.2.3 Envelope Detector

As with the band-pass filter, the filtering components in the envelope detector were changed for the final prototype. The envelope detection modules consisted of two major features: a rectifier and a low-pass filter (Figure 4.26). The rectifier was kept the same as in the single board prototype, consisting of a half-wave rectifier in the form of a Schottky diode. However, the low-pass filter design was altered. The low-pass filter used in the previous prototype encountered several issues that lead to many sections of the filtering ICs being bypassed. The low-pass filter IC was therefore exchanged for a two-pole active low-pass filter. Due to the modulation carrier frequencies being several decades higher than the frequencies found to occur during a swallowing sequence a lower-order filter could be used. As shown previously in Chapter 3, all of the information in a manometry waveform that relates to the swallowing sequence (not noise) is found to occur below 20 Hz, where no significant frequency components are present at greater frequencies. A filter with a lower-order than the previously designed eighth-order filter would help to minimize noise created by the filter and circuit complexity.

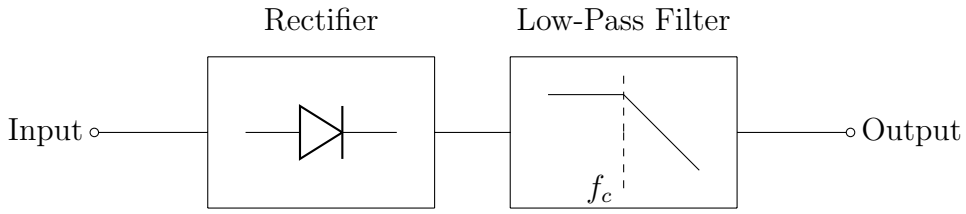

Figure 4.26: *Block diagram of the components used in the circuit detector for the final prototype for envelope detection.*

The active low-pass filter design shown in Figure 4.27 was used as the filtering stage in the envelope detection module. This filter has the characteristics of a unity gain and a cut-off frequency of 21 Hz. This filter was designed using the FilterPro software by Texas Instruments [98]. The MCP6H01 op-amp by Microchip Technology [96] was used for this low-pass filter as a low noise rail-to-rail op-amp was desired. An example of the output of the envelope detection module can be seen in Figure 4.28, where the measured impedance signal is the result. The protocol for the changing impedance measurement

was to quickly iterate the variable resistor over the 10 Ω impedance range three times and then slowly change the variable resistor over the range twice. These actions can be seen in this figure, where the first three peaks are the fast transition changes and the final two peaks and the step change are the slow transitions.

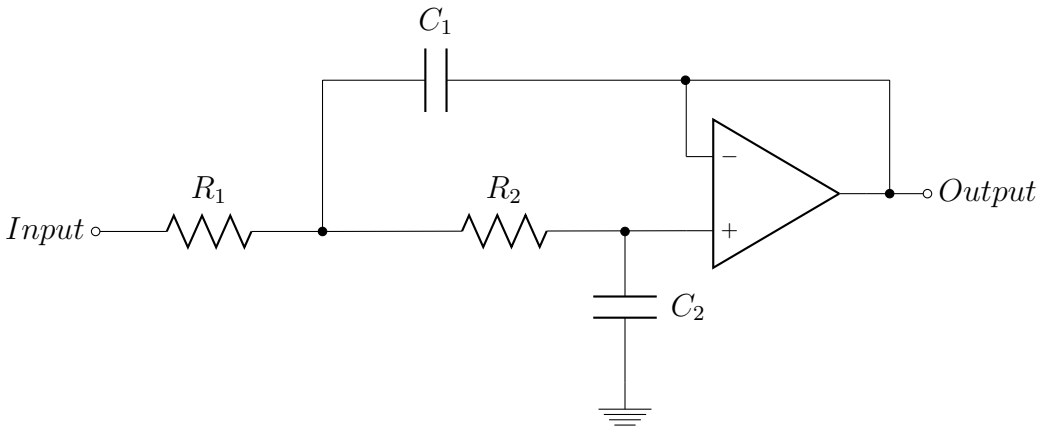

Figure 4.27: *Circuit diagram of the 2nd-order Sallen-Key low-pass filter used in the final prototype.*

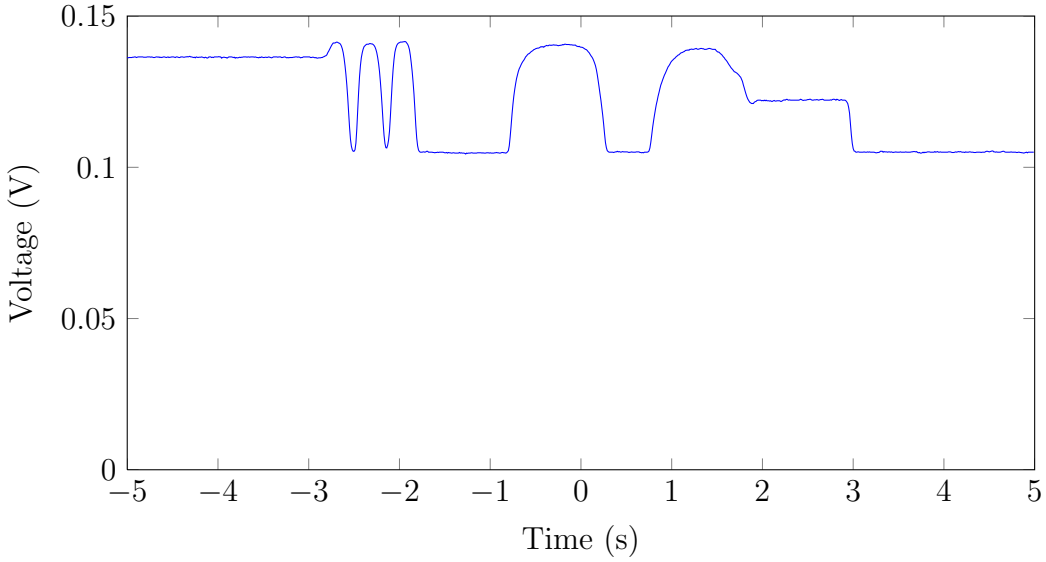

Figure 4.28: *Output of the envelope detection module during the final prototype, where the load being measured was the dummy load. The load was adjusted over its full 10 Ω range.*

With the active filter following the Schottky diode, it was found that the the op-amp characteristic of not drawing current through the input pin meant that no current would flow through the diode. In order to counter this, a 1 kΩ resistor was placed to ground from the output of Schottky diode in order allow for the current through the rectifier. The rectifier load resistor decreased the input impedance of the low-pass filter, but

the low output impedance and reasonably high current limit of the band-pass filter were determined to be sufficient for this change in impedance not to make a significant difference to the signal. This fix was not ideal and in future designs an alternative rectifying method should be investigated, where a precision half-wave rectifier, or a full precision rectifier would provide a better solution [99]. The final circuit diagrams are shown in Figure A.5 (Appendix A.1) and Figure A.12 (Appendix A.2).

4.3.2.4 High-pass Filter

In order to create a stable and predictable prototype, the high-pass filter used for removing the dc component of the impedance measurement was redesigned for the final prototype. The high-pass filter used in the previous prototypes consisted of a passive filter, where a very large 1 mF electrolytic capacitor was in combination with a resistor. This circuit had major variation in its behaviour between prototypes. The filter, when used in this prototype, took several minutes to reach a steady output voltage when the prototype was turned on, and any large variation in the input voltage would again cause the output to need to settle again. The issue was found to be centred around the 1 mF capacitor, where variation between capacitors of this size caused variation in the circuit's response. Large electrolytic capacitors are normally only used for filtering power supplies [95]. The resulting delay and different cut-off frequencies, as well as the design producing a response that was difficult to estimate, caused an alternative design to be investigated.

The high-pass filter used in the final prototype was a two pole Sallen-Key active high-pass filter with unity gain and a cut-off frequency of 0.05 Hz. This cut-off frequency is ten times smaller than the lowest frequency seen in a changing impedance signal during a swallow (approximately 0.5 Hz). The choice of the cut-off frequency for this filter was found to be an important decision in the design process. Choosing a frequency that was too high would result in lost information, but choosing a frequency that was too low would result in a slow response time for the filter to any changes in the base impedance. A 0.05 Hz cut-off frequency was found to provide a well balanced response. The output from the filter can be seen in Figure 4.30. This is the same impedance measurement protocol shown in Figure 4.28. It can be seen that the higher frequency components of the measured impedance remain intact, where the features such as the peak and trough of the waveform remain similar. The lower frequencies of the impedance change are slightly attenuated resulting in a sloping plateau of the stepped impedance change (centred around 3 s). This slope was very gradual and was evaluated to be an acceptable compromise for having a reasonable response time to a changing base impedance. A

changing base impedance would occur if the electrodes were moved or upon power-on of the device. The response time for a changing electrode position would be in the order of 5 to 10 s, where power-on of the device would have a response time of closer to 30 s.

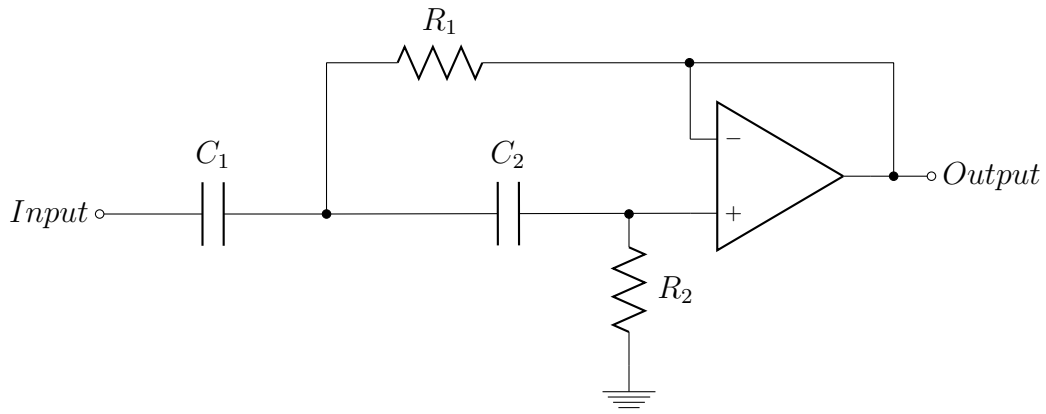

Figure 4.29: *Circuit diagram of the 2nd-order Sallen-Key high-pass filter used for filtering the dc component of the impedance signal in the final prototype.*

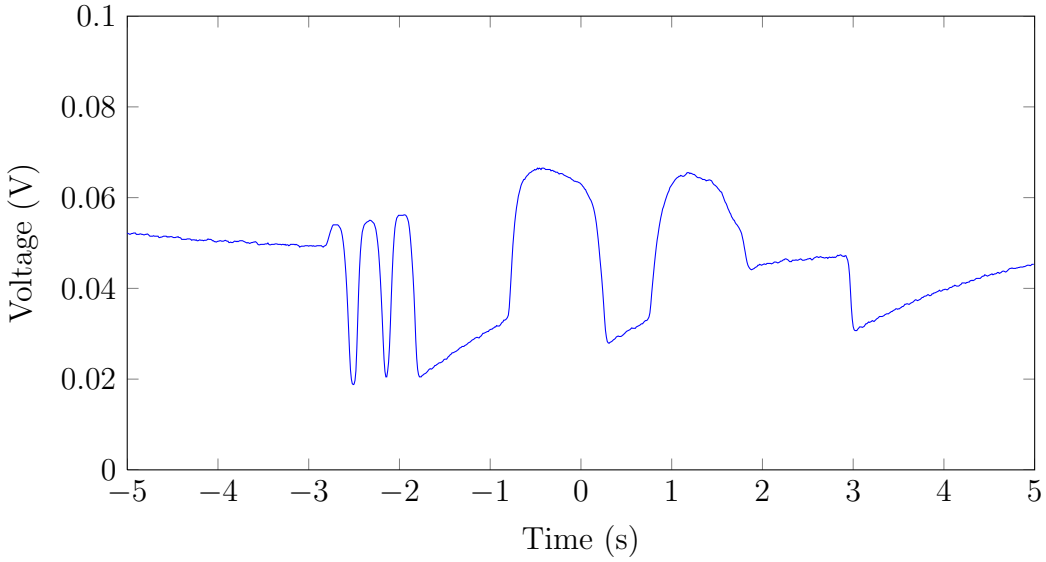

Figure 4.30: *Output of the high-pass filter used for removing the dc component of the impedance signal in the final prototype.*

The op-amp used for this module was the LM358N low power op-amp by Texas Instruments [100]. This op-amp was chosen due to its availability and its low input offset voltage of 2 mV. The final circuits for the dc removal filters can be seen in Figure A.6 (Appendix A.1) and Figure A.13 (Appendix A.2). An example output of this module can be seen in Figure 4.30.

The high-pass filter modules can be seen to remove the dc component from the signal (Figure 4.30), but it has also created an offset of its own. One explanation for this is that due to the impedances seen at both the inputs of the op-amp not being identical in value there will be a finite difference in the input currents seen at each input. This mismatch in currents could lead to the output voltage being non-zero when there is no voltage difference between the input pins [87]. As counter-productive as it seems, this offset was not much of an issue. The offset created by the high-pass filter module was a constant dc value of about 50 mV which could be removed by compensation in the next amplifying module. This could not be done with the original signal as the dc value would change depending on the impedance being measured. The impedance could change by a shift in the electrodes or measuring a completely different neck.

4.3.2.5 Final Amplifiers

As with earlier prototypes, a final amplifier was needed in order to boost the signal to a level where it could be easily sampled by the microcontroller. In the final prototype however, an additional amplifier was implemented in order to provide an auxiliary analogue output. The analogue output was added to allow for the device to connect easily to external analogue signal measuring equipment, such as an oscilloscope or the swallowing workstation used for pharyngeal manometry [32]. The only difference between the digital and analogue amplifiers was the off-set voltage used, where the digital amplifier offset the output voltage by about 1.32 V, and the analogue amplifier had no offset. The auxiliary analogue output was chosen to have no dc offset due to the swallowing workstation's limited ability to change its y-axis scale. The workstation has two options in regard to the scaling the y-axis: the axis scale could be symmetrical about 0 V with a specified maximum, or the scale could be between 0 V and a specified maximum value. This was not ideal if the waveform being displayed contained an offset voltage, where the waveform would occupy a smaller region of the monitor. This shrinking of the waveform made observing and detecting small changes in the impedance waveform difficult. Having a waveform with no offset allowed for the region of the monitor occupied to be increased by using the scaling option of making the axis symmetrical about 0 V.

The op-amp used for both amplifiers in each channel was the TLE2022CD by Texas Instruments [101]. This IC was chosen due to its low noise characteristics of 19 nV/$\sqrt{Hz}$. This chip was again set-up in an inverting amplifier configuration for both the analogue and digital outputs, similar to that shown in Figure 4.10. A gain of 56 V/V was used in both analogue and digital amplifiers for each channel to amplify the signal. This gain was found to amplify the signal measured, due to changing impedance, to a 1.5 V peak-to-peak signal. This allowed the ADC to sample the signal without the risk of

exceeding the range of the ADC with a larger impedance change; the input voltage swing from an auxiliary port of the swallowing workstation could be greater than 20 V [32]. The gain of 56 V/V was greater than that used in the previous prototype of 22 V/V, so as to counter the attenuation added in the band-pass filter modules of the final prototype. BNC co-axial connectors were used as the analogue output interface.

In order to create the appropriate output offsets for each amplifier the dc voltage on each op-amp's non-inverting input had to be set. Due to the previous dc filtering module not creating a purely ac signal an additional 0.05 V had to be subtracted from the input voltage. For the analogue output filter this 0.05 V was the only compensation needed, where the 4.4 V positive rail voltage was divided through 1.2 kΩ and 100 kΩ resistors to achieve this voltage. The digital output amplifiers required an offset of around 1.5 V. This equates to a biasing voltage of 0.026 V needing to be applied to the positive pin when the gain of 56 V/V was taken into consideration. Combining this voltage with the 0.05 V required to counteract the previous module gave the required offset of 0.076 V. The 4.4 V positive rail voltage was divided through 1.2 kΩ and 100 kΩ resistors to achieve a biasing voltage of 0.08 V. This resulted in a output offset voltage of 1.74 V which would allow for the 1.5 V peak-to-peak signal to be measured by the ADCs.

The passive anti-aliasing filter used in the previous prototype was kept in the amplifier circuit for the digital output of each channel. This filter was not required for the analogue output and was therefore removed, allowing the low output impedance of the inverting amplifier to be utilized [84]. Since this output was likely to be connected to various external devices, having a low output impedance was highly desired.

With the final amplifier module circuit design finished the outputs of the module could be tested. The final circuit diagrams for each channel can be seen in Figure A.7 (Appendix A.1) and Figure A.14 (Appendix A.2). An example output waveform for the final amplifier circuitry can be seen in Figure 4.31, where this figure is the output of the analogue filter. This figure shows how a changing voltage signal centered about 0 V is the output of the amplifier. This output has a higher peak-to-peak voltage than the output for a standard swallow as the dummy load was designed to have a greater impedance change than that due to a standard swallow.

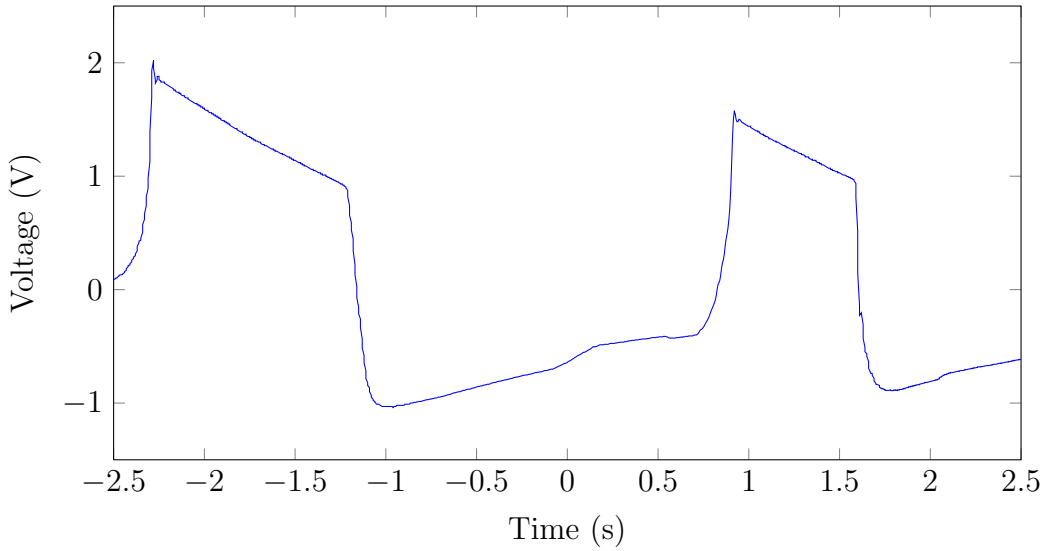

Figure 4.31: *Output of the final amplifier circuitry in the final prototype. This signal is for the output of the analogue amplifier circuit. The dummy impedance load was used as the changing impedance, where rapid transitions over the 10 Ω impedance range were applied.*

4.3.3 Microcontroller

The microcontroller design was kept the same as used in the previous prototype, where the dsPIC30F3013 microcontroller by Microchip Technology [74] was used. However, the interface to the computer was replaced with a separate internal USB to UART module in preference to a cable adaptor.

4.3.4 USB to UART Converter

In order to simplify the set-up of the device, as well as to minimize the number of external components needed, a USB to UART conversion module was included in the final prototype. In addition to reducing the external component count, the on-board chip allowed for a consistent driver to be used with the computer, where previously changing the USB to UART conversion cable often required new driver software to be installed on the computer used. The USB to UART conversion IC used was the FT231X by Future Technology Devices International Ltd [102]. Software that came with the microcontroller allowed for a level-shifting IC to be bypassed when using a USB to UART converter, where the USB to UART converter was connected directly to the UART interface pins of the microcontroller. The microcontroller used a USB type B connector as the interface terminal between the GULPS device and the PC.

4.3.5 Power Supply

The power supply used in the final design was the same used in the second prototype as outlined in Section 4.2. This module used an external ac-to-dc transformer-isolated +6V external adaptor as the power source. An internal voltage inverting circuit was then used to create a negative voltage rail. These two voltages were then maintained by voltage regulators to constant ±4.4 V levels.

4.3.6 GULPS Instrument

The final prototype board was placed inside a 1598D instrument case by Hammond Manufacturing [103] which, together with the external power source, created a portable solution i.e., the electrode-impedance biofeedback or GULPS instrument. This has three external connections: to the external power source, to the USB port on a computer, and leads to the electrodes. Custom electrode collars were used which connected to the device via a RJ45 cable. Two external BNC connectors are also available for auxiliary outputs from the device. This connection arrangement can be seen in Figure 4.32.

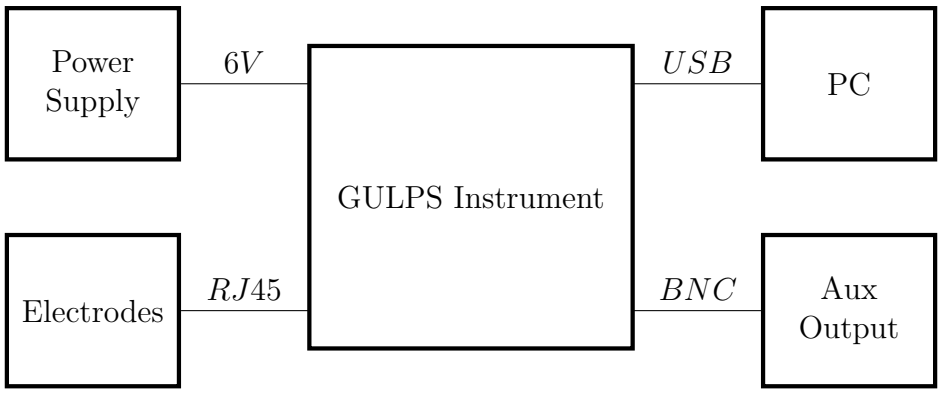

Figure 4.32: *Block diagram of connections to the final GULPS instrument prototype.*

4.3.7 Evaluation - Dummy Load

An evaluation of the final prototype instrument was undertaken to determine its ability to provide consistent results when measuring a changing impedance. This evaluation was conducted on-top of the testing of all the individual modules conducted in Sections 4.3.1 - 4.3.5. It was hoped that the final prototype would provide similar results to the second prototype but with the advantages of having set component values and an easier to manage device. One of the key features observed in the second prototype was its similarity in operation between channels. This again was investigated in the final prototype. Figure 4.33 shows the output of the circuit for the dummy impedance,

where it can be seen that changes in each channel's signals are similar for a varying impedance. These tests used a protocol of first quickly changing the variable resistor over two seconds, creating a slow decrease in impedance and then a slow increase in impedance. Following this a fast change in impedance was applied, again both an increase and a decrease in impedance was used. This was done for each channel. In addition to being able to detect a channel's response to a changing impedance the ability for each channel to operate independently can be seen in this figure. It can be seen that there is only a change in the output waveform of the channel experiencing a change in impedance, therefore any capacitive coupling between channels does not affect the output.

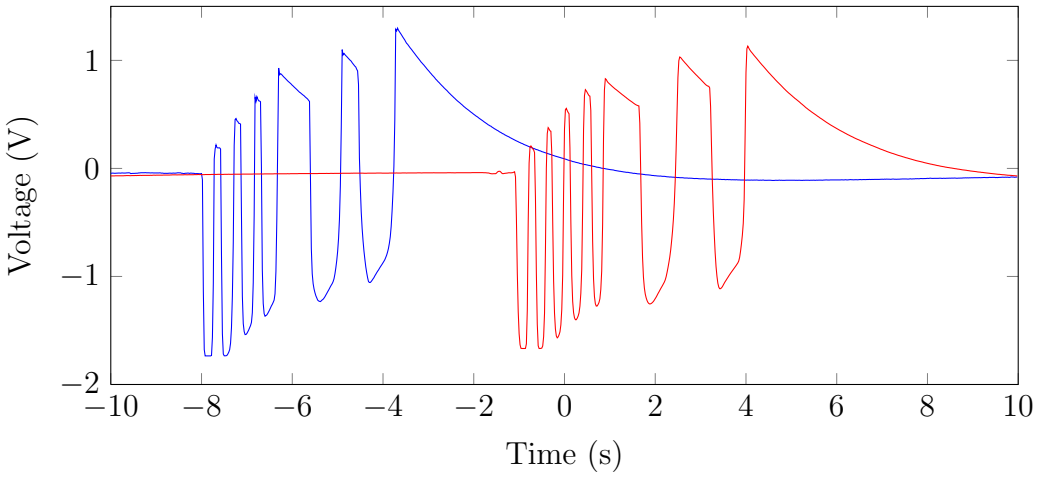

Figure 4.33: *Output waveforms of the final prototype, where the device was measuring the impedance across the dummy impedance circuit. The red waveform is the output of the 70 kHz channel and the blue channel is the 40 kHz channel.*

Inter-channel interference had the potential to be significant issue for this prototype due to the band-pass filters' orders being significantly less than desired. In order to determine the effect of inter-channel interference on the final prototype the sensing probes from each channel were used to measure the opposite channel's signal, using the dummy impedance load. Measuring the inter-channel interference of both channels in the same medium was difficult due to both the medium and the signals changing (as mentioned in Section 4.1.4.4). It was therefore decided that measuring the other channel's signal exclusively was the best way to test each channel's susceptibility to inter-channel interference, where ideally the output waveforms would no longer indicate a changing impedance. The responses following the band-pass filters for the mismatched measurements can be seen in Figure 4.34 and Figure 4.35, where the response of putting the 70 kHz signal through the 40 kHz band-pass filter is shown and vice versa. As expected, the signal present after the band-pass filter in the 40 kHz channel was about

four times larger than that in the 70 kHz channel; the attenuation provided by the band-pass filter on the 40 kHz channel was about 25 V/V. This attenuation was not as desired and its potential effect on the output of the device had to be investigated.

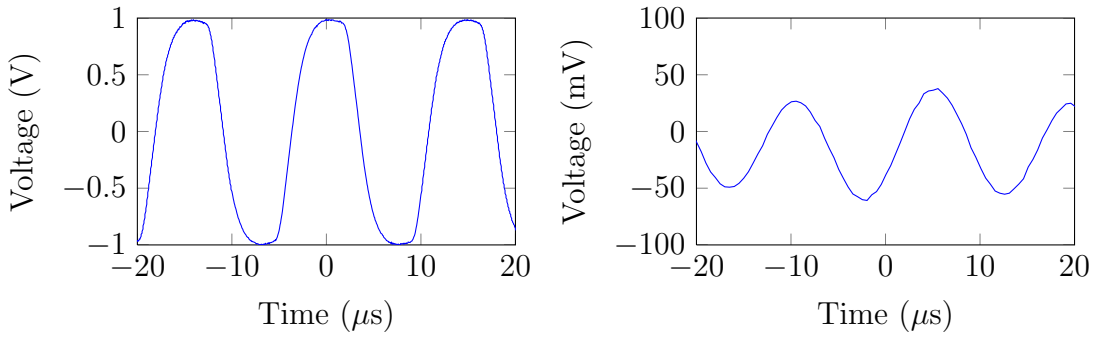

Figure 4.34: *Waveforms produced when the 70 kHz signal is placed on the 40 kHz channel of the dummy load. (a) is the waveform detected by the instrumentation amplifier and (b) is the signal remaining after the band-pass filter.*

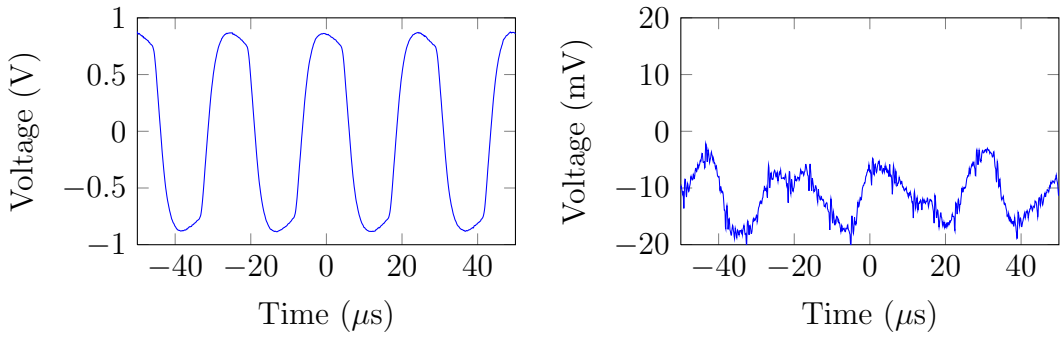

Figure 4.35: *Waveforms produced when the 40 kHz signal is placed on the 70 kHz channel of the dummy load. (a) is the waveform detected by the instrumentation amplifier and (b) is the signal remaining after the band-pass filter.*

In order to determine the effect of the inter-channel interference on each channel the outputs of the GULPS device were analysed for the inter-channel interference set-up. It was found that the output waveforms' responses to a changing impedance when the opposite channels were measured was insignificant. Figure 4.36 shows that the analogue outputs of the final amplifier stage were constant value waveforms, even when the dummy load's impedance was varied over its full 10 Ω range. This response was as desired, where it was found that the inter-channel interference present after the band-pass filters did not contain frequencies that would pass unattenuated through the

envelope detection modules (due to distortion from the band-pass filter). This result allowed further investigation into the final prototype to be completed without the issue of inter-channel interference corrupting the results.

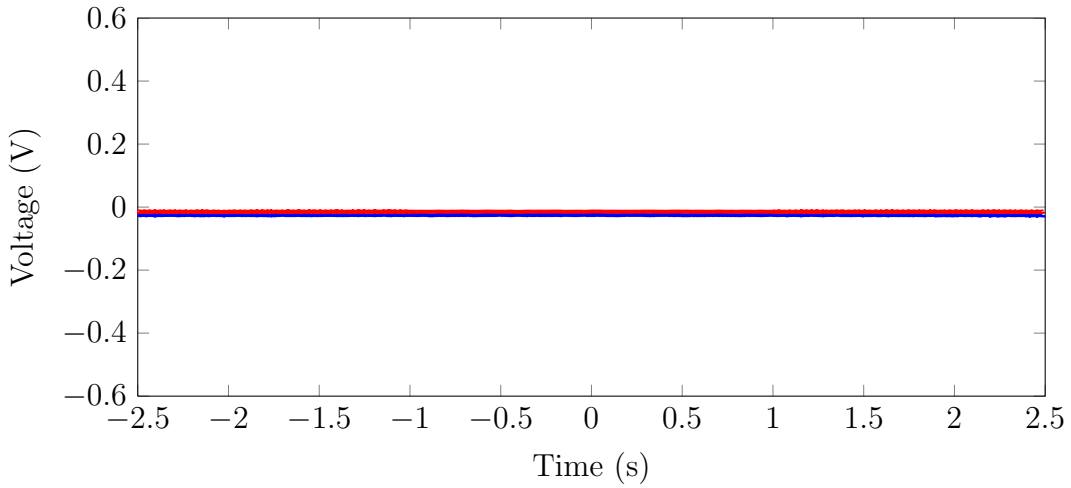

Figure 4.36: *Output waveforms of the final prototype where the 70 kHz voltage sensing probes are on the 40 kHz channel (blue waveform) of the dummy prototype, and vice versa (red waveform). The impedance values of both channels were being altered during this measurement over the dummy impedance's 10 Ω range.*

4.3.8 Evaluation - Impedance Changes Across a Throat

With the circuit's performance for the dummy impedance load analysed, the circuit's performance for measuring the changing impedance of a throat during a swallowing event could be investigated. The response of the output waveforms during three swallowing events can be seen in Figure 4.37, where the electrode positioning had not yet been altered from the previous investigation. This figure showed that the outputs from the device were relatively consistent, with differing outputs from each swallow due to non-identical swallows, rather than a difference in the way they were measured. The only exceptional variations that occurred between outputs happened when either the electrodes or electrode positioning were changed. In addition to a channel providing a similar response between swallows, both of the channels' responses were similar. This was desired as it was hoped that the channels would provide similar, temporally separated, responses. It was therefore concluded that this impedance measuring prototype could be used to investigate the practicality of impedance measurement as a method of detecting pharyngeal sequencing and to determine the potential for further development of this prototype.

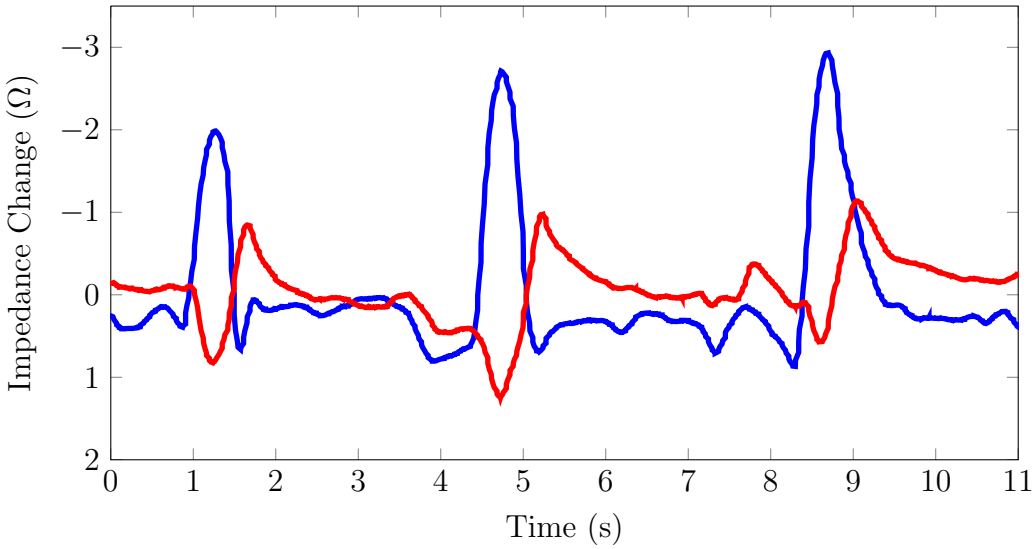

Figure 4.37: *Changing impedance of three swallows measured by the final prototype, recorded from the GULPS software on a computer. The line in blue shows the upper position channel and the red line is the lower position channel. The impedance values have been inverted to somewhat emulate the manometry waveforms - an increasing pressure relates to a decreasing impedance.*

4.4 Summary

The pre-existing hardware that had been developed for the GULPS device suffered from several issues, including one channel not working at all, the other channel not working as expected, and the device not being portable. Three subsequent prototypes were designed and built to obtain a device that would be able to measure the impedance across two positions of the neck. Initially, several independent modules were created that could be joined to create a working prototype. This allowed for easy replacement of faulty modules and modules needing to be upgraded. Following this, the second prototype was built. The second prototype was constructed on a single board, with a second board eventually being incorporated for the power module. This prototype was able to achieve similar performance on both of its impedance measuring channels, but required tuning and had several modules that were inconsistent. A third and final prototype was then constructed. This prototype allowed for consistent, similar impedance measurements for each channel, where fixed component values and a change in design allowed for a much shortened set-up time for use.

The final prototype had several modules that were not ideal but, overall, its performance was satisfactory and was chosen to be used for further investigation. The current generation, instrumentation amplifier, and envelope detection modules were all found to have a circuit design that could be improved upon. The designs used degraded the performance

of the circuit through undesired attenuation and should be improved upon in future developments. These undesired attenuations did not drastically affect the performance of the circuit however, and the impedance measurements of both a dummy neck impedance and a changing real neck impedance were as expected. In addition to these modules, the band-pass filter module should also be improved upon in future designs, where higher-order filters should be used to decrease inter-channel interference. Though inter-channel interference was present in the final prototype, it did not significantly affect the output waveforms. Therefore, the final prototype was chosen to be used for further investigation into whether impedance measurement could detect the sequencing of the pharynx during a swallow.

CHAPTER 5

Electrodes

An important aspect in achieving appropriate results is the type of electrodes chosen to be used, and their placement on the neck. Multiple types of electrodes were tested in different containment apparatus in order to gain results that were of interest and repeatable. Electrode placement was also taken into consideration to ensure informative results were gained from the impedance change during a swallowing sequence. This chapter details the various types of electrode prototypes used, as well as the different electrode positions tested in order to obtain the desired results.

5.1 Electrode Development

The choice of electrode was found to be an important component of the GULPS device, where an electrode that provided consistent and informative results was desired. The type of electrode to be used and how those electrodes would be placed in a consistent position on the neck were investigated. Multiple types of electrodes were trialled in order to find the type that would best detect small changes in the impedance of the neck when combined with the hardware detailed in Chapter 4.

Individual electrodes: The first technique used for placing the electrodes was to attach the electrodes individually by using adhesive gel electrodes. The first electrode trialled was the Blue Sensor NF by Ambu [66] which is a skin-friendly solid-gel electrode that ensures optimal skin-electrode contact during long-term applications. These were the same electrodes used in the previous project and offered a high-quality method of injecting and receiving signals through the throat; the electrodes can be seen in

Figure 5.1. These electrodes were placed individually onto the subject's neck in order to determine the changing impedance. Other electrodes trialled include the Norotrode by Myotronics [104] and the Blue Sensor N by Ambu [105]. Both of these electrodes were found to be less effective than the Blue Sensor NF electrodes due to the signals often being hard to distinguish or becoming noisy. The wet-gel used in these electrodes would often bridge the sensing and current input electrodes, bypassing the tetrapolar configuration. As already detailed earlier in 3.2.1.1 a tetrapolar electrode set-up was used for this project due its ability to minimize the effect of the changing impedance of the skin's surface due to an alternating current being applied and of the changing impedance of the electrode-skin interface [65].

The main issue found with the individual solid-gel electrode configuration was difficulty in achieving appropriately accurate placement for reapplication of the electrodes. This is important in the use of biofeedback as differing electrode placements could lead to differing results, potentially providing patients with unfamiliar waveforms, limiting the ability for ongoing treatment. Limited reusability was also an issue as the adhesive of the electrodes would deteriorate after several reapplications. Positioning the electrodes for use in the same position each time proved to be very time consuming and difficult, especially if the subject had to place the electrodes themselves. The Blue Sensor NF stray electrodes worked well, but their long-term use was limited by needing to replace electrodes often and the issue of placement.

Figure 5.1: *Ambu Blue Sensor [66]*

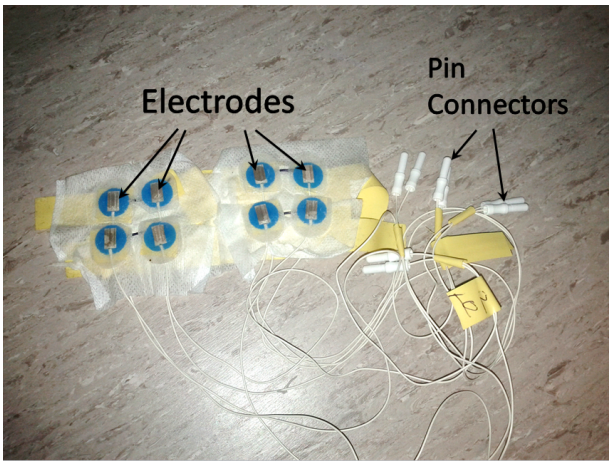

Figure 5.2: *Blue Sensor Collar*

Initial electrode positioning prototype: Electrode positioning prototypes were created so as for users to be able to more easily reapply the electrodes to effectively the same positions. The first prototype contained the previously used gel electrodes housed within a collar of medical tape, with electrodes paced in a symmetrical formation on the

tape as shown in Figure 5.2. This collar solved the problem of adjusting each individual position of the electrodes but the issue of the degradation of electrode contacts remained, where the replacement of an electrode was now more difficult. This collared solution, though having a limited number of uses, was still preferred to using individually placed electrodes for measurement due to the ease of positioning. Using a frame to house the electrodes was useful and was the premise behind the next electrode prototype.

Collared dry electrode prototype: The next prototype combined the use of a cervical collar with easily replaceable dry electrodes. The dry electrodes used were Triode electrodes from Thought Technology Ltd [106]. These electrodes had been removed from their three electrode configuration and combined with pin-to-snap connectors in order to attain the eight electrode set-up needed. They were then combined with a cervical collar from Gordon's Manufacturing [107] to produce the collar seen in Figure 5.3. This collar allowed for easy application of the electrodes to the neck, as well as more permanent, easily replaceable electrodes.

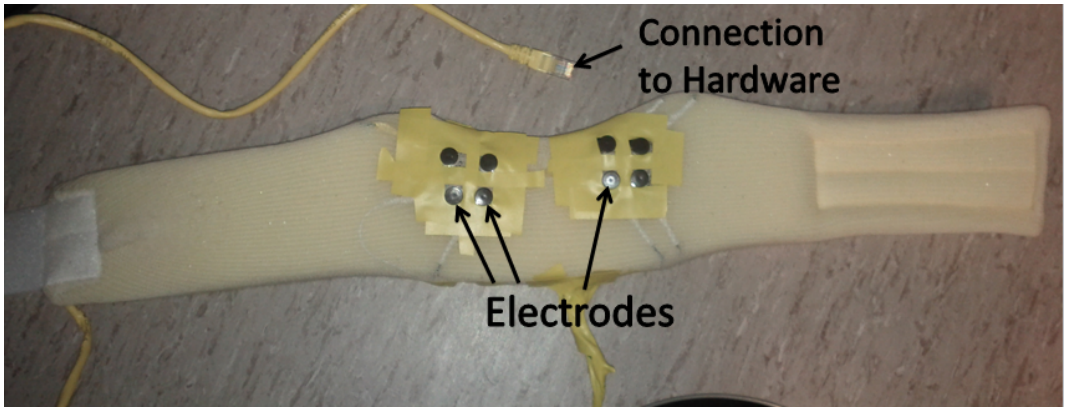

Figure 5.3: *Neck collar with dry electrodes*

Though the combination of the cervical collar and the dry electrodes provided a solution which was able to give consistent placement results, there were drawbacks in this design. The positions at which the electrodes could be placed on the cervical collar were limited to the lower positions of the neck and could not be positioned so as to be in contact with the neck at the position of the pharynx. This meant that the measured changing impedance was most likely due to the movement of other structures in the throat, rather than the pharynx. The electrode positioning for this prototype relative to a human throat can be seen in Figure 5.4, where the electrode positioning was not centred at the pharynx. In order to be able to position the electrodes in the desired area a new prototype was needed.

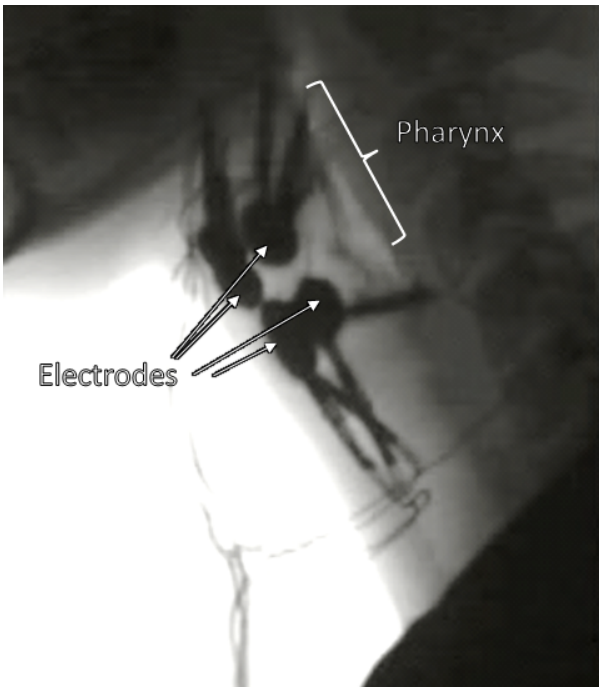

Figure 5.4: *Videofluoroscopy image of the electrode positioning of the cervical collared electrode prototype.*

Wafer prototype: Due to complex movements in the throat during a swallowing event (as described in Chapter 2), reasonably accurate electrode positioning was desired. It was hoped that these precise placements would enable identification of the sequencing of the pharynx using bio-impedance. It was therefore decided that a finely adjustable arrangement of the electrodes should be used in preference to an electrode set-up that is easy to implement. The final electrode prototype consisted of two electrode placement wafers with embedded dry-electrodes to accurately position the electrodes. This prototype used Stomachesive ® skin barrier pads from ConvaTec [108] as a frame to embed the electrodes (Figure 5.5), which would adhere the electrodes to the skin surface at various positions on the neck. This, combined with the ability to place the electrodes in different positions in the wafer, allowed for several electrode position combinations to be trialled. This final electrode prototype had the advantage of being able to be reapplied to specific locations in the neck, without the drawback of needing to replace the components in the prototype after every trial. Double-sided adhesive tape could be reapplied to the wafer in order to use the same wafer over multiple trials.

Figure 5.5: *Final electrode prototype consisting of a adhesive wafer with four electrodes placed into it. Two of these wafers are used for the GULPS device.*

5.2 Electrode Positioning

Electrode placement was found to be one of the key features in achieving a device that would be able to detect the sequencing of the pharynx. Both the signal generating and signal detection electrodes needed to be positioned in specific locations in order to measure the changing impedance across the pharynx. In order to determine the optimal electrode placements of both the top and bottom channels, an investigation was performed into the results gained at various positions.

The main electrodes of interest for this investigation were the signal transmitting electrodes, where the positioning of the signal detection electrodes was kept relatively constant. The detection electrodes were to be positioned close (20 mm) to their corresponding transmitting electrodes. Kushuhara *et al.* [41] found that positioning of the signal detection electrodes had little effect on the characteristics of the signal detected for distances less than 40 mm The main difference found was the level of attenuation, where a greater attenuation occurred when the detection electrodes were positioned further away from the transmitting electrodes (both horizontally and vertically). This led to the signal generation electrodes to be placed relatively close to the signal generating electrodes to maximise the signal measured. However, these electrode positions were chosen to still maintain a reasonable separation from the signal generating electrodes in order to maintain the benefits of the tetrapolar electrode circuit. The boundary tissue can be polarized by the introduction of an electric current, causing the resulting resistance across the throat to change with an ac current. This change is not in phase with the ac current [65]. The tetrapolar configuration prevents this changing impedance

to impact the analysis of the internal tissue by measuring the voltage drop at a separate location. A 20 mm horizontal separation was therefore chosen between the transmission and detection electrodes to satisfy both of the proximity constraints.

An electrode grid was configured to determine the best electrode positioning for detecting the sequencing of the pharynx. A three-by-four electrode grid was created on two wafers of the Stomachesive ® skin barrier pads used in the final electrode prototype [108], one for each side of the neck. The electrodes used were the same dry Triode Electrodes as used in the final prototype [106]. Each electrode was placed with a 20 mm, centre-to-centre, separation in a mesh design, with a 20 mm gap between the outer electrodes and the edge of the adhesive pad. A diagram of the layout can be seen in Figure 5.6. This wafer was able be used to attempt several different combinations of upper and lower channel electrode positions, as well as signal generation and detection electrode positions. To do this, a protocol was established to ensure thoroughness and completeness of the results.

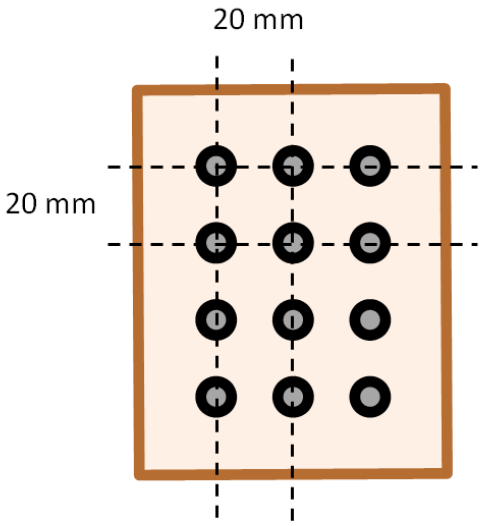

Figure 5.6: *Electrode placement wafer containing 12 Triode electrodes embedded in a Stomachesive ® wafer.*

5.2.1 Placement Protocol

A protocol was used in pursuit of determining the best electrode placement for the GULPS device. Three main procedures needed to be followed when testing the electrode positioning. These procedures encompassed the positioning of the wafer, the electrode combinations to try, and the procedure for swallowing when testing each electrode set. These procedures were clearly outlined before the testing to ensure a consistent, repeatable testing environment and are detailed below.

Wafer Placement: The wafer placement procedure was broken down into three steps which allowed for repeatable positions to be produced. These steps were:

- Place the top edge of the wafer directly under and as close as possible to the ear.
- Place the row of electrodes closest to the jawline as close to the jawline as possible, without having the electrodes on the jaw bone (mandible).
- Line the electrode columns up parallel with the sternocleidomastoid (the muscle running down the side of the neck).

An example of the set-up can be seen in Figure 5.7, where the wafer is placed in the location specified in the protocol.

Note: In some cases, the subject's hair may need to be pinned back to expose the back of the neck.

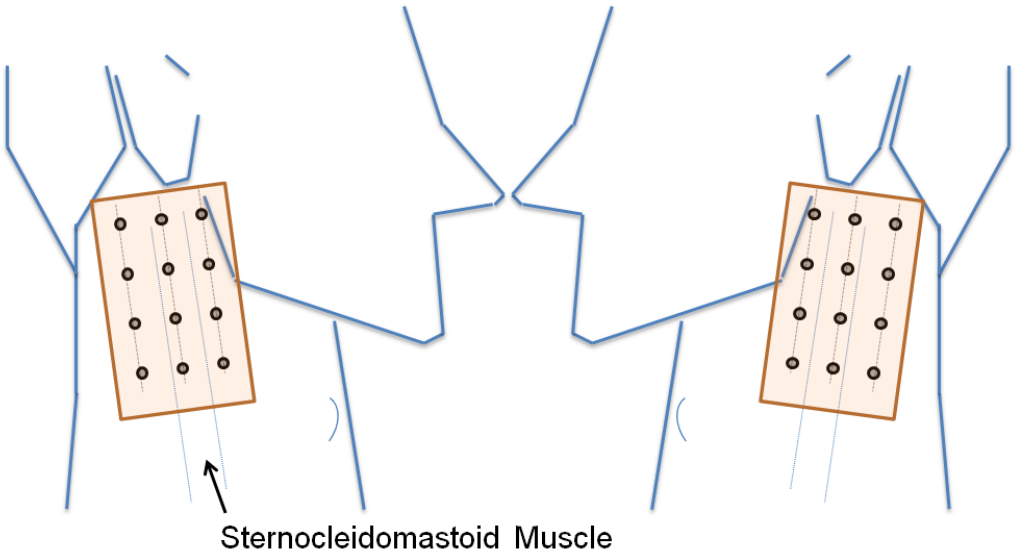

Figure 5.7: *Placement of the electrode mesh wafer used for the electrode positioning trials.*

These electrode positions were chosen due to their relative position to the pharynx, and the lack of movement of the electrodes during a swallow. Rahilly *et al.* [109] stated that the pharynx extends from the base of the skull down to around the C6 vertebral level (Figure 5.8), where it becomes continuous with the oesophagus. The electrodes were therefore placed in order to encompass as much of the region between the base of the skull and C6 vertebral level as possible. The electrode placement was also positioned in order to avoid any movement during a swallow. Due to mandible movement during the swallowing sequence, it was decided that the electrodes should not be in direct contact with the mandible. This resulted in the inner-most electrodes being placed by the edge of the jaw line, where the position of the pharynx is roughly half-way between the chin and the back of the neck (Figure 5.8). This position is roughly the same position as the edge of the mandible.

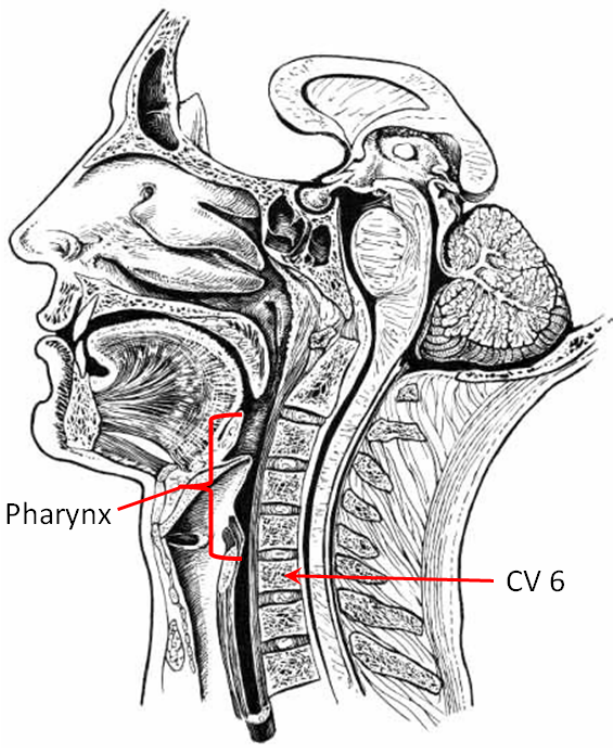

Figure 5.8: *The position of the cervical vertebrae in relation to the jaw [109].*

Electrode Combinations: The set of electrode combinations tried encompassed a systematic shifting of the upper and lower sets of electrodes both forwards and backwards, as well as up and down. The combinations tried were outlined beforehand and can be seen in Figure 5.9, where an identical mirrored wafer for each combination was placed on the other side of the neck. For each of these positions, the signal generating electrodes of each channel were trialled at both the front and the back highlighted columns of

the wafer, where the detection electrodes would be placed in the remaining positions. This meant for the first electrode placement trialled (top left of Figure 5.9), the signal generating electrodes were trialled in both the second and third columns. In addition to this, the signal generating electrodes were trialled in a diagonal formation, were the signal electrodes were at the back position on one wafer and the front position of the other. The combinations trialled corresponded to 24 different electrode placements (more combinations were available but were not tested). The additional combinations included further use of the bottom set of electrodes. These electrodes were located far down the neck and were unlikely to provide any useful information about the sequencing of the pharynx. There was an ability to investigate these positions in further tests if it was found that these positions provided informative results.

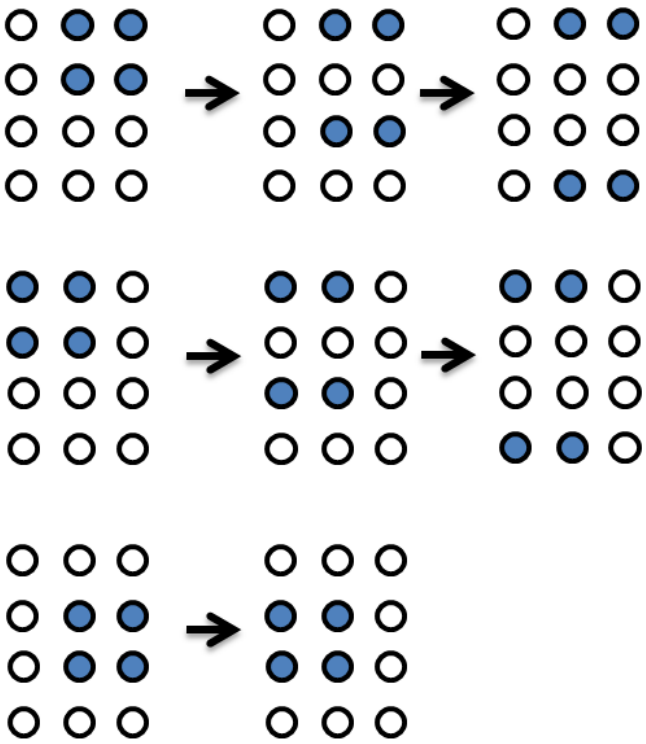

Figure 5.9: *Electrode placements used in the electrode positioning trials.*

Swallowing Procedure: To ensure that not only the placement of the electrodes is correct but also a similar swallowing movement was produced, the third and final protocol stage was implemented. The swallowing protocol outlined that both dry and wet swallows should be performed to investigate the resulting impedance change. Dry swallows are when only saliva is swallowed and it was stated in the protocol that these should be done smoothly with the mouth closed and as little tongue movement as possible; a wet swallow was defined as a swallow using water as a bolus. The protocol for these swallows

stated that the swallows should be done with a constant (30 ml) water sample, where the water is put in the mouth and then swallowed only once the output waveforms have settled from this movement. Again, these swallows were aimed to be done smoothly with minimal force. Five swallows of each style were to be done to assess repeatability of individual swallows.

5.2.2 Results

With the protocol specified, the electrode position trials were able to be performed. The resulting waveforms for several of the positions can be seen in Figure 5.10 and Figure 5.11. Figure 5.10 shows the investigation into the physical positioning of the electrodes and Figure 5.11 shows the investigation into which electrodes should generate the signal and which should detect the signal. These trials showed a variation in the clarity of the features as well as the temporal separation between the two channels' waveforms depending on electrode positioning. These trials were only performed on one subject.

5.2.3 Placement Choice

The results of the various positions needed to be analysed to select the position that produced the best results. Firstly, however, the term 'best results' needs to be defined. The desired result would include two similar, but temporally separated, waveforms with clearly defined features (such as peaks). These features would ideally have a temporal separation similar to that found in pharyngeal manometry. This consistent and definable temporal separation could then be used for biofeedback purposes.

The waveforms that best matched the criteria for the electrode positioning all occurred with the electrodes placed in the foremost positions, around the expected position of the pharynx. This is shown in Figure 5.10, where the waveforms that provided the 'best results' are the top two positions. These waveforms correspond to the electrode positions being in the front two columns and in the top three rows of the positioning wafer. Out of these two arrangements the arrangement consisting of electrodes in the first and third rows of the positioning wafer was found to provide the best results. This arrangement provided a greater temporal separation on average between features than the first and second row arrangement. The average separation between the two peaks in the two channels was 112 ms and 64 ms respectively for the two positions. This temporal separation was closer to the desired separation, where the mean temporal separation found in pharyngeal manometry is around 240 ms [27]. This temporal separation could

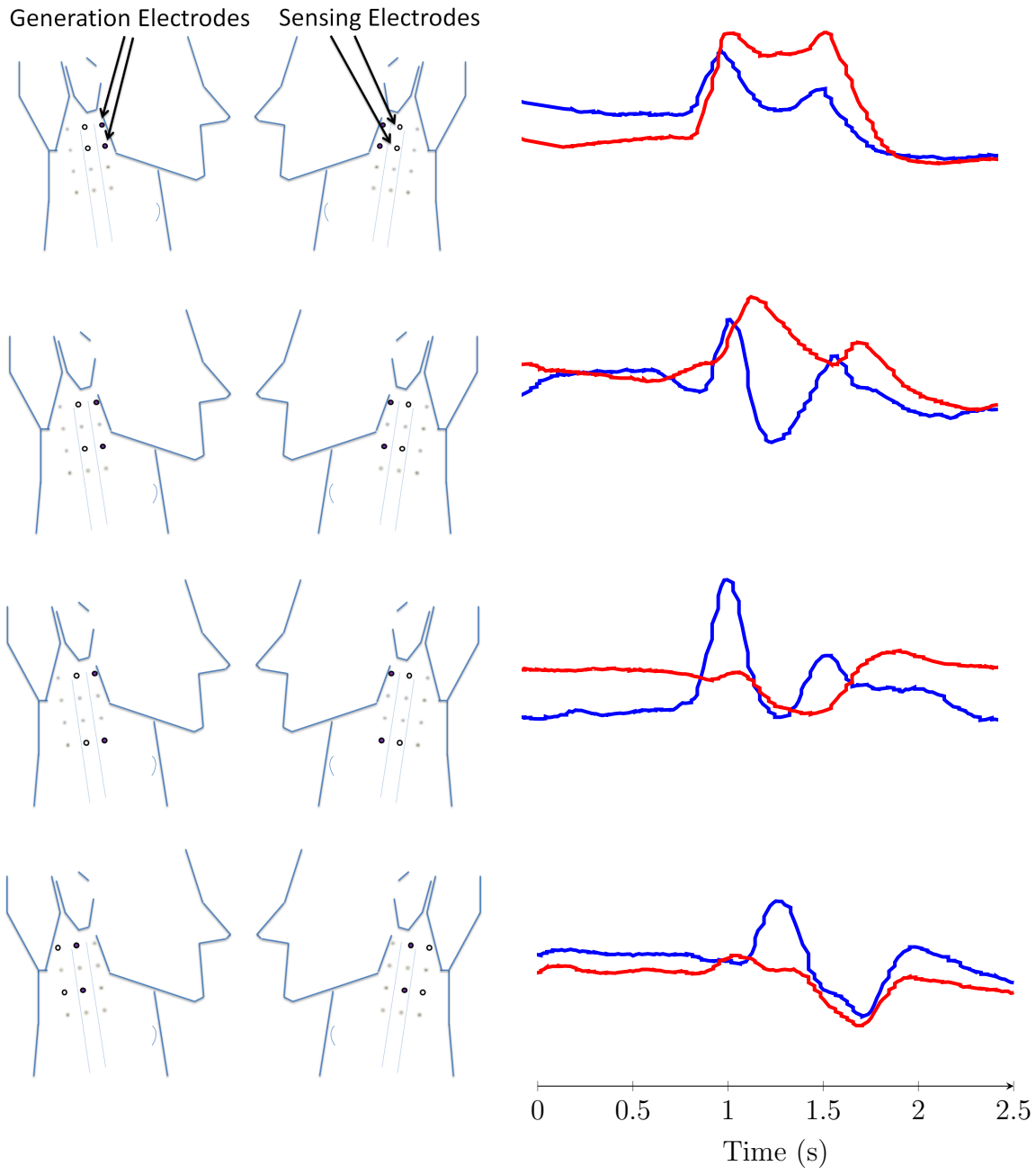

Figure 5.10: *Responses from GULPS device when using different electrode positioning. The signal generating electrodes (purple) are at the foremost position. The blue waveforms are the upper channel and the red waveforms are the lower channel.*

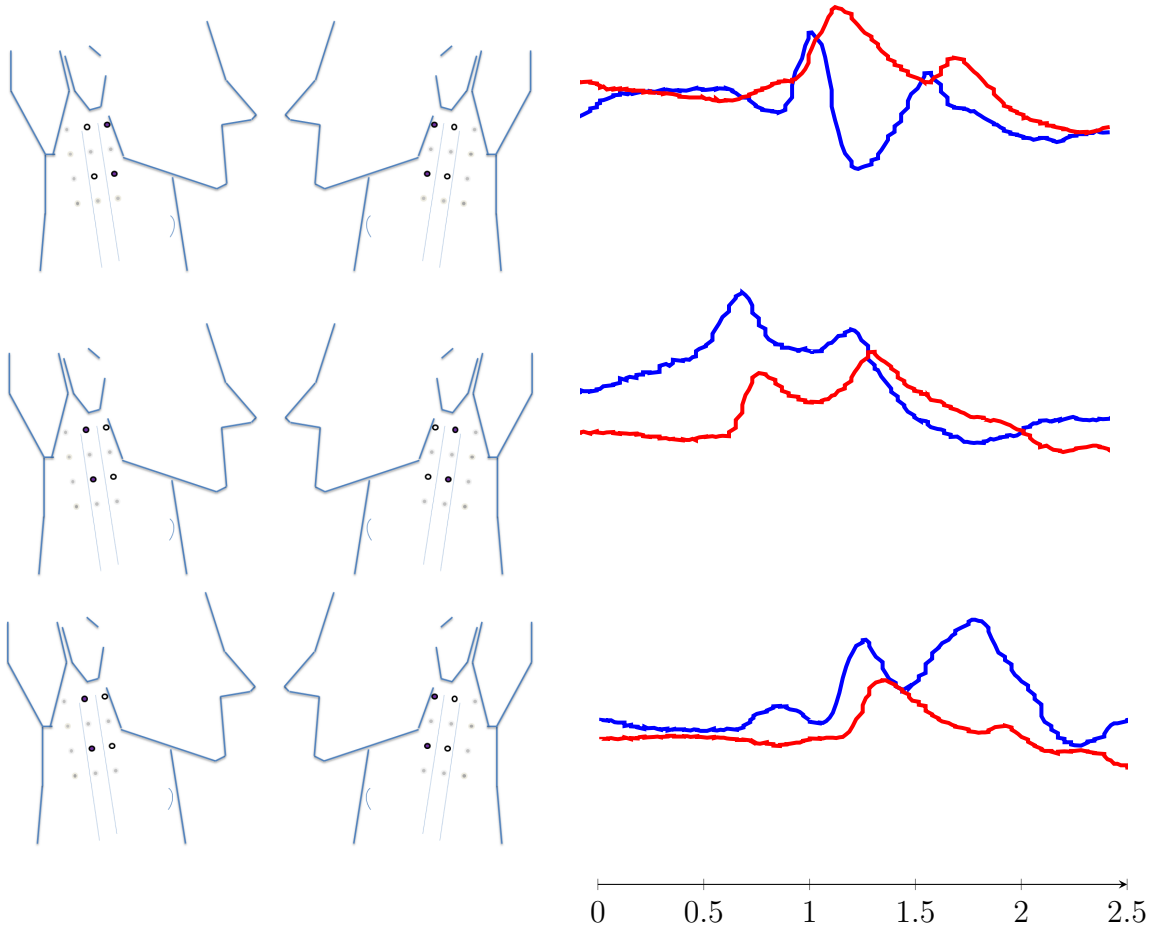

Figure 5.11: *Impedance waveforms for electrodes positioned in the same locations, with differing allocations of the signal generating and detection electrodes. The signal generating electrodes are the electrodes seen in purple. The blue waveforms are for the upper channel and the red waveforms are the lower channel.*

be improved by further separating the two channels, however this heavily impacts upon the other desired features such as signal similarity and defined features. The electrode positioning of the first and third rows in the front two columns was therefore chosen.

In addition to what electrode positions would be used, the arrangement of the signal generation and detection electrodes had to be chosen. The results from the various arrangements of the signal generation and detection electrodes in the chosen electrode positioning can be seen in Figure 5.11. This figure shows that having the signal generating electrodes in the foremost position of each channel provided the results that

best corresponded to the desired response. This positioning provided waveforms that had larger impedance changes during a swallow, as well as more clearly defined peaks. This was the final electrode positioning chosen and can be seen in Figure 5.12.

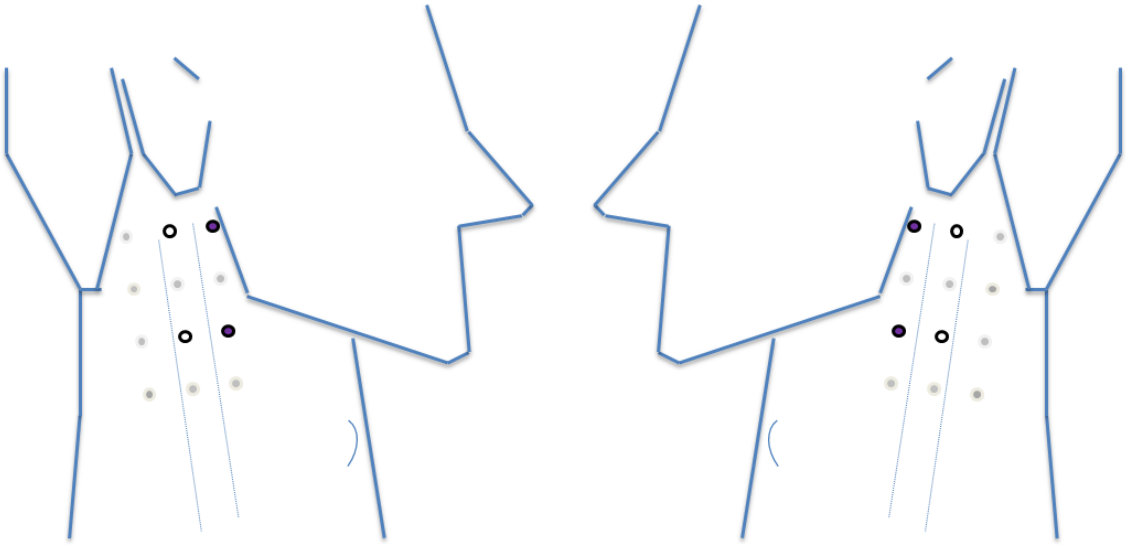

Figure 5.12: *Chosen electrode positions, the signal detection electrodes are the electrodes with a white centre (central) and the generation electrodes have a purple centre (by the jaw).*

In order to validate the placement of these electrodes, several videofluoroscopic images were taken of a throat with the final electrode wafer attached. An image from this testing can be seen in Figure 5.13. This image shows that the electrodes were in the area of the throat containing the pharynx. This electrode positioning therefore not only produced the best results but was also in the location desired to be investigated.

5.3 Summary

The electrodes were found to be an important part of developing a device to investigate bio-impedance for detection of sequencing of the pharynx. Both the electrode type and positioning were investigated in order to determine the optimum set-up for measuring a changing impedance due the movement in the pharynx. Several electrode types were trialled to obtain the best solution, where easily positioned dry electrodes by Thought Technology Ltd [106] were the final choice. These electrodes were chosen to be applied to the neck using easily re-positionable adhesive wafers by ConvaTec [108]. The electrodes were positioned symmetrically in two wafers, one for each side of the neck.

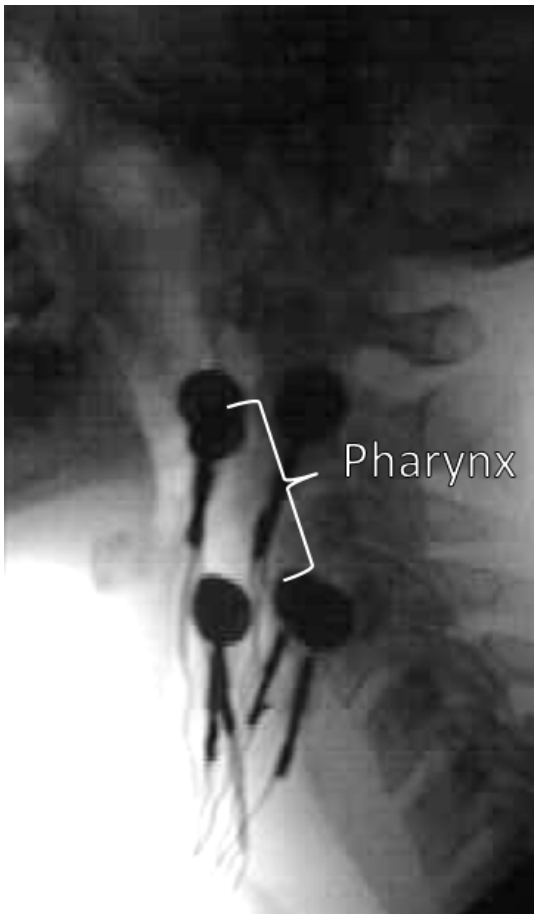

Figure 5.13: *Videofluoroscopy image from the final electrode prototype. This figure shows the positing of the electrodes relative to the pharynx.*

The positioning of the electrode wafers was then investigated in order to obtain the desired results. An array of electrodes was set-up in two adhesive wafers to trial 24 different electrode placements, where the electrode positions were able to be placed in 12 different locations on each wafer. The different positioning not only included changing the electrode separation and locations but also which positions the signal generating and signal sensing electrodes should be placed. The set-up chosen to produce the best results had a 40 mm vertical gap between the two channels and a 20 mm horizontal gap between each set of sensing and generating electrodes. The positioning of these electrodes relative to the pharynx was then investigated. A videofluoroscopic image of the electrodes attached to the throat was taken, where the electrodes were found to be located around the pharynx. With the optimum electrode positioning chosen, the only feature of the GULPS device limiting the continuation of research was the software.

CHAPTER 6

Software

One of the features that severely limited the pre-existing biofeedback device was the operation of the software responsible for interfacing the device with a computer. As stated in Chapter 3, only one channel of the impedance signal was able to be displayed on a computer and the display speed of this channel was unacceptably slow. This chapter outlines the work performed on the software elements involved in this project to enable the hardware prototype to effectively interface with a computer. A section on the adaptations made to the firmware of the microcontroller on-board the hardware prototype is first presented. Following this, a section on the improvements made to the *Microsoft Windows* application for the GULPS device is detailed. This section contains the adaptations made and modules added to the software to appropriately display and record two-channels of data.

6.1 Firmware

For the microcontroller to operate in the manner desired for the final prototype, the firmware from the previous project had to be rewritten. The firmware used for the dsPIC30F3013 microcontroller by Microchip Technology [74] was written in the C programming language. To apply this software to the microcontroller the MPLAB IDE V8.87 by Microchip Technology [110] was used as the programming platform. This platform was used in conjunction with the PICKit3 in-circuit programmer by Microchip Technology [111] to program and debug the microcontroller.

In order to develop the pre-existing firmware further, the aims of what was required from the firmware first had to be outlined. Those were: (1) improve the operating speed of the system to be able to display results in 'real-time' and (2) adapt the firmware to allow for two channels to be measured and transmitted.

6.1.1 Improving Performance

After examination, the firmware in the pre-existing device was found to be the limiting factor in the speed of the system. The microcontroller was previously set-up to operate at 26.67 million instructions per second (MIPS) through Equation 6.1 from the microcontroller's datasheet [74]. The external oscillator had a frequency of 20 MHz, the PLL frequency increase value was set to 16, and the post-scaler was set to 3. This value was previously interpreted as the frequency that the microcontroller would step through the main-loop in the code, rather than the frequency that the microprocessor would complete a single instruction. To try and obtain the desired operating frequency of 10 Hz, the main-loop was set-up in the pre-existing code to only transmit the information via UART once every 2.6 million iterations. Due to an iteration of the loop requiring more than one instruction to complete, this would not result in the frequency of transmission being 10 Hz, but a much lower value [112]. An alternative approach was therefore needed to increase the system's speed and to achieve a more constant transmission frequency.

$$MIPS = \frac{\text{External Oscillator} \times PLL}{\text{Programmable post-scaler} \times 4} \tag{6.1}$$

The solution used to increase the transmission rate of data was to remove the counters previously used to limit the transmission rate of the information. This meant that the speed of transmission of the new firmware would be governed by the ADC's sample frequency of 9.26 kHz per channel, the time for transmission of the information via UART, and the time delay added between transmissions. This set-up was designed as a simple method of increasing the speed of operation. The structure of the code used in the main-loop is shown in Figure 6.1. The time delay used during the transmission of the data was required to send the three bytes of information for each data measurement without data corruption. The transmission of each byte via the UART protocol was found to take approximately 60 μs. If a transmission was attempted while a previous transmission was being performed, the new transmission would override the previous transmission. This was found to often corrupt the data if several transmissions were attempted in sequence. A time delay was therefore implemented between transmissions to allow for the previous transmission to be completed before sending a new transmission. This time delay was chosen to allow for ample time for the transmissions to be completed as well as to govern the frequency of transmissions. Delays that would correspond to a

frequency of about 50 Hz were chosen, where it was assumed that delay length would be substantially larger than any other operation in the microcontroller. A frequency of 50 Hz correspond to a delay of 20 ms in total. The chosen solution did not create an exactly determinable constant frequency of data transmission, where the frequency was still governed by the speed of the various operations occurring during the main-loop. However, it was found to be always in the region of 50 Hz allowing the signal to be viewed in 'real-time'; this rate exceeds the Nyquist rate for the 20 Hz swallowing data.

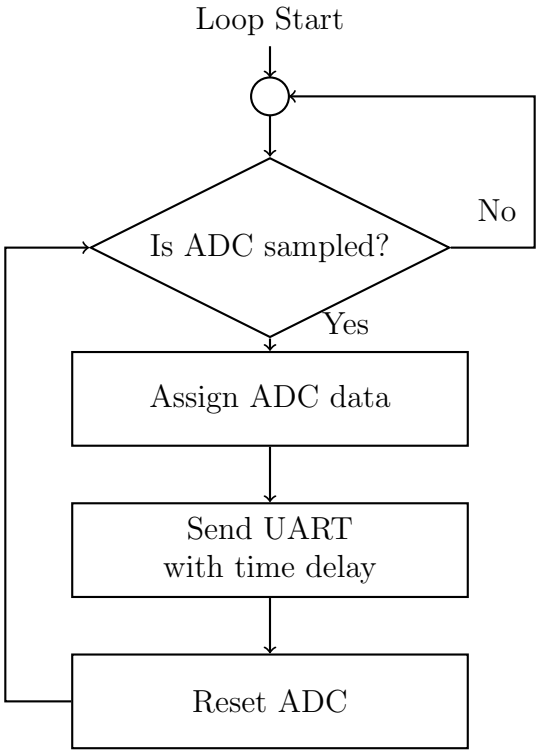

Figure 6.1: *Structure of the main loop in the firmware used to increase the data rate.*

6.1.2 Two Channel Performance

The majority of the code needed to implement two channels of measurement and transmission was already present in the pre-existing firmware, with only additions to the transmitting section of the code being required. The code relating to the measurement of the two ADCs was already in place and being used in the pre-existing firmware, where only one chosen channel's data was transmitted. The transmission of two channels of measurement required the serial data protocol discussed in Chapter 3 to be extended to allow for two channels of measurement. The protocol chosen was essentially the same as the previous protocol, except four bytes of information were sent instead of the previous

two bytes (Figure 6.2). In order to decode and display the data sent through this new protocol, the software used on the *Microsoft Windows* based system also needed to be adapted.

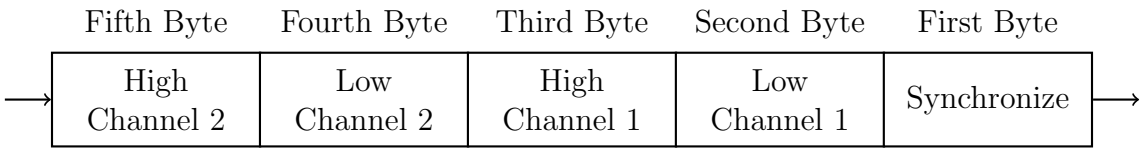

Figure 6.2: *New data packet format sent through the UART connection.*

The final firmware code used in the main function is shown in Appendix C.1. This code's operation is not ideal as the rate of transmissions is still dependent on the speed of the system, rather than a known time value. However, the system performed as required and, therefore, further improvement of the code was not a priority. Notwithstanding, if further investigation requires a constant known frequency of transmission to be used, the code should be adapted to implement a set-up using an in-built timer.

6.2 Bio-impedance Software (GULPS.exe)

In order to display both of the impedance measuring channels on a monitor simultaneously the GULPS software was created. This software was a continuation of software written to interact with the pre-existing hardware device (described in Chapter 3). This pre-existing software was written in the Python programming language and allowed for one channel of data to be viewed in real-time (while using correctly functioning firmware). The GULPS software was designed with the goals of adapting the pre-existing software to interface with the GULPS device, display two channels of impedance measurements simultaneously, and be easy to use and set-up.

The GULPS software was designed to inherit several modules from the pre-existing software as a basis for the code. This pre-existing software was an adaptation of a software called BiSSkiT which was created in another research project. As mentioned in Chapter 3, the BiSSkiT software was designed to be used for EMG biofeedback and rehabilitation purposes. The pre-existing GULPS software inherited all of the features from the BiSSkiT software to display one channel of impedance measurement data. This was excessive as only a few of these modules were actually required to display this data. It was therefore decided that only the required modules would be inherited by the GULPS software. These modules included the main module, three user interface modules, a module for connecting to the bio-impedance measuring device, and, finally,

a module to plot the received data. The structure of the GULPS software, including the inherited modules and additional added modules can be seen in Figure 6.3. The majority of the modules were inherited from the pre-existing software, with only the *Serial Find*, *Save Plot*, *Review Frame*, and *View Plot* modules being created for this project. However, all of the inherited modules were required to be adapted to create software specific to the GULPS device.

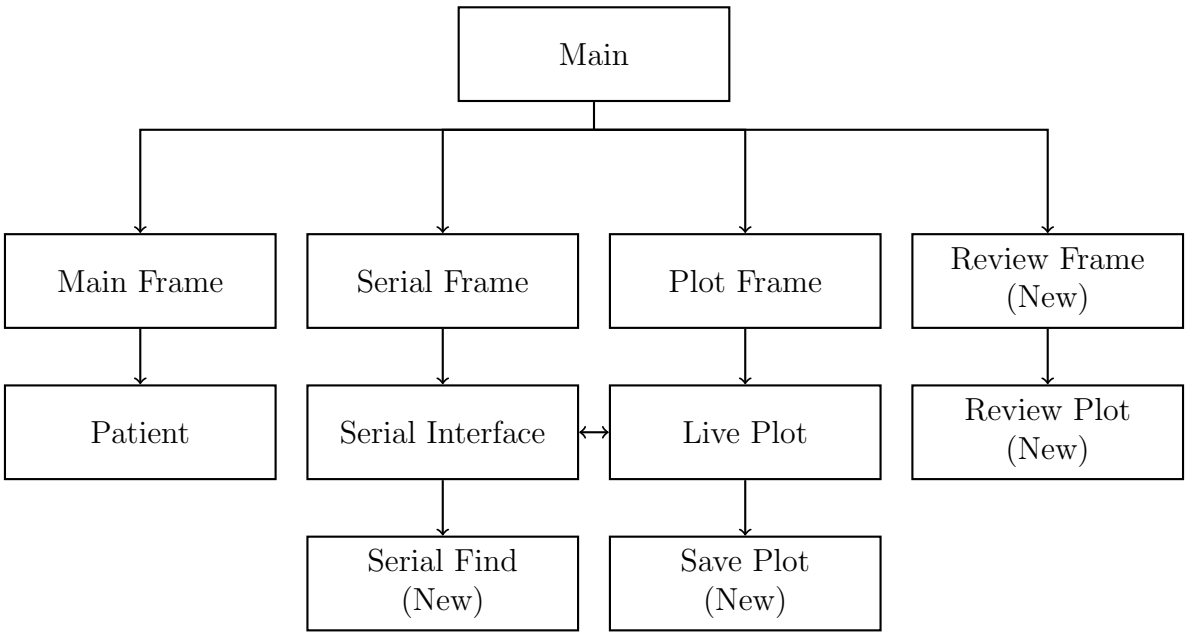

Figure 6.3: *Structure of the GULPS software. The modules labelled New were created for this project and the remaining modules were inherited.*

6.2.1 Inherited Modules

To be able to display the impedance measurement waveforms several pre-existing software modules could be inherited and adapted in order to set-up a 'real-time' display of two channels of impedance measurement.

6.2.1.1 User Interface Modules

Three graphical user interface (GUI) modules were inherited from the pre-existing hardware modules to create an application that was easy for the user to operate. The BiSSkiT software was designed to be operated by clinicians and researchers, where ease of use was of high priority. Due to the GULPS software fitting similar criteria, the three relevant GUI modules were inherited. The three modules were: *Main Frame*, *Serial Frame*, and *Plot Frame*. Each of these modules were adapted in order to be specific to the GULPS system, where options not related to this system were removed.

Main Frame: This module produced the main screen GUI for the software which is presented when the software is opened. This module was used to display and interface with three main areas: the patient information, the creation of a session, and the revision of a previous session. An example of the interface produced by this module is shown in Figure 6.4. The primary difference between this adapted module and the pre-existing module was the inclusion of the review session interface. The ability to review a session within the software was a feature added to the GULPS system. The sections of the GUI relating to the patient information and session creation were also adapted from the pre-existing software. The patient interface now provided session information relevant to this project, where swallows per session and the characteristics of those swallows were available to displayed but are not used in the current software. The interface to start a session was simplified from the pre-existing software to a single 'Start Session' button; the pre-existing software allowed for several session types to be chosen relating to the BiSSkiT swallowing training.

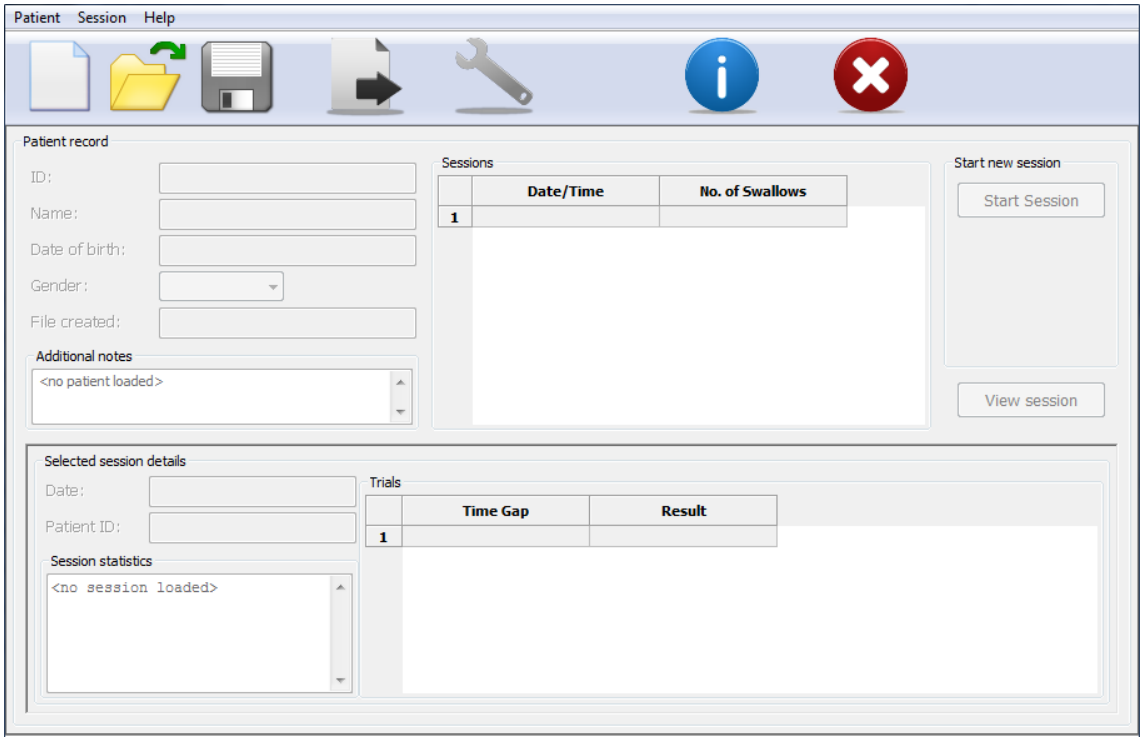

Figure 6.4: *Main screen of the GULPS software*

Serial Frame: When a session is started in the GULPS software, the user is presented with a GUI prompting them to connect to the GULPS device. The module governing this interface was inherited from the pre-existing software. This module was adapted to allow for an auto-connection function to be used to automatically connect to the GULPS device, where previously the port that the device was connected to had to be manually found and entered. The final layout of the serial screen is shown in Figure 6.5.

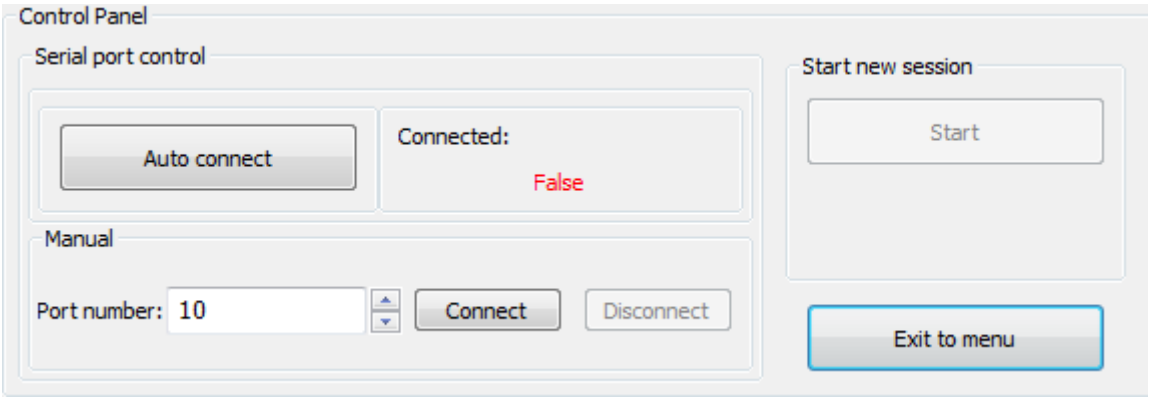

Figure 6.5: *Serial connection screen of the GULPS software*

Plot Frame: With a connection to the GULPS device established, the waveforms could be viewed through the use of the final inherited GUI module. Due to research being the primary objective of this project, a simplistic GUI was designed for displaying the waveforms, as more advanced controls could be added in future development. The GUI was centred around the *Live Plot* module, which is responsible for displaying the output waveforms. Several plotting controls were also present in this GUI. These controls consisted of the ability to pause the display, scale the output, and save the received data. This frame can be seen in Figure 6.6.

6.2.1.2 Background Modules

The modules controlling the functionality of the information displayed in the GUIs were edited in order to be relevant to this project.

Patient: The pre-existing software had a module designed to manage patient information, in which each patient would have their own user data. This user data would consist of the patient's information, such as their name and date of birth, as well as session information. This module was inherited and implemented in a similar way in the GULPS software, where the module was adapted to record relevant information for the GULPS

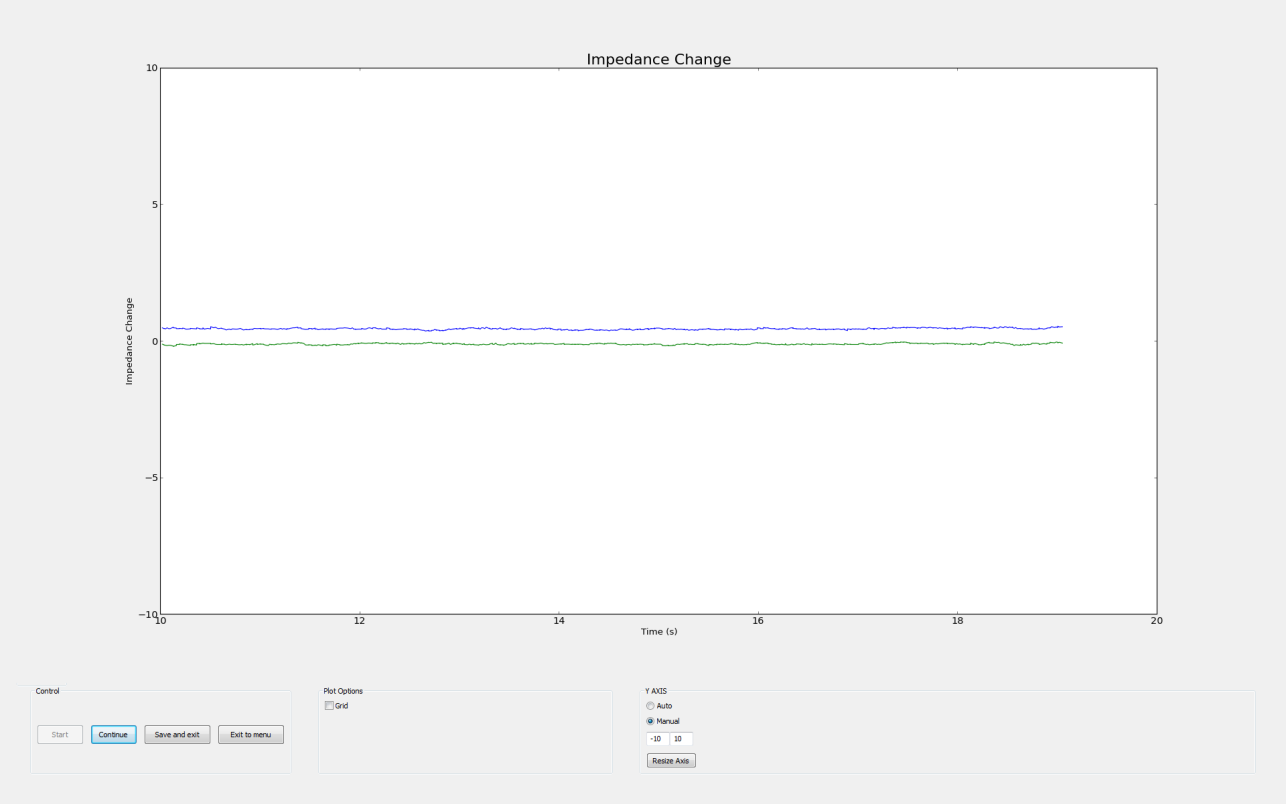

Figure 6.6: *Waveform display from the GULPS application*

device such as the number of sessions conducted and the length of each session. These features allowed for the bio-impedance data to be effectively labelled and stored. Again, this module was developed to allow for future improvement. The inclusion of data on each specific swallow in a session was included.

Serial Interface: In order to interface with the GULPS device, the *Serial interface* module was inherited from the pre-existing software. This module was able to communicate with the device via the UART connection in order to retrieve the data from the device. The data was interpreted by using the protocol shown in Figure 6.2 to decode the received data from the UART connection, where the software would first locate the synchronization byte to be able to decode the data. These extracted data values were initially paired with the time values provided by the pre-existing software in order to produce a two-dimensional waveform. However, these time values were found to be inaccurate due to the time values being generated by iterating a pre-specified time step. Due to the time between data points not always being a constant value, an alternative approach was taken. The chosen method was to determine the time elapsed since the start of the trial by an actual time difference, rather than an estimated difference. To

achieve this the system clock of the computer was used to obtain an accurate time base for the measurements. With an accurate two-dimensional representation of the impedance data available the data could be transmitted to the *Live Plot* module which controlled the display of the data.

Live Plot: To display two channels of data simultaneously the inherited plotting module of the pre-existing software needed to be adapted. The matplotlib python package [113] was used to display the output waveforms inside a two-dimensional axis. This display was able to be continuously updated to create an animated waveform. In the GULPS software this module was updated to accept and display two channels of impedance measurement data. This was completed by simply providing the plotting function with the additional x and y data points to display. With the ability to display two channels simultaneously without delay, the main two limiting features from the pre-existing software had been corrected. However, several improvements were still required to increase the ease of use of the software.

6.2.2 Created Modules

To add additional functionality to the GULPS device, several additional modules were added to the software. These modules allowed for the session data to be effectively saved and reviewed at a later time. In addition, the connection to the serial device was simplified, where an automatic connection protocol was established.

Save Plot: The *Save Plot* module was written to save the session data into a comma-separated variable (.csv) file at the end of each session. This data was arranged in a four row arrangement, two rows for each channel (one row for time and one row for the GULPS data). This data format was chosen as a comprehensive csv module exists for the Python language [114] as well as being a commonly-used format in external data processing programs such as *Matlab* [115].

Review Frame: A further GUI module was created in order to view previously recorded sessions. This module was very similar to the *Plot Frame* module, where the main differences were the controls available. The controls used for the review plot included the use of 'left' and 'right' buttons to shift the window of time viewed forwards or backwards; the plot was displayed in ten second intervals. These controls, paired with the same plot scaling controls used in the *Plot Frame* module, allowed for certain areas

of the saved waveforms to be investigated. In addition to the controls, a central graph was present as the focal point of the GUI. This was as with the *Plot Frame* module, except the module was the *Review Plot* module instead of the *Live Plot* module. An example of the complete GUI provided by this module is shown in Figure 6.7.

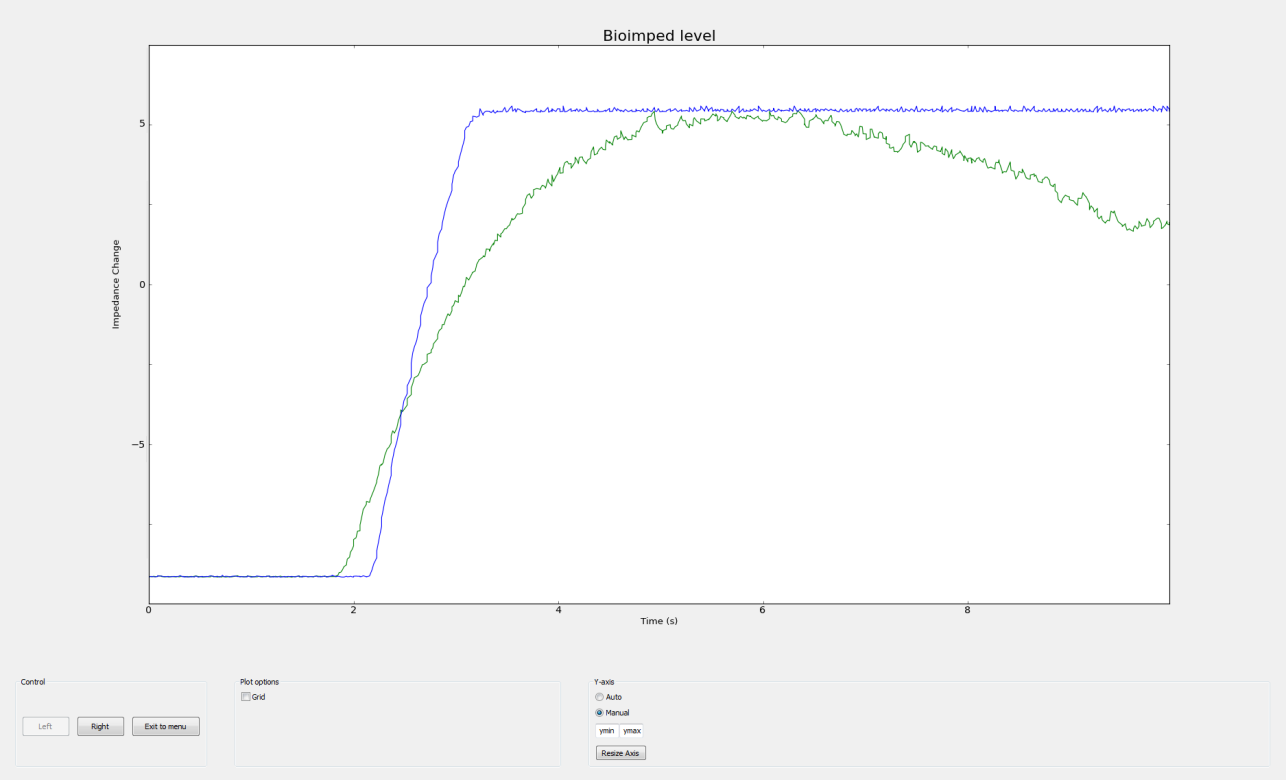

Figure 6.7: *Session review from the GULPS application*

Review Plot: The *Review Plot* module was similar to the *Live Plot* module, as the *Review Frame* was similar to the *Plot Frame*. This module received its data from saved csv data files and displayed the two waveforms in a static format, where ten second intervals of data would be presented. This differed from the *Live Plot* module which displayed its received data in an animated format, resetting the display when the data reaches the right-hand side of the screen.

Serial Find: In order to improve the ease of use of the GULPS system, the *Serial Find* module was created to automatically establish a UART connection between the software and hardware. In the pre-existing software the COM port of the computer that the device was connected to had to be manually input into the software for a connection to be made to the device. Due to this not being very 'user-friendly', where users not familiar with computers would struggle to find this information, the automatic connection module was

created. The use of the FT231X UART-to-USB converter IC by FTDI allowed for a constant COM port name of 'VCP0' to be created [102]. This name remained the same even when a different computer was used and allowed for the port to be found using recognition algorithms.

6.2.3 Distribution

To enable the GULPS software to be used without the need to install additional software, the GULPS application was packaged into an executable (.EXE) format. This executable included all of the modules required to run the application, both Python distribution modules and GULPS software modules. Traditionally, to run applications written in Python requires the Python interpreter to be installed on the computer [116]. In addition, several Python packages were required to be installed to operate the GULPS software. This limited the ability to use the GULPS software on different computers, where administration rights would be needed to install these distributions. To negate these issues the GULPS code was packaged into an executable file using the PyInstaller program [117]. The PyInstaller program created a frozen binary executable to allow for the code to be launched in the same ways other executable programs are. This created the final GULPS.exe application.

6.3 Summary

Both the firmware and software existing from the previous system had to be altered in order to obtain the desired operation of the system. In order to fix the issue of a slow transmission rate present in the pre-existing system, the firmware of the microcontroller used in the hardware had to be rewritten. The pre-existing firmware used an inexact method of limiting the transmission rate of the data over the UART connection. This was found to cause the transmissions to occur at a rate far slower than the desired 10 Hz. This code was rewritten to create a firmware capable of transmitting the data at 50 Hz, allowing for a 'real-time' display of the waveform to be achieved.

The software used to interact with the GULPS device was a Python-based application that inherited the majority of its functionality from the pre-existing BiSSkiT software. The GULPS software allows for the user to create a profile and then connect to the device to view a 'real-time' display of the impedance measurement data. Several modules were added to the inherited modules to added additional functionality. These modules included modules for saving and reviewing session data as well as a module to automatically connect to the GULPS device. This software was packaged using the PyInstaller program to create an executable application which could be used without prior installations.

CHAPTER 7

Results

This chapter details the results of preliminary trials of the GULPS system's ability to detect pharyngeal sequencing using bio-impedance. An ethics application and approval process is first highlighted outlining the steps undertaken to ensure the research was ethical. Following this, the results of testing the system on healthy subjects aimed at quantifying pharyngeal sequencing is covered. This section analyses the results of the GULPS system in both a standalone configuration and when used alongside pharyngeal manometry. Finally, the results of the GULPS system's ability to detect pharyngeal sequencing in a dysphagic subject who presents the condition of pharyngeal mis-sequencing are presented.

7.1 Ethics

Before the GULPS system could be trialled on any subjects, a concerted effect was made to ensure that the study was ethical. To achieve this, an application was made to the Southern Health and Disability Ethics Committee (HDEC) requesting ethical approval. Jointly with any other health and disability ethics committee(s), the Southern HDEC has responsibility for reviewing health and disability research occurring anywhere in New Zealand [118]. An application for ethical approval was made through the expedited review pathway in the HDEC's application process. The device was to be evaluated on up to four 'healthy' and up to four dysphagic subjects. The GULPS device was classified as a low-medium risk (IIa) device using the Australian Regulatory Guidelines for Medical Devices [119].

The application for ethical approval was approved by the Southern HDEC allowing for further research to be ethically conducted. This approval was received on 13 June 2013 (reference *13/STH/50*). This approval was conditioned upon subjects being required to give informed consent, advertisement material being required to include information relating to the new impedance method and how it will be trialled against the nasal monitor so that participants are aware that a nasal tube will be inserted.

7.2 Healthy Subjects

In order to evaluate whether the developed GULPS system could detect the sequencing of the pharynx, testing was initially performed with subjects who had correctly operating swallowing mechanisms. The use of the device on these 'healthy' subjects allowed for the investigation into whether any temporal separation between waveforms related to pharyngeal sequencing could be detected.

7.2.1 Standalone Device

Initially the GULPS system was trialled in a standalone fashion to examine the device's ability to create two similar channels of impedance data with a temporal separation. The device was trialled on three healthy subjects, two male and one female, aged 20-24 years, to ensure similar outputs could be achieved between subjects. These trials were conducted using the same swallowing and wafer positioning protocols established for the electrode positioning trials (outlined in Chapter 5). These protocols allowed for two channels of similar temporally separated waveforms to be achieved. Examples of the waveforms received from the three 'healthy' subjects effortfully swallowing a wet bolus are shown in Figure 7.1. These waveforms were as desired, with each subject's waveforms being of similar size and contained similar features.

The results in Figure 7.1 show two peaks and a trough in both waveforms of each subject's results. These features are different to those produced in pharyngeal manometry which usually contains only one large peak for each channel, rather than two. Additional information was therefore needed to categorize these features. The large number of muscles used during a swallowing sequence means that several movements could potentially be responsible for the features in the GULPS waveform. To gain a better understanding of these waveforms, pharyngeal manometry was used simultaneously with the GULPS system to provide additional spatiotemporal information.

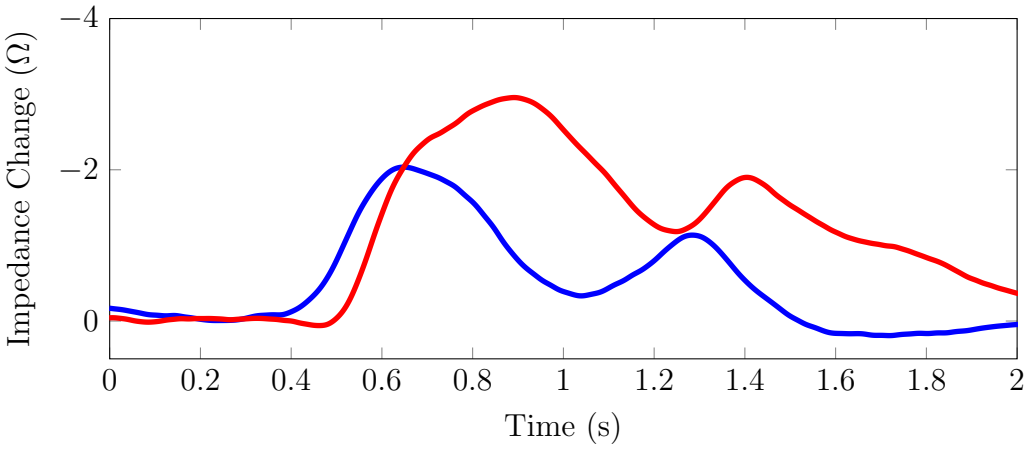

(a) *First male subject*

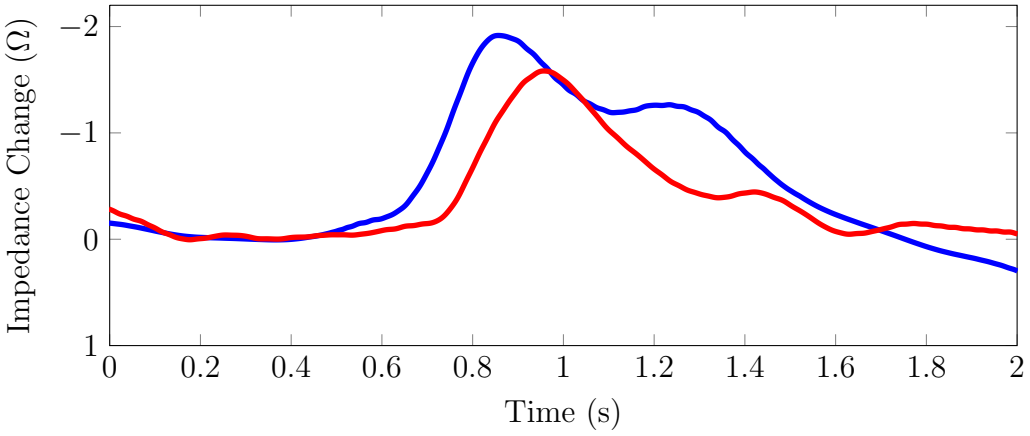

(b) *Second male subject*

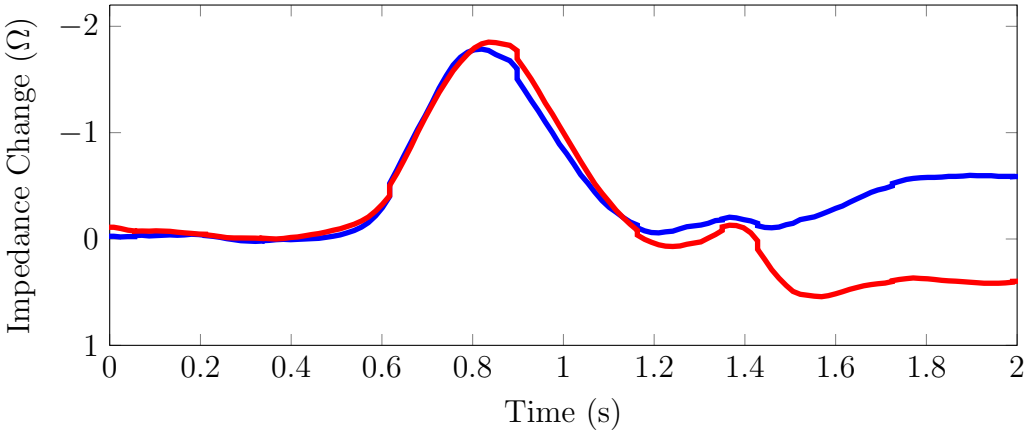

(c) *Female subject*

Figure 7.1: *Output waveforms of the three 'healthy' subjects using the GULPS device. The swallows were of wet boluses with a effortful swallow. The blue waveform corresponds to the top channel and the red waveform to the bottom channel.*

The results for each subject in Figure 7.1 show that similar features can be achieved from each subject, but this is not the case for every swallow. These features were not always visible in a swallowing sequence, with the trough and second peak often not detectable. This loss of detail most commonly occurred when a reapplication or readjustment of electrodes was performed. This problem meant that often the electrodes would have to be reapplied several times before the desired waveforms could be reproduced. In addition to electrode positioning, the type of swallow was found to affect the waveform received. An effortful swallow, using water as the bolus, was found to be the most effective at producing the second peak and trough. An effortful swallow with water was found to produce a swallow containing all of these features in 64% of swallows, after a correct electrode application was performed. This was in contrast to 22% for a normal water swallow and 16% for a regular dry swallow. Sample results of output waveforms not containing one or more of these features can be seen in Appendix D.

7.2.2 GULPS alongside Manometry

In an attempt to identify the features of the GULPS waveforms, pharyngeal manometry was used alongside the GULPS system. To achieve this, the pharyngeal manometer was inserted into the pharynx at the same time the GULPS system was connected to a subject. This set-up allowed for the investigation into whether any of the features produced by the GULPS waveforms aligned with the features in the pharyngeal manometry waveforms. An example of the waveforms produced by both of these systems during a swallowing sequence can be seen in Figure 7.2. The GULPS system's outputs for these trials were collected from the auxiliary outputs of the GULPS device. These outputs were connected to the manometry workstation to allow for synchronization of the time scales.

The output waveforms of the GULPS system to varied substantially more during a session in which pharyngeal manometry was used, potentially due to the invasive nature of pharyngeal manometry. The subjects often were unable to follow the swallowing protocol due to discomfort. It was found that 23% of effortful swallows with water as the bolus presented the three outlined features, down from the 64% without manometry. Though obtaining these three features was more difficult, data containing these three features was still able to be obtained and compared with the manometry data.

Analysis of an initial eight selected swallows using both the manometry and GULPS systems found that none of the features could be categorically determined to align with the pressure peaks in the manometry waveforms. The results chosen to be analysed at this stage only included waveforms that contained all three of the identified features,

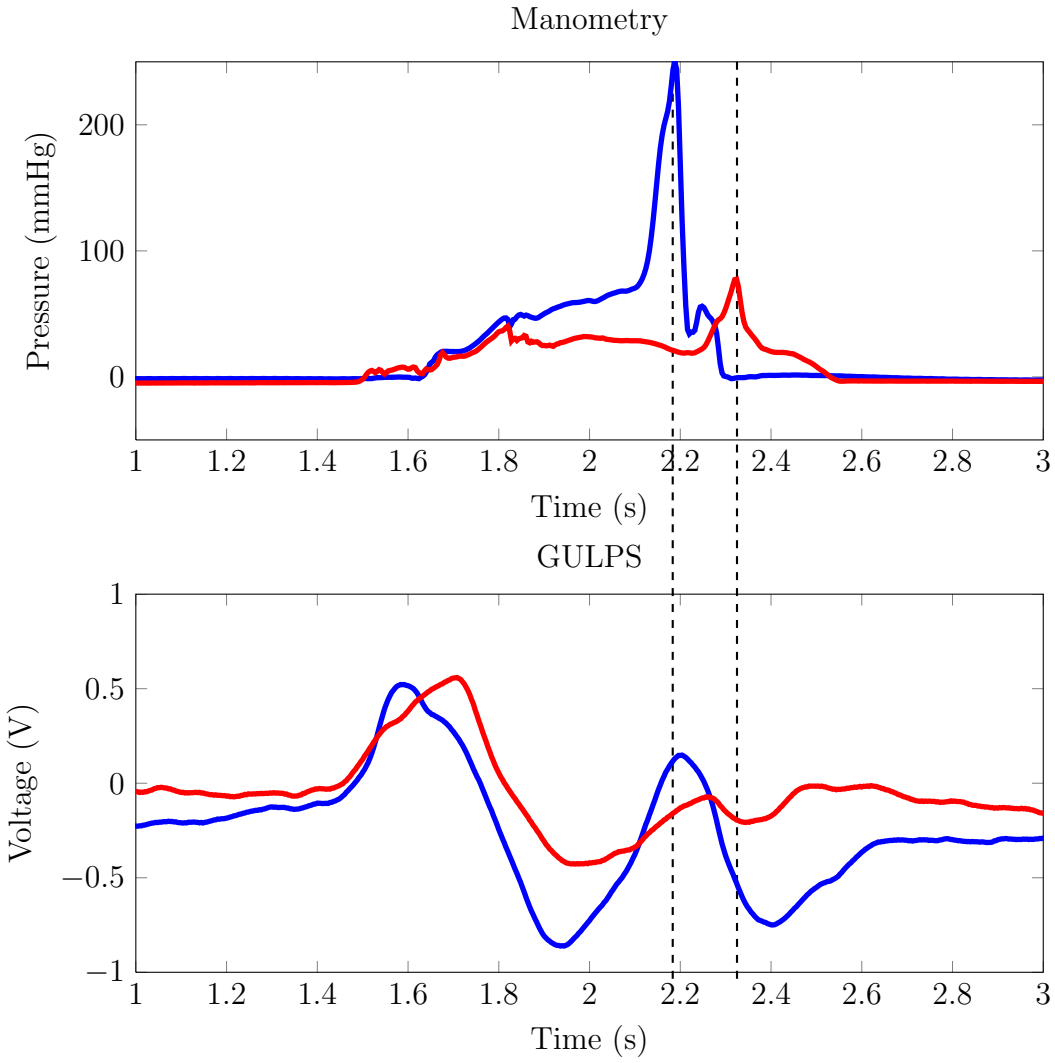

Figure 7.2: *Manometry and GULPS used alongside each other. The blue waveform the upper channel of measurement and the red waveform of each waveform is for the lower channel of measurement of each device respectively.*

where the features were required to be prominent for this initial identification process. It was found that the first peaks of the GULPS device occur substantially before the pressure peaks in all of the examined waveforms, where they are more likely to correspond to the onset of pressure. The troughs and second peaks present a closer temporal relationship to the pressure peaks but a constant temporal relationship could not be found. Both the troughs and second peaks were found to occur both before and after the pressure peak of the relating channel of pharyngeal manometry in the same session. This can be seen in Figure 7.2 and Figure 7.3, where the blue waveform's peak in the GULPS waveform occurs approximately at the same time as the pressure peak in the first figure and then substantially after in the second figure.

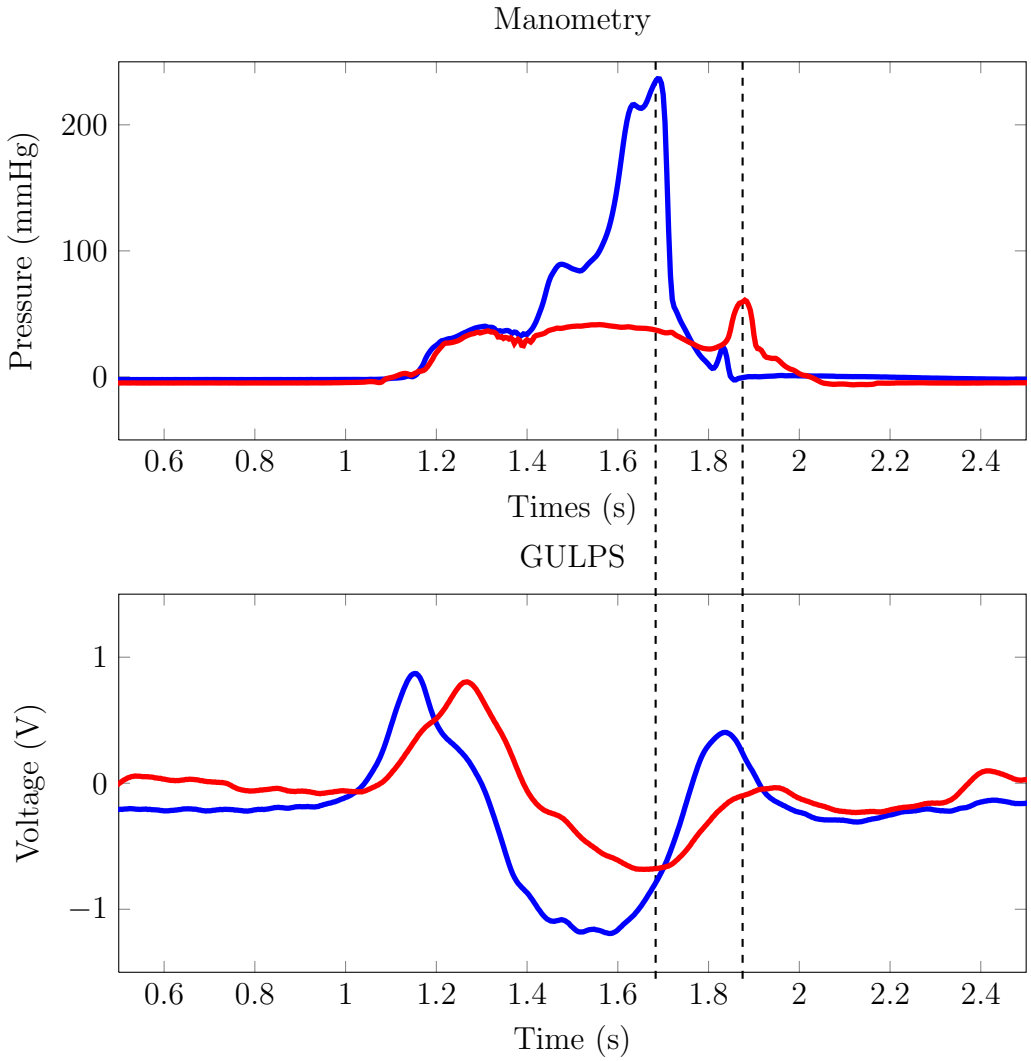

Figure 7.3: *Second example of manometry and GULPS used alongside each other. The blue waveform the upper channel of measurement and the red waveform of each waveform is for the lower channel of measurement of each device respectively.*

Due to no clear relationship being observed between the features of these two systems, an investigation was performed into a potential correlation between the temporal separation of features. The manometry peak separation was compared to the temporal separation between the GULPS waveform's first peaks, second peaks, and finally the separation between the trough that occurs between the two peaks. The chosen eight swallows containing prominent features were re-analysed in order to determine the correlation of the temporal separations. In this initial investigation, the criteria of using the eight waveforms with clearly defined features was chosen to obtain easily identifiable

temporal separations. The resulting characteristics of each of these features can be seen in Table 7.1, where linear regression analysis was performed between the temporal separation of each of the features and the temporal separation between the manometry peaks.

Feature	**Mean Separation (s)**	**vs manometry linear regression**		
		β	α	R^2 Value
Manometry Peaks	0.208	-	-	-
First Peak	0.120	-0.085	0.138	0.175
Second Peak	0.159	1.0646	- 0.06	0.6907
Trough	0.160	2.233	- 0.305	0.5756

Table 7.1: *Initial statistics of the temporal separations between features using GULPS alongside manometry for the first male subject (n=8). The linear regression equation relating the temporal separation of each feature to that of pharyngeal manometry is in the form of $y = x\beta+\alpha$, where β is the regression model's slope and α is the y-intercept. The variable y is the manometry separation and x is the GULPS feature's temporal separation.*

As shown in Table 7.1, the R^2 values of the second peak and trough temporal separation values suggested a potential correlation between these separations and the separation of the manometry pressure peaks. In contrast, the first GULPS peak separation was reasonably constant over all of the swallows, such that a change in temporal separation in the manometry waveforms was not reflected in the first peak temporal separation. To further investigate a potential relationship for the second peak and trough temporal separations, the number of swallows investigated was expanded to 33. These included all of the swallows in which both the trough and second peak could be detected in both of the GULPS system's waveforms. These features were often not as distinct as in the first eight waveforms used. The results from this further regression analysis again provided results that suggested the temporal separation of these features may be correlated to the temporal separation of pharyngeal manometry. The linear regression values can be seen in Table 7.2. Again the linear regression values for the trough and second peak separations both had similar R^2 values, where scatter plots of these separations are shown in Figure 7.4a and Figure 7.4b. These figures indicate that both the second peak and the trough separations are reasonably correlated to the separation of the pharyngeal manometry peaks.

Feature	Mean Separation (s)	vs manometry regression values		
		β	α	R^2 Value
Manometry Peaks	0.228	-	-	-
Second Peak	0.152	0.74	-0.018	0.347
Trough	0.160	1.61	-0.208	0.365

Table 7.2: *Follow-up statistics of the temporal separations between features using GULPS alongside manometry for the first male subject (n=33). The linear regression equation relating the temporal separation of each feature to that of pharyngeal manometry is in the form of $y = x\beta + \alpha$, where β is the regression model's slope and α is the y-intercept. The variable y is the manometry separation and x is the GULPS feature's temporal separation.*

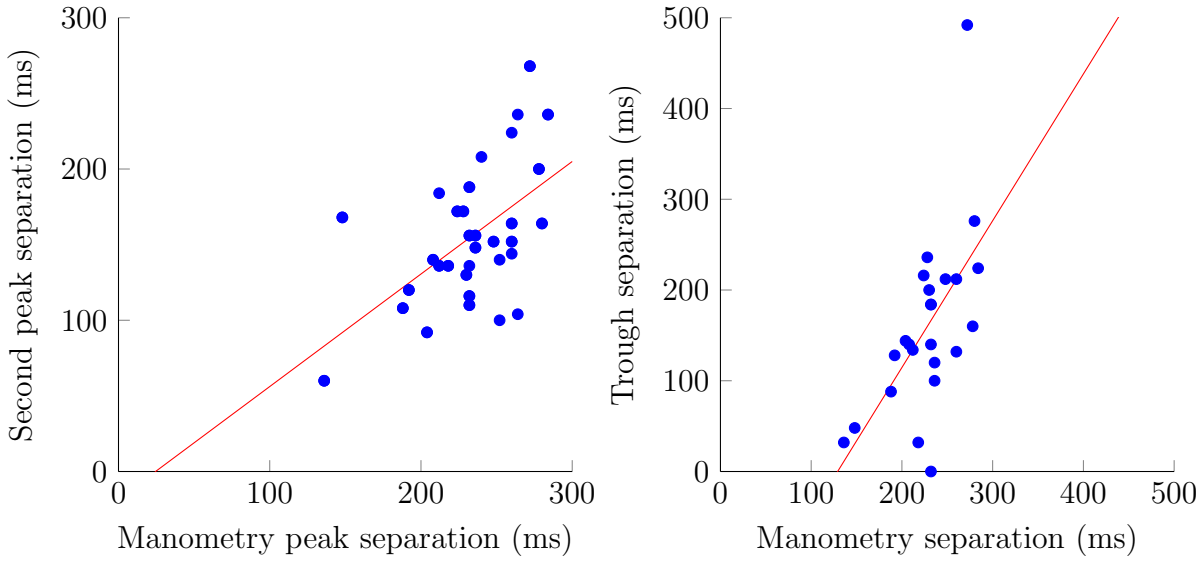

(a) *Second Peak.* ***(b)*** *Trough.*

Figure 7.4: *Linear regression plots of the GULPS second peak and trough temporal separations against the corresponding manometry peak separation. The blue dots are the data points and the red line is the linear regression model of each plot.*

Of the two features investigated, the second peak was chosen to be that primarily investigated. Due to both devices being designed to measure the temporal information of the same object (the pharynx), the features relating to this were expected to measure similar temporal data, rather than just mathematically related. In terms of the linear regression modules this meant having a slope of close to 1.0, where a change in the temporal separation in one device would be equally represented in the other. The second peak

separation's linear regression model had a slope of 0.74 which is closer to the desired unity slope than the trough regression model's slope of 1.61. The closer match, along with a smaller offset value led to the choice of the second peak for further investigation of GULPS in a dysphagic patient.

7.3 Dysphagic Subject

To further determine if the second peak separation could detect pharyngeal mis-sequencing, the GULPS device was trialled on a subject who exhibited pharyngeal mis-sequencing (male). An example of the resulting waveforms for this subject can be seen in Figure 7.5. The typical features were different than for the 'healthy' subjects, but were still present with different amplitudes. These features were again found to not directly line-up with the peaks in the manometry waveforms. As for the 'healthy' subject, the correlation between temporal separations was investigated. The regression plot for the second peak separation is shown in Figure 7.6. This figure shows that there is still an approximately linear relationship between the two separations, but that this relationship is a poorer fit than for the healthy subject (as shown by a lower R^2 value). Again the data from all swallows could not be used, with 76% of swallows showing a distinct second peak. This was a much higher percentage of usable waveforms than for the 'healthy' subjects and the second peaks were regularly found to be larger than the first peak in the dysphagic subject. These changing features and apparent correlation between the second peak separation and the temporal separation found in manometry are aspects that could provide rewarding results in future studies.

7.4 Summary

By trialling the GULPS system in both a standalone configuration and alongside pharyngeal manometry, the device's ability to detect pharyngeal sequencing could be determined. It was found that a swallow would often produce three distinct features in the output waveforms of the GULPS device, two peaks and one trough. These features were not always visible but were the most repeatable of all of features able to be produced. To determine if these features relate to the application of pressure in the pharynx the GULPS device was used alongside pharyngeal manometry. None of the features in GULPS consistently aligned with the pharyngeal pressure, measurements. In a further attempt to evaluate if these features relate to pharyngeal pressure the temporal separation between the two channels of each of these features was investigated. These separations were compared to the temporal separation between the pressure peaks measured in pharyngeal manometry for the same swallow to determine any

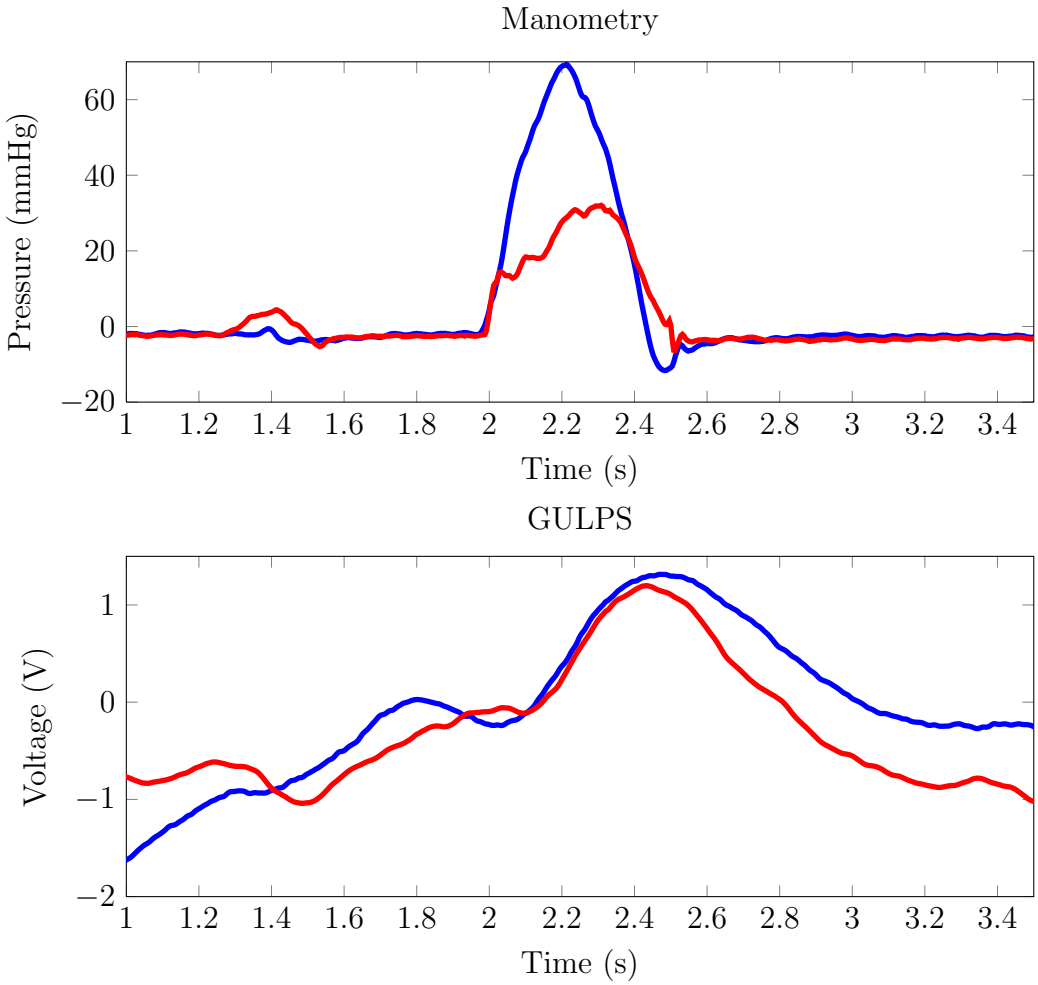

Figure 7.5: *Output waveforms of the GULPS system alongside manometry from a subject who presents pharyngeal mis-sequencing. The red waveform of each waveform is for the lower channel of measurement and the blue waveform the upper channel of measurement of each device respectively.*

correlation. To achieve this, linear regression modules relating each temporal separation to pharyngeal manometry were created. The features that were found to best correlate to the pressure sequencing were those of the second peak and the trough. The R^2 values of the regression plots for both these features were 0.347 and 0.365 respectively, where a conceivable linear relationship existed for both of these features. The feature chosen to most likely relate to the pharyngeal sequencing was the temporal separation between the second peaks of the waveform. These values were found to match the pharyngeal manometry peak separation values better than the trough separations.

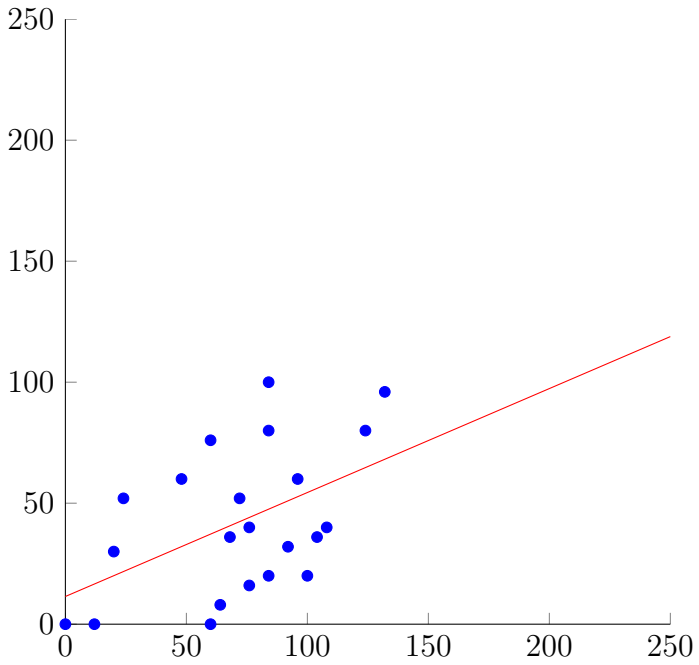

Figure 7.6: *Regression plot of the GULPS second peak temporal separation against the corresponding manometry peak separation for a dysphagic subject. The blue dots correspond to the data point and the red line is the linear regression model. The linear regression model had the equation of* $y = 0.56x + 48.4$ *(ms) with a* R^2 *value of 0.241 (*$n = 22$*).*

In an attempt to further investigate the relationship between the second peak temporal separation and the temporal separation found in pharyngeal manometry, the GULPS device was trialled on a subject who exhibited pharyngeal mis-sequencing characteristics. Again, pharyngeal manometry was used alongside the GULPS system to evaluate the presence of a relationship. The resulting linear regression model did not fit the data as well as in the healthy subject, where a R^2 value of 0.241 was obtained. The resultant grouping of the data did however still suggest that the values could be correlated. In addition, the resultant output waveforms of the GULPS device from a dysphagic subject were different to those of the healthy subjects. The waveforms produced by the dysphagic subject presented second peaks that were larger in amplitude than the first peaks, where it was the opposite to the waveforms found for 'healthy' subjects.

The main issues with the results of the GULPS device were the inconsistencies when detecting the swallowing characteristics. Electrodes often had to be reapplied and specific swallowing strategies enforced to gain the desired waveforms. Even when these steps were taken the waveforms were not always available, with the 'healthy' subjects only able to

produce a waveform containing these features in 64% of swallows using the standalone set-up. When paired with manometry, this number decreased to 23%. However, the dysphagic subject however had waveforms with the desired second peak in 76% of swallows.

CHAPTER 8

Discussion

This chapter outlines the key findings and implications of the research conducted in this project. The key findings cover the ability to use bio-impedance as a form of biofeedback, as well as its ability to be used for detection of the sequencing of the pharynx. Guidelines for further research are then detailed, suggesting alternative methods and designs that should be investigated. These guidelines include alternative hardware development techniques to obtain a more reliable device for detecting pharyngeal sequencing. Additional features of the software are also discussed for future research, where data processing algorithms have the ability to be introduced into the software architecture.

8.1 Key Findings and Developments

The GULPS system has been substantially improved from the pre-existing device with several advances in hardware, electrode prototypes and positioning, and software. During an examination of the pre-existing device several limitations to the system were found, which included:

- Faults in both current generation modules.
- Faults in the signal detection module of one channel.
- The power supply did not provide steady rail voltages.

To fix these issues a new hardware prototype was developed to provide an impedance measuring device which is able to provide two channels of impedance measurement data. Using the frequencies of 40 kHz and 70 kHz it was found that the impedance across a human throat was of the order of 60 Ω, with a changing in impedance during a swallow of around 2 Ω. This new hardware prototype was found to produce consistent impedance waveform data for a changing impedance load of variable resistors.

With an improved prototype device available the issues with the software in the pre-existing system could be addressed. These issues included:

- Only one channel of impedance measurement was able to be displayed.
- The displayed measurements experienced a significant delay.

Modifications were made to both the *Windows* based software as well as the firmware for the microcontroller in the device to fix these issues. The modifications to the firmware allowed for the transmission rate to be increased to close to 50 Hz, removing the delay from the transmission. The improvements to the *Windows* software allowed for two channels of impedance data to be displayed simultaneously.

Through various electrode positioning trials it was found that the best electrode positioning for the GULPS device was near the top and front of the throat. Four electrodes were placed on each side of the throat with a 40 mm gap between each channel. Using these locations an electrode positioning prototype was developed to place the electrodes in the desired locations. The electrodes that were found to operate best with the GULPS device were dry electrodes.

The performance of the system was determined to be sufficiently reliable and accurate to warrant trials on subjects. Three 'healthy' subjects and one subject who presented pharyngeal mis-sequencing were investigated. Three main features were able to be found in each subject's waveforms from the GULPS device (GULPS inverted the measured impedance waveforms). These features included two peaks and one trough. The detection of all of these features was not always possible, where the electrodes often had to be reapplied to be able to view the second peak and the trough. Even when the electrodes were applied in a position where the features could be seen the feature of the second peak could only be found in 64% of swallows in the 'healthy' subjects when using the GULPS device in a standalone manner.

In relation to pharyngeal sequencing, a relationship was found between the temporal separation of the second peaks of the GULPS waveforms and the temporal separation found in pharyngeal manometry. A similar relationship was found for the temporal separation of the trough in the GULPS waveforms. A linear relationship was found between the peak separation in manometry and these second peaks, where a linear regression model relating the two produced an R^2 value of 0.35 in the 'healthy' subject and 0.24 in the dysphagic subject; only one 'healthy' subject was trialled with pharyngeal manometry alongside GULPS. This R^2 value was greater in a regression module only containing waveforms that were considered to have distinctive peaks, where the use of eight of these waveforms from the 'healthy' subject produced an R^2 value of 0.69.

Due to the apparent increase in correlation between these two temporal separations when the second peaks in the GULPS waveforms are distinctive, future research should attempt to improve the detection of these peaks and/or troughs. The current system's inability to consistently provide these features limits its use for future research and its ability to be used as a biofeedback instrument, were adaptations and modifications are needed to overcome these limitations. Further investigations should therefore improve upon this device for future research.

8.2 Further Research: Hardware

Future research should include further investigations into the development of the GULPS prototype. The design of this new prototype should include several alternate module designs to those used in the current prototype, where several limitations of the current system have been outlined in Chapter 4. Altering these modules should allow for more stable waveforms to be produced without significant noise. In addition, alternative design techniques should be attempted to determine if a different design approach can better isolate the desired features. These design techniques include changing the operating frequency or using a different demodulation technique.

8.2.1 Improvements on Current Module Designs

As mentioned in Chapter 4, several of the modules in the final prototype's design were not ideal. Unnecessary attenuation was present in several of the modules, where alternative design techniques could be used to avoid attenuation. The modules that provided unwanted attenuation were:

- The current generation module.
- The instrumentation amplifier module.

- The envelope detection module.

Current Generation: The current generation module's unwanted attenuation was due to using a passive band-pass filter to convert the square-wave to a sine-wave. In future designs an alternative to this waveform generator should be investigated to provide a purely sinusoidal waveform without the need for wave conversion. Saulnier [77] stated that recent designs of bio-impedance measuring systems generally utilize digital waveform synthesis to achieve constant frequency waveforms. Direct digital synthesizer (DDS) ICs can be used to produce an analogue waveform by feeding the digital samples through a digital-to-analogue converter (DAC). Another alternative technique is to store all or part of a sinusoid in programmable read-only memory (PROM) and sequentially step through these stored values. Again, this would use a DAC to convert digital values to an analogue waveform.

Instrumentation Amplifier: Improving upon the instrumentation amplifier module simply requires removing the circuitry that reduces the module's input impedance. A high-pass filter is present at the input of the instrumentation amplifier in the final prototype. This filter was present from the pre-existing hardware design and served no design purpose. The data-sheet from the AD620 IC used for the instrumentation amplifier stated that the amplifier could be used with a direct connection from the amplifier inputs to the electrodes for medical applications [70].

Envelope Detection: The envelope detection module contains a half-wave rectifier in the form of a Schottky diode with a current draining load resistor following it. This Schottky diode causes a voltage drop in the signal, requiring additional amplification later in the circuit. An alternative design that could be implemented is that of a precision rectifier. A precision rectifier allows for rectification of the signal without the voltage drop caused by the diode to affect the output signal [99]. An example of the circuit that could be used is shown in Figure 8.1. The gain of this circuit is set by the ratio of R_2/R_1, where both resistors were given a value of 1 kΩ to achieve a unity gain. This circuit requires a voltage buffer following it as the output impedance is set by the resistor R_2. Due to a low-pass filter module with a relatively low input impedance following this stage, the buffer is needed to avoid unwanted coupling between these modules. It should also be noted that this module's input impedance is governed by the 1 kΩ resistor R_1. This is not an issue in the current design as the high-pass filter module present before the rectifier has a very low output impedance. However, if any changes are applied to the band-pass filter module compensation for this low input impedance may be needed.

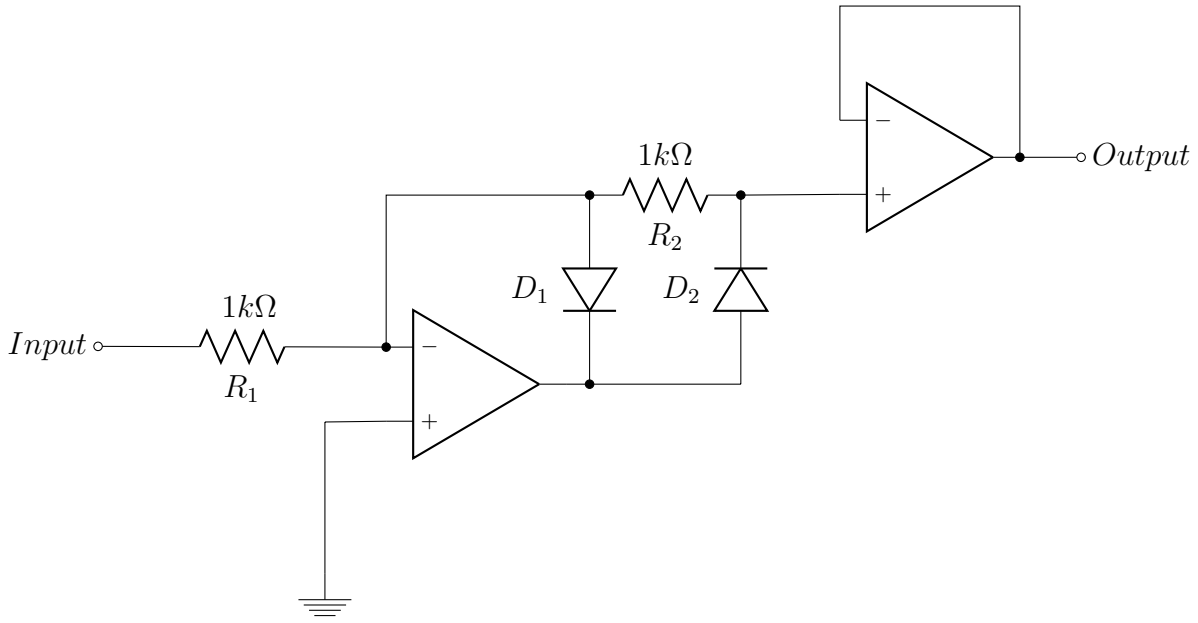

Figure 8.1: *Circuit diagram of the precision rectifier circuit that could be used in a future prototype.*

Band-pass Filter: In addition to the modules with unwanted attenuation, the band-pass filter module was not as desired in the final prototype in this project. The band-pass filter order was far less for each channel than desired, where a 4^{th} order filter was implemented in each channel instead of the desired 16^{th} order filter. This lower filter order allowed for inter-channel interference to be present after the band-pass filtering module. Though this signal was found not to substantially corrupt the resulting output data of the device it is still not ideal. In future designs, the order of the filter should be increased to further attenuate the inter-channel interference. Potential methods to complete this are cascading more of the implemented filtering modules together to obtain a high-order filter, or to use a new design technique to gain this higher order. The use of the Texas Instruments Filter Pro [98] designer allows for the design of a band-pass filter using only discrete components and op-amp ICs.

8.2.2 Potential Design Changes

All of the changes stated in Section 8.2.1 allow for improvements of the current design, but may not functionally improve quantification of pharyngeal sequencing. Alternative design approaches may be taken in future research in an attempt to gain more meaningful results for the detection of the sequencing of the pharynx. Design changes such as changing the frequency of operation or taking into account the in-phase and quadrature components of the signal may be investigated.

Frequency Change: Due to human tissue being a combination of resistive and capacitive elements, the frequencies used will affect impedance measurements [1]. Over the frequency range of 100 Hz to 100 MHz, there are certain frequency bands where the phase angle increases, because mechanisms come into play which provide more capacitance. One of these bands is around 100 Hz and is called the alpha dispersion range. This is where the outer cell membrane of most cells is able to charge and discharge fully. A further effect occurs from 10 kHz - 10 MHz and is called beta dispersion. This effect causes the impedance measured to be sensitive to intracellular changes from structural relaxation due to the current flowing through lipid cell membranes, introducing a capacitive component. However at higher frequencies the capacitance has a reduced effect on the overall impedance; above the beta dispersion range the cell membranes have a negligible impedance [120].

This project used frequencies that could potentially be affected by an increase in capacitance due to beta dispersion. The frequencies of 40 kHz and 70 kHz are both reasonably close to the implied beta dispersion frequency of 100 kHz [38]. The changing impedance effect due to this dispersion could potentially be a limiting factor in detecting the changing impedance in the throat due to a swallow. Further research should investigate using alternative frequencies to reduce the effects due to these dispersions.

Quadrature Modulation: Quadrature demodulation can be used to isolate either the resistive or reactive features of the throat's impedance. Both in-phase and quadrature components of the voltage signal need to be detected to correctly measure the bio-impedance [121]. An envelope detector is able to detect both the in-phase and quadrature components of the signal, but it is not able to differentiate between the two [122]. Several alternate studies into both bio-impedance and electrical impedance tomography (EIT) have used the quadrature demodulation technique to extract the in-phase and quadrature components of the impedance signal [121, 123]. The study performed by Kushuhara *et al.* [41] on using bio-impedance to assess swallowing function used only the in-phase component of the signal to measure a change in the impedance of the throat. This allowed for just the series resistance component of the impedance to be assessed. This investigation of the separate components of the impedance (resistive and reactive) could provide rewarding results in the application of detection of pharyngeal sequencing.

Quadrature demodulation is performed by using either a sine-wave or cosine-wave multiplier at the same carrier frequency as the modulated waveform to extract the in-phase or quadrature component of the signal. A block diagram of the potential architecture to implement this system is shown in Figure 8.2. This figure shows that the quadrature demodulation method has the ability to replace both the bandpass filter and the envelope detection modules in the GULPS system, where the output of this module is to the dc removal filter.

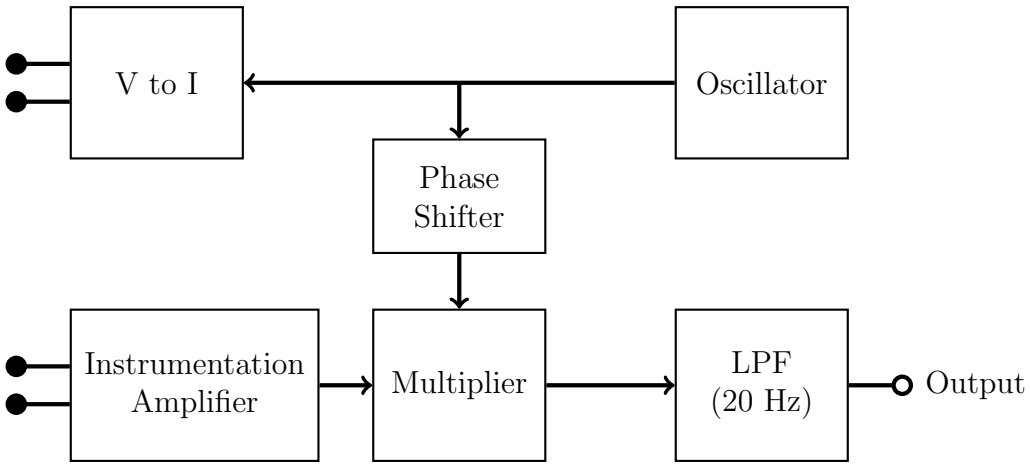

Figure 8.2: *Block diagram of the architecture for one channel of a quadrature demodulator.*

8.3 Further Research: Software

Further developments in the software are available to be implemented to allow for improvement of the GULPS system. One of the main features that has the ability to be implemented in future investigation is that of peak detection. Due to the second peak of the impedance waveform being identified as a feature of interest an algorithm in the software that could detect these peaks would be a valuable tool. Currently the peaks are detected by analysis of the collected data after a session has been conducted. This requires each waveform to be individually analysed to first detect if two peaks are present, and then determine the location in time of the second peak. An automated system which achieves this is therefore highly desirable, especially if an improvement to the peak detection in the hardware can be implemented.

A further potential development in the software is an active feedback of the temporal separation between features in the two channels. This feature is more critical for a clinical instrument rather than a tool researching the ability to detect pharyngeal sequencing, but is still important. For an effective biofeedback instrument to be produced the feedback

should be presented in such a way that it is easy for a patient to interpret. As mentioned in Chapter 2, patients who mis-sequence their swallows often have suffered head injuries and could have cognitive impairment. Therefore, if further research proves the existence of a relationship between any of the features in the GULPS output waveforms additional feedback should be provided to simplify this information for the patients. Options to display the whole waveforms or just a feedback of the temporal separation could provide useful tools for rehabilitation purposes.

CHAPTER 9

Conclusions

The GULPS system was created to research the potential of using bio-impedance measurements of the throat to detect the sequencing of the pharynx during a swallow. This initial system was a continuation from a pre-existing system developed at the University of Canterbury. This system was found to have both faulty hardware and software features limiting its use. The hardware was tested and redesigned to achieve a prototype which is able to achieve two channels of impedance measurement. Various electrode prototypes and positioning arrangements were trialled with this final prototype in an attempt to create two channels of impedance measurement with similar features, where a temporal separation between these features was present. The software of the system also had to be improved upon, where both the firmware for the microcontroller in the final prototype and the *Windows* based interfacing application had to be adapted. With these features implemented the GULPS system was able to be trialled on both 'healthy' and dysphagic subjects to determine its ability to detect the sequencing of the pharynx. Trials of the GULPS device alongside pharyngeal manometry provided evidence that there is a potential relationship between the GULPS waveforms and the sequencing of the pharynx detected by pharyngeal manometry. A linear regression model of the temporal separation between the second peaks seen in the GULPS waveforms and the temporal separation between pressure peaks in manometry had a R^2 value of 0.347 for a healthy subject and 0.241 in the dysphagic subject. These second peaks were not always visible however and often would require certain swallowing techniques and electrode positioning to achieve. Even when these conditions were met the second peaks could only be found in 64% of swallows for 'healthy' subjects.

Future research is able to be conducted about this study with additional investigation of the relationship between the features shown in the GULPS waveforms and pharyngeal sequencing. This further research should attempt to further isolate the second peaks in the GULPS waveforms to allow for conclusions about their relationship with pharyngeal manometry to be drawn. Improvements in hardware as well as different approaches to measuring these changing impedances are able to be examined. Different frequencies of operation and demodulation techniques of the received signals are two methods that could be investigated. For the potential use of this system as a clinical tool additional improvements should be made to the software as well. Peak detection modules and a better biofeedback methods are able to be investigated for further applications of this system.

References

[1] L. Geddes and L. Baker, *Principles of Applied Biomedical Instrumentation.* Wiley-Interscience, 1975, ch. Ch.10 : Detection of Physiological Events by Impedance, pp. 1312–1319.

[2] A. V. Sokolov, "Medical stimulators for biological feedback," *Meditsinskaya Tekhnika*, no. 3, pp. 6–8, 1995. [Online]. Available: www.scopus.com

[3] W. Edmonds and G. Tenenbaum, *Case Studies in Applied Psychophysiology: Neurofeedback and Biofeedback Treatments for Advances in Human Performance.* Wiley, 2011. [Online]. Available: http://books.google.co.nz/books?id=q7NXpB9IqLIC

[4] L. Guan, G. Deng, and L. Xu, "Effect of biological feedback therapy on clinical symptoms and pelvic floor muscle surface electromyography in elderly patients with chronic functional constipation," *World Chinese Journal of Digestology*, vol. 21, no. 20, pp. 2000–2004, 2013. [Online]. Available: www.scopus.com

[5] J. B. Storrie, "Biofeedback: a first-line treatment for idiopathic constipation," *British journal of nursing (Mark Allen Publishing)*, vol. 6, no. 3, pp. 152–158, 1997.

[6] M. I. Anokhin, V. N. Sergeev, and V. L. Domanskij, "Biological feedback correction of respiration in the treatment of bronchial asthma," *Meditsinskaya Tekhnika*, no. 1, pp. 26–29, 1996.

[7] L. N. Kornilova, V. V. Temnikova, I. A. Naumov, and A. D. Solovieva, "Treatment of patients with vertigo and balance disorders," *Neuroscience and behavioral physiology*, vol. 41, no. 1, pp. 57–63, 2011. [Online]. Available: www.scopus.com

[8] O. Ekberg, *Dysphagia: Diagnosis and Treatment*, ser. Medical Radiology. Springer, 2012.

[9] C. W. Howden, "Management of acid-related disorders in patients with dysphagia," *American Journal of Medicaine*, vol. 117, pp. 44–48, Sep 2004.

[10] E. Domench and J. Kelly, "Swallowing disorders," *Medical Clinics of North America*, vol. 83, no. 1, pp. 97–113, Jan 1999.

[11] S. Langmore, *Endoscopic evaluation and treatment of swallowing disorders*. Thieme Medical Publishers, Incorporated, 2001.

[12] New Zealand Brain Research Institute (NZBRI), "UC Swallowing Rehabilitation Research Laboratory," Sep 2013. [Online]. Available: http://www.cmds.canterbury.ac.nz/researchcentre/

[13] S. Daniels and M.-L. Huckabee, *Dysphagia Following Stroke*, ser. Clinical Dysphagia Series. Plural Publishing, 2008, ch. Normal Swallowing Anatomy and Physiology, pp. 41–53.

[14] N. A. Leopold and M. C. Kagel, "Dyspagia – Ingestion or deglutition? A proposed paradigm." *Dysphagia*, vol. 12, no. 4, pp. 202–206, 1996.

[15] B. E. Murdoch and D. Theodoros, *Traumatic Brain Injury: Associated Speech, Language, and Swallowing Disorders*, ser. Neurogenic communication disorders series. Singular Thomson Learning, 2001. [Online]. Available: http://books.google.co.nz/books?id=OubPfsqqh_kC

[16] T. Ebihara, s Ebihara, M. Maruyama, M. Kobayashi, A. Itou, and H. A. . H. Sasaki, "A randomized trial of olfactory stimulation using black pepper oil in older people with swallowing dysfunction." *Journal of American Geriatric Society*, vol. 54, no. 9, pp. 1401–1406, 2006.

[17] B. Jones, *Normal and Abnormal Swallowing: Imaging in Diagnosis and Therapy*. Springer, 2003.

[18] B. Oto, "Mastering BLS Ventilation: Supplemental Methods," Aug. 2012. [Online]. Available: http://emsbasics.com/2012/08/05/mastering-bls-ventilation-supplemental-methods/

[19] S. Daniels and M.-L. Huckabee, *Dysphagia Following Stroke*, ser. Clinical Dysphagia Series. Plural Publishing, 2008, ch. The Neural Control of Swallowing, pp. 36–38.

[20] R. Drake, A. Vogl, and A. Mitchell, *Gray's Anatomy for Students*, ser. Gray's Anatomy. Elsevier Health Sciences, 2009. [Online]. Available: http://books.google.co.nz/books?id=_ozrqnzzhFwC

[21] D. J. S. Burks and D. K. P. Johnson, *Multiple Sclerosis: Diagnosis, Medical Management, and Rehabilitation: Diagnosis, Medical Management, and Rehabilitation*, ser. Springer Demos Medic Series. Demos Medical Publishing, 2000.

[22] N. A. Leopold and M. C. Kagel, "Prepharyngeal dysphagia in Parkinson's disease," *Dysphagia*, vol. 11, no. 1, pp. 14–22, 1996.

[23] D. W. Buchholz, "Dysphagia associated with neurological disorders," *Acta Otorhinolaryngol Belg*, vol. 48, no. 2, pp. 143–155, 1994.

[24] J. A. Logemann, "Swallowing Disorders," *Best Practice & Research Clinical Gastroenterology*, vol. 21, no. 4, pp. 563–573, 2007, Severe Gastrointestinal Motor Disorders .

[25] S. Daniels and M.-L. Huckabee, *Dysphagia Following Stroke*, ser. Clinical Dysphagia Series. Plural Publishing, 2008, ch. Diagnosis of dysphagia in stroke, pp. 185–193.

[26] M. Huckabee, "The complexities of pharyngeal pathophysiology: Limitations in diagnosis lead to limitations in rehabilitation," in *International Journal of Stroke*, vol. 8. Risk, Recovery and Reorganisation 9th Australasian Nursing and Allied Health Stroke Conference, 2013, pp. 27–29.

[27] M. Huckabee, K. Lamvik, and R. Jones, "Pharyngeal mis-sequencing: Motor programming or maladaptive compensation?" To be published.

[28] Z. Gao, M. Taniwaki, H. Shimada, S. Ishihara, M. Nakauma, T. Funami, and K. Kohyama, "Ultrasound Analysis of the Effects of Food Bolus Volume on Tongue Movement at the Initiation of Swallowing," *Journal of Texture Studies*, 2013, article in Press. [Online]. Available: www.scopus.com

[29] M. Komori, M. Hyodo, and K. Gyo, "A swallowing evaluation with simultaneous videoendoscopy, ultrasonography and videofluorography in healthy controls," *Journal for Oto-Rhino-Laryngology*, vol. 70, no. 6, pp. 393–398, 2008.

[30] A. Buettner, A. Beer, C. Hannig, and M. Settles, "Observation of the swallowing process by application of videofluoroscopy and real-time magnetic resonance imaging-consequences for retronasal aroma stimulation," *Chemical Senses*, vol. 26, no. 9, pp. 1211–1219, 2001.

[31] O. Sella, "Skill versus strength in swallowing training: Neurophysiological, biomechanical, and structural assessments," Ph.D. dissertation, The University of Canterbury, Christchurch, New Zealand, 2012.

[32] *Digital Swallowing Workstation Model 7200*, D ed., kayPENTAX, Lincoln Park, NJ, USA, Aug 2007, Instruction Manual.

[33] M. Milosevic, K. M. V. McConville, E. Sejdic, K. Masani, M. J. Kyan, and M. R. Popovic, "Visualization of trunk muscle synergies during sitting perturbations using Self-Organizing Maps (SOM)," *IEEE Transactions on Biomedical Engineering*, vol. 59, no. 9, pp. 2516–2523, 2012.

[34] G. van Elswijk, B. U. Kleine, S. Overeem, B. Eshuis, K. D. Hekkert, and D. F. Stegeman, "Muscle imaging: Mapping responses to transcranial magnetic stimulation with high-density surface electromyography," *Cortex*, vol. 44, no. 5, pp. 609–616, 2008.

[35] J. R. Daube and D. I. Rubin, "Needle electromyography," *Muscle Nerve*, vol. 39, no. 2, pp. 244–270, Feb 2009.

[36] V. R. Edgerton, S. L. Wolf, D. J. Levendowski, and R. R. Roy, "Evaluating Patterns of EMG Amplitudes for Trunk and Neck Muscles of Patient and Controls," *International Journal of Rehabilitation and Health*, vol. 2, no. 1, 1996.

[37] S. H. Doeltgen, A. Hofmayer, F. Gumbley, U. Witte, C. Moran, G. Carroll, and M. L. Huckabee, "Clinical measurement of pharyngeal surface electromyography: exploratory research," *Neurorehabil Neural Repair*, vol. 21, no. 3, pp. 250–262, 2007.

[38] D. S. Holder, *Electrical Impedance Tomography: Methods, History and Applications*, ser. Series in Medical Physics and Biomedical Engineering. Taylor and Francis, 2004.

[39] S. Lovin, R. Bercea, C. Cojocaru, G. Rusu, and T. Mihescu, "Body composition in obstructive sleep apneahypopnea syndrome: Bio-impedance reflects the severity of sleep apnea," *Multidisciplinary Respiratory Medicine*, vol. 5, no. 1, pp. 44–49, 2010.

[40] B. Rigaud, J. P. Morucci, and N. Chauveau, "Bioelectrical impedance techniques in medicine. Part I: Bioimpedance measurement. Second section: impedance spectrometry," *Critical Reviews in Biomedical Engineering*, vol. 24, no. 4-6, pp. 257–351, 1996.

[41] T. Kusuhara, T. Nakamura, Y. Shirakawa, K. Mori, Y. Naomoto, and Y. Yamamoto, "Impedance Pharyngography to Assess Swallowing Function," *The Journal of International Medical Research*, vol. 32, pp. 608–616, 2004.

[42] F. H. Gravesen, P. Funch-Jensen, H. Gregersen, and A. M. Drewes, "Axial force measurement for esophageal function testing," *World Journal of Gastroenterology*, vol. 15, no. 2, pp. 139–143, 2009.

[43] R. Leonard and K. Kendall, *Dysphagia Assessment and Treatment Planning: A Team Approach*, ser. Dysphagia series. Singular Publishing Group, 1997.

[44] F. H. Gravesen, B. P. McMahon, A. M. Drewes, and H. Gregersen, "Measurement of the axial force during primary peristalsis in the oesophagus using a novel electrical impedance technology," *Physiological Measurement*, vol. 29, no. 3, pp. 389–399, 2008.

[45] F. H. Gravesen, H. Gregersen, L. Arendt-Nielsen, and A. M. Drewes, "Reproducibility of axial force and manometric recordings in the oesophagus during wet and dry swallows," *Neurogastroenterology and Motility*, vol. 22, no. 2, pp. 142–149, 2010.

[46] F. Gravesen, N. Behan, A. Drewes, and H. Gregersen, "Viscosity of food boluses affects the axial force in the esophagus," *World Journal of Gastroenterology*, vol. 17, no. 15, pp. 1982–1988, 2011.

[47] O. Ekberg, *Dysphagia: Diagnosis and Treatment*, ser. Medical radiology. Springer, 2012. [Online]. Available: http://books.google.co.nz/books?id=TjVV8VoR8NEC

[48] S. E. Langmore, K. Schatz, and N. Olsen, "Fiberoptic endoscopic examination of swallowing safety: a new procedure," *Dysphagia*, vol. 2, no. 4, pp. 216–219, 1988.

[49] S. Sun, C. Hsu, H. Lin, H. Sun, P. Chang, W. Hsieh, and J. Wang, "Combined Neuromuscular Electrical Stimulation (NMES) with Fiberoptic Endoscopic Evaluation of Swallowing (FEES) and Traditional Swallowing Rehabilitation in the Treatment of Stroke-Related Dysphagia," *Dysphagia*, 2013, article in Press.

[50] KayPENTAX, "Hospital FEES System, Model 7190 ," dec 2013. [Online]. Available: http://www.kayelemetrics.com/index.php?option=com_product&Itemid=3&controller=product&task=learn_more&cid[]=20

[51] V. Cherepenin, A. Karpov, A. Korjenevsky, K. V, A. Mazaletskaya, D. Mazourov, and D. Meister, "A 3D electrical impedance tomography (EIT) system for breast cancer detection," *Physiological Measurement*, vol. 22, no. 1, pp. 9–18, 2001.

[52] J. Jossinet, "Variability of impedivity in normal and pathological breast tissue," *Medical and Biological Engineering and Computing*, vol. 34, no. 5, pp. 346–350, 1996.

[53] L. Baker, "Applications of the impedance technique to the respiratory system," *Engineering in Medicine and Biology Magazine*, vol. 8, no. 1, pp. 50–52, Mar 1989.

[54] L. M. Yamokoski, G. J. Haas, B. Gans, and W. T. Abraham, "Optivol fluid status monitoring with an implantable cardiac device: A heart failure management system," *Expert Review of Medical Devices*, vol. 4, no. 6, pp. 775–780, 2007.

[55] D. S. Holder, *Electrical Impedance Tomography: Methods, History and Applications*, ser. Series in Medical Physics and Biomedical Engineering. Taylor and Francis, 2004.

[56] A. Hartov, N. Soni, and R. Halter, "Breast Cancer Screening with Electrical Impedance Tomography," in *Electrical Impedance Tomography: Methods, History and Applications*, ser. Series in Medical Physics and Biomedical Engineering. Taylor and Francis, 2004, pp. 107–123.

[57] D. Holder and T. Tidswell, "Electrical Impedance Tomography of Brain Function," in *Electrical Impedance Tomography: Methods, History and Applications*, ser. Series in Medical Physics and Biomedical Engineering. Taylor and Francis, 2004, pp. 127–146.

[58] H. J. Smit, A. V. Noordegraaf, H. R. van Genderingen, and P. W. A. Kunst, "Imaging of the Thorax by EIT," in *Electrical Impedance Tomography: Methods, History and Applications*, ser. Series in Medical Physics and Biomedical Engineering. Taylor and Francis, 2004, pp. 167–182.

[59] W. Lionheart, N. Polydorides, and A. Borsic, "The reconstruction problem," in *Electrical Impedance Tomography: Methods, History and Applications*, ser. Series in Medical Physics and Biomedical Engineering. Taylor and Francis, 2004, pp. 10–17.

[60] Q. Acton, *Advances in Heart Research and Application: 2013 Edition*. ScholarlyEditions, 2013. [Online]. Available: http://books.google.co.nz/books?id=HXLz4UKjjAwC

[61] W. J. Hannan, S. J. Cowen, C. E. Plester, K. C. H. Fearon, and A. De Beau, "Comparison of bio-impedance spectroscopy and multi-frequency bio-impedance analysis for the assessment of extracellular and total body water in surgical patients," *Clinical Science*, vol. 89, no. 6, pp. 651–658, 1995.

[62] C. Cornelius, J. Sorber, R. Peterson, J. Skinner, R. Halter, and D. Kotz, "Who wears me? Bioimpedance as a passive biometric," in *Proceedings of HealthSec*, 2012. [Online]. Available: https://www.usenix.org/conference/healthsec12/tech-schedule/workshop-program

[63] T. A. T. Hughes, P. Liu, H. Griffiths, B. W. Lawries, and C. M. Wiles, "An analysis of studies comparing electrical impedance tomography with x-ray videofluoroscopy in the assessment of swallowing," *Physiological Measurement*, vol. 15, pp. 199–209, 1994.

[64] WikiBooks, "Medical Physiology/Gastrointestinal Physiology/Motility," Apr. 2013. [Online]. Available: http://en.wikibooks.org/wiki/Medical_Physiology/Gastrointestinal_Physiology/Motility

[65] H. P. Schwan and C. D. Ferris, "Four-electrode null techniques for impedance measurement with high resolution," *Review of Scientific Instruments*, vol. 39, no. 4, pp. 481–485, 1968.

[66] Ambu, "Ambu Blue Sensor NF," Aug. 2012. [Online]. Available: http://www.ambu.com/corp/products/patient_monitoring_and_diagnostics/product/blue_sensor_nf.aspx

[67] *AD9833: Low Power, 12.65 mW, 2.3 V to 5.5 V, Programmable Waveform Generator*, Analog Devices, 2012, datasheet. [Online]. Available: www.analog.com/static/imported-files/data_sheets/AD9833

[68] *LTC6900 Low Power, 1kHz to 20MHz Resistor Set SOT-23 Oscillator*, A ed., Linear Technology Corporation, 2002, datasheet. [Online]. Available: www.linear.com/product/LTC6900

[69] *LM13700: Dual Operational Transconductance Amplifiers with Linearizing Diodes and Buffers*, Texas Instruments, 2013, datasheet. [Online]. Available: www.ti.com/lit/gpn/lm13700

[70] *AD620: Low Cost, Low Power Instrumentation Amplifier*, Analog Devices, 1999, datasheet. [Online]. Available: www.analog.com/static/imported-files/data_sheets/AD620

[71] *LTC1562-2: Very Low Noise, Low Distortion Active RC Quad Universal Filter*, Linear Technology, 1998, datasheet. [Online]. Available: www.linear.com/product/LTC1562-2

[72] *LTC1068:Clock-Tunable, Quad Second Order, Filter Building Blocks*, Linear Technology, 1996, datasheet. [Online]. Available: www.linear.com/product/LTC1068

[73] *AD8622:Low Power, Precision Rail-to-Rail Output Op Amp*, Analog Devices, 2011, datasheet. [Online]. Available: www.analog.com/static/imported-files/data_sheets/AD8622

[74] *dsPIC30F2011/2012/3012/3013, High-Performance, 16-bit Digital Signal Controllers*, Microchip Technology Inc, 2010, datasheet. [Online]. Available: ww1.microchip.com/downloads/en/DeviceDoc/70139E

[75] Python Software Foundation, "Python Programming Language Official Website," Jun. 2012. [Online]. Available: http://www.python.org/

[76] M. Frank-Stromborg and S. Olsen, *Instruments for Clinical Health-care Research*, ser. Jones and Bartlett series in oncology. Jones and Bartlett Publishers, 2004.

[77] G. J. Saulnier, "EIT Instrumentation," in *Electrical Impedance Tomography: Methods, History and Applications*, ser. Series in Medical Physics and Biomedical Engineering. Taylor and Francis, 2004, pp. 67–103.

[78] Element14, "Element14: Frequency Synthesizers," Jun. 2013, formally Farnel. [Online]. Available: http://nz.element14.com/frequency-synthesizers

[79] *Sine Wave Oscillator Circuits*, Texas Instruments, Mar 2001. [Online]. Available: www.ti.com/lit/an/sloa060/sloa060.pdf

[80] *AN-263 Sine Wave Generation Techniques*, Texas Instruments, Apr 2013. [Online]. Available: www.ti.com/litv/pdf/snoa665c

[81] *74HC/HCT4046A Phase-locked-loop with VCO*, Philips Semiconductors, 1997, datasheet. [Online]. Available: www.nxp.com/documents/data_sheet/74HC_HCT4046A_CNV

[82] E. Bogatin, *Signal Integrity: Simplified*, ser. Prentice Hall modern semiconductor design series. Prentice Hall, 2004, ch. The Spectrum of an Ideal Square Wave, p. 53. [Online]. Available: http://books.google.co.nz/books?id=_IiONSphoB4C

[83] S. Winder, *Analog and Digital Filter Design*, ser. EDN Series for Design Engineers. Elsevier Science, 2002, ch. introduction, p. 27. [Online]. Available: http://books.google.co.nz/books?id=NuRvHVMuzI4C

[84] D. Crecraft and S. Gergely, *Analog Electronics: Circuits, Systems and Signal Processing*. Elsevier Science, 2002. [Online]. Available: http://books.google.co.nz/books?id=lS7qN6iHyBYC

[85] *LTC1562-2 Very Low Noise, Low Distortion Active RC Quad Universal Filter*, Linear Technology, 1997.

[86] *FilterCAD Users Manual*, 1st ed., Linear Technology Corporation, Nov 1990, application Note 38.

[87] A. Peyton and V. Walsh, *Analog Electronics with Op-amps: A Source Book of Practical Circuits*, ser. Electronics Texts for Engineers and Scientists. Cambridge University Press, 1993. [Online]. Available: http://books.google.co.nz/books?id=io36-F1cPu8C

[88] *Calculating settling time for switched capactior ADCS*, 1st ed., Jul.

[89] *TPS6755, Adjustable Inverting DC/DC Cconverter*, Texas Instruments, 1996, datasheet. [Online]. Available: www.ti.com/product/tps6755

[90] *RBE850 Adjustable 3-12VDC Transformer-Isolated Voltage Rectifier*, Avico Electronics Pty Ltd, 1997, datasheet. [Online]. Available: http://www.avico.com.au/power-surge/RBE850

[91] P. Resca, "Medical Power Supplies," *Power Electronics Technology*, Apr 2007.

[92] *LM117/LM217/LM317: 1.2V to 37V Adjustable voltage regulators*, Texas Instruments, 2007, datasheet. [Online]. Available: www.ti.com/product/lm317

[93] *LM137/LM337-N: 3-Terminal Adjustable Negative Regulators*, Texas Instruments, 2013, datasheet. [Online]. Available: www.ti.com/lit/gpn/lm137

[94] K. Wildes and N. Lindgren, *A Century of Electrical Engineering and Computer Science at MIT, 1882-1982*. MIT Press, 1985. [Online]. Available: http://books.google.co.nz/books?id=6ZX-GwvhcnkC

[95] T. Băjenescu and M. Bâzu, *Component Reliability for Electronic Systems*, ser. Artech House Remote Sensing Library. Artech House, 2010. [Online]. Available: http://books.google.co.nz/books?id=mNnaCSKP9WMC

[96] *MCP6H01/2/4, 1.2 MHz, 16V Op Amps*, Microchip Technology, 2011, datasheet. [Online]. Available: www.microchip.com/wwwproducts/Devices.aspx?dDocName=en547495

[97] *UAF42: Universal Active Filter*, Texas Instruments, Oct 2010, datasheet. [Online]. Available: www.ti.com/product/uaf42

[98] *FilterPro MFB and Sallen-Key Low-Pass Filter Design Program User Guide (Rev. C)*, C ed., Texas Instruments, Feb 2011.

[99] T. Wilmshurst, *Analog Circuit Techniques: With Digital Interfacing*. Newnes, 2001. [Online]. Available: http://books.google.co.nz/books?id=AE49Vqm5ioYC

[100] *LM158/LM258/LM358/LM2904: Low Power Dual Operational Amplifiers*, Texas Instruments, 2013, datasheet. [Online]. Available: www.ti.com/product/lm358

[101] *TLE202x, TLE202xA, TLE202xB, TLE202xY Excalibur High-speed Low-power Precision Operational Amplifiers*, Texas Instruments, 2010, datasheet. [Online]. Available: www.ti.com/product/tle2022

[102] *FT231X (USB to FULL HANDSHAKE UART IC)*, Future Technology Devices International Ltd., 2013, datasheet. [Online]. Available: www.ftdichip.com/Products/ICs/FT231X

[103] *ABS1598 Adjustable 3-12VDC Transformer-Isolated Voltage Rectifier*, Hammond Manufactoring, 2013, datasheet. [Online]. Available: http://nz.element14.com/hammond/1598jsgy/enclosure-abs-1598/dp/1876956

[104] Myotronics, "Norotrode 20 Bipolar SEMG Electrodes," 2013. [Online]. Available: https://myotronics.worldsecuresystems.com/norotrodes

[105] Ambu, "Ambu BlueSensor N," 2013. [Online]. Available: http://www.ambu.com/corp/products/patient_monitoring_and_diagnostics/product/ambu%C2%AE_bluesensor_n-prod844.aspx

[106] Sten's Corportation, "Tripletrode Electrodes," 2013. [Online]. Available: http://stens-biofeedback.com/products/tripletrode-electrodes

[107] Gordon's: Manufactorers and Wholesalers of Medical Softgoods, "Cervical Collars - Standard," Sep 2011. [Online]. Available: http://www.gordons.co.nz/index.php?page=cervical-collars---standard

[108] ConvaTec, "Stomahesive Wafer," 2013. [Online]. Available: http://www.convatec.co.nz/products/ostomy/stomahesive-wafer/p-b91cba9a-efd4-4dd4-833c-8d7a858f7ef9/1_0043/

[109] R. O'Rahilly, F. Mller, S. Carpenter, and R. Swenson, *Basic Human Anatomy: A Regional Study of Human Structure*. Saunders, 1983, ch. Chapter 53: The pharynx and larynx. [Online]. Available: http://www.dartmouth.edu/~humananatomy/part_8/chapter_53.html

[110] Microchip Technology Inc., "MPLAB Integrated Development Environment ," 2013. [Online]. Available: www.microchip.com/mplab8

[111] ——, "PICkit 3 In-Circuit Debugger," 2013. [Online]. Available: www.microchip.com/pickit3

[112] D. Godse, *Elements Of Microprocessors*. Technical Publications, 2007. [Online]. Available: http://books.google.co.nz/books?id=8LqTavxvspwC

[113] J. Hunter, D. Dale, E. Firing, and M. Droettboom, "Matlibplot," dec 2012. [Online]. Available: http://matplotlib.org/

[114] P. S. Foundation, "CSV File Reading and Writing," dec 2013. [Online]. Available: http://docs.python.org/2/library/csv.html

[115] M. Inc., "csvread," dec 2013. [Online]. Available: http://www.mathworks.com.au/help/matlab/ref/csvread.html

[116] M. Lutz, *Learning Python*, ser. Safari Books Online. O'Reilly Media, 2013. [Online]. Available: http://books.google.co.nz/books?id=4pgQfXQvekcC

[117] "Pyinstaller official website," Jun 2013. [Online]. Available: http://www.pyinstaller.org/

[118] S. Health and D. E. Committee, "Terms of reference," 2012. [Online]. Available: http://ethics.health.govt.nz/about-committees/southern-health-and-disability-ethics-committee

[119] A. G. D. of Health, "Australian regulatory guidelines for medical devices," dec 2012. [Online]. Available: http://www.tga.gov.au/pdf/devices-argmd-p1.pdf

[120] K. R. Foster, "Dielectric Properties of Tissues," ser. Electrical engineering handbook series. CRC Press, 2000, pp. 89–2.

[121] T. I. Oh, J. W. Lee, K. S. Kim, J. S. Lee, and E. J. Woo, "Digital phase-sensitive demodulator for electrical impedance tomography," in *Engineering in Medicine and Biology Society, 2003. Proceedings of the 25th Annual International Conference of the IEEE*, vol. 2, 2003, pp. 1070–1072 Vol.2.

[122] *Synchronous Vs Envelope Detection*, Television Measurement Services, Oct 2001. [Online]. Available: http://www.tvms.net/Tech_Articles/Synchronous_vs_Envelope_Detection.htm

[123] N. Bqo, G. Sze, B. Tunstall, G. Qiao, A. Zarafshani, and W. Wang, "A flexible and configurable hardware for the combined eim and ultrasound device," in *Journal of Physics: Conference Series*, ser. International Conference on Electrical Bioimpedance, vol. 224, 2010.

APPENDIX A

Hardware Diagrams

A.1 40 kHz Channel

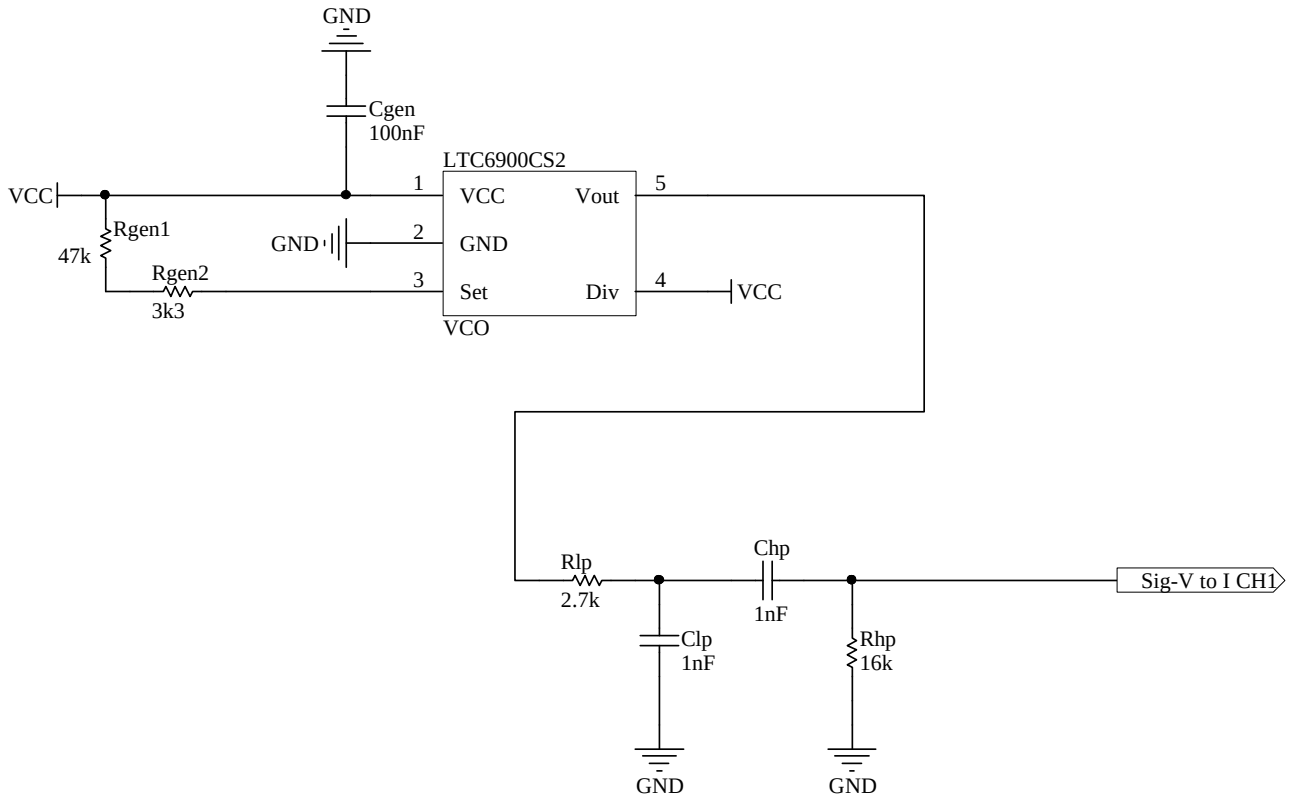

Figure A.1: *Circuit diagram of the signal generating module of the 40 kHz channel.*

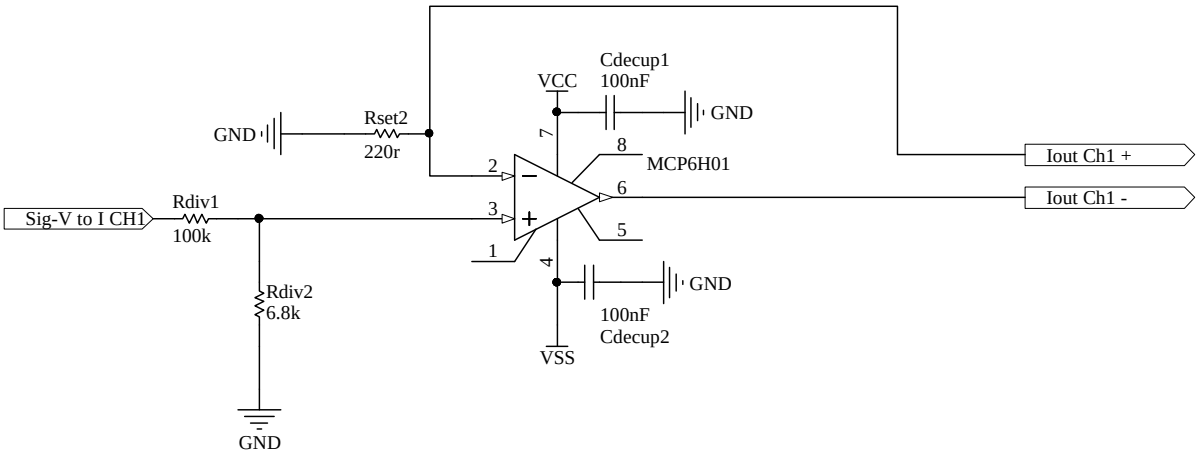

Figure A.2: *Circuit diagram of the voltage to current conversion module of the 40 kHz channel.*

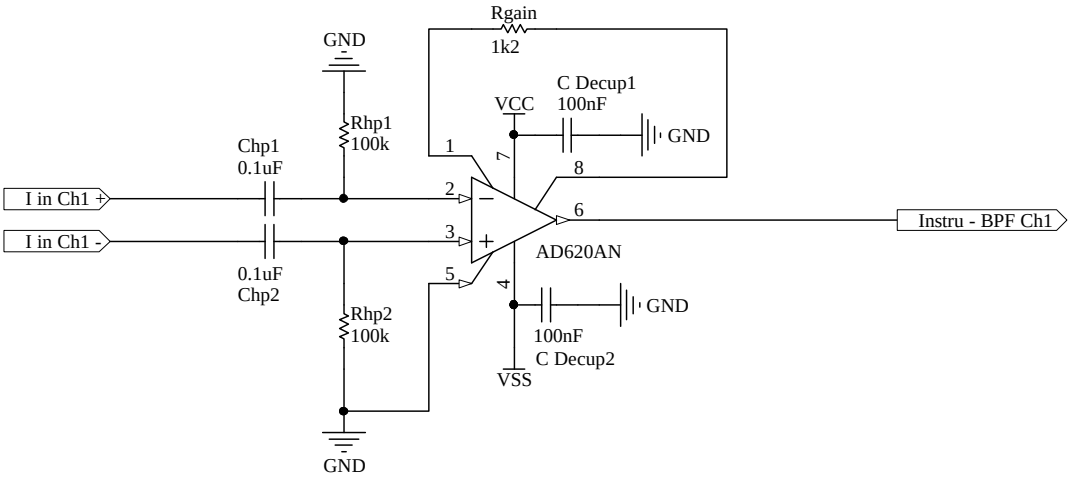

Figure A.3: *Circuit diagram of the instrumentation amplifier module of the 40 kHz channel.*

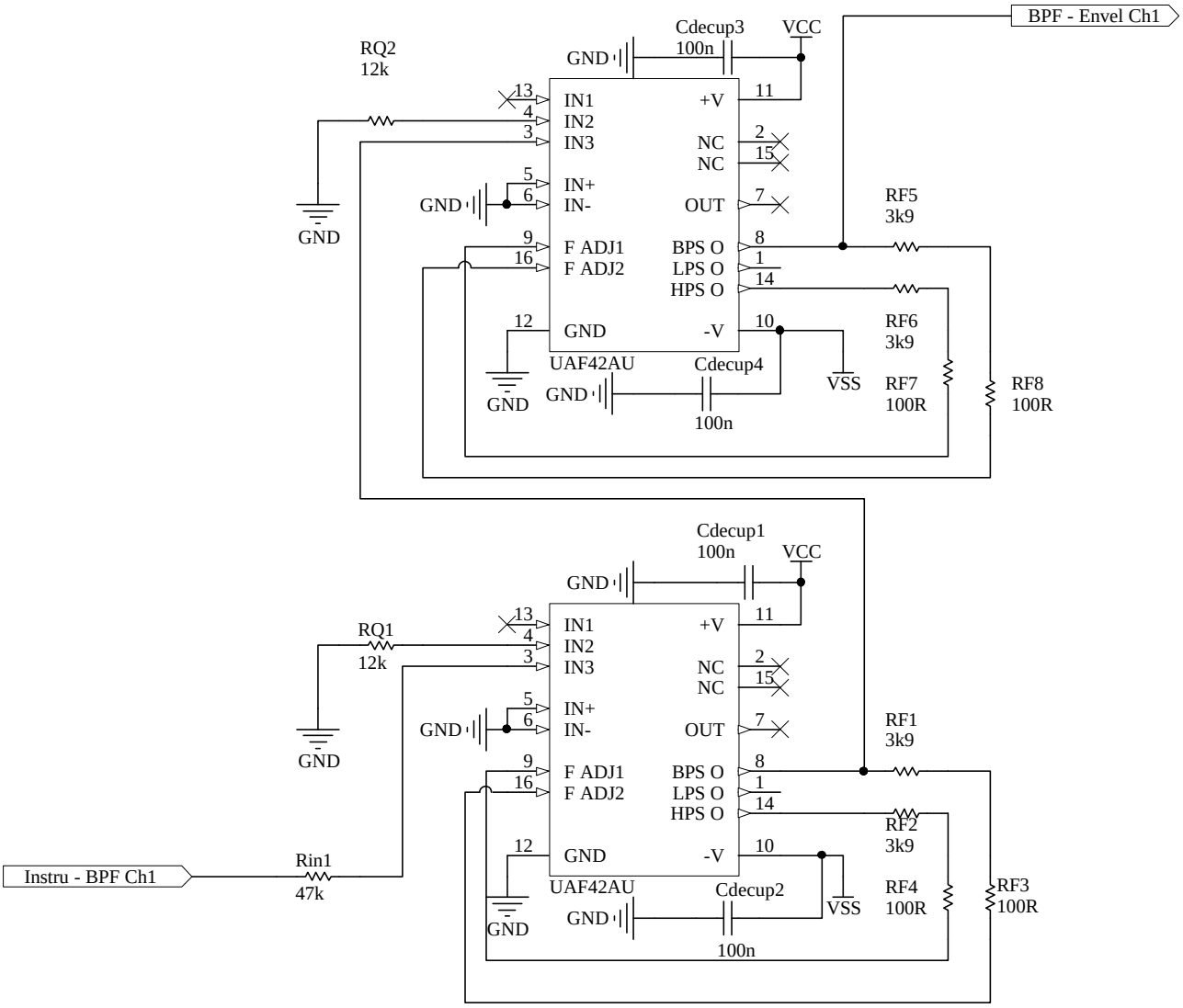

Figure A.4: *Circuit diagram of the band-pass filter module of the 40 kHz channel.*

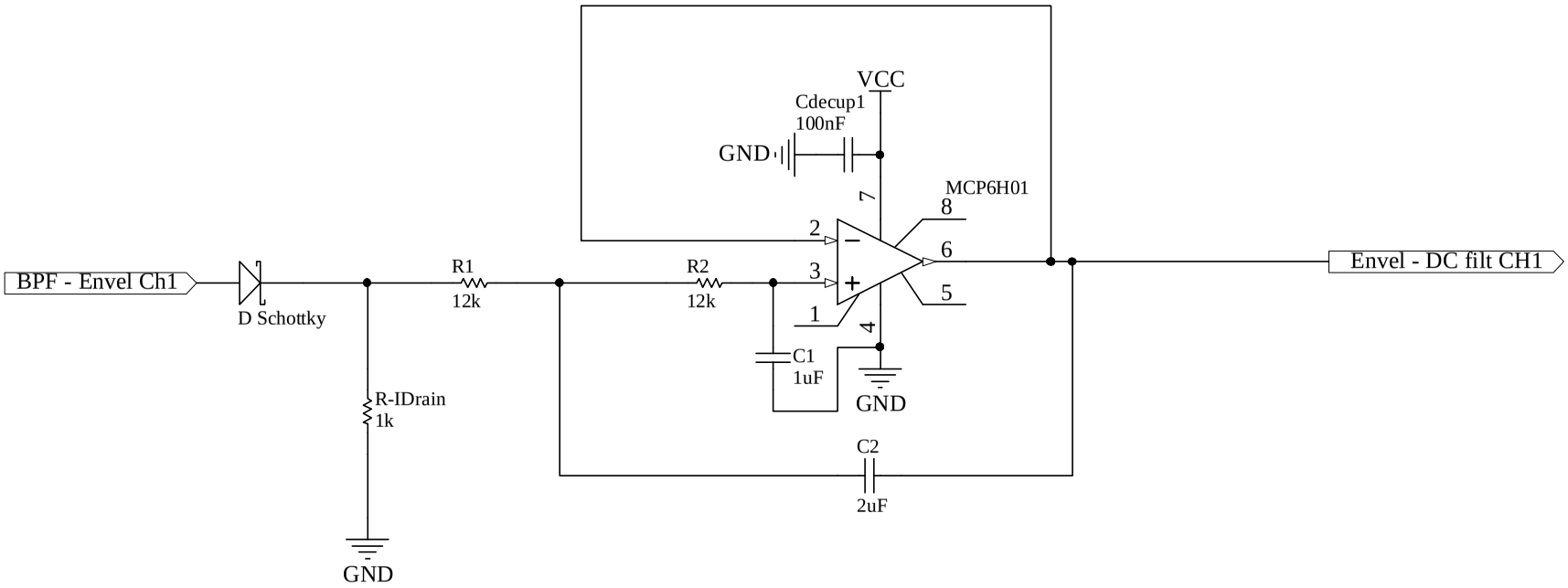

Figure A.5: *Circuit diagram of the envelope detection module of the 40 kHz channel.*

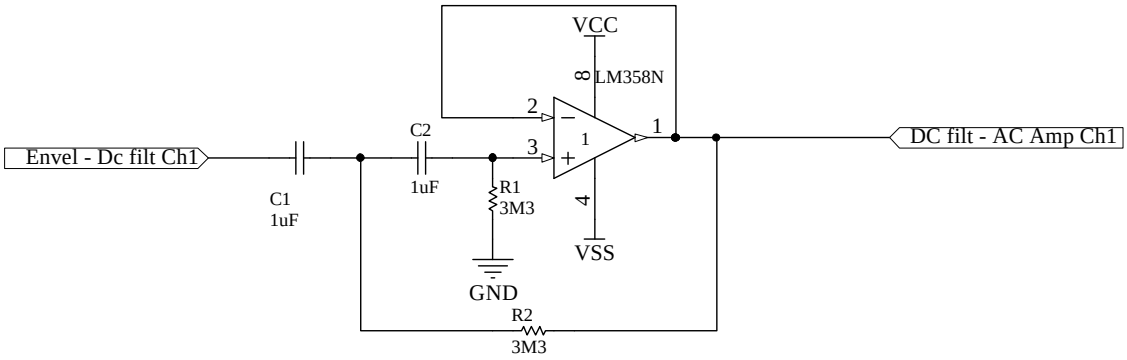

Figure A.6: *Circuit diagram of the DC filtering module of the 40 kHz channel.*

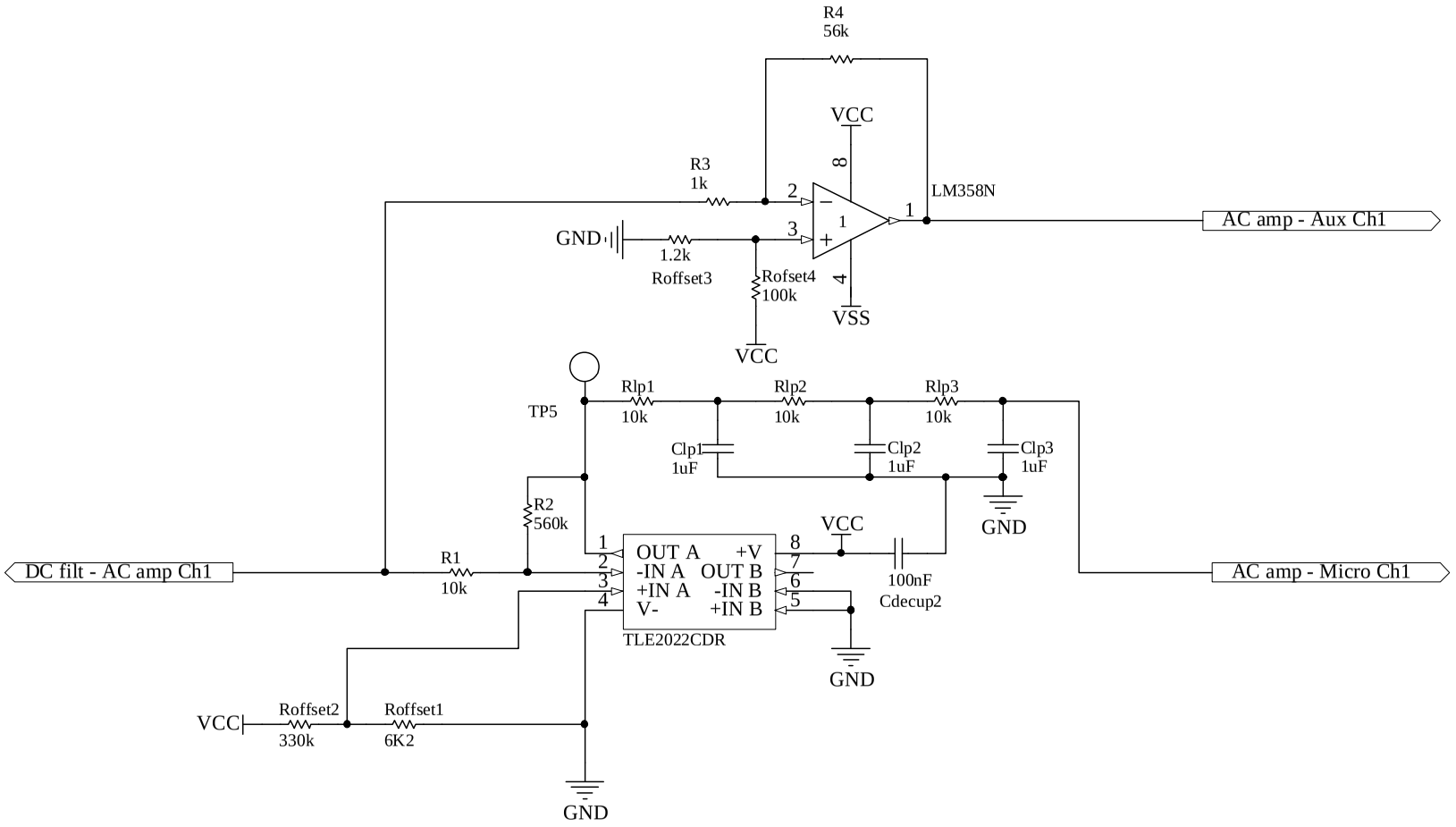

Figure A.7: *Circuit diagram of the AC amplifier module of the 40 kHz channel.*

A.2 70 kHz Channel

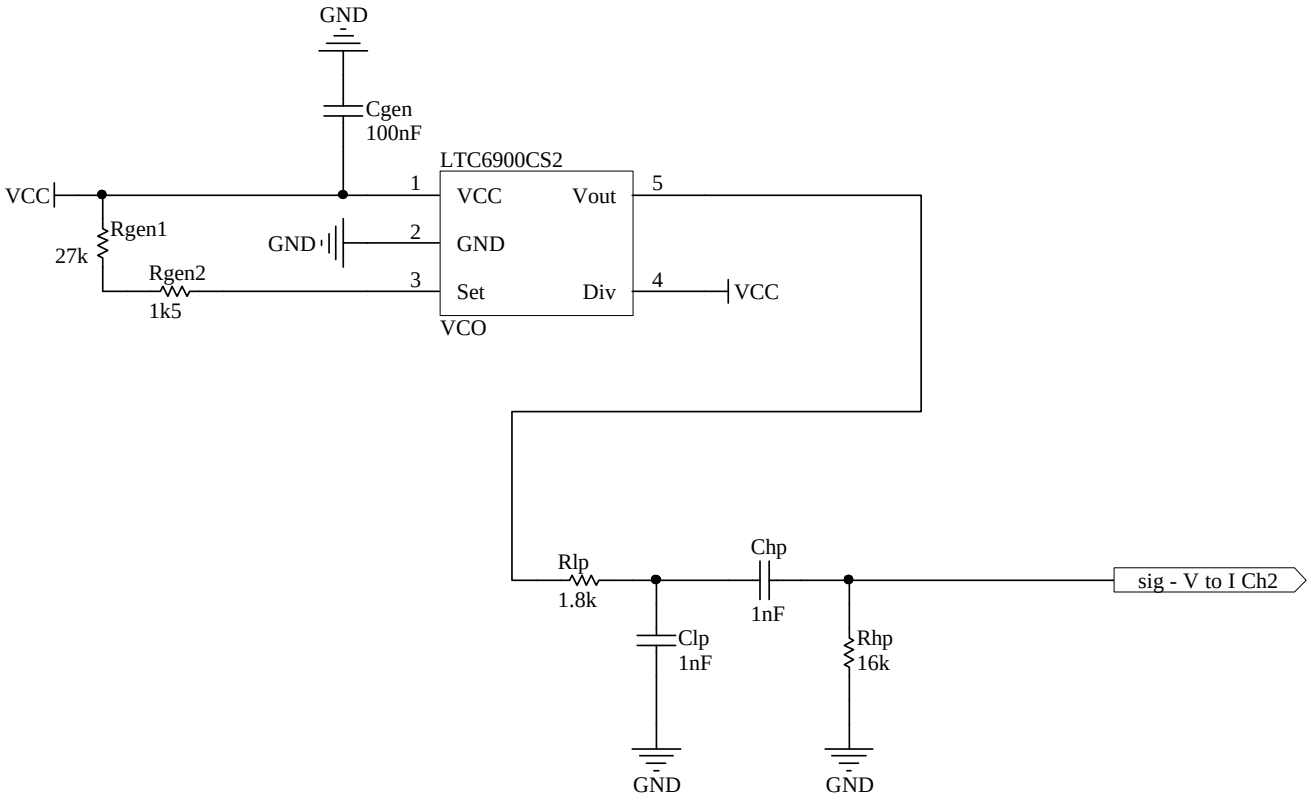

Figure A.8: *Circuit diagram of the signal generating module of the 70 kHz channel.*

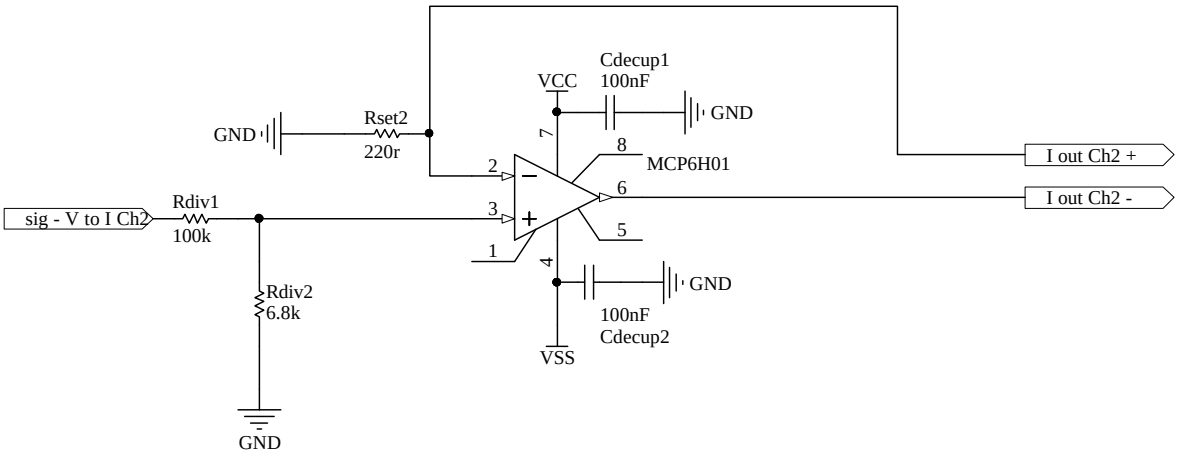

Figure A.9: *Circuit diagram of the voltage to current conversion module of the 70 kHz channel.*

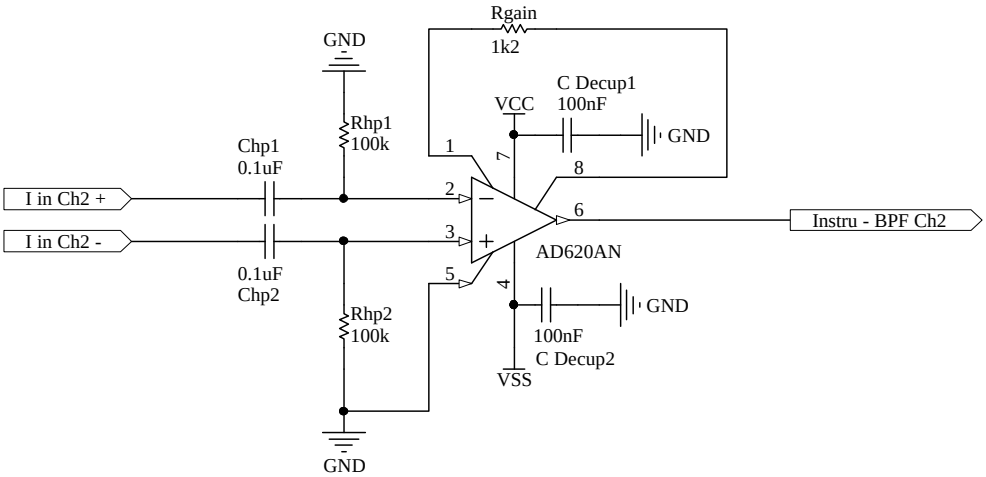

Figure A.10: *Circuit diagram of the instrumentation amplifier module of the 70 kHz channel.*

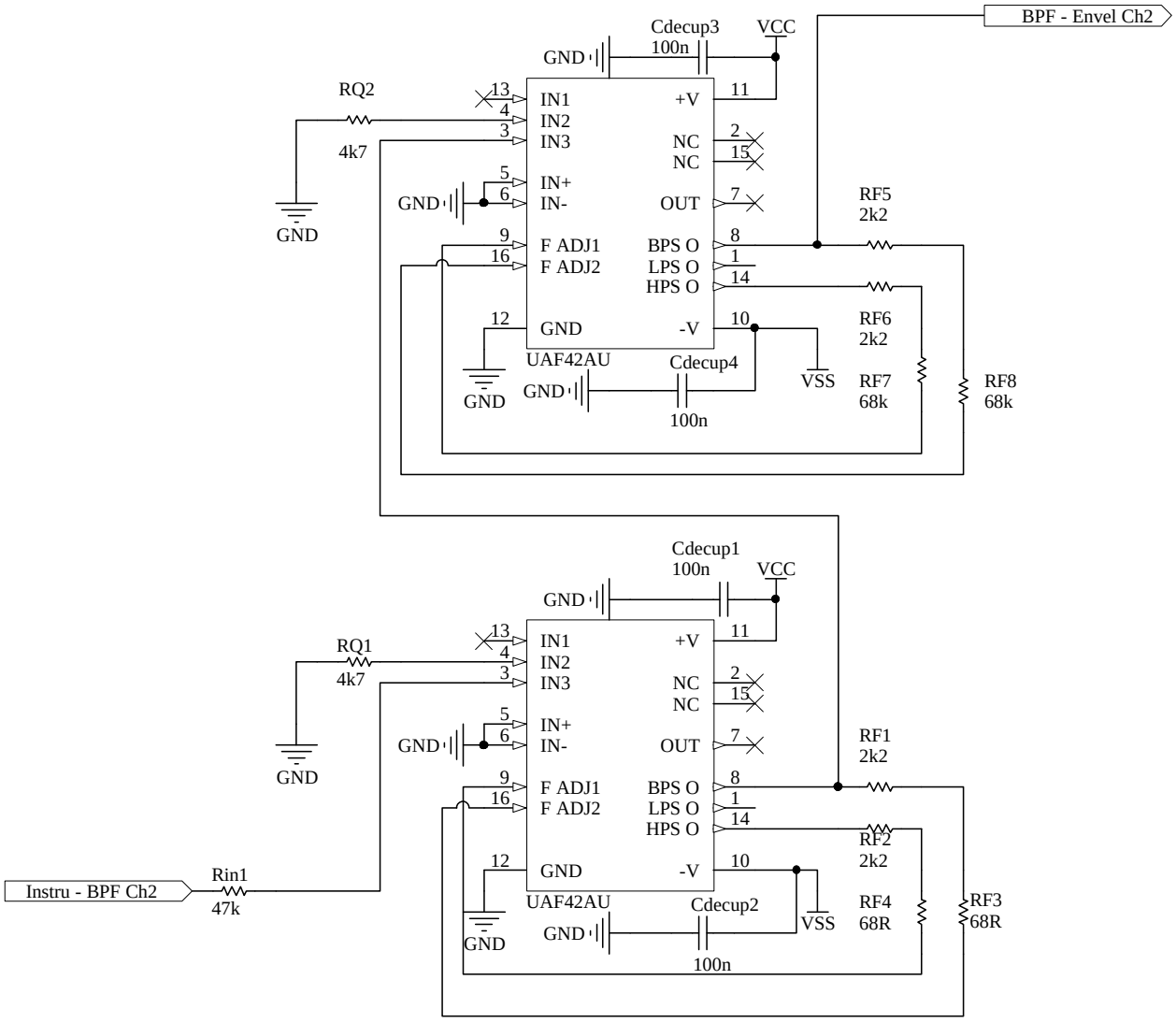

Figure A.11: *Circuit diagram of the band-pass filter module of the 70 kHz channel.*

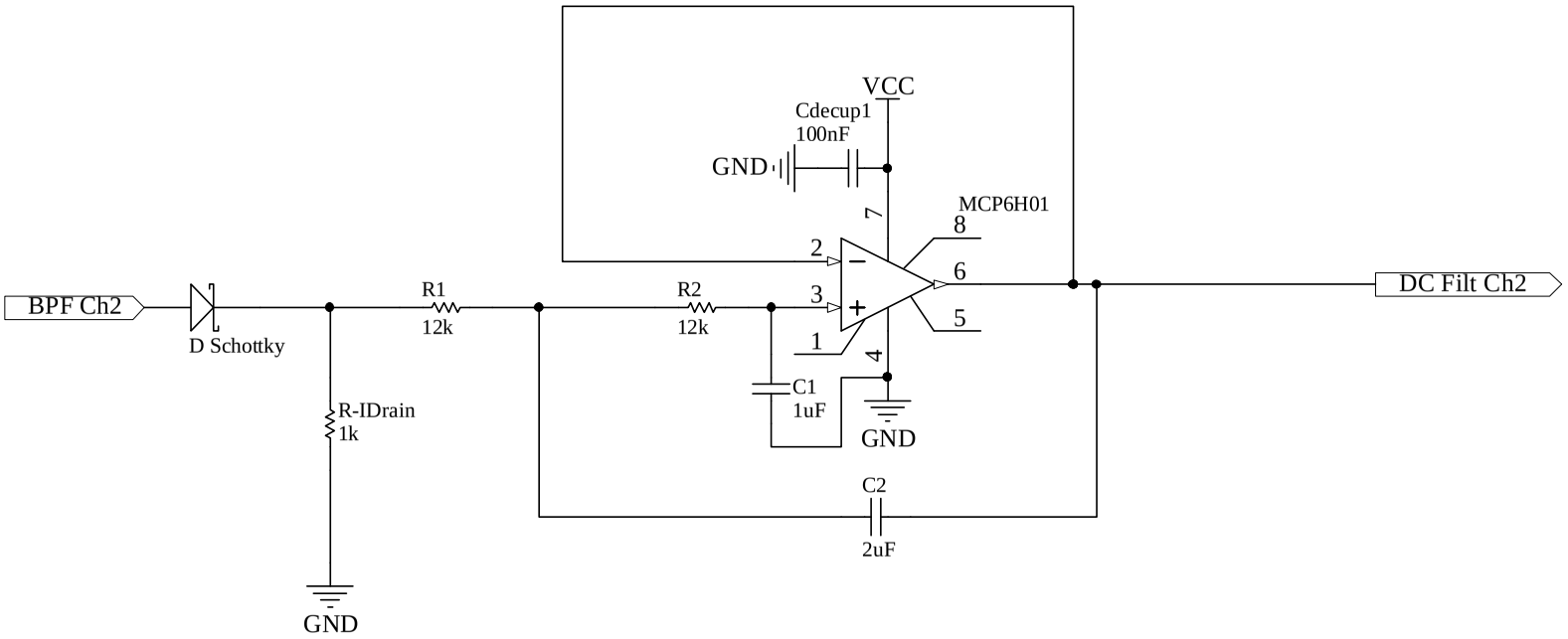

Figure A.12: *Circuit diagram of the envelope detection module of the 70 kHz channel.*

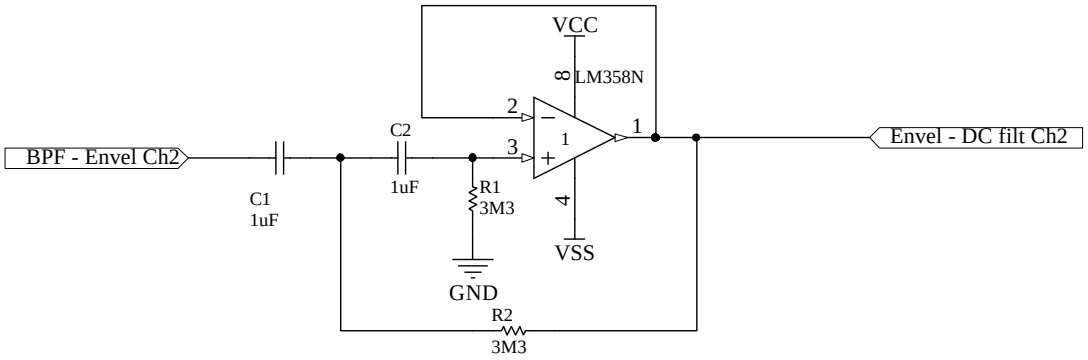

Figure A.13: *Circuit diagram of the DC filtering module of the 70 kHz channel.*

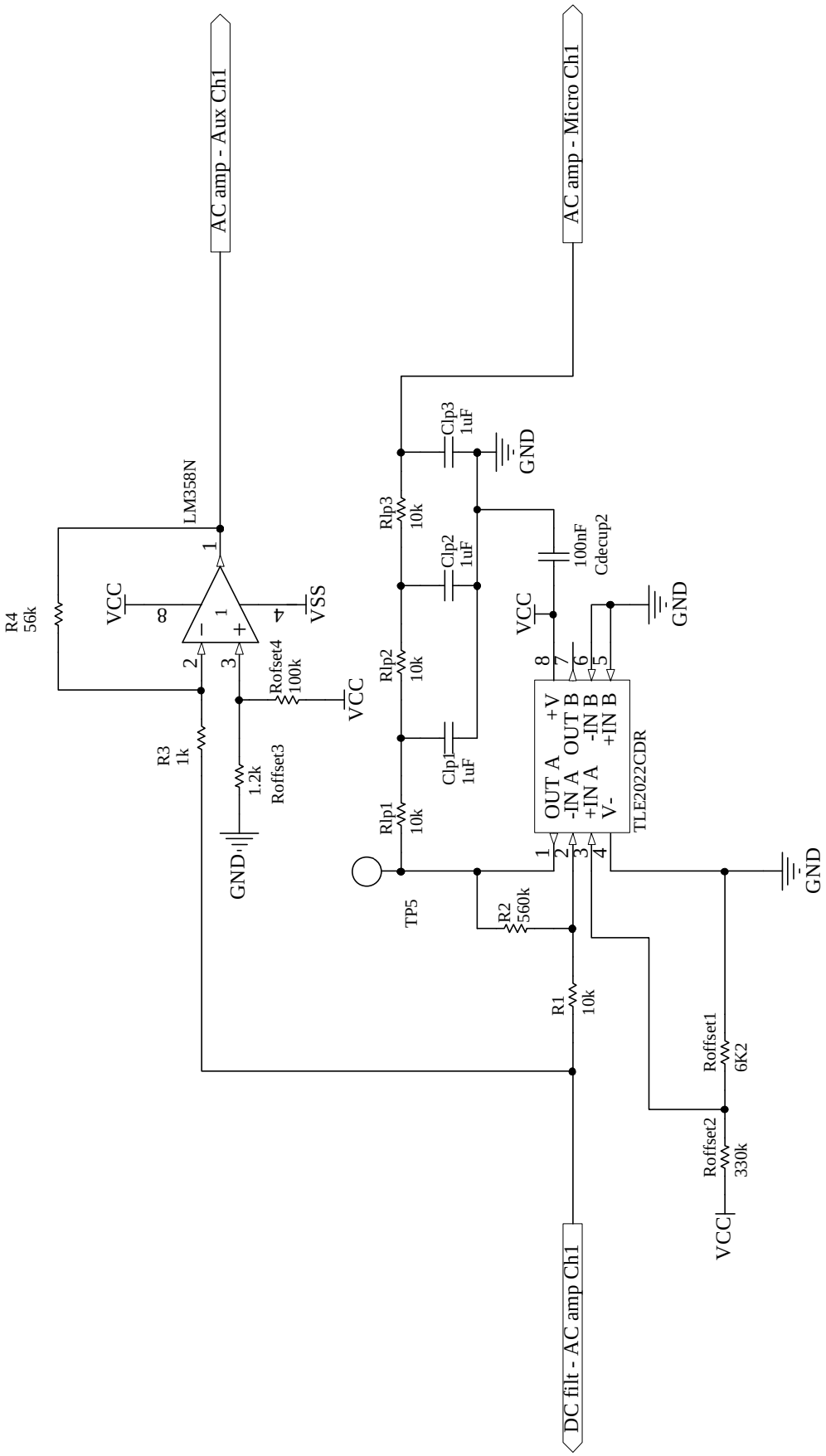

Figure A.14: *Circuit diagram of the AC amplifier module of the 70 kHz channel.*

A.3 Universal Sections

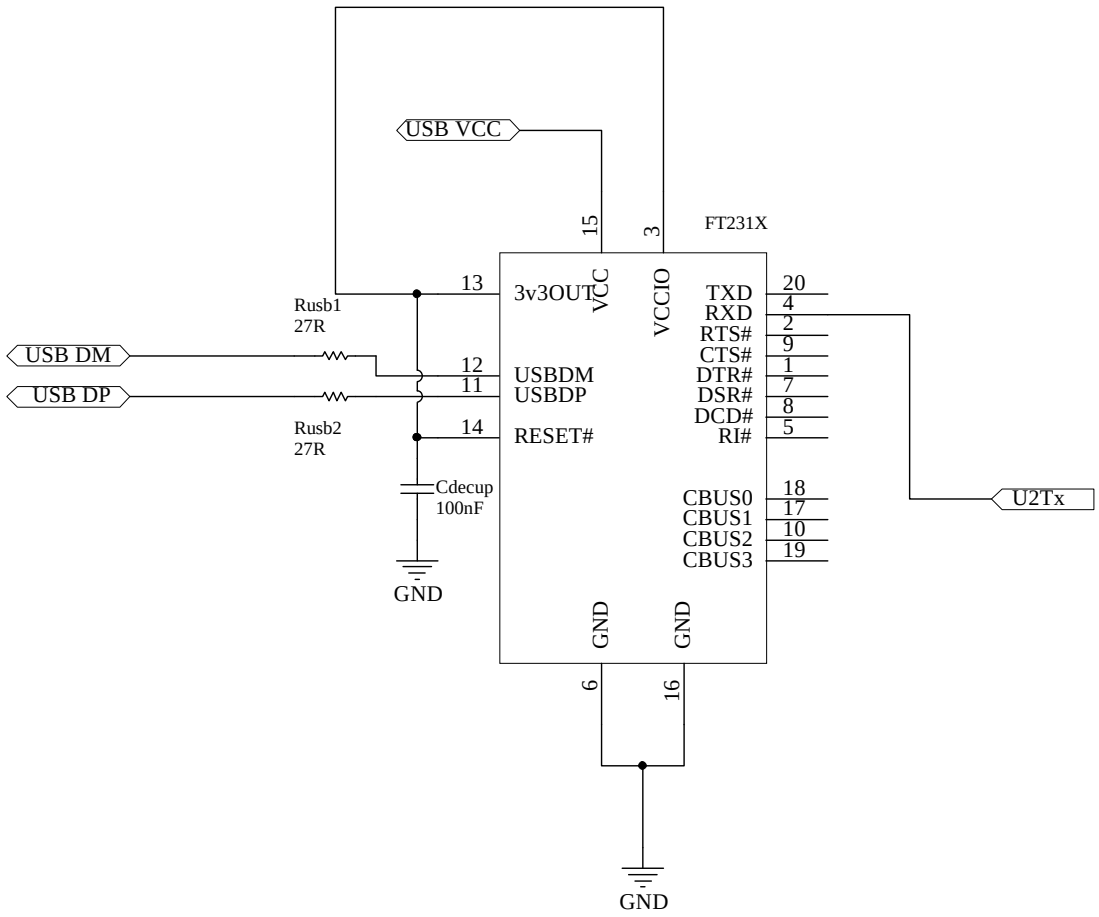

Figure A.15: *Circuit diagram of the Serial to USB module.*

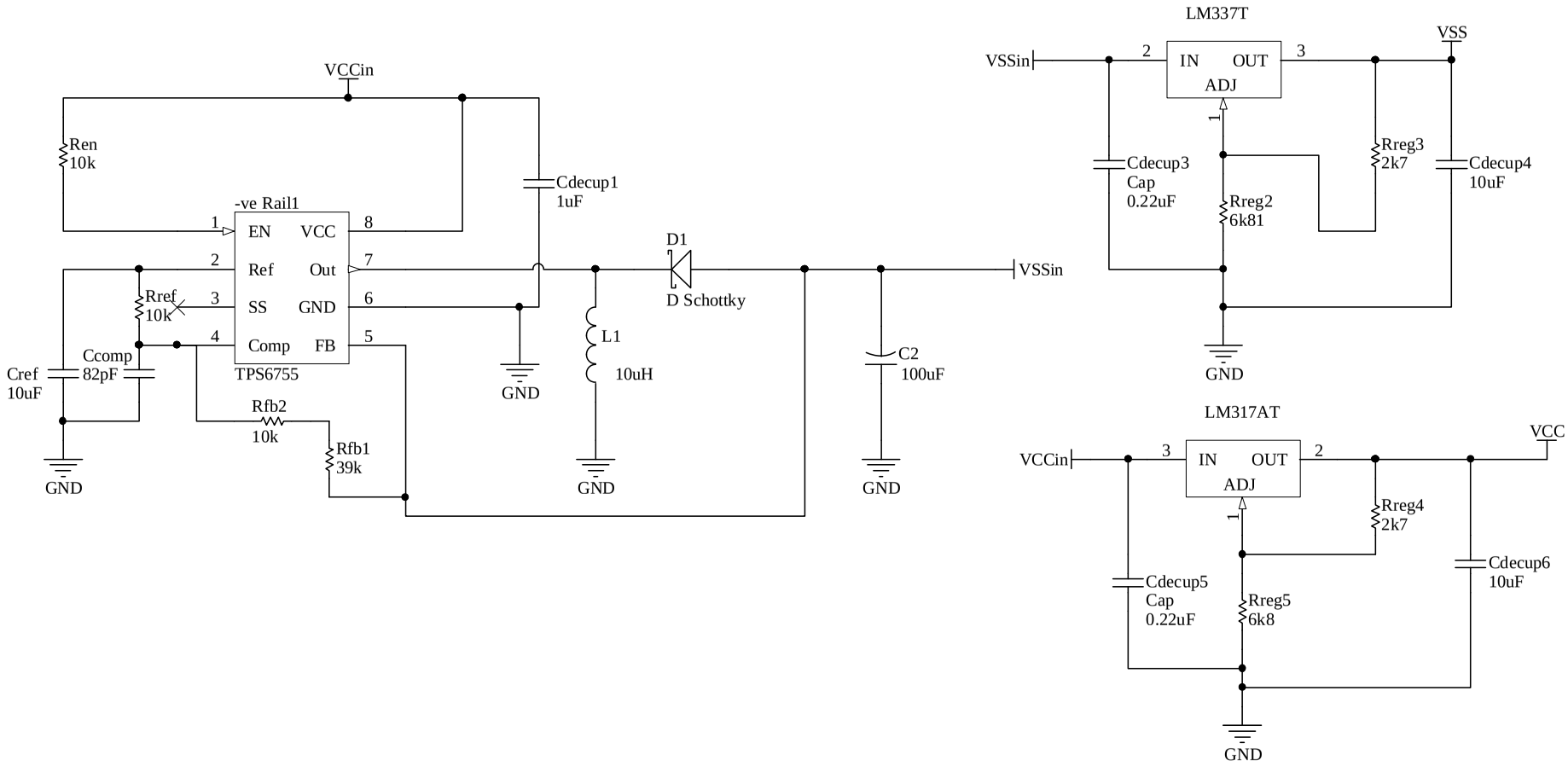

Figure A.16: *Circuit diagram of the Power module.*

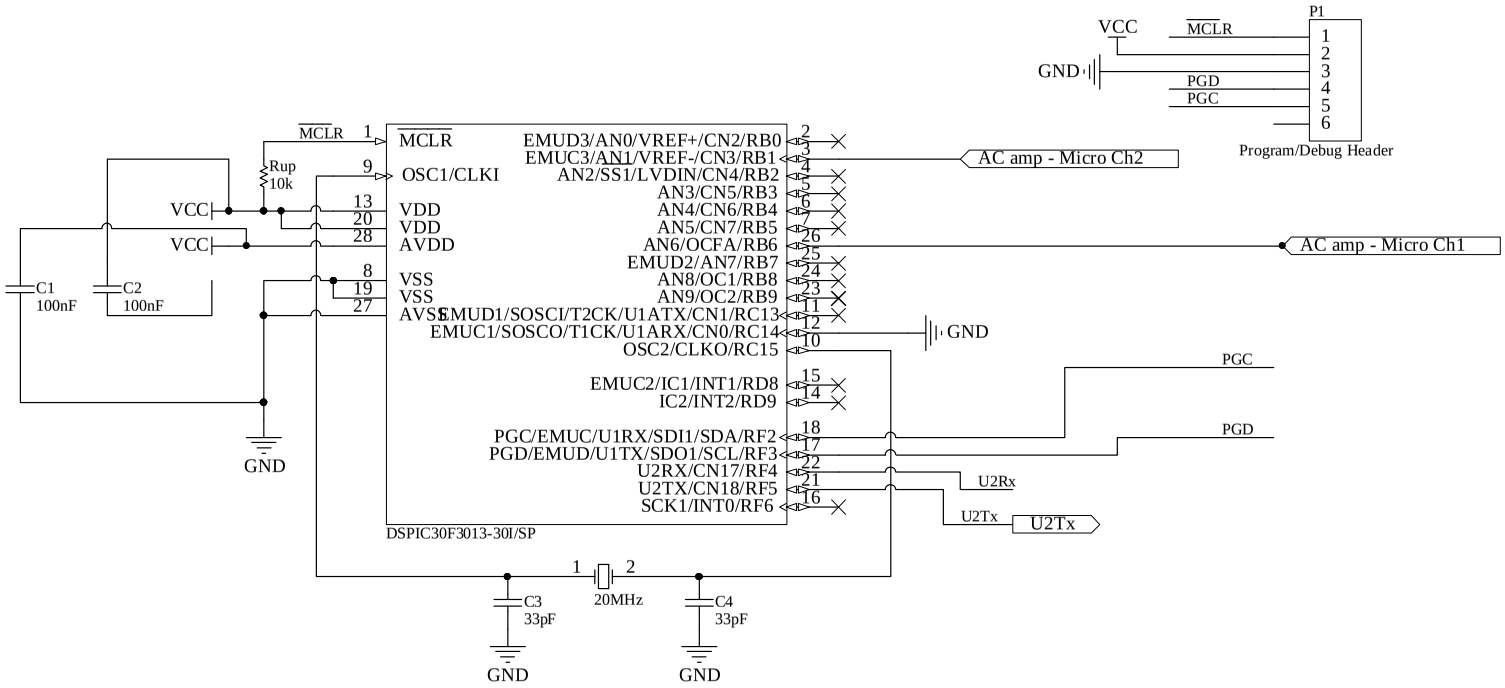

Figure A.17: *Circuit diagram of the Microcontroller module.*

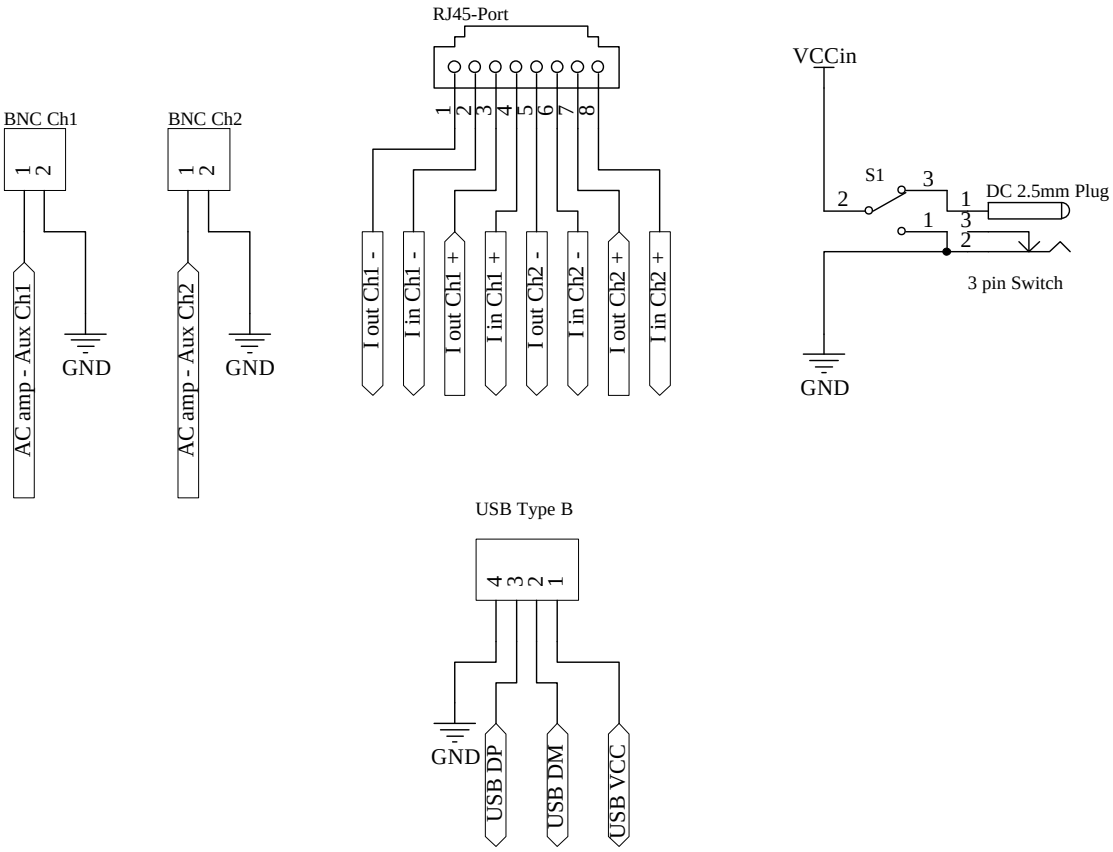

Figure A.18: *Circuit diagram of the Serial to USB module.*

APPENDIX B

Hardware Images

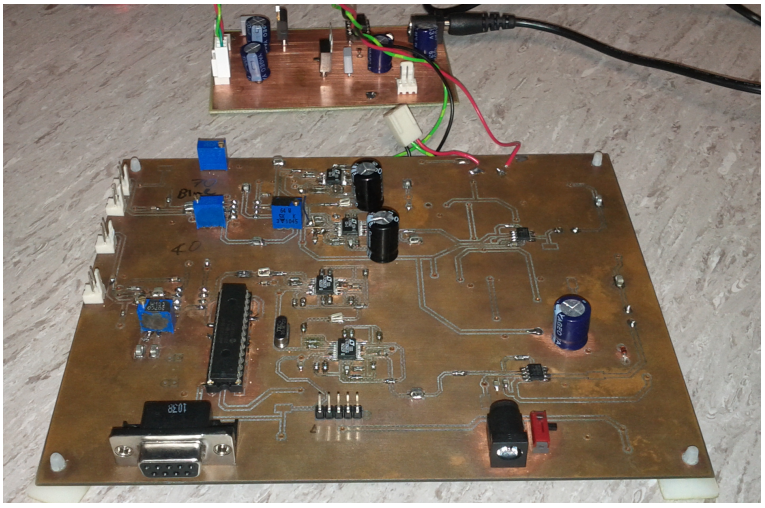

Figure B.1: *Developed Circuit for the First Full Prototype.*

Figure B.2: *Developed Circuit for the final enclosed prototype, including cables used for its operation.*

APPENDIX C

Software

C.1 Firmware

```
/* Filename: adc.c
    Author: Chris Chester
   Date: 20/09/2012
   Notes: This code was adapted from code created by Andrew Nicholas

   Description: The main code designed to be operated with a PIC micro
   to work with the GULPS device.
*/
#define FCY 26000000UL // Defining the system speed for delays, 26 MHz
#include <libpic30.h>
#include <p30f3013.h>
#include <stdlib.h>
#include <stdio.h>

#include "uart_bisskit.h"
#include "adc.h"

#define SYNC_BYTE 0xFF

#define BORV_SET 0x30  // Brown out voltage set to not in operating
```

```
// range

#define ADC_MAX 0xFD

#define DOWNSAMPLE_TIME 100 // Iterations used to slow transmissions
#define HIGH_BIT_SHIFT 8    // Shift needed to convert highest 8 bits
// of a conversion down

#define TRANSFER_DELAY 4      // Delay in milli seconds between transmissions

//Channel 1 data
uint16_t adc_data_ch1 = 0;
uint8_t high_byte_ch1 = 0;
uint8_t low_byte_ch1 = 0;

// Channel 2 data
uint16_t adc_data_ch2 = 0;
uint8_t high_byte_ch2 = 0;
uint8_t low_byte_ch2 = 0;

uint16_t timer_count_1 = 0;

// Initial Microcontroller Configuration
_FOSC(CSW_FSCM_OFF & HS3_PLL16);
_FWDT(WDT_ON & WDTPSA_512 & WDTPSB_16);
_FBORPOR(PBOR_ON & BORV_SET & PWRT_64 & MCLR_EN);
_FGS(CODE_PROT_OFF);
_ICD(ICS_PGD1);

/* Function prototypes */
void UART_test();
void ADC_test();

int main (void){

// Initialise LED's for debugging
    led_init();
```

```
// Initialise UART and ADC
    uart_init();
    adc_init();

    while(1)
    {
        if (adc_is_new_data())
        {
            adc_data_ch1 = adc_read_ch1();

            // Check to make sure the data value isn't the same as a
            // sync bit
            if(adc_data_ch1 == SYNC_BYTE)
            {
                adc_data_ch1 = ADC_MAX;
            }
            low_byte_ch1 = adc_data_ch1;
            high_byte_ch1 = adc_data_ch1 >> HIGH_BIT_SHIFT;

            adc_data_ch2 = adc_read_ch2();

            // Check to make sure the data value isn't the same as a
            // sync bit
            if(adc_data_ch2 == SYNC_BYTE)
            {
                adc_data_ch2 = ADC_MAX;
            }

            low_byte_ch2 = adc_data_ch2;
            high_byte_ch2 = adc_data_ch2 >> HIGH_BIT_SHIFT;

            //Send data

            uart_send(SYNC_BYTE);
            __delay_ms(TRANSFER_DELAY);
            // Channel 1 data
            uart_send(low_byte_ch1);
            __delay_ms(TRANSFER_DELAY);
```

```
            uart_send(high_byte_ch1);
            __delay_ms(TRANSFER_DELAY);

            // Channel 2 data
            uart_send(low_byte_ch2);
            __delay_ms(TRANSFER_DELAY);
            uart_send(high_byte_ch2);
            __delay_ms(TRANSFER_DELAY);

            adc_set_data_received(0); // turn flag off to indicate
            // data received.
        }
    }
}
```

APPENDIX D

Unused Results

During the investigation of the GULPS system the results gained would often not provide the features desired, where the second peak was often unable to be determined. Examples of these results can be seen in the figures below, these figures all contained data from the same session of a male subject.

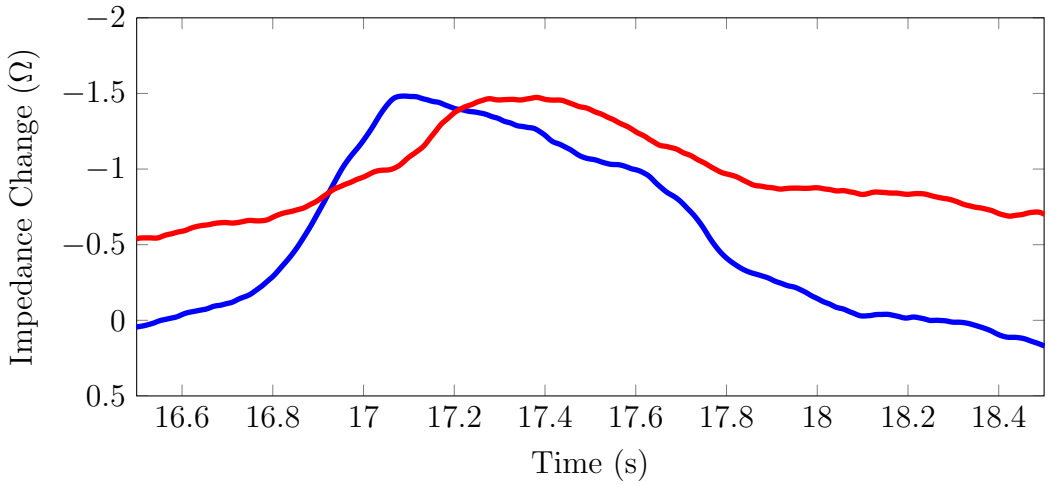

Figure D.1: *Resultant output waveform for the first swallow of a poor session on male subject 2. The blue waveform is from the upper positioned channel and the red dashed waveform is from the lower positioned channel.*

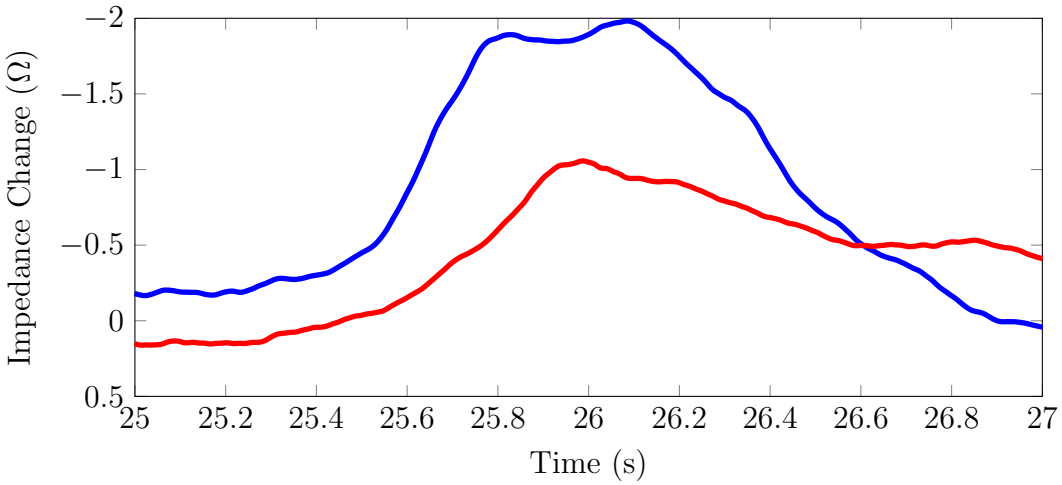

Figure D.2: *Resultant output waveform for the second swallow of a poor session on male subject 2. The blue waveform is from the upper positioned channel and the red dashed waveform is from the lower positioned channel.*

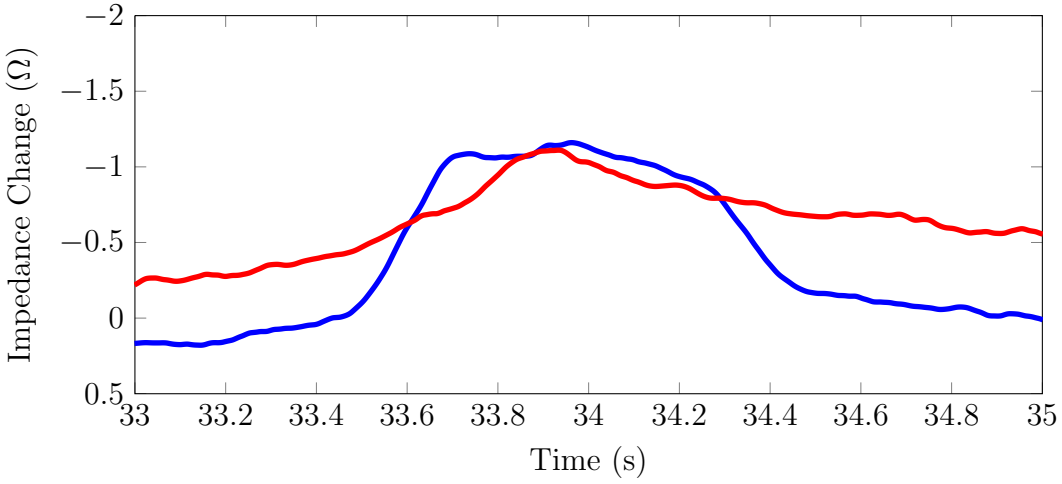

Figure D.3: *Resultant output waveform for the third swallow of a poor session on male subject 2. The blue waveform is from the upper positioned channel and the red dashed waveform is from the lower positioned channel.*

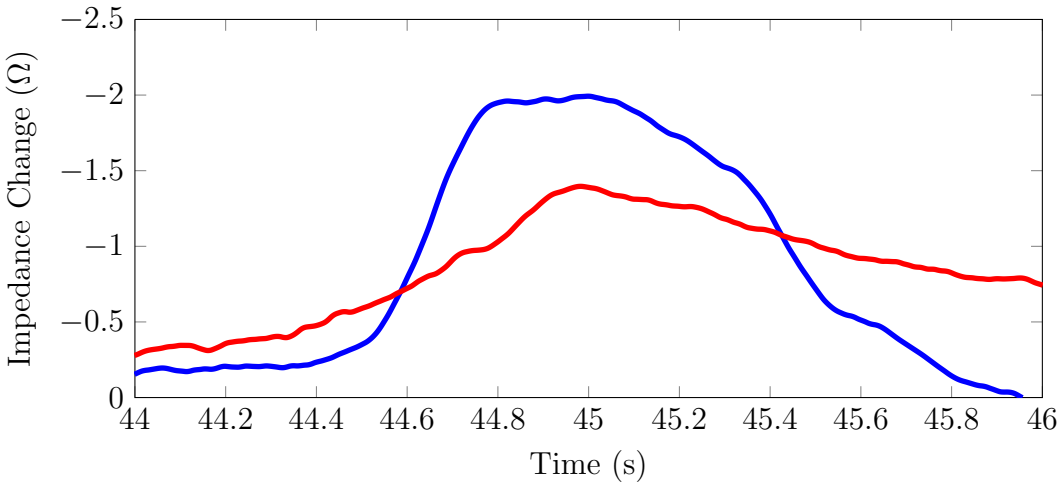

Figure D.4: *Resultant output waveform for the fourth swallow of a poor session on male subject 2. The blue waveform is from the upper positioned channel and the red dashed waveform is from the lower positioned channel.*